The H2A.Z-associated protein ZNF512B acts as a transcriptional repressor, aggregates chromatin and binds RBBP4 via an alternative NuRD interaction motif

By

Tim Marius Wunderlich

A dissertation submitted to the

Institute for Genetics

Justus Liebig University Giessen

for the degree of *Doctor rerum naturalium*

December 2024

Dean:

Prof. Dr. Holger Zorn

Institute of Food Chemistry and Food Biotechnology

Justus Liebig University Giessen

First Referee:

Prof. Dr. Sandra B. Hake

Institute for Genetics

Justus Liebig University Giessen

Second Referee:

Prof. Dr. Alexander Brehm

Institute for Molecular Biology and Tumor Research

Philipps University Marburg

Publications associated with this dissertation

Wunderlich, T. M., Deshpande, C., Paasche, L. W., Friedrich, T., Diegmüller, F., Haddad, E., Kreienbaum, C., Naseer, H., Stebel, S. E., Daus, N., Leers, J., Lan, J., Trinh, V. T., Vázquez, O., Butter, F., Bartkuhn, M., Mackay, J. P., & Hake, S. B. (2024). ZNF512B binds RBBP4 via a variant NuRD interaction motif and aggregates chromatin in a NuRD complex-independent manner. *Nucleic acids research*, *52*(21), 12831–12849. https://doi.org/10.1093/nar/gkae926

Herchenröther, A., Wunderlich, T. M., Lan, J., & Hake, S. B. (2023). Spotlight on histone H2A variants: From B to X to Z. *Seminars in cell & developmental biology*, *135*, 3–12. https://doi.org/10.1016/j.semcdb.2022.03.025

Eidesstattliche Versicherung

Ich erkläre: Ich habe die vorgelegte Dissertation selbstständig und ohne unerlaubte fremde Hilfe und nur mit den Hilfen angefertigt, die ich in der Dissertation angegeben habe. Alle Textstellen, die wörtlich oder sinngemäß aus veröffentlichten Schriften entnommen sind, und alle Angaben, die auf mündlichen Auskünften beruhen, sind als solche kenntlich gemacht. Ich stimme einer evtl. Überprüfung meiner Dissertation durch eine Antiplagiat-Software zu. Bei den von mir durchgeführten und in der Dissertation erwähnten Untersuchungen habe ich die Grundsätze guter wissenschaftlicher Praxis, wie sie in der „Satzung der Justus-Liebig-Universität Gießen zur Sicherung guter wissenschaftlicher Praxis“ niedergelegt sind, eingehalten.

Ort, Datum

Unterschrift

Abstract

Chromatin serves as the substrate for a multitude of essential biological functions within the cell and is dynamically regulated, for instance through the incorporation of histone variants. The evolutionarily conserved histone variant H2A.Z is involved in nearly all DNA-related processes but the mechanisms underlying its diverse roles remain largely unknown. One potential approach for further elucidation of these mechanisms is the investigation of H2A.Z-specific interacting proteins. Recently, the zinc finger (ZF) protein ZNF512B has been identified as an interactor of H2A.Z and its associated proteins HMG20A and PWWP2A. This study demonstrates that elevated levels of ZNF512B induce protein and chromatin aggregation in the nucleus, presumably facilitated by DNA binding and oligomerization of its ZF domains. Biochemical and mass spectrometry-based experiments show that ZNF512B interacts with the nucleosome remodeling and deacetylase (NuRD) complex. The solved crystal structure of ZNF512B bound to the NuRD member RBBP4 and biophysical assays reveal an alternative, internal NuRD interaction motif as necessary for this high-affinity interaction. Moreover, transcriptome analyses and reporter assays identify ZNF512B as a transcriptional repressor acting in NuRD-dependent and -independent manners. Collectively, this study may have implications for diseases in which ZNF512B expression is deregulated, such as neurodegenerative diseases and cancer, suggests the existence of additional proteins as potential NuRD interactors and contributes to a better understanding of the mechanisms underlying H2A.Z's activity.

Zusammenfassung

Chromatin stellt die Grundlage für eine Vielzahl wesentlicher biologischer Funktionen innerhalb der Zelle dar und unterliegt einer dynamischen Regulation, beispielsweise durch den Einbau von Histonvarianten. Die evolutionär konservierte Histonvariante H2A.Z ist an einer Vielzahl von DNA-bezogenen Prozessen beteiligt, jedoch sind die zugrunde liegenden Mechanismen noch weitgehend unbekannt. Ein vielversprechender Ansatz zur weiteren Aufklärung dieser Mechanismen ist die Untersuchung von Proteinen, die spezifisch mit H2A.Z interagieren. In jüngster Zeit konnte das Zinkfingerprotein ZNF512B als Interaktor von H2A.Z und dessen assoziierten Proteinen HMG20A und PWWP2A identifiziert werden. Diese Studie zeigt, dass eine erhöhte Expression von ZNF512B zur Bildung von Protein- und Chromatin-Aggregaten im Zellkern führt. Dieser Prozess wird vermutlich durch DNA-Bindung und Oligomerisierung der Zinkfinger-Domänen des Proteins verursacht. Die Ergebnisse biochemischer und massenspektrometrischer Experimente legen dar, dass ZNF512B mit dem Nukleosomenremodellierungs- und Deacetylase-Komplex (NuRD) interagiert. Die Kristallstruktur von ZNF512B, welches an das NuRD-Protein RBBP4 gebunden ist, sowie biophysikalische Untersuchungen zeigen auf, dass ein alternatives, internes NuRD-Interaktionsmotiv für diese hochaffine Interaktion erforderlich ist. Des Weiteren belegen Transkriptomanalysen und Reporterassays, dass ZNF512B sowohl abhängig als auch unabhängig von NuRD als Transkriptionsrepressor wirkt. Die Ergebnisse dieser Studie könnten zukünftig Auswirkungen auf die Behandlung von Krankheiten haben, bei denen die Expression von ZNF512B dereguliert ist, wie beispielsweise neurodegenerative Erkrankungen und Krebs. Zudem deuten die Ergebnisse auf die Existenz weiterer Proteine als potenzielle NuRD-Interaktoren hin und tragen zu einem besseren Verständnis der Mechanismen bei, die der Aktivität von H2A.Z zugrunde liegen.

List of abbreviations

3C	Chromosome conformation capture
4PL	Four parameter logistic
5mC	5-methylcytosine
AAVS1	Adeno-associated virus integration site 1
ADAMTS3	ADAM metallopeptidase with thrombospondin type 1 motif 3
AEBP2	Adipocyte enhancer-binding protein 2
ALS	Amyotrophic lateral sclerosis
ANP32E	Acidic nuclear phosphoprotein 32 family member E
APOBEC	Apolipoprotein B mRNA editing enzyme, catalytic polypeptide
APS	Ammonium persulfate
AR	Androgen receptor
ATAC	Assay for transposase-accessible chromatin
ATP	Adenosine triphosphate
B1H	Bacterial one-hybrid
BAM	Binary alignment map
BCL11A	B-cell CLL/lymphoma 11A
BET	Bromodomain and extra-terminal domain
BIRC3	Baculoviral IAP repeat containing 3
BLAST	Basic local alignment search tool
BPTF	Bromodomain PHD finger transcription factor
BRD2	Bromodomain containing 2
BSA	Albumin fraction V
BSD	Blasticidin S deaminase
CARM1	Coactivator-associated arginine methyltransferase 1
Cas9	CRISPR associated protein 9
CDK1	Cyclin dependent kinase 1
CDK2AP1/2	Cyclin-dependent kinase 2-associated protein 1/2
cDNA	Complementary DNA
CECR2	Cat eye syndrome critical region protein 2
CGAS	Cyclic GMP-AMP synthase
CHD	Chromodomain helicase DNA-binding
ChIP	Chromatin immunoprecipitation
CIM	Critical illness myopathy
CKAP2	Cytoskeleton associated protein 2
CLIP	Crosslinking immunoprecipitation
CM	Cardiomyocyte
CoREST	Corepressor of RE1 silencing transcription factor
CpG	Cytosine-phosphate-guanine
CRC	Chromatin remodeling complex
CRISPR	Clustered regularly interspaced short palindromic repeats
CTCF	CCCTC-binding factor
Ctrl	Control

CUT&RUN	Cleavage under targets and release using nuclease
DACOR1	DNMT1-associated colon cancer repressed lncRNA 1
DAPI	4′,6-diamidino-2-phenylindole
DBD	DNA-binding domain
DIP	DNA immunoprecipitation
DMEM	Dulbecco’s Modified Eagle Medium
DMSO	Dimethyl sulfoxide
DNA	Deoxyribonucleic acid
DNMT1/3A/3B	DNA methyltransferase 1/3A/3B
DSLR	Digital single-lens reflex
DTT	Dithiothreitol
E2F1	E2F transcription factor 1
EDTA	Ethylenediaminetetraacetic acid
EGTA	Ethylene glycol-bis(β-aminoethyl ether)-*N*,*N*,*N*′,*N*′-tetraacetic acid
EIF4H	Eukaryotic translation initiation factor 4H
EMSA	Electrophoretic mobility shift assay
EMT	Epithelial to mesenchymal transition
ERV	Endogenous retrovirus
ESI	Electrospray ionization
FAM	Fluorescein
FCS	Fetal calf serum
FHS	Floating-Harbor syndrome
FOG-1	Friend of GATA protein 1
FOXJ1	Forkhead box J1
FP	Fluorescence polarization
FPLC	Fast protein liquid chromatography
FSC	Forward scatter
GAS2L3	Growth arrest specific 2 like 3
GATA3	GATA-binding factor 3
GATAD2A/B	GATA zinc finger domain containing 2 A/B
GFP	Green fluorescent protein
GNAI1	G protein subunit alpha I1
GO	Gene ontology
GSEA	Gene set enrichment analysis
GTF3C2	General transcription factor IIIC subunit 2
HA	Homology arm
HCD	Higher-energy collisional dissociation
HDAC	Histone deacetylase
HeLaK	HeLa Kyoto
HEPES	4-(2-hydroxyethyl)-1-piperazineethanesulfonic acid
His	Histidine
HMBS	Hydroxymethylbilane synthase
HMG20A	High mobility group 20 A
HOTAIR	HOX transcript antisense RNA

HOXD	Homeobox D
HPRT1	Hypoxanthine phosphoribosyltransferase 1
HRMS	High-resolution mass spectrometry
HRP	Horseradish peroxidase
HSA	Helicase/SANT-associated
HSS	HAND-SANT-SLIDE
IF	Immunofluorescence
IGF2	Insulin-like growth factor 2
IKZF1	IKAROS family zinc finger 1
IL6	Interleukin 6
iNIM	Internal NuRD interaction motif
INO80	Inositol requiring 80
IP	Immunoprecipitation
ISWI	Imitation switch
ITC	Isothermal titration calorimetry
JAZF1	Juxtaposed with another zinc finger protein 1
KAP1	KRAB-associated protein-1
KD	Knock-down
KEGG	Kyoto Encyclopedia of Genes and Genomes
KPNA3/4	Karyopherin subunit alpha 3/4
KRAB	Krüppel-associated box
LB	Lysogeny broth
lfqMS/MS	Label free quantitative mass spectrometry
LLPS	Liquid-liquid phase separation
lncRNA	Long non-coding RNA
MARCS	Modification Atlas of Regulation by Chromatin States
MB21D1	Mab-21 domain-containing protein 1
MBTD1	Mbt domain containing 1
MDB1/2/3	Methyl-CpG binding domain protein 1/2/3
MeCP2	Methyl-CpG binding protein 2
MEF	Mouse embryonic fibroblast
MEL	Mouse erythroleukemia
mESC	Mouse embryonic stem cell
miRNA	MicroRNA
MLL	Mixed lineage leukemia
MNase	Micrococcal nuclease
mRNA	Messenger RNA
MS	Mass spectrometry
MTA1/2/3	Metastasis-associated 1/2/3
MuSC	Muscle stem cells
MYRF	Myelin regulatory factor
NCAPG/H	Non-SMC condensin I complex subunit G/H
NCC	Neural crest cell
ncRNA	Non-coding RNA

NIM	NuRD interaction motif
NLS	Nuclear localization signal
NMR	Nuclear magnetic resonance
NOL9	Nucleolar protein 9
NP-40	Nonidet P-40 substitute
NPC	Neural progenitor cell
NuRD	Nucleosome remodeling and deacetylase
NURF	Nucleosome remodeling factor
ORA	Over-representation analysis
P/S	Penicillin/streptomycin
PBS	Phosphate-buffered saline
PCA	Principal component analysis
PCR	Polymerase chain reaction
PDAC	Pancreatic ductal adenocarcinoma
PDB	Protein data bank
PEG	Polyethylene glycol
PFA	Paraformaldehyde
PHF14	PHD finger protein 14
PHF6	PHD finger protein 6
PHIP	Pleckstrin homology domain interacting protein
PI	Propidium iodide
PMSF	Phenylmethanesulfonyl fluoride
PRC2	Polycomb repressive complex 2
PRDM3/16	PR domain zinc finger proteins 3/16
PTEN	Phosphatase and tensin homolog
PTM	Post-translational modification
PWM	Position weight matrix
PWWP2A	PWWP domain containing 2A
qPCR	Quantitative PCR
RBBP4/7	Retinoblastoma-binding protein 4/7
RIP	RNA immunoprecipitation
RIPA	Radioimmunoprecipitation assay
RNA	Ribonucleic acid
RNA-Pol II	RNA polymerase II
RPL11	Ribosomal protein L11
rRNA	Ribosomal RNA
RRP9	Ribosomal RNA processing 9
RT-qPCR	Reverse transcription-qPCR
RYR3	Ryanodine receptor 3
SA	Senescence associated
SALL1/4	Sal-like protein 1/4
SAM	S-adenosyl methionine
SANT	Swi3, Ada2, N-Cor, and TFIIIB
SCR	Scrambled

SD	Standard deviation
SDS	Sodium dodecyl sulfate
SDS-PAGE	SDS-polyacrylamide gel electrophoresis
SEC-MALS	Size-exclusion chromatography with multi-angle light scattering
SELEX	Systematic evolution of ligands by exponential enrichment
seq	Sequencing
sgRNA	single guide RNA
SILAC	Stable isotope labeling by amino acids in cell culture
siRNA	Small interfering RNA
SIRT1	Sirtuin 1
SNP	Single-nucleotide polymorphism
SPATA18	Spermatogenesis associated 18
SRCAP	Snf2-related CREBBP activator protein
SSC	Sideward scatter
STAMP	Surveying targets by APOBEC-mediated profiling
SUV39H1/2	Suppressor of variegation 3–9 homolog 1/2
SWI/SNF	Switch/sucrose non-fermentable
SWR1	Swi2/Snf2-related 1
TCGA	The Cancer Genome Atlas
TdT	Terminal deoxynucleotidyl transferase
TEMED	Tetramethylethylenediamine
Tet	Tetracycline
TEX10	Testis expressed 10
TF	Transcription factor
TFA	Trifluoroacetic acid
Tip60	Tat interacting protein, 60 kDa
TNBC	Triple negative breast cancer
TOPO	Topoisomerase-based
TRE	Tet-responsive
TRIM28	Tripartite motif-containing 28
Tris	Tris (hydrxymethyl)aminomethan
TSA	Trichostatin-A
TSS	Transcription start site
TUNEL	Terminal deoxynucleotidyl transferase dUTP nick end labeling
UBE2D1	Ubiquitin conjugating enzyme E2 D1
UL	Uterine leiomyoma
URB1	URB1 ribosome biogenesis homolog
UV	Ultraviolet
ZBTB20	Zinc finger and BTB domain-containing protein 20
ZBTB7B	Zinc finger and BTB domain containing 7B
ZEB2	Zinc-finger E-box binding-homeobox 2
ZF	Zinc finger
ZFP	Zinc finger protein
ZID	H2A.Z interacting domain

ZNF148	Zinc finger protein 148
ZNF219	Zinc finger protein 219
ZNF410	Zinc finger protein 410
ZNF512	Zinc finger protein 512
ZNF512B	Zinc finger protein 512B
ZNF558	Zinc finger protein 558
ZNF827	Zinc finger protein 827

1 Introduction

1.1 Chromatin structure and function are dynamically regulated

The DNA molecule of every single chromosome in a eukaryotic organism is several magnitudes longer than the diameter of a cell nucleus (Widom, 1989). Therefore, it is inevitable for eukaryotes to compact their genetic material in a structured and organized way. The resulting complex of DNA and proteins, that is making up the chromosomes, is called chromatin (Flemming, 1882; Kornberg, 1977). The smallest unit of chromatin is the nucleosome core particle consisting of 145–147 bp DNA wrapped around an octamer of two of each of the four core histones H2A, H2B, H3 and H4 (Figure 1.1) (Luger et al., 1997). Together with the so-called 'linker' DNA it forms the nucleosome, the primary repeating unit of chromatin (McGhee & Felsenfeld, 1980). Nucleosomes can form the chromatosome, when 'linker' DNA is bound by histone H1, and further pack into higher order structures, being the chromatin fiber and, eventually, the chromosome (Bednar & Dimitrov, 2011; Bharath et al., 2003). However, chromatin is the substrate for several essential processes like replication, transcription, DNA repair, recombination and chromosome segregation (Richmond & Davey, 2003). In order for these processes to occur effectively, chromatin must be accessible, for example to polymerases. Consequently, chromatin structure and compaction need to be highly dynamic. First evidence of chromatin segments with varying degrees of compaction was already discovered in the early 20th century, when Emil Heitz coined the terms 'euchromatin' and 'heterochromatin', due to their different behavior during chromosomal stains (Heitz, 1928). Today, euchromatin (or 'open' chromatin) is known as accessible, gene-rich and (mostly) transcriptionally active in comparison to the condensed, gene-poor and transcriptionally silent heterochromatin (or 'closed' chromatin) (Oberdoerffer & Sinclair, 2007; Olins & Olins, 2003). The latter is further categorized into constitutive heterochromatin, which consists of repetitive DNA sequences and composes genetic elements localizing to the nuclear periphery, like centromeres and telomeres, and facultative heterochromatin, which is found throughout the nucleus and able to switch to a transcriptionally active state by decondensation (Fritz et al., 2019). While constitutive heterochromatin-induced silencing is thought to be unspecific and more important in maintaining genome stability, silencing by facultative heterochromatin is specifically regulated in regard to the developmental stage of the cell or external triggers. Several interconnected epigenetic mechanisms – meaning that they can influence the phenotype

of a cell without altering the DNA sequence – have evolved that can dynamically affect chromatin structure, such as DNA methylation, non-coding RNAs, histone post-translational modifications, chromatin remodeling and the incorporation of histone variants. These mechanisms will be described in more detail in the following chapters.

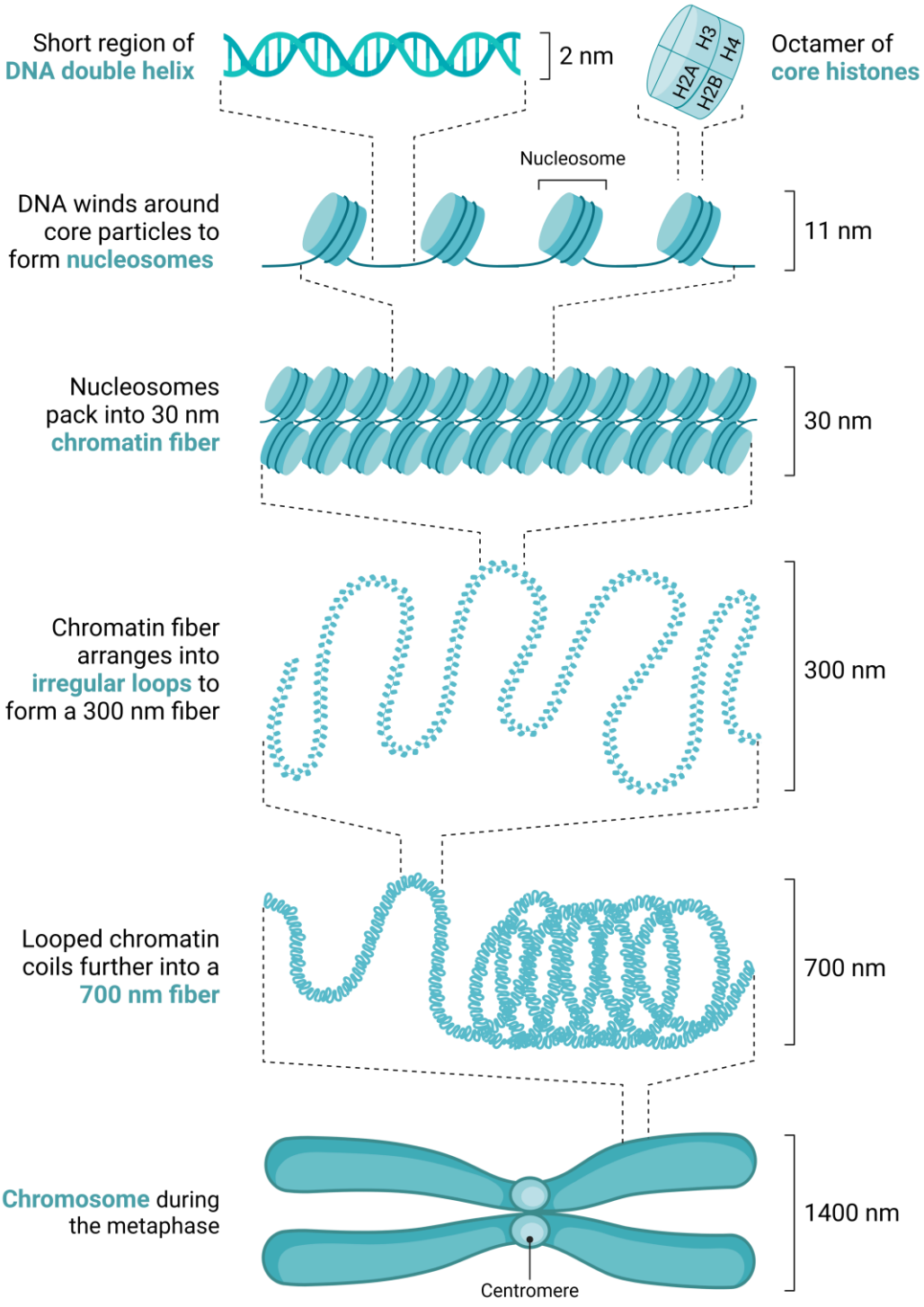

Figure 1.1: DNA of a cell is compacted in the form of a chromosome. *DNA is wrapped around octameric complexes of core histones, making up the nucleosomes (Jansen & Verstrepen, 2011). Nucleosomes further pack into chromatin fibers and, in the end, the chromosome. Created in BioRender.com.*

1.1.1 DNA methylation at promoters leads to transcriptional repression

DNA methylation describes the establishment of 5-methylcytosine (5mC) through the transfer of a methyl (CH_3) group from *S*-adenosyl methionine (SAM) to the fifth position of cytosine resulting in changes in chromatin density and accessibility of DNA (Hotchkiss, 1948; Lister et al., 2009; Xiao et al., 2019). DNA methyltransferases (DNMT) mediate this transfer, and several have been identified in mammalian cells, including DNMT1, DNMT3A and DNMT3B (Yanagisawa et al., 2002). While DNMT3A and DNMT3B function as *de novo* methyltransferases without a substrate DNA preference, DNMT1 acts as a maintenance methyltransferase during replication, preferring hemimethylated DNA (Moore et al., 2013). DNA methylation typically occurs in the context of cytosine-phosphate-guanine (CpG) dinucleotides (Bird, 1986). Most CpG dinucleotides in humans are methylated, with the exception of those clustered in CpG islands in the promoter region of genes. Here, DNA methylation is generally connected to transcriptional repression (Figure 1.1.1). Methylated DNA prevents the interaction of transcription factors (TFs) by blocking their binding site and in contrast recruits methyl-CpG-binding domain containing proteins like MeCP2 and MBD1/2/3, which in turn recruit repressive complexes containing histone deacetylases (HDACs) (Ballestar & Wolffe, 2001; Becker et al., 1987). Since DNA methylation plays a pivotal role in embryonic development, genome stability, genomic imprinting and the regulation of transcription, aberrations in the DNA methylation machinery can lead to a variety of diseases like immunodeficiency, centromeric instability, facial anomalies syndrome or cancer (Robertson, 2005).

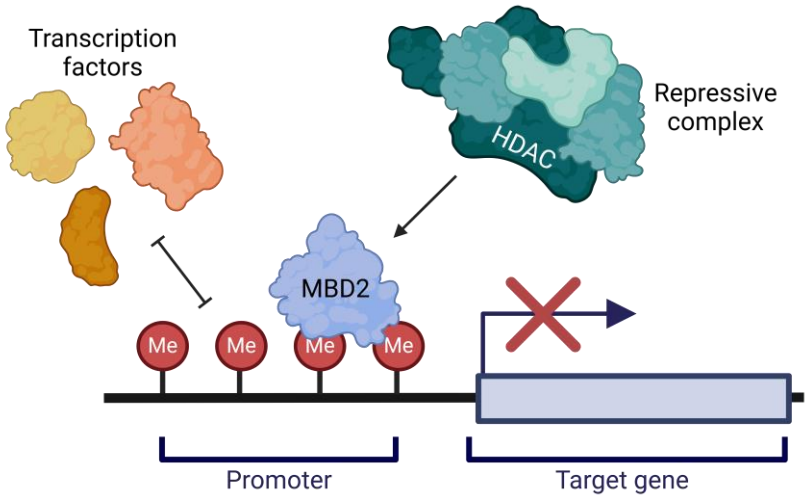

Figure 1.1.1: DNA methylation at a gene promoter represses transcription. *Methylated CpG dinucleotides prevent the interaction of TFs and lead to the recruitment of repressive complexes by methyl-CpG-binding domain containing proteins, like MBD2 (Koschmann et al., 2017). Created in BioRender.com.*

1.1.2 Non-coding RNAs can influence chromatin in various ways

Non-coding RNAs (ncRNAs) are defined as RNA molecules not encoding for proteins (Ignarski et al., 2019). However, they play a vital role in regulating gene expression and maintaining cellular functions and constitute a substantial proportion of the human transcriptome with over 90 % of all transcripts being ncRNAs. Long non-coding RNAs (lncRNAs), which are ncRNAs over 200 nucleotides long, are particularly influential in chromatin-related processes (Statello et al., 2021). This is achieved through recruiting chromatin-modifying complexes, altering higher-order chromatin structure or regulating gene expression at specific genomic loci (Figure 1.1.2).

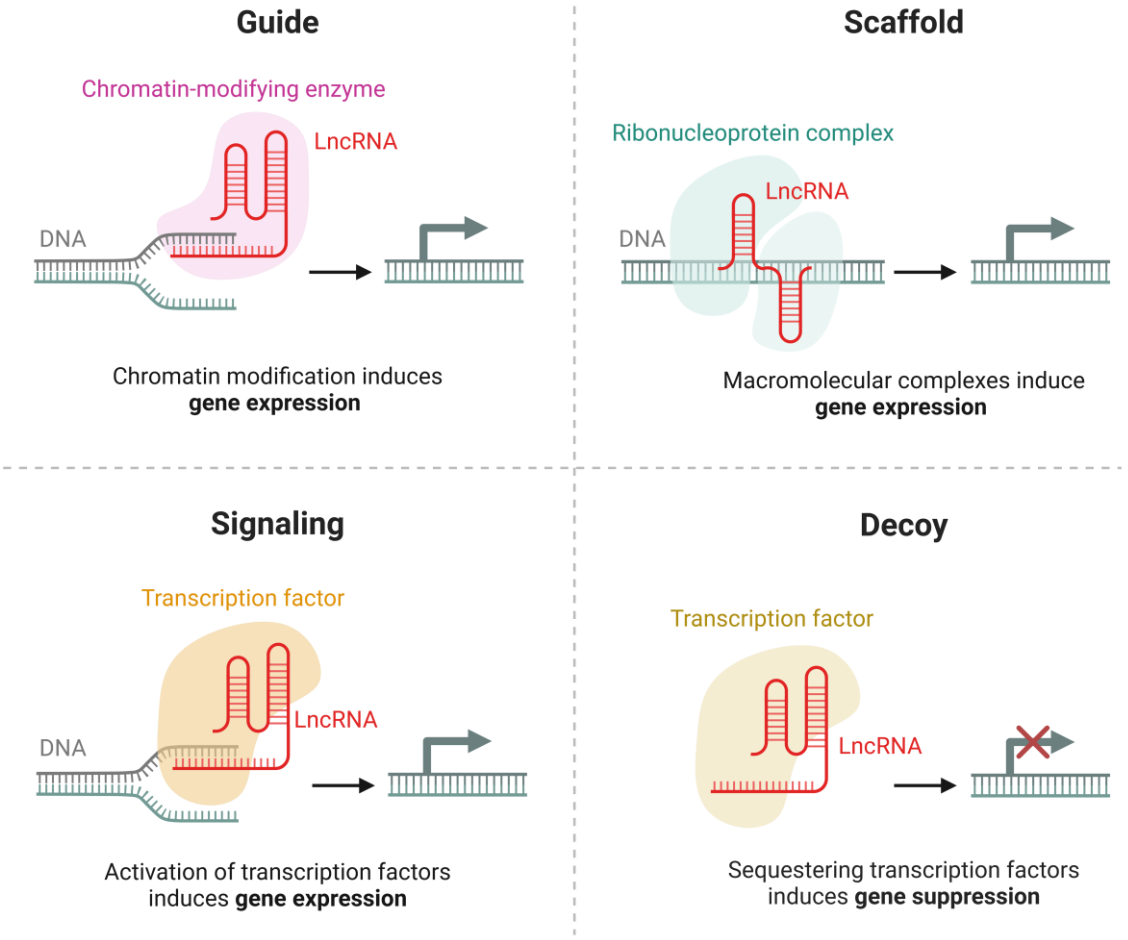

Figure 1.1.2: lncRNAs regulate gene expression through different processes. *lncRNAs can recruit chromatin-modifying or other complexes and activate or sequester TFs to induce gene expression or suppression (Gao et al., 2020). Created in BioRender.com.*

The lncRNA HOX transcript antisense RNA (HOTAIR), for instance, represses transcription of the HOXD locus by acting as a scaffold for the chromatin-modifying polycomb repressive complex 2 (PRC2) (Rinn et al., 2007). DNMT1-associated colon

cancer repressed lncRNA 1 (DACOR1), on the other hand, can interact with the DNA methyltransferase DNMT1 to regulate DNA methylation patterns (Merry et al., 2015). Nevertheless, other classes of ncRNAs can influence chromatin structure and function, too. MicroRNAs (miRNAs) can regulate TFs involved in epithelial to mesenchymal transition (EMT), which can indirectly affect chromatin configuration, and other small ncRNAs can participate in the transgenerational transmission of epigenetic information, affecting phenotypes across generations (Hussen et al., 2021; Larriba & del Mazo, 2016). Overall, the roles of ncRNAs in chromatin dynamics underscore their potential as therapeutic targets in diseases such as cancer.

1.1.3 Histone proteins are extensively post-translationally modified

The post-translational modification (PTM) of histone proteins is a crucial biochemical process that plays a fundamental role in the regulation of chromatin structure and function (Connacher et al., 2022). Histone PTMs are predominantly associated with the N-terminal tails of histones, which protrude from the nucleosome core and are accessible for enzymes that facilitate the deposition of particular modifications (Demetriadou et al., 2020; Etier et al., 2022). These enzymes are called ‘writers’, while proteins involved in the removal of modifications are called ‘erasers’ (Figure 1.1.3) (Bannister & Kouzarides, 2011; Kouzarides, 2007). Histone PTMs can either directly alter chromatin structure by changing the physicochemical environment around the histones or recruit proteins, called ‘readers’, that recognize and interact with specific modifications and initiate downstream biological effects (Li & Li, 2021).

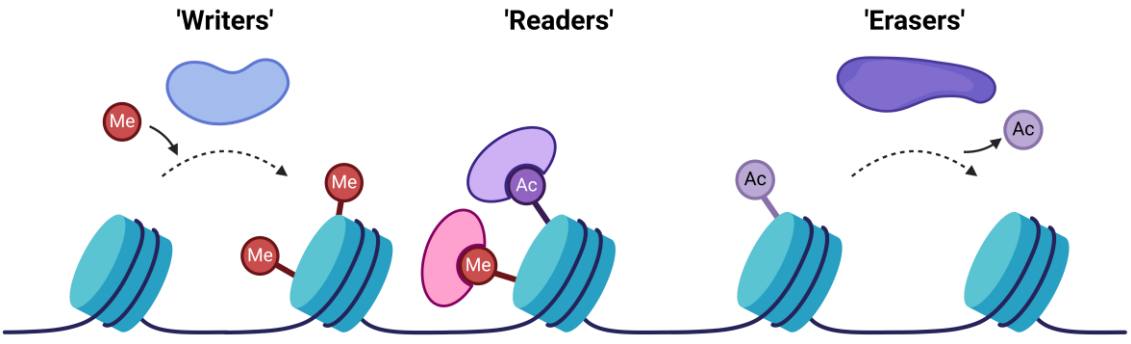

Figure 1.1.3: The ‘histone code’ is written, read and erased. *Proteins called ‘writers’ deposit histone PTMs, while ‘readers’ recognize and interact with them and ‘erasers’ remove them (Bannister & Kouzarides, 2011; Fardi et al., 2018). Created in BioRender.com.*

One of the most important findings in the field was the revelation that the combination of different histone modifications creates distinct patterns that affect chromatin dynamics and gene activity, leading to the 'histone code' hypothesis (Jenuwein & Allis, 2001; Strahl & Allis, 2000). This combinatorial aspect greatly extends the informational capacity of the genetic code itself. Several well-studied histone PTMs have been identified, like acetylation, methylation, phosphorylation, ubiquitination and sumoylation, that can fulfill both similar and distinct functions. Acetylation, for instance, is associated with gene activation by reducing the positive charge of histones, thereby decreasing their affinity for DNA and making chromatin more accessible (Romhanyi et al., 2023). Methylation, on the other hand, can either activate or repress gene expression, depending on the specific site and number of methyl groups added (Yang et al., 2021). While monomethylation of the lysine at position four in histone H3 (H3K4me1) is associated with transcriptional activation (Beisel et al., 2002), trimethylation of the lysine at position nine in histone H3 (H3K9me3) is associated with transcriptional repression (Johnson et al., 2002). Phosphorylation is often involved in chromosome condensation during cell division, but also plays roles in DNA repair processes and transcriptional regulation (Komar & Juszczynski, 2020; Sawicka & Seiser, 2012), and ubiquitination is also involved in DNA damage response and transcriptional regulation (Yadav et al., 2022). Sumoylation is typically associated with transcriptional repression and can influence chromatin structure and gene expression by recruiting chromatin modifiers (Wang et al., 2013). In addition, there is a number of more recently identified histone PTMs, such as crotonylation, benzoylation, lactylation, malonylation, succinylation and glutarylation (Jing et al., 2022). A short (not conclusive) overview of some important histone PTMs and their functional association can be found in Table 1.1.3.

Table 1.1.3: Overview of selected histone PTMs and their functional association.

Modification	Functional association	Reference
H3K4me1	transcriptional activation, enhancer priming, poised enhancers, promoters	(Beisel et al., 2002; Nakamura et al., 2002; Sedkov et al., 2003)
H3K4me3	transcriptional activation, active promoters	(Wang et al., 2001)
H3K9me1	transcriptional repression, heterochromatin formation, enhancers	(Tachibana et al., 2001)
H3K9me3	transcriptional repression, heterochromatin formation, DNA methylation	(Johnson et al., 2002; Schultz et al., 2002; Tamaru & Selker, 2001)
H3S10ph	mitosis, meiosis	(Hendzel et al., 1997; Hsu et al., 2000)
H3K27me3	transcriptional repression, inactive promoters, X inactivation	(Cao et al., 2002; Tachibana et al., 2001)
H3K27ac	transcriptional activation, active enhancers, promoters	(Tie et al., 2009; Zhang et al., 2013)
H3K36me3	transcriptional activation, RNA splicing, gene bodies	(Krogan et al., 2003)
H4K16ac	transcriptional activation, chromatin decondensation, gene bodies, enhancers, promoters	(Kimura & Horikoshi, 1998; Kuo et al., 1996; Suka et al., 2001)

1.1.4 Chromatin remodeling is catalyzed by ATP-dependent complexes

Chromatin remodeling complexes (CRCs) are essential molecular machines that regulate the accessibility of chromatin, thereby influencing gene expression, DNA replication, repair and recombination (Clapier et al., 2017). CRCs work by altering histone-DNA interactions through the use of ATPase subunits (Chen et al., 2013). These subunits are responsible for the catalytic activity that drives the remodeling process. They all encompass a translocase domain for DNA translocation and utilize energy derived from ATP hydrolysis to facilitate the repositioning, ejection or restructuring of nucleosomes. Non-catalytic subunits also play significant roles by enhancing the efficiency of the catalytic subunits or by targeting the complexes to specific genomic locations. There are over 20 known CRCs, which are conserved from yeast to humans and can be categorized into four major families based on their ATPase subunits (Figure 1.1.4) (Magana-Acosta & Valadez-Graham, 2020). Members of the switch/sucrose non-fermentable (SWI/SNF) family, for instance, contain, in addition to their translocase domain, an N-terminal helicase/SANT-associated (HSA) domain, that binds actin-related proteins, followed by

a post-HSA domain and a C-terminal bromodomain recognizing acetylated lysine residues (Mohrmann & Verrijzer, 2005; Schubert et al., 2013). SWI/SNF CRCs typically facilitate sliding and ejection of nucleosomes. Similar to the SWI/SNF family, inositol requiring 80 (INO80) ATPases comprise N-terminal HSA and post-HSA domains but lack the C-terminal bromodomain (Bao & Shen, 2011; Morrison & Shen, 2009). INO80 family CRCs have distinct functions. The mammalian p400 and Snf2-related CREBBP activator protein (SRCAP) complexes can catalyze the replacement of H2A-H2B dimers with histone variant H2A.Z-containing dimers, whereas the INO80 complex evicts H2A.Z-H2B dimers (Mizuguchi et al., 2004; Papamichos-Chronakis et al., 2011). ATPases of the imitation switch (ISWI) family incorporate a C-terminal HAND-SANT-SLIDE (HSS) domain, in addition to their translocase domain, that can bind the H3 tail and linker DNA (Corona & Tamkun, 2004; Dang & Bartholomew, 2007; Grune et al., 2003). Most ISWI CRCs are involved in nucleosome assembly and spacing to negatively regulate transcription, while some, like the nucleosome remodeling factor (NURF) complex, have subunits promoting transcription (Hochheimer et al., 2002; Xiao et al., 2001). Finally, chromodomain helicase DNA-binding (CHD) family ATPases have a C-terminus similar to the ISWI family but are missing the HAND domain in the DNA-binding domain (DBD) (Ryan et al., 2011). The N-terminus uniquely consists of two tandem chromodomains for binding of methylated histones (Kunert & Brehm, 2009; Tran et al., 2000). In general, CHD CRCs can catalyze all remodeling functions. One major CRC in the CHD family is the nucleosome remodeling and deacetylase (NuRD) complex, which will be described in more detail in the following chapter.

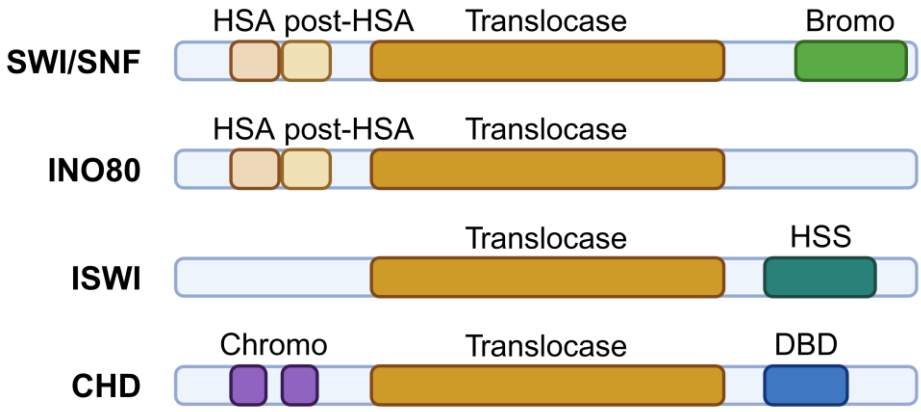

Figure 1.1.4: CRCs can be categorized into four families based on the ATPase subunit. *All ATPase subunits contain a DNA translocase domain. SWI/SNF and INO80 members encompass HSA and post-HSA domains, SWI/SNF members an additional bromodomain. ISWI members incorporate an HSS domain. CHD members include a DBD and tandem chromodomains. Adapted from (Clapier et al., 2017). Created in BioRender.com.*

1.1.4.1 The NuRD complex facilitates chromatin remodeling and histone deacetylation

The NuRD complex is an important chromatin remodeling complex that uniquely integrates ATP-dependent nucleosome remodeling with histone deacetylation (Xue et al., 1998). This dual functionality makes the NuRD complex a critical regulator of gene expression and chromatin architecture in eukaryotic cells. The NuRD complex is composed of several subunits, each contributing to its diverse functions (Figure 1.1.4.1). The chromodomain helicase DNA-binding (CHD) family of ATPases, particularly CHD3, CHD4 and CHD5, are integral to the NuRD complex's function (Shi et al., 2023). These ATPases leverage the energy from ATP hydrolysis to facilitate nucleosome sliding and repositioning. This activity is crucial for altering chromatin structure to either expose or occlude specific DNA regions, thereby regulating access for transcriptional machinery. The histone deacetylase (HDAC) activity within the NuRD complex is primarily mediated by HDAC1 and HDAC2 (Zhang et al., 2021). These enzymes remove acetyl groups from lysine residues on histone tails, resulting in chromatin condensation and transcriptional repression. This deacetylation process plays a pivotal role in modulating gene expression by influencing chromatin accessibility. Other essential components include metastasis-associated 1/2/3 (MTA1/2/3), retinoblastoma-binding proteins 4/7 (RBBP4/7), GATA zinc finger domain containing 2 A/B (GATAD2A/B), methyl-CpG-binding domain proteins 2/3 (MBD2/3) and cyclin-dependent kinase 2-associated protein 1/2 (CDK2AP1/2) (Reddy et al., 2012; Torchy et al., 2015). These proteins contribute to the structural integrity and functional specificity of the complex. They facilitate interactions with other proteins and complexes and help target the NuRD complex to specific genomic loci through DNA-binding domains (Banks et al., 2018). For instance, the MBD2 and MBD3 subunits can recognize and bind to methylated DNA, linking the complex to DNA methylation-dependent gene silencing (Hashimoto et al., 2012). The GATAD2A/B subunit has been demonstrated to interact directly with coactivator-associated arginine methyltransferase 1 (CARM1), thereby expanding the activities of NuRD to include protein arginine methylation (X. Chen et al., 2024). MTA1 can interact with the histone variant H2A.Z-associated proteins PWWP domain containing 2A (PWWP2A), which regulates mitosis and neural crest differentiation, and high mobility group 20 A (HMG20A), which controls early head and heart developmental transcription programs (Herchenrother, Gossen, et al., 2023; Link et al., 2018; Punzeler et al., 2017). Finally, several TFs, such as friend of GATA protein 1 (FOG-1), Sal-like protein 1/4

(SALL1/4) and B-cell CLL/lymphoma 11A (BCL11A), have been shown to bind RBBP4 via a conserved N-terminal motif called NuRD interaction motif (NIM) or FOG-1-like motif (Hong et al., 2005; Lauberth & Rauchman, 2006; Miller et al., 2016; Sankaran et al., 2008).

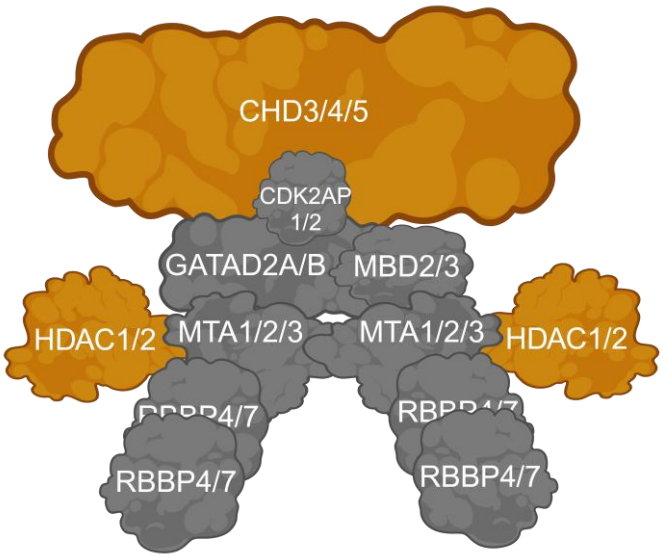

Figure 1.1.4.1: The NuRD complex has two distinct enzymatic functions. *The NuRD complex consists of several subunits that facilitate chromatin remodeling, histone deacetylation, DNA-binding and interactions with other proteins and complexes. The enzymatic subunits are indicated in yellow. Adapted from (Reid et al., 2023). Created in BioRender.com.*

Since the NuRD complex has the ability to incorporate and exchange different subunits, called 'paralog switching', it is involved in a wide array of cellular processes (Reid et al., 2023). By orchestrating chromatin remodeling and histone deacetylation, the NuRD complex can either repress or activate gene expression (Hoffmann & Spengler, 2019). This regulation is crucial during development and differentiation, where precise control over gene expression patterns is necessary for proper cell fate determination and tissue development. The NuRD complex is, for example, essential for spermatogonia survival and normal meiotic progression in mouse testis development (de Castro et al., 2022). In cardiac tissue it represses skeletal muscle-specific genes in cardiomyocytes in conjunction with the TF ZNF219 (El Abdellaoui-Soussi et al., 2022). This repression is essential for maintaining cardiac cell identity and proper heart function. Further, the NuRD complex is engaged in the DNA damage response by facilitating chromatin remodeling at sites of DNA breaks (Li & Kumar, 2010). This activity helps to recruit repair machinery to damaged sites, ensuring genomic stability and preventing mutations.

During DNA replication, particularly in the S phase, the NuRD complex maintains chromatin structure, ensuring proper progression through the cell cycle (Basta & Rauchman, 2015). This function is critical for preventing replication stress and maintaining genomic integrity, which are essential for normal cellular proliferation. In the nervous system, the NuRD complex is essential for brain development and maintaining neuronal circuits (Boulasiki et al., 2023). It regulates genes involved in neuronal differentiation, synaptic plasticity and neurogenesis, which are indispensable for cognitive functions such as learning and memory. This involvement in a multitude of important biological processes makes the NuRD complex a key player in various diseases and cancer types, like breast cancer, leukemia, colorectal cancer and prostate cancer (Andrade de Oliveira et al., 2023; Lai & Wade, 2011). In critical illness myopathy (CIM), muscle stem cells (MuSC) with altered NuRD complex function exhibit impaired DNA repair capabilities (Schneider et al., 2023). In breast cancer, the MTA1 subunit of the NuRD complex plays a role in genotoxic adaptation and chemoresistance (Xie et al., 2021). On the other hand, this renders the NuRD complex also a promising therapeutic target. In triple negative breast cancer (TNBC), for instance, it associates with SALL4 in cancer cells, contributing to the silencing of tumor-suppressor genes like phosphatase and tensin homolog (*PTEN*) (Zhang et al., 2024). Here, a novel small-molecule nucleotide analog, R9, has been recently discovered as a first-in-class NuRD inhibitor, showing promise in TNBC treatment. In conclusion, the NuRD complex is a versatile chromatin remodeling complex with significant implications for cellular function and disease. Exploring the broader network of proteins, that interact with and regulate the NuRD complex, and developing new strategies to selectively modulate NuRD activity will be of high interest for future research.

1.1.5 Histone variants fulfill specialized functions through diverse mechanisms

As mentioned previously, the four histone proteins H2A, H2B, H3 and H4 constitute the octameric complex within the nucleosome core particle. These core histones are encoded by multiple intronless genes, which are predominantly distributed in large clusters throughout the genome (Albig & Doenecke, 1997; Albig et al., 1997). They are expressed in a replication-dependent manner during the S phase of the cell cycle, to ensure that newly synthesized DNA is properly packaged, and their mRNAs usually include a

3′ stem-loop structure (Cakmakci et al., 2008). In addition to these 'canonical' histones an increasing number of specialized histone variants have been identified (Buschbeck & Hake, 2017). These variants differ in genomic arrangement, expression timing, transcript processing and amino acid composition. Their sometimes intron-containing genes appear as single-copy genes (e.g. H2A.X) or as a gene duplication (e.g. H2A.Z), they are expressed throughout the cell cycle and their mRNAs typically contain a 3′-poly-A tail and can be alternatively spliced, when containing introns (Marzluff et al., 2008). The differences in amino acid composition range from only a few amino acids (e.g. H2A.X) to large regions (e.g. H2A.Z) or even additional domains (e.g. macroH2A) (Figure 1.1.5). Histone variants fulfill specialized functions through either directly influencing the nucleosome structure and stability, by being uniquely post-translationally modified or by recruiting variant specific interactors. One well-studied but still enigmatic variant is the functionally distinct H2A variant H2A.Z, which will be discussed in more detail in the next chapter.

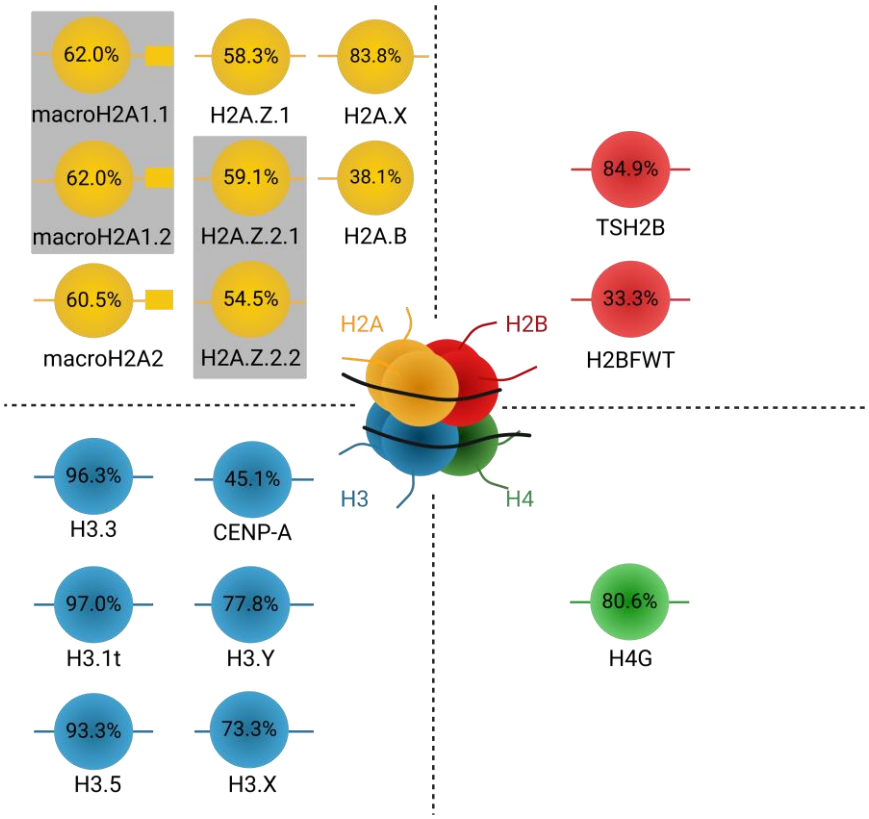

Figure 1.1.5: A variety of histone variants have been identified in humans. *Variants show differences in genomic arrangement, expression timing, transcript processing and amino acid composition, which range from a few amino acids to large regions or additional domains. Percentages indicate sequence identity with the 'canonical' counterparts (for H3 variants, sequence identity was calculated with H3.1). Grey rectangles indicate alternative splice isoforms. Adapted from (Buschbeck & Hake, 2017) with help from Lena Paasche (Institute for Genetics, Justus-Liebig University Giessen, Germany). Information on H4G from (Long et al., 2019). Created with BioRender.com.*

1.1.5.1 The histone variant H2A.Z is functionally diverse

The histone variant H2A.Z was first identified in 1980 in mouse L1210 cells, making it one of the longest-known H2A variants (West & Bonner, 1980). Remarkably, H2A.Z has a single evolutionary origin (Eirin-Lopez et al., 2008; Thatcher & Gorovsky, 1994). It was later found to be essential in various organisms, such as *Drosophila* (van Daal & Elgin, 1992), *Tetrahymena* (Liu et al., 1996) and mammals (Faast et al., 2001). This variant is present in all higher eukaryotes and is highly conserved, showing approximately 90 % sequence identity (Iouzalen et al., 1996). In contrast, H2A.Z shares only about 60 % of its amino acid sequence with 'canonical' H2A, suggesting a distinct function (Figure 1.1.5.1) (Suto et al., 2000).

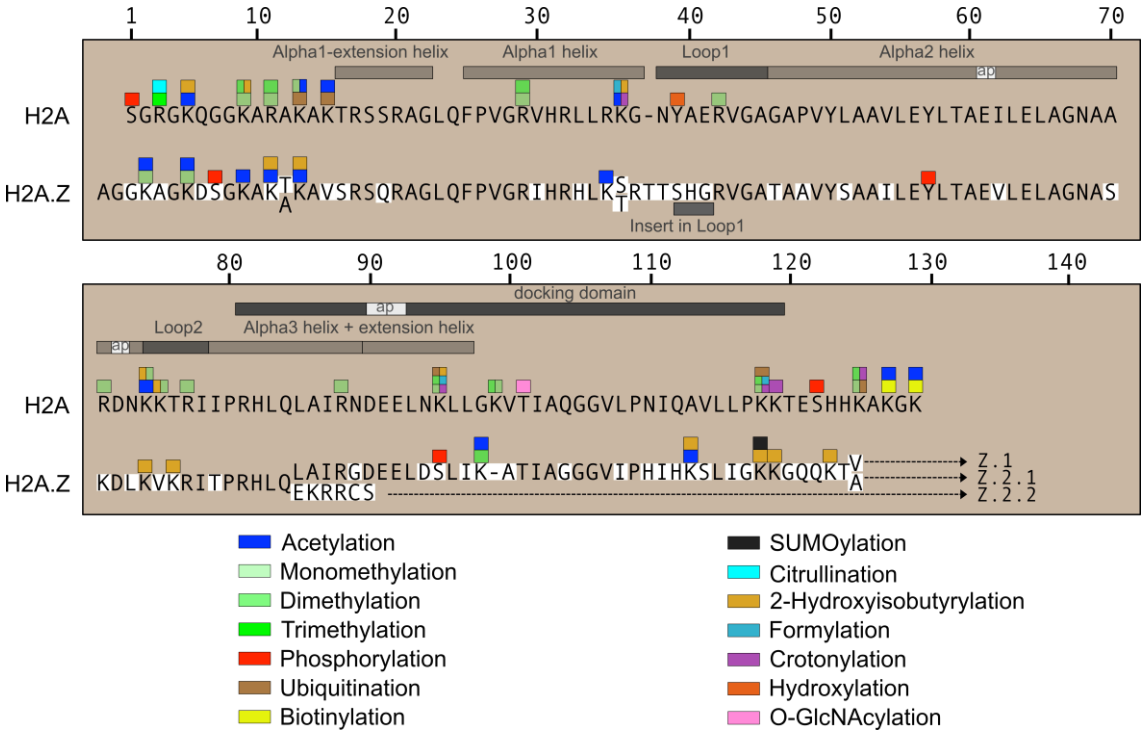

Figure 1.1.5.1: H2A.Z shares about 60 % of its sequence with H2A. *H2A.Z.1 and H2A.Z.2.1 differ in only three amino acids. H2A.Z.2.2 is an alternative splice isoform of H2A.Z.2.1. PTMs and structural motifs are indicated. ap: acidic patch. Adapted from (Herchenrother, Wunderlich, et al., 2023). Created in BioRender.com.*

A significant development in H2A.Z research occurred in 2005 when Coon and colleagues identified two isoforms via mass spectrometry (MS) that differ by only three amino acids (Coon et al., 2005). These isoforms were designated as H2A.Z.1 and H2A.Z.2 (Talbert et al., 2012). They are encoded by two separate genes, *H2AFZ* and *H2AFV*, which are highly conserved across chordates (Eirin-Lopez et al., 2009). In 2012, the discovery of an alternatively spliced isoform of H2A.Z.2, which was named

H2A.Z.2.1 from there on, added a new layer of complexity. This primate-specific form, known as H2A.Z.2.2, differs at the C-terminus and is predominantly expressed in human brain tissues (Bonisch et al., 2012; Wratting et al., 2012). Overall, H2A.Z is implicated in a wide variety of biological processes (Zlatanova & Thakar, 2008). However, some proposed functions appear to contradict one another, leaving the roles of H2A.Z somewhat controversial. Further research into the distinct isoforms may help resolve these discrepancies. Despite differing by only three amino acids, H2A.Z.1 and H2A.Z.2 exhibit specialized functions (Giaimo et al., 2019). It is plausible that these isoforms, along with chromatin occupancy, PTMs and specific interacting proteins, contribute to the functional diversity of this intriguing histone variant.

1.1.5.1.1 Highly conserved remodeling complexes facilitate the deposition and eviction of H2A.Z

The process by which histone variants such as H2A.Z are incorporated into nucleosomes has puzzled scientists for a significant period. A breakthrough came in 2004 when Mizuguchi and colleagues discovered the Swi2/Snf2-related 1 (SWR1) complex in *S. cerevisiae*, which facilitates the deposition of H2A.Z in an ATP-dependent manner (Mizuguchi et al., 2004). This complex partially unwraps DNA from the histone core, while its SWR1 subunit, a member of the Snf2 ATPase family, acts as a histone chaperone to deliver the H2A.Z-H2B dimer to the DNA-$(H3\text{-}H4)_2$ tetrasome (Hong et al., 2014; Willhoft et al., 2018). The incorporation of H2A.Z by SWR1 occurs in a sequential manner, first forming heterotypic nucleosomes with one H2A.Z, then homotypic nucleosomes with two H2A.Z variants (Luk et al., 2010). SWR1 recruitment requires acetylation of the N-terminal tails of either H2A or H4, which is recognized by the bromodomain of the BDF1 subunit within SWR1 (Altaf et al., 2010). This acetylation is carried out by the NuA4 complex, a multi-subunit acetyltransferase that shares six subunits with SWR1 and is also responsible for acetylating H2A.Z through its ESA1 subunit (Auger et al., 2008; Keogh et al., 2006; Kobor et al., 2004). Both SWR1 and NuA4 complexes are evolutionarily conserved. In mammals and *Drosophila*, there exists a single complex that combines homologous subunits from SWR1 and NuA4, effectively merging chromatin remodeling and acetyltransferase functions (Cai et al., 2005; Cai et al., 2003; Choi et al., 2009; Doyon et al., 2004; Scacchetti et al., 2020). This hybrid complex is known as p400/Tip60 in mammals and Domino in *Drosophila* (Gevry et al.,

2007; Kusch et al., 2004). In addition to p400/Tip60, mammals also possess another complex called SRCAP, which functions as a SWR1 homolog but lacks acetyltransferase activity (Figure 1.1.5.1.1) (Robert et al., 2006; Ruhl et al., 2006). All these complexes have been shown to facilitate the incorporation of H2A.Z into nucleosomes.

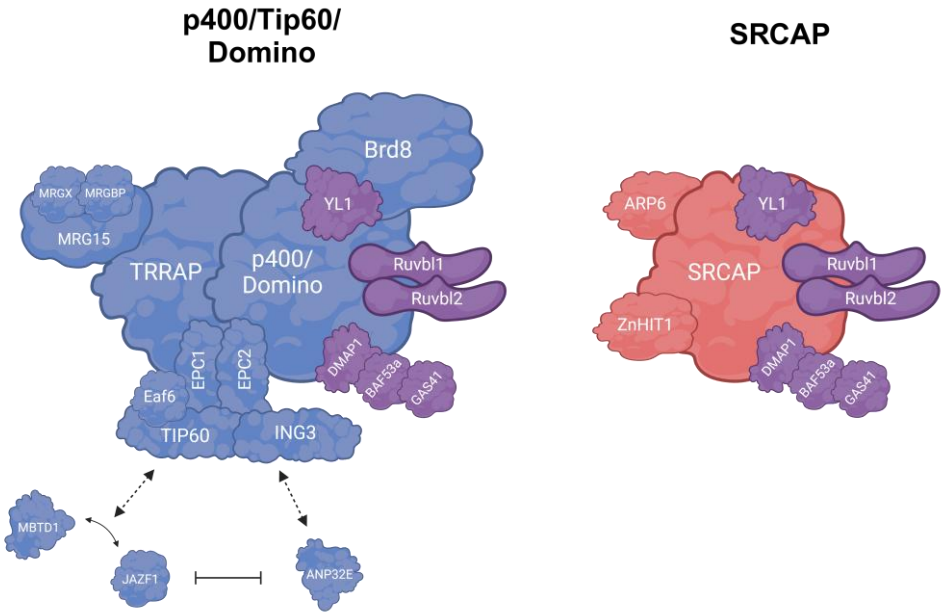

Figure 1.1.5.1.1: p400/Tip60/Domino and SRCAP share several subunits. *Both complexes can deposit H2A.Z, but SRCAP lacks the acyltransferase function. JAZF1 is part of a p400/Tip60 subcomplex containing MBTD1 but excluding ANP32E. Adapted from (Billon & Cote, 2013). Created in BioRender.com.*

On the flip side, two proteins have been identified as key players in removing H2A.Z from chromatin. The first is acidic nuclear phosphoprotein 32 family member E (ANP32E), which is part of the p400/Tip60 complex (Mao et al., 2014; Obri et al., 2014). ANP32E specifically interacts with the extended αC-helix of H2A.Z through a newly identified motif called the H2A.Z interacting domain (ZID), enabling it to evict H2A.Z from nucleosomes in dividing human cells. Recent findings by Stefanelli and colleagues showed that depletion of ANP32E leads to an accumulation of H2A.Z in post-mitotic neuronal chromatin but does not prevent its removal in response to neuronal activity (Stefanelli et al., 2021). This suggests that ANP32E may primarily regulate basal turnover of H2A.Z, while other mechanisms likely govern activity-induced removal. The second protein involved in evicting H2A.Z is INO80, which belongs to the same ATP-dependent chromatin remodeler family as Swr1/p400/SRCAP/Domino (Alatwi & Downs, 2015; Brahma et al., 2017). INO80 facilitates the selective removal of H2A.Z-H2B dimers from

nucleosomes and is essential for removing H2A.Z from damaged chromatin. Interestingly, a recent study by Yu and colleagues linked INO80 to the deposition of H2A.Z at bivalent promoters marked by both H3K4 and K27 trimethylation in primed pluripotent stem cells (Yu et al., 2021), suggesting that INO80 may have more complex roles in both deposition and eviction than previously understood. In addition to ANP32E and INO80, active transcription has also been implicated in opposing random incorporation of H2A.Z. When transcription is globally inhibited, there is an accumulation of H2A.Z at transcription start sites (TSSs) and within gene bodies (Hardy et al., 2009; Lashgari et al., 2017). In summary, both deposition and eviction of H2A.Z are orchestrated by highly conserved remodeling complexes, histone chaperones and transcriptional activity, all working together in a dynamic interplay that still requires further investigation for full comprehension.

1.1.5.1.2 Acetylation of H2A.Z is linked to transcriptional activity

Like their 'canonical' equivalents, histone variants can undergo diverse post-translational modifications. In the case of H2A.Z, several modifications have been identified, including acetylation (Vavra et al., 1982), methylation (Binda et al., 2013), phosphorylation (Hornbeck et al., 2015), ubiquitination (Mertins et al., 2013) and SUMOylation (Lumpkin et al., 2017). Among these, acetylation stands out as the most prominent. The acetylated form of H2A.Z, known as H2A.Zac, was first identified in *Tetrahymena* and has since been associated with active transcription across various organisms (Bellucci et al., 2013; Bruce et al., 2005; Valdes-Mora et al., 2012; Vavra et al., 1982). As previously noted, in *S. cerevisiae*, the NuA4 complex subunit Esa1 is responsible for H2A.Z acetylation, while its homologs Tip60 in mammals and dTip60 in *Drosophila* have been shown to perform the same function (Giaimo et al., 2018). More recently, the nuclear/nucleolar protein juxtaposed with another zinc finger protein 1 (JAZF1) was identified as part of a p400/Tip60 subcomplex that likely recruits the acetyltransferase to genomic regulatory regions (Procida et al., 2021). However, it has been suggested that other enzymes may also play a role in H2A.Z acetylation. Research by Colino-Sanguino and colleagues revealed that p300 can acetylate H2A.Z at multiple lysine residues, a process enhanced by the interaction between p300's bromodomain and H4 acetylation (Colino-Sanguino et al., 2019). Their results also support Tip60's involvement, as they observed reduced levels of H2A.Zac following genetic inhibition of

Tip60. Ultimately, their study demonstrated that both Tip60 and p300 contribute to H2A.Z acetylation and highlighted a writer/reader interaction between H2A.Z and H4 acetylation via p300. Despite these findings, they could not determine whether H2A.Z acetylation occurs through independent pathways or involves a sequential cascade initiated by H4ac. On the other hand, the process governing H2A.Z deacetylation remains largely unknown. It was shown that inhibiting histone deacetylases with Trichostatin-A (TSA) increased H2A.Z acetylation without affecting overall H2A.Z levels (Narkaj et al., 2018). Additionally, it was found that depletion of PWWP2A, a direct interactor of H2A.Z, led to elevated levels of H2A.Z acetylation – likely due to impaired chromatin recruitment of an HDAC1/2-containing subcomplex of the NuRD complex (Link et al., 2018). One of the few known proteins capable of recognizing specific acetylated forms of H2A.Z is the bromodomain PHD finger transcription factor (BPTF) (Olson et al., 2020; Perell et al., 2017). BPTF is the largest subunit of the NURF complex, plays a role in transcriptional regulation and has been linked to high gene expression and poor prognosis in several cancers. In summary, the mechanisms underlying H2A.Z acetylation and deacetylation are not yet fully elucidated and identifying additional reader proteins for specific acetylation patterns on H2A.Z will be an interesting task for future research.

1.1.5.1.3 H2A.Z isoforms can offer insights into its functional diversity

H2A.Z plays a crucial role in almost all DNA-related processes (Colino-Sanguino et al., 2022). Further, it is critical for development, cellular differentiation and brain functions such as memory formation (Figure 1.1.5.1.4) (Ramzan, Baumbach, et al., 2020; Ramzan, Creighton, et al., 2020). Consequently, alterations or mutations in H2A.Z can have severe effects, linking this histone variant to a wide range of diseases. This has sparked increasing interest in understanding the specific mechanisms through which H2A.Z operates. In a recent study, Cole et al. demonstrated that active chromatin in cancer cell lines is characterized by H2A.Z nucleosomes resistant to MNase digestion either upstream or downstream of the TSS, while an H2A.Z nucleosome at the TSS remains accessible to MNase (Cole et al., 2021). Notably, the absence of H2A.Z led to an increase in accessible TF binding sites, indicating that H2A.Z's role in gene regulation is influenced by its positioning within the promoter. Additionally, Papin et al. found that histone variants specifically target CpG-rich promoters, with CpG island boundaries – rather than transcriptional activity – being the primary determinant of H2A.Z positioning

around these promoters (Papin et al., 2021). As a result, transcriptional activity in arrested mouse embryonic fibroblasts (MEFs) remained unaffected by H2A.Z depletion. Conversely, another study proposed a dual function for H2A.Z.1 at the +1 nucleosome of promoters, showing that this isoform slows RNA-Pol II pause release and also restricts pre-initiation complex re-loading (Mylonas et al., 2021). Moreover, the incorporation of H2A.Z into nucleosomes results in a less stable structure with more flexible DNA ends, which lowers the activation energy required for RNA-Pol II during transcription initiation but simultaneously allows H2A.Z-containing nucleosomes to form compacted and repressive chromatin (Lewis et al., 2021).

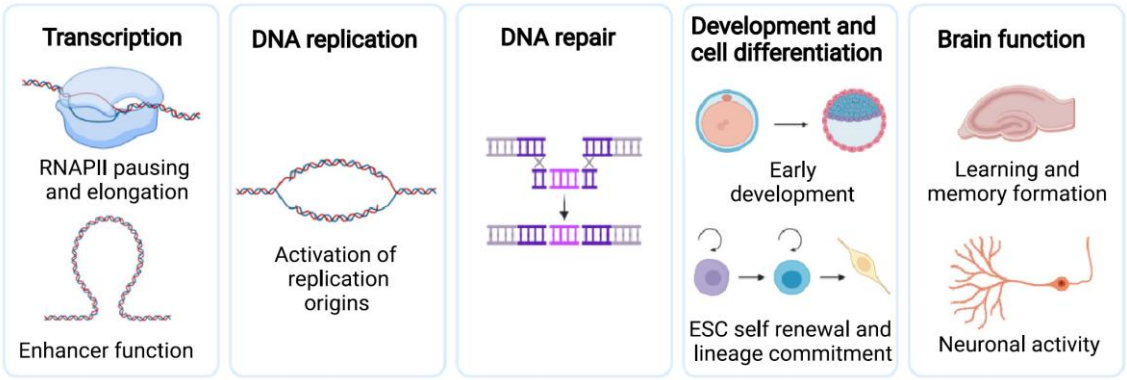

Figure 1.1.5.1.4: H2A.Z is implicated in a wide range of mechanisms. *H2A.Z is crucial for nearly all DNA-based processes, development, differentiation and brain functions. Adapted from (Colino-Sanguino et al., 2022).*

Given these occasionally contradictory roles attributed to H2A.Z, there is a growing focus on elucidating the distinct functions of its isoforms, as these may provide insights into the histone variant's functional diversity. For instance, a study led by Greenberg and colleagues investigated Floating-Harbor syndrome (FHS) (Greenberg et al., 2019). FHS is a developmental disorder caused by heterozygous truncating mutations in SRCAP, one of the chromatin remodelers responsible for incorporating H2A.Z. Greenberg et al. revealed that FHS mutations disrupt SRCAP's nuclear localization, leading to altered neural crest gene expression and defects in craniofacial cartilage development in *X. laevis*. Remarkably, they found that depleting H2A.Z.2.1 alone could replicate this phenotype and that only overexpressing this isoform could reverse it. They further pinpointed the reason for this selective rescue to one of the three single amino acid differences between H2A.Z.1 and H2A.Z.2.1, S38/T38. They hypothesized that substituting S38 with T38 modifies the conformation of the adjacent L1 loop, affecting nucleosome mobility and its

sensitivity to SRCAP (Bowerman & Wereszczynski, 2016; Horikoshi et al., 2013; Osakabe et al., 2018). Of note, Berta et al. recently demonstrated the involvement of H2A.Z in tumorigenesis of uterine leiomyomas (ULs), which also arise from SRCAP mutations that impair deposition (Berta et al., 2021). Greenberg and colleagues further identified distinct but overlapping genomic occupancy patterns for H2A.Z.1 and H2A.Z.2.1. Lamaa et al. later supported these findings by conducting an integrated analysis of how H2A.Z isoforms influence gene expression in non-transformed cells using endogenously-tagged proteins (Lamaa et al., 2020). Their work underscored the critical role of H2A.Z in gene regulation: after depleting either H2A.Z.1, H2A.Z.2.1 or both isoforms in WI38 and U2OS cells, approximately 25 % of expressed genes were deregulated. Interestingly, each isoform activated and repressed a similar number of genes, reaffirming the dual role of H2A.Z in gene regulation (Dunn et al., 2017; Subramanian et al., 2015). Moreover, they showed that while both isoforms regulate overlapping sets of genes, they also control distinct gene groups, confirming the earlier results from Greenberg et al. (Greenberg et al., 2019). Upon closer examination of shared gene sets, Lamaa et al. found that both isoforms often play similar roles and can compensate for each other at certain genes but act antagonistically at others, further emphasizing their separate functions (Lamaa et al., 2020). To investigate how these isoforms differentially affect gene regulation, Lamaa and colleagues identified isoform-specific interactors through MS experiments – PHD finger protein 14 (PHF14) for H2A.Z.1 and sirtuin 1 (SIRT1) for H2A.Z.2.1. Olson et al. took a similar approach by using protein-observed fluorine NMR, surface plasmon resonance and X-ray crystallography to analyze the acetylation patterns of both H2A.Z isoforms and their affinities for BPTF (Olson et al., 2020). They made two significant discoveries: first, the acetylation pattern K7acK13ac on H2A.Z.2.1 exhibited the strongest affinity for BPTF's bromodomain; second, the cat eye syndrome critical region protein 2 (CECR2) bromodomain showed high specificity for H2A.Z.1ac but barely interacted with H2A.Z.2.1ac. This suggests that each isoform may have distinct PTM patterns or that identical PTMs can interact differently depending on the isoform. These findings could have important implications since BPTF has been linked to various cancers and was shown to co-immunoprecipitate with H2A.Z-containing nucleosomes in bladder cancer (Kim et al., 2013). The distinct acetylation patterns of H2A.Z isoforms might allow them to function independently in cancer contexts due to their differing affinities for BPTF. In addition to BPTF, bromodomains from cancer-associated BET family proteins interact

with H2A.Z through the diacetylated K4acK7ac motif, with bromodomain containing 2 (BRD2) showing a preference for H2A.Z.1 over H2A.Z.2.1 (Draker et al., 2012; Patel et al., 2021). Tang and colleagues demonstrated that these isoforms play unique roles in cancer (Tang et al., 2020). They examined the expression levels of both H2A.Z isoforms in hepatocellular carcinoma tissues using RT-qPCR, ChIP-seq, RNA-seq experiments and meta-analysis techniques. Their findings related both isoforms to overexpression in hepatocellular carcinoma and poorer patient survival outcomes. However, genes associated with H2A.Z.1 were linked to RNA splicing/exporting functions, while those associated with H2A.Z.2 were linked to microtubule depolymerization and chromatin binding processes. Further research by Dong et al. showed that overexpression of H2A.Z.1 in hepatocellular carcinoma is regulated by P53 mutations and promotes cell proliferation while being associated with immune infiltrations (Dong et al., 2021). These findings suggest that immune checkpoint inhibitors could be a potential treatment option for patients overexpressing this isoform. Ávila-López et al.'s recent work demonstrated elevated expression levels of all H2A.Z isoforms in pancreatic ductal adenocarcinoma (PDAC) cell lines and patient samples (Avila-Lopez et al., 2021). Depleting H2A.Z induced senescence and sensitized cells to gemcitabine treatment while reducing tumor size *in vivo*; however, overexpression of either H2A.Z.1 or H2A.Z.2.1 could more effectively reverse these effects than overexpression of H2A.Z.2.2. Therefore, they proposed that targeting these isoforms could serve as a diagnostic or therapeutic strategy for PDAC. Vardabasso et al.'s research identified H2A.Z as a driver of malignant melanoma by regulating E2F target genes through reduced histone acetylation and BRD2 binding – ultimately affecting cell proliferation (Vardabasso et al., 2015). Interestingly, reducing levels of the histone variant sensitized melanoma cells to chemotherapy. Tang et al.'s findings suggested that both H2A.Z isoforms have oncogenic potential but play distinct roles in hepatocellular carcinoma without redundancy between them. The recent study by Sales-Gil and colleagues explored how these isoforms impact cell cycle regulation differently (Sales-Gil et al., 2021). They used siRNA-mediated knockdowns to selectively deplete either H2A.Z.1 or H2A.Z.2 in HeLa cells and found that depletion of H2A.Z.1 caused G1 arrest due to its role in MYC transcription regulation and p21/p27 suppression, ultimately leading to cellular senescence, while depletion of H2A.Z.2 affected centromere integrity and sister chromatid cohesion. In summary, research indicates that H2A.Z.1 and H2A.Z.2 may have overlapping yet distinct roles in various cellular processes and disease states. These unique functions can be influenced by factors

such as their genomic localization, modification patterns or even a single amino acid variation. However, efforts to unravel the specific roles of the H2A.Z isoforms are still in their early stages. The number of investigations remains limited, partly because isolating the isoforms individually has been challenging, for instance, due to the absence of isoform-specific antibodies. Despite this, advancements in techniques like gene editing now offer new opportunities to perform isoform-specific studies and have the potential to reveal more about the specialized roles of H2A.Z isoforms.

1.1.5.1.4 Several H2A.Z-specific interactors have been characterized

Another factor in H2A.Z's functional diversity is the recruitment of specific interaction partners. In the last years, there have been various studies to uncover the H2A.Z interactome (Figure 1.1.5.1.3) (Fujimoto et al., 2012; Kreienbaum et al., 2022; Punzeler et al., 2017; Zhang et al., 2017).

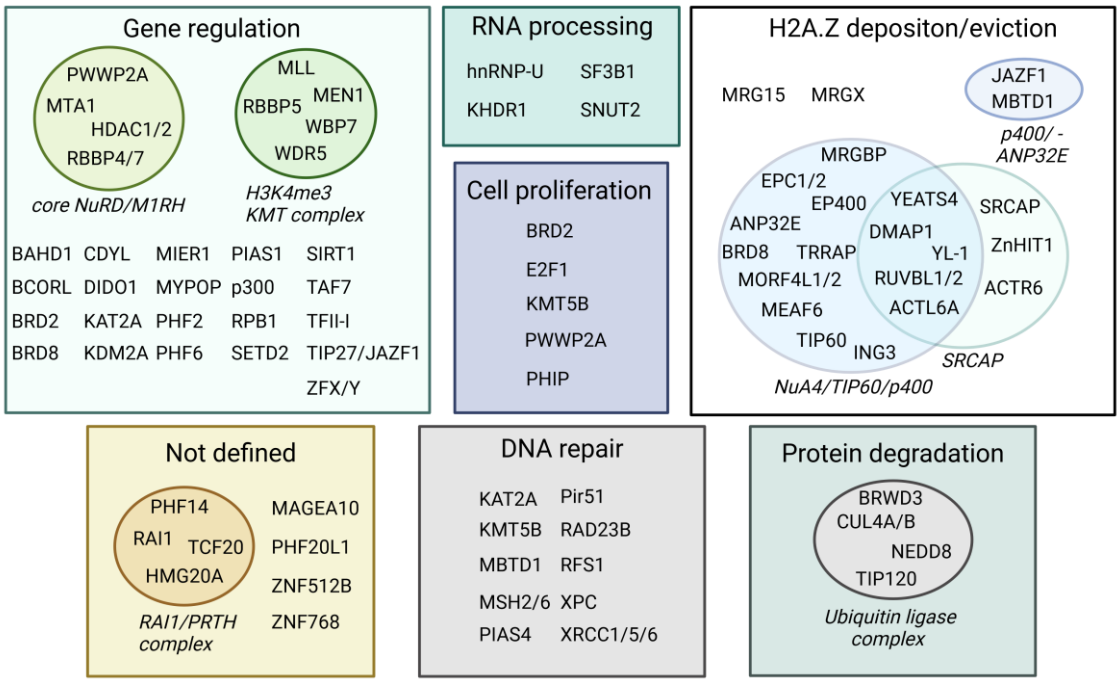

Figure 1.1.5.1.3: H2A.Z binding partners are involved in a multitude of biological functions. *The mammalian H2A.Z-associated proteins that have been identified to date are ordered in boxes based on their respective functions. Circles indicate known complexes. Adapted from (Kreienbaum et al., 2022). Created in BioRender.com.*

One noteworthy binding partner is the vertebrate-specific protein PWWP2A that was identified as a direct H2A.Z interactor via label-free quantitative MS/MS (Punzeler et al., 2017). PWWP2A binds tightly to chromatin through a concerted multivalent binding

mode. Two internal protein regions mediate H2A.Z-specificity and nucleosome interaction, whereas the PWWP domain exhibits direct DNA binding, H3K36me3 recognition via an aromatic cage and possible interaction with another histone variant. Further, loss of PWWP2A in human cells impairs proper mitosis progression, while in *Xenopus* PWWP2A depletion results in severe craniofacial defects arising from neural crest cell differentiation and migration problems. In addition, PWWP2A promotes changes in histone acetylation levels at defined regulatory regions by recruiting an MTA1-specific NuRD subcomplex (M1HR) to H2A.Z-containing chromatin. M1HR consists exclusively of MTA1, RBBP4/7 and HDAC1/2, which are, notably, also interaction partners of H2A.Z (Link et al., 2018). Recently, HMG20A was described as an H2A.Z/PWWP2A-associated protein (Herchenrother, Gossen, et al., 2023). HMG20A interacts with multiple chromatin modifiers, like the NuRD and corepressor of RE1 silencing transcription factor (CoREST) complexes. Depletion of HMG20A in *X. laevis* results in significant abnormalities in craniofacial development, including defects in the head and heart. These developmental failures are replicated in HMG20A-depleted mouse embryonic stem cells (mESCs), which demonstrate impaired differentiation into neural crest cells (NCCs) and cardiomyocytes (CMs). Consequently, HMG20A is suggested to play a pivotal role in regulating developmental transcription programs that orchestrate the differentiation of NCCs and CMs. In conclusion, while some interesting members of the H2A.Z interactome have already been characterized, several remain whose functions are still unclear, like the zinc finger protein ZNF512B.

1.2 Zinc finger proteins constitute the largest family of transcription factors

Zinc finger proteins (ZFPs) are a large and diverse family of proteins characterized by their ability to bind zinc ions, which stabilize their structural domains, and constitute the largest group of transcription factors in the human genome (Li et al., 2022). The zinc finger (ZF) motif was first discovered in the late 1980s by Aaron Klug and his colleagues while studying the transcription factor TFIIIA in *X. laevis* (Gibson et al., 1988; Vrana et al., 1988). TFIIIA contains repeated domains that were found to coordinate zinc ions, giving rise to the term 'zinc finger.' The discovery of ZFPs was a milestone in molecular biology because it revealed a new way that proteins could interact with DNA and regulate gene expression. Since then, ZFPs have been identified across different organisms, from bacteria to humans, where they play crucial roles in a wide range of biological processes, most notably in gene regulation, DNA recognition, RNA binding and protein-protein interactions (Malgieri et al., 2015). Their functions have been linked to both normal physiological processes and diseases such as cancer, neurological disorders and developmental abnormalities (Cassandri et al., 2017). The defining feature of ZFPs is the presence of one or more zinc finger motifs, which are small protein domains that coordinate zinc ions (Eom et al., 2016; Hossain et al., 2015; Klug, 2010; Laity et al., 2001; Matthews et al., 2009). This coordination of zinc ions is critical for maintaining the structural integrity of these motifs. It stabilizes the folding of the protein domain into a loop or 'finger' structure that can interact with other molecules such as DNA, RNA or proteins. Without the presence of zinc, these domains would lose their functional conformation and become unstable. The zinc ion acts as a scaffold around which the protein folds into its functional shape. In addition to stabilizing the structure, the zinc ion also contributes to the ability of these proteins to interact with nucleic acids or other proteins. The zinc ion is typically coordinated by cysteine and histidine residues within the protein sequence. There are several types of zinc finger motifs, each with distinct structural features and functions, with the most common type found in eukaryotic TFs being the C_2H_2 zinc finger motif (Wolfe et al., 2000). It consists of two cysteine (C) residues and two histidine (H) residues that coordinate a single zinc ion. The C_2H_2 motif typically forms an α-helix and a β-sheet structure (ββα fold) that can bind to specific sequences of DNA (Figure 1.2). When it binds to its target site, it aligns three base pairs on the DNA with specific amino acids in the α-helix structure. These amino acids at the contact site determine the DNA sequence recognition specificity (Peng et al., 2014). C_2H_2

ZFPs often contain multiple zinc finger motifs arranged in tandem, allowing them to recognize longer stretches of DNA.

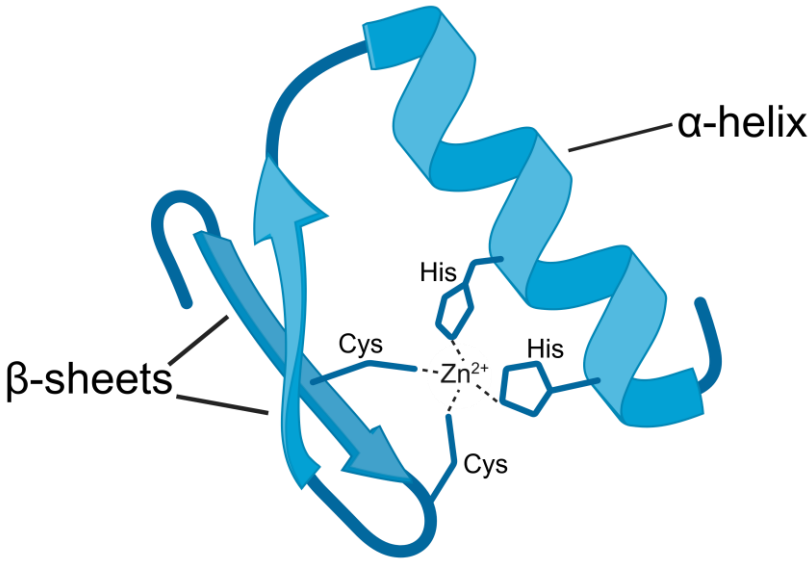

Figure 1.2: The C_2H_2 zinc finger motif forms a ββα fold. *Two N-terminal β-sheets and a C-terminal α-helix coordinate a zinc ion. Adapted from (Wolfe et al., 2000). Created in BioRender.com.*

One of the most well-known functions of ZFPs is their role as TFs. ZFPs can bind to promoters or enhancers of target genes through their zinc finger motifs to either activate or repress gene transcription (Liu et al., 2022). For instance, a subclass of C_2H_2 ZFPs, that contain a Krüppel-associated box (KRAB) domain at their N-terminus, act as transcriptional repressors by recruiting co-repressors such as KRAB-associated protein-1 (KAP1), also known as tripartite motif-containing 28 (TRIM28), which modifies chromatin structure through histone deacetylation and methylation to silence target genes (Al-Naama et al., 2020; Urrutia, 2003). In mammals, KRAB-ZFPs play an essential role during early embryonic development by silencing endogenous retroviruses (ERVs) that could otherwise disrupt genomic integrity (Yang, Wang, & Macfarlan, 2017). This co-evolution between KRAB-ZFPs and ERVs has been essential for shaping species-specific regulatory networks. Another well-known ZFP, that functions as an insulator protein, is the CCCTC-binding factor (CTCF) (Phillips & Corces, 2009). CTCF binds to specific sites in the genome and regulates chromatin architecture by creating boundaries between active and inactive chromatin regions. This insulator function helps control long-range gene regulation by preventing inappropriate interactions between enhancers and promoters. A noteworthy development in recent years has been the identification of

multiple ZFPs that display an exceptionally high degree of selectivity, specifically regulating a single gene. The KRAB-ZFP ZFP568, for example, acts as a direct repressor of a placental-specific insulin-like growth factor 2 (IGF2) transcript in mice (Yang, Wang, Hoang, et al., 2017). In leukemia, ZFP64 plays a crucial role in maintaining the expression of the Mixed Lineage Leukemia (*MLL*) gene (Lu et al., 2018). This occurs through binding to the *MLL* promoter, where an extensive number of ZFP64 motifs allows for highly specific binding. Zinc finger protein 558 (ZNF558) is involved in the maintenance of mitochondrial function and brain development and exclusively regulates the expression of the mitophagy gene spermatogenesis associated 18 (*SPATA18*) (Johansson et al., 2022). Lastly, ZNF410 exerts its function through the direct silencing of one gene, the NuRD component CHD4 (Lan et al., 2021). This results in the silencing of fetal-type β-globin genes in adult erythroid cells. The identification of additional highly specific TFs represents an intriguing path for future research, particularly given the vast number of ZFPs that have been identified to date.

1.2.1 The zinc finger protein ZNF512B is well conserved among vertebrates

In multiple MS-based screens utilizing the histone variant H2A.Z and its associated proteins PWWP2A and HMG20A, a common identified protein was ZNF512B (Herchenrother, Gossen, et al., 2023; Link et al., 2018; Punzeler et al., 2017; Vardabasso et al., 2015). ZNF512B (previously named ZFp/GAM) was first expressed and characterized from isolated chicken cDNA in 2005 (Michaille et al., 2005). It is a vertebrate-specific nuclear zinc finger protein comprising eight ZF domains (Figure 1.2.1). These are organized into four pairs, with each pair consisting of one atypical C_2HC ZF followed by one typical C_2H_2 ZF. The first and second pairs are separated by a large internal region (I). Further, ZNF512B contains a repeat region (P-V-T/S-K/R or V/I-P/S-K/R or V/I) at the beginning of its internal region and a putative leucine zipper between the third and fourth ZF pairs. ZNF512B is well conserved across species, showing 60 % homologies and 71 % similarities between mammalian and chicken orthologs. However, the number of studies on ZNF512B is fairly limited. It was shown to modulate levels of E2F transcription factor 1 (E2F1) and Ras, leading to apoptosis when overexpressed (Tili et al., 2010). It was identified as a hub gene negatively correlated with nut allergy in children (K. H. Lee et al., 2022), predicted to regulate genes

connected with feather morphogenesis in ducks (Xu et al., 2022), and suggested as a prognostic biomarker for colon adenocarcinoma (Wang et al., 2024). Several studies have linked ZNF512B to the neurodegenerative disorder amyotrophic lateral sclerosis (ALS) (Jiang et al., 2021; Ning et al., 2018). A single-nucleotide polymorphism (SNP) situated within the enhancer region of the *ZNF512B* gene is associated with reduced activity of the ALS susceptibility allele in a luciferase reporter assay. Recently, it has been proposed that ZNF512B, in conjunction with ZNF512, plays a role in the initiation of pericentric heterochromatin formation. This is thought to occur through the binding of the protein to repetitive and non-consecutive TTC sequences and the subsequent recruitment of the methyltransferases suppressor of variegation 3–9 homolog 1/2 (SUV39H1/2) (Ma et al., 2024). Finally, ZNF512B has been found to be part of the interactomes of the NuRD complex members MBD3 and GATAD2B in different MS studies (Kloet et al., 2015; Spruijt et al., 2016).

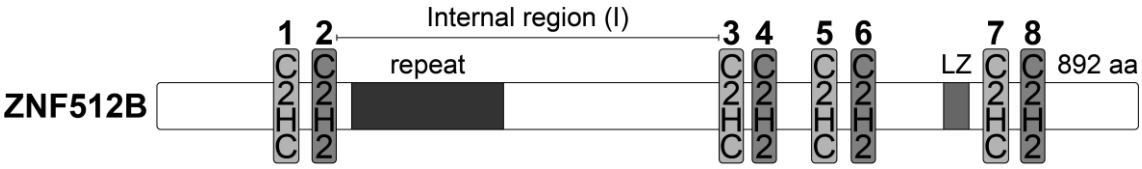

Figure 1.2.1: ZNF512B's ZFs are arranged in four pairs. *Schematic depiction of the human ZNF512B protein with four pairs of atypical C_2HC (light grey) and typical C_2H_2 (dark grey) ZFs, a repeat region and a putative leucine zipper (LZ).*

1.3 Aim of this study

The histone variant H2A.Z is involved in nearly all DNA-related processes and crucial for development, cellular differentiation and brain functions, linking it to a broad range of pathological conditions (Colino-Sanguino et al., 2022). However, the mechanisms underlying H2A.Z's diverse functions remain largely unknown. A potential approach to better understand these mechanisms is the comprehensive analysis of H2A.Z-specific interacting proteins. The zinc finger protein ZNF512B has been identified as a common interactor of H2A.Z and its associated proteins HMG20A and PWWP2A in several mass spectrometry-based screens (Herchenrother, Gossen, et al., 2023; Link et al., 2018; Punzeler et al., 2017; Vardabasso et al., 2015), and its function remains largely elusive.

The aim of this study is to confirm the interactions between ZNF512B and H2A.Z, HMG20A and PWWP2A, and to uncover ZNF512B's functionality through analysis of its structural domains, its interactome and its role in gene regulation.

2 Material & Methods

2.1 Technical devices

Table 2.1: Important technical devices and their manufacturer

Description	Name	Manufacturer
Automated cell counter	Countess	Invitrogen
	Countstar Mira FL	Shanghai Ruiyu Biotech
Chemiluminescence imager	ECL Chemostar	Intas
DSLR	D3000	Nikon
Flow cytometer	Accuri C6 Plus	Becton Dickinson
Fluorometer	Qubit 4	Invitrogen
FPLC	Äkta Start	Cytiva
Gel documentation system	GelStick Touch	Intas
HPLC	EASY-nLC 1000	Thermo Fisher Scientific
Mass spectrometer	Q Exactive Plus	
Microscope	Axio Observer.Z1	Carl Zeiss
Microscope camera	Axiocam 506 mono	
Nano photometer	NP80	Implen
PCR-thermocycler	Labcycler basic	SensoQuest
	Labcycler gradient	
Plate reader	Spark 20M	Tecan
	Orion L	Titertek-Berthold
Real-time PCR system	CFX Opus	Bio-Rad
	CFX96	
RNA/DNA extraction instrument	QIAcube	Qiagen
Ultrapure lab water system	Milli-Q	Millipore
UV-Crosslinker	BLX-254	Bio-Link

2.2 Chemicals

Table 2.2: Chemicals and their supplier

Description	Supplier
4-(2-hydroxyethyl)-1-piperazineethanesulfonic acid (HEPES)	Carl Roth
Acetic acid (CH_3COOH)	
Agar	
Agarose	
Albumin fraction V (BSA)	
Ammonium persulfate (APS)	
Ampicillin	
Aprotinin	AppliChem
bisBenzimide H 33342 trihydrochloride (Hoechst)	Sigma-Aldrich
Bromophenol blue sodium salt	Carl Roth

Calcium chloride dihydrate ($CaCl_2$ 2×H_2O)	Carl Roth
Coomassie brilliant blue R-250	Fluka
DharmaFECT1 transfection reagent	Horizon Discovery
Dimethyl sulfoxide (DMSO)	Carl Roth
Disodium hydrogen phosphate dihydrate (Na_2HPO_4 2×H_2O)	
Dithiothreitol (DTT)	
Dulbecco's Modified Eagle Medium (DMEM)	Gibco
Ethanol	Carl Roth
Ethidium bromide	
Ethylene glycol-bis(β-aminoethyl ether)-N,N,N′,N′-tetraacetic acid (EGTA)	
Ethylenediaminetetraacetic acid (EDTA)	
ExpiFectamine Sf transfection reagent	Gibco
Fetal calf serum (FCS)	Thermo Fisher Scientific
Fluoromount-G mounting medium	VWR
Formaldehyde	Thermo Fisher Scientific
FuGENE HD transfection reagent	Promega
GFP-Trap Magnetic Particles M-270	Chromotek
Glycerol	Carl Roth
Glycine	
Hydrochloric acid (HCl)	
Immersol 518 F immersion oil	Th. Geyer
Isopropanol	Carl Roth
Kanamycin	
Leupeptin	AppliChem
Magnesium chloride ($MgCl_2$)	Carl Roth
Magnesium sulfate heptahydrate ($MgSO_4$ 7×H_2O)	
McCoy's 5A Modified Medium	Gibco
Methanol	Carl Roth
Milk powder	
Nonidet P-40 substitute (NP-40)	Sigma-Aldrich
Opti-MEM	Gibco
Paraformaldehyde	Carl Roth
Penicillin	Gibco
Pepstatin A	AppliChem
Phenylmethanesulfonyl fluoride (PMSF)	Carl Roth
Potassium chloride (KCl)	
Potassium dihydrogen phosphate (KH_2PO_4)	
Propidium iodide (PI)	Sigma-Aldrich
Rotiphorese Gel 30	Carl Roth
Sf-900 II SFM medium	Gibco
Sodium chloride (NaCl)	Carl Roth

Sodium deoxycholate	Sigma-Aldrich
Sodium dodecyl sulfate (SDS)	Carl Roth
Sodium hydroxide (NaOH)	
Streptomycin	Gibco
Sulfuric acid (H_2SO_4)	Carl Roth
Tetramethylethylenediamine (TEMED)	
Trident femto Western HRP substrate	GeneTex
Trifluoroacetic acid (TFA)	Thermo Fisher Scientific
Tris(hydroxymethyl)aminomethan (Tris)	Carl Roth
Triton X-100	
Trypan blue solution	Thermo Fisher Scientific
Tryptone	Carl Roth
Tween20	
Yeast extract	

2.3 General buffers / solutions

Table 2.3: Composition of general buffers / solutions

Buffer / solution	Concentration	Component
Coomassie destaining solution	10 %	Acetic acid
	30 %	Methanol
Coomassie staining solution	10 %	Acetic acid
	50 %	Methanol
	0.1 %	Coomassie brilliant blue R-250
LB agar	1.5 %	LB agar
LB medium	1 %	NaCl
	1 %	Tryptone
	0.5 %	Yeast extract
PBS (10×)	100 mM	Na_2HPO_4 2×H_2O pH 7.4
	20 mM	KCl
	14 mM	KH_2PO_4
	1.37 M	NaCl
Protease inhibitor mix	1 mg/mL	Aporotinin
	1 mg/mL	Leupeptin
	0.7 mg/mL	Pepstatin
	0.2 M	PMSF
	1 M	DTT
SDS running buffer (10×)	1.29 M	Glycine
	0.25 M	Tris
	1 %	SDS

SDS sample buffer (5×)	500 mM	DTT
	250 mM	Tris pH 8
	0.02 %	Bromophenol blue
	30 %	Glycerol
	10 %	SDS
Separating gel (10, 12, 15 or 18 %)	375 mM	Tris/HCl pH 8.8
	33, 40, 50 or 60 %	Rotiphorese Gel 30
	0.1 %	SDS
	0.13 %	TEMED
	0.13 %	APS
Stacking gel (6 %)	125 mM	Tris/HCl pH 6.8
	20 %	Rotiphorese Gel 30
	0.1 %	SDS
	0.15 %	TEMED
	0.14 %	APS
Semi-dry transfer buffer (1×)	48 mM	Tris
	39 mM	Glycine
	0.0375 %	SDS
	20 %	Methanol
TAE buffer (50×)	2 M	Tris pH 7.8
	0.1 M	EDTA
Trypsin/EDTA	0.6 mM	$CaCl_2$ 2×H_2O
	3 mM	EDTA
	2.6 mM	KCl

2.4 Antibodies

Table 2.4: Antibodies and their supplier, application and dilution

Antibody	Host	Supplier	Order Number	Application	Dilution
α-CHD4	Mouse	Abcam	ab70469	IF	1:100
α-FLAG	Mouse	Sigma-Aldrich	F3165	WB	1:6,000
				IF	1:100
α-GFP	Mouse	Roche	11814460001	WB	1:3,000
α-H2A	Mouse	Active Motif	91325	WB	1:1,000
α-H2A.X	Rabbit	Sigma-Aldrich	07-627	WB	1:1,000
α-H2A.Z	Rabbit	Abcam	ab4174	WB	1:1,000
α-H2A.Zac	Rabbit	Abcam	ab232908	IF	1:100
α-H3	Rabbit	Abcam	ab1791	WB	1:5,000
α-H3K27ac	Rabbit	Active Motif	39133	IF	1:100
α-H3K27me3	Rabbit	Diagenode	C15410195	IF	1:100
α-H3K4me3	Rabbit	Diagenode	C15410003	IF	1:100
α-H3K9me3	Rabbit	Invitrogen	49-1008	IF	1:100
α-H3S10ph	Rabbit	Invitrogen	PA5-17869	IF	1:100
α-HDAC1	Rabbit	Proteintech	10197-1-AP	WB	1:1,000
α-HDAC2	Rabbit	Abcam	ab7029	WB	1:1,000
α-HMG20A	Rabbit	Proteintech	12085-1-AP	WB	1:1,000
α-KPNA4	Rabbit	Proteintech	12463-1-AP	WB	1:1,000
α-macroH2A	Rabbit	Abcam	ab13923	WB	1:1,000
α-MBD2	Rabbit	Abcam	ab188474	WB	1:1,000
α-MTA1	Rabbit	Cell Signaling Technology	5647	WB	1:1,000
				IF	1:100
α-PWWP2A	Rabbit	Norvusbio	NBP2-13833	WB	1:1,000
α-RBBP4	Rabbit	Abcam	ab79416	WB	1:1,000
				IF	1:100
α-URB1	Rabbit	Bethyl Laboratories	A305-215A	WB	1:1,000

α-ZNF512B	Rabbit	BJ-Diagnostik BioScience	not applicable	WB	1:1,000
				IF	1:100
anti-Mouse IgG (H+L), HRP	Goat	Invitrogen	31430	WB	1:20,000
anti-Rabbit IgG (H+L), HRP	Goat	Invitrogen	31460	WB	1:20,000
F(ab')2 anti-Rabbit IgG (H+L) Cross-Adsorbed, Alexa Fluor 488	Goat	Invitrogen	A-11070	IF	1:200
F(ab')2 anti-Rabbit IgG (H+L) Cross-Adsorbed, Alexa Fluor 594	Goat	Invitrogen	A-11072	IF	1:200
F(ab')2 anti-Mouse IgG (H+L) Cross-Adsorbed, Alexa Fluor 594	Goat	Invitrogen	A-11020	IF	1:200

2.5 Primers / oligonucleotides

All primers and oligonucleotides were synthesized at Thermo Fisher Scientific or Integrated DNA Technologies.

Table 2.5: Primers / oligonucleotides and their application

Target / oligo	Application	Forward (5´ to 3´)	Reverse (5´ to 3´)
ZNF512B	Cloning into pIRESneo-eGFP	TCATCGTTCGAAG TCCGGATCTATGA CGGATCCTTTCTG CGTTGGAG	TAGTAAGCGGCC GCTCACTATCACT TTTCAGGCGCCTT GCTG
	Cloning into pEGFP-N2	ATGACGGATCCTT TCTGCGTTGGAG	CTTTTCAGGCGCC TTGCTGACTC
	Cloning into p3xFLAG-CMV-10	ATGACGGATCCTT TCTGCGTTGGAG	TCACTTTTCAGGC GCCTTGCTG
	Cloning into pFastBac1	ACTACTGAATTCA TGGATTACAAGG ATGACGATGACA AGGGTGGTTCTG GTACGGATCCTTT CTGCGTTGGAG	GTGGTGGGTACCT CACTTTTCAGGCG CCTTGCT
	Cloning into pAB-Gal94	TTTTGTCGACACG GATCCTTTCTGCG TTGGA	TTTTTCTAGACTA CTTTTCAGGCGCC TTGCTGA
eGFP-ZNF512B	Cloning into pTetLS	TCATCGTTCGAAG CCACCATGGTGA GCAAGG	TAGTAAGTCGACT CACTATCACTTTT CAGGCGCCTTG
eGFP	Cloning into pTetLS		TAGTAAGTCGACT CACTTGTACAGCT CGTCCATGCCG
FOXJ1	Cloning into pIRESneo-eGFP	TCATCGTTCGAAG GCGGAGAGCTGG CTG	TAGTAAGCGGCC GCCTATCATTACA AGAAGGCCCCCA CG
ZBTB20	Cloning into pIRESneo-eGFP	TTCGAAGTCCGG ATCTCTAGAACG GAAGAAACCCAA GACAG	GCGGCCGCTCACT ATTATCCGTCAGA CACATGCATCC

ZNF148	Cloning into pIRESneo-eGFP	TTCGAAGTCCGGATCTAACATTGACGACAAACTGGAAGGATT	GCGGCCGCTCACTATTAGCCAAAAGTCTGGCCAGTT
	Cloning into p3xFLAG-CMV-10	GCGGCCGCAAACATTGACGACAAACTGGAAGGATT	GGATCCTTAGCCAAAAGTCTGGCCAGTT
ZNF512B	Cloning of GFP-ZNF512B_ΔZF	TCATCGTTCGAAGTCCGGATCTATCAGCAGGCCGGTCACCATC	TAGTAAGCGGCCGCTCACTACTCTTCAGGGCCACCTGGAG
	Cloning of GFP-ZNF512B_ΔI fragment 1	TCATCGTTCGAAGTCCGGATCTATGACGGATCCTTTCTGCGTTGGAG	CACCTGGAGCGATGGTGACCGGCCTGCT
	Cloning of GFP-ZNF512B_ΔI fragment 2	GGTCACCATCGCTCCAGGTGGCCCTGAA	TAGTAAGCGGCCGCTCACTACACCTTCCGCTTCTTCTTGGGCTTTTCAGGCGCCTTGCTGACTC
	Cloning of GFP-ZNF512B_ΔZF1-2	TCATCGTTCGAAGTCCGGATCTATCAGCAGGCCGGTCACCATC	TAGTAAGCGGCCGCTCACTATCACTTTTCAGGCGCCTTGCTG
	Cloning of GFP-ZNF512B_ΔZF3-8	TCATCGTTCGAAGTCCGGATCTATGACGGATCCTTTCTGCGTTGGAG	TAGTAAGCGGCCGCTCACTACTCTTCAGGGCCACCTGGAG
	Cloning of GFP-ZNF512B_ZF1-2	TCATCGTTCGAAGTCCGGATCTGATGAGTTCAAGGCACACTCGAG	TAGTAAGCGGCCGCTCACACCTTCCGCTTCTTCTTGGGAGGCTTGGAGGCAGGC
	Cloning of GFP-ZNF512B_ZF3-4	TCATCGTTCGAAGTCCGGATCTAGGGCCATCCATGAGCG	TAGTAAGCGGCCGCTCACACCTTCCGCTTCTTCTTGGGGGAGGCCTCGGCGT
	Cloning of GFP-ZNF512B_ZF5-6	TCATCGTTCGAAGTCCGGATCTAAGGTGCTGAAGCAGATGGG	TAGTAAGCGGCCGCTCACACCTTCCGCTTCTTCTTGGGGTCTGTGGGCTCCTCAGG
	Cloning of GFP-ZNF512B_ZF7-8	TCATCGTTCGAAGTCCGGATCTAATGAAGTGAAGGAGAAAGGCCACG	TAGTAAGCGGCCGCTCACACCTTCCGCTTCTTCTTGGGGTCTGCTGATGTTCGGAACCAG

ZNF512B	Cloning of GFP-ZNF512B_iNIM	TCATCGTTCGAAG TCCGGATCTTCCC CGCCTGAGGAGG	TAGTAAGCGGCC GCTCACACCTTCC GCTTCTTCTTGGG GGTCCCTGAGAT GGATGGCT
	Cloning of GFP-ZNF512B_IN	TCATCGTTCGAAG TCCGGATCTATGG ACCGACCCCTGC	TAGTAAGCGGCC GCTCACACCTTCC GCTTCTTCTTGGG TGTGGCACGAGG TGCTTT
	Cloning of GFP-ZNF512B_IC	TCATCGTTCGAAG TCCGGATCTGGG AGGAACAGTGGT AAGAAAAGGG	TAGTAAGCGGCC GCTCAGACGGCTT CCCCGC
ZNF512B	Cloning of FLAG-ZNF512B_ΔZF	ATCATCGAATTCA GCTTCGAAGTCCG	ATCATCGGTACCC TACTCTTCAGGGC C
	Cloning of FLAG-ZNF512B_ΔI	ATAACAGAATTC AATGACGGATCC TTTCTGC	AAAGCAAGATCT CTACACCTTCCGC TTCTTC
ZNF512B	Cloning of GAL-ZNF512B_ΔZF Gibson vector	CAGGTGGCCCTG AAGAGTGATTTC GGATCCAAAGCT TGATCCG	ATGGTGACCGGC CTGCTGATGAATT CCAATCTAGATTG CGGCG
	Cloning of GAL-ZNF512B_ΔZF Gibson fragment	CGCAATCTAGATT GGAATTCATCAG CAGGCCGGTCAC	ATCAAGCTTTGGA TCCGAAATCACTC TTCAGGGCCACCT
	Cloning of GAL-ZNF512B_ΔI Gibson vector	GAGTCAGCAAGG CGCCTGAATTTCG GATCCAAAGCTT GATCG	CCAACGCAGAAA GGATCCGTGAATT CCAATCTAGATTG CGGC
	Cloning of GAL-ZNF512B_ΔI Gibson fragment	CGCAATCTAGATT GGAATTCACGGA TCCTTTCTGCGTT GG	ATCAAGCTTTGGA TCCGAAATTCAG GCGCCTTGCTGAC
ZNF512B	SDM K419A	GCGCACAGAAGG AAACAGAAAACA CCCAAAAAGTTT ACAGGGGAGC	TTTCTGTTTCCTT CTGTGCGCTGTGC GCTCCGGGTC
	SDM H420A	AGGCCAGAAGGA AACAGAAAACAC CCAAAAAGTTTA CAGGGGAGC	TTTCTGTTTCCTT CTGGCCTTTGTGC GCTCCGGGTC

ZNF512B	SDM R421A	AGCACGCAAGGA AACAGAAAACAC CCAAAAAGTTTA CAGGGGAGC	TTTCTGTTTCCTT GCGTGCTTTGTGC GCTCCGGGTC
	SDM R422A	AGCACAGAGCGA AACAGAAAACAC CCAAAAAGTTTA CAGGGGAGC	TTTCTGTTTCGCT CTGTGCTTTGTGC GCTCCGGGTC
	SDM K423A	CACAGAAGGGCA CAGAAAACACCC AAAAAGTTTACA GGGGAGCAGC	GTTTTCTGTGCCC TTCTGTGCTTTGT GCGCTCCGGGTCC T
	SDM Q424A	AGCACAGAAGGA AAGCGAAAACAC CCAAAAAGTTTA CAGGGGAGC	TTTCGCTTTCCTT CTGTGCTTTGTGC GCTCCGGGTC
	SDM K425A	AGCACAGAAGGA AACAGGCAACAC CCAAAAAGTTTA CAGGGGAGC	TGCCTGTTTCCTT CTGTGCTTTGTGC GCTCCGGGTC
	SDM T426A	AGCACAGAAGGA AACAGAAAGCAC CCAAAAAGTTTA CAGGGGAGC	TTTCTGTTTCCTT CTGTGCTTTGTGC GCTCCGGGTC
	SDM P427A	AGCACAGAAGGA AACAGAAAACAG CCAAAAAGTTTA CAGGGGAGC	TTTCTGTTTCCTT CTGTGCTTTGTGC GCTCCGGGTC
	SDM K428A	AGCACAGAAGGA AACAGAAAACAC CCGCAAAGTTTAC AGGGGAGC	TTTCTGTTTCCTT CTGTGCTTTGTGC GCTCCGGGTC
	SDM K429A	AGCACAGAAGGA AACAGAAAACAC CCAAAGCGTTTAC AGGGGAGC	TTTCTGTTTCCTT CTGTGCTTTGTGC GCTCCGGGTC
	SDM K429R	AGCACAGAAGGA AACAGAAAACAC CCAAAAGGTTTA CAGGGGAGC	TTTCTGTTTCCTT CTGTGCTTTGTGC GCTCCGGGTC
	SDM F430A	AGCACAGAAGGA AACAGAAAACAC CCAAAAAGGCTA CAGGGGAGC	TTTCTGTTTCCTT CTGTGCTTTGTGC GCTCCGGGTC
	SDM K419A_R421A	GCGCACGCAAGG AAACAGAAAACA CCCAAAAAGTTT ACAGGGGAGCAG	GTTTCCTTGCGTG CGCTGTGCGCTCC GGGTCC

ZNF512B	SDM C107A_C112A	GGTGAAGGCTCCAAACTCAGGGGCCTGGCTGG	GTTTGGAGCCTTCACCCTCGAGTGTGCCTTGAACTCATCCTTC
	SDM C512A_C515A	GGAAGCCGTCGCCCCCACCGCCAACGTG	GCGACGGCTTCCCCGCGCTCATGGATGGC
	SDM C596A_C601A	CGCCCCCCAGGAGGGTGCCGGGGCT	CCTGGGGGGCGCGCAGCCGTCCCATCTG
	SDM C752A_C757A	GTCAACGCTCCCAACGACTGCGCTGAAGCCATCTACTCC	GTTGGGAGCGTTGACGTGGCCTTTCTCCTTCACTTCATTCTTCCA
	SDM C142A_C145A	CCCCGCCCCCTTCGCCGAGGCCGCA	GGGGGCGGGGAAGGCCAGGCGATCTGAGATGG
	SDM C542A_C545A	GCACTCAAGGCCCAGCACGCCCGGAAGCAGTTCAAG	CTGGGCCTTGAGTGCATCCTGAAGCTTCTGACACACCTCCATG
	SDM C632A_C635A	GCCACCCACGCTGGCAAGACGTACCGATCCAAGGC	CAGCGTGGGTGGCGGGGAAGGAGGGGCTGTC
	SDM C786A_C789A	GAAGTACCGCGCTCTGCTGGCTCCGAAGGAGTTCAGTTCTGA	CAGAGCGCGGTACTTCCCTGCCAGGTGGGCC
ZNF512B	RT-qPCR	TCCCAACGACTGCTGTGAAG	TGAACTCCTTCGGACACAGC
HPRT1		AAGGGTGTTTATTCCTCATGGA	AATCCAGCAGGTCAGCAAAG
BIRC3		CACAGAAGATGTTTCAGATCTACCA	TGTACGAACTGTACCCTTGATTGT
IL6		GCCCACCGGGAACGAAAG	CGAAGGCGCTTGTGGAG
MYRF		GCAAGTCATCGTCCGTGGTT	CACGGCAAAAGAGCCATCAGT
ADAMTS3 gene body	ChIP-qPCR	CGTTCCTTTCCACTGGTCTTTTC	CTCTCCTTCCTGCTGTGTGG

EIF4H promoter	ChIP-qPCR	TCTCCAGGTCACCTCCCG	CCTACGCGGCCCATTATGT
GNAI1 gene body		AGAACAAAAGCATGGATGACAGC	AGCCAAGATTGTTGTGCCAACTACA
RPL11 gene body		ACAGCTTTGGGTGATGCAGT	TTGTTGGACCAAAACACGGC
	EMSA		
H19		CACCCGGTGCTTCGGGCCCTCTAGCCCGGGCTTTTTCTAACTGGAGTGGCTCCGCCCA	
Predicted		CCCATAATCTTATAATTATTCTACTAGGGG	
Ma & Zhang et al.		GGACCTGGAATATGGCGAGAAAACTGAAAATC	

2.6 Peptide characterization

2.6.1 ZNF512B-FAM (fluorescence polarization)

H_2N-KHRRKQKTPKKFTGE-Ahx-Ahx-K(FAM)-$CONH_2$; peptide was synthesized in 5 µmol scale. After purification (5–50 % MeCN), the 9 x TFA salt product (7.47 mg, 2.07 µmol, 41 % yield) was obtained as a white solid. t_R = 9.43 min. Purity ≥ 98 %. Formula: $C_{121}H_{186}N_{34}O_{29}$. Molecular weight: 2580.98 Da. HRMS-ESI+ (m/z): $[M+1H]^{1+}$ calcd.: 1291.2150; found: 1291.2137.

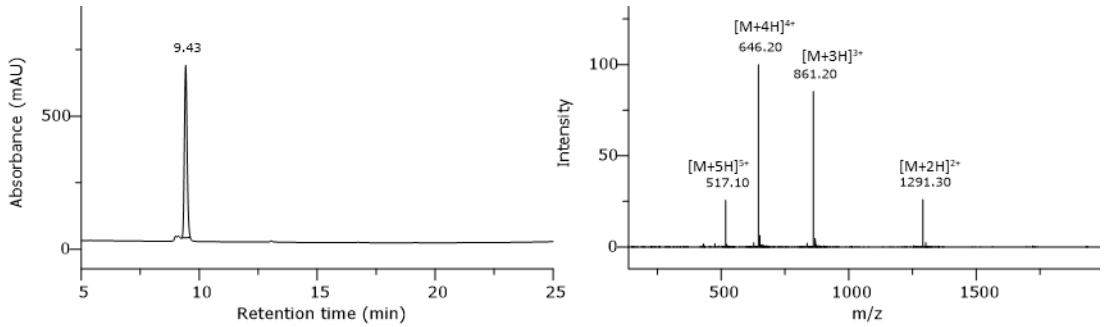

Figure 2.6.1: HPLC chromatogram of purified peptide ZNF512B-FAM. *Gradient 5–95 % MeCN monitored at 220 nm.*

2.6.2 ZNF512B WT (fluorescence polarization / peptide competition)

H_2N-KHRRKQKTPKKFTGE-$CONH_2$; peptide was synthesized in 5 µmol scale. After purification (5–50 % MeCN), the 9 x TFA salt product (3.06 mg, 1.06 µmol, 21 % yield) was obtained as a white solid. t_R = 6.47 min. Purity ≥ 99 %. Formula: $C_{82}H_{142}N_{30}O_{20}$. Molecular weight: 1868.19 Da. HRMS-ESI+ (m/z): $[M+3H]^{3+}$ calcd.: 624.0429; found: 624.0427.

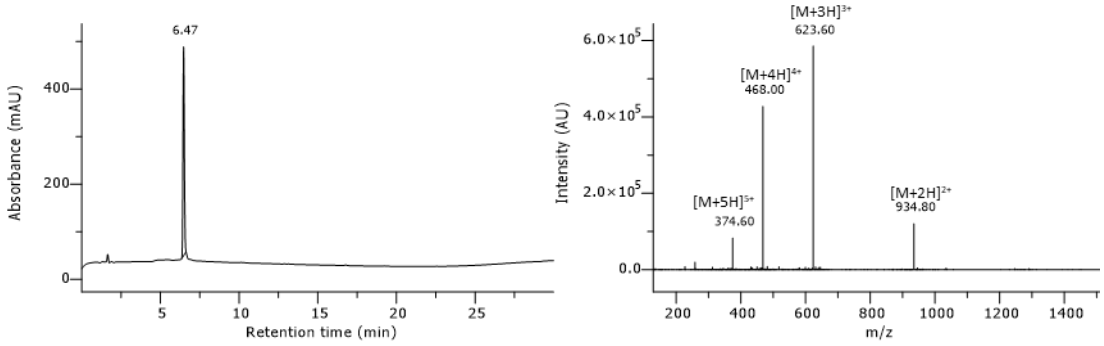

Figure 2.6.2: HPLC chromatogram of purified peptide ZNF512B WT. *Gradient 5–95 % MeCN monitored at 220 nm.*

2.6.3 ZNF512B SCR (fluorescence polarization / peptide competition)

H_2N-KQHGKTEKTPRKRFK-$CONH_2$; peptide was synthesized in 5 µmol scale. After purification (5–50 % MeCN), the 9 x TFA salt product (2.10 mg, 0.72 µmol, 14 % yield) was obtained as a white solid. t_R = 6.12 min. Purity ≥ 99 %. Formula: $C_{82}H_{142}N_{30}O_{20}$. Molecular weight: 1868.19 Da. HRMS-ESI+ (m/z): $[M+3H]^{3+}$ calcd.: 624.0429; found: 624.0431.

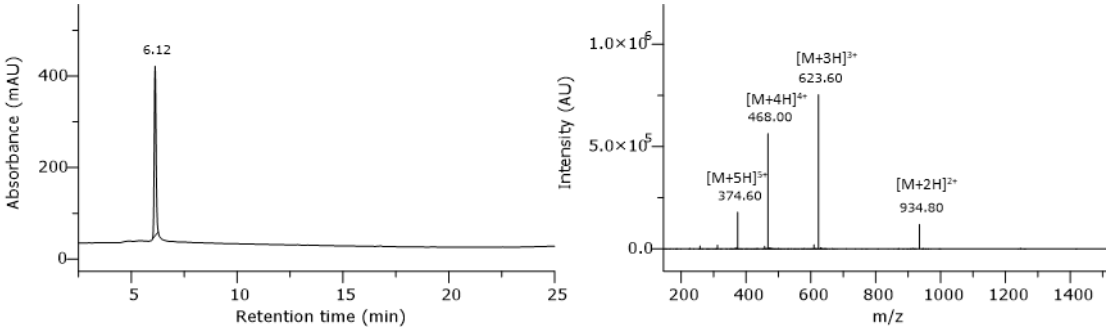

Figure 2.6.3: HPLC chromatogram of purified peptide ZNF512B SCR. *Gradient 5–95 % MeCN monitored at 220 nm.*

2.6.4 FOG-1 (fluorescence polarization)

H_2N-MSRRKQSNPRQI-$CONH_2$; peptide was synthesized in 5 µmol scale. After purification (5–50 % MeCN), the 5 x TFA salt product (3.49 mg, 1.67 µmol, 34 % yield) was obtained as a white solid. t_R = 6.23 min. Purity ≥ 99 %. Formula: $C_{60}H_{110}N_{26}O_{17}S_1$. Molecular weight: 1499.7443 Da. HRMS-ESI+ (m/z): $[M+2H]^{2+}$ calcd.: 750.4204; found: 740.4191.

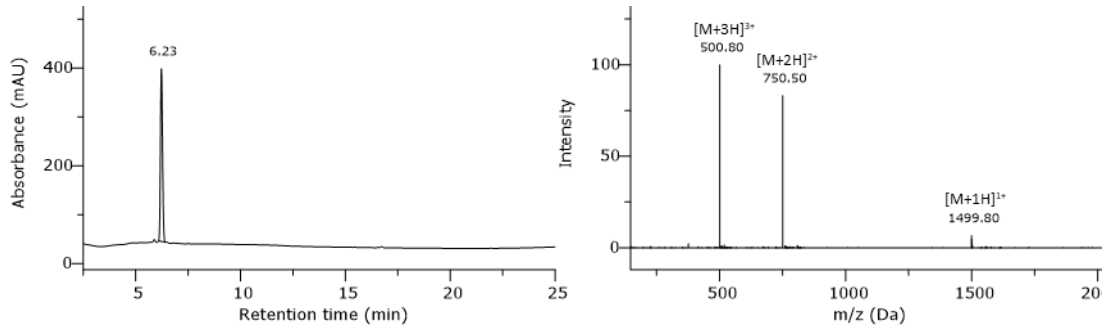

Figure 2.6.4: HPLC chromatogram of purified peptide FOG-1. *Gradient 5–95 % MeCN monitored at 220 nm.*

2.6.5 FOG-1 WT (peptide competition)

H_2N-MSRRKQSNPRQIKRS-Ahx-Ahx-K-$CONH_2$; peptide was synthesized in 5 µmol scale. After purification (5–50 % MeCN), the 8 x TFA salt product (2.23 mg, 0.71 µmol, 14 % yield) was obtained as a white solid. t_R = 6.56 min. Purity ≥ 99 %. Formula: $C_{93}H_{173}N_{37}O_{24}S$. Molecular weight: 2224.32 Da. HRMS-ESI+ (m/z): $[M+3H]^{3+}$ calcd.: 742.7806; found: 742.7887.

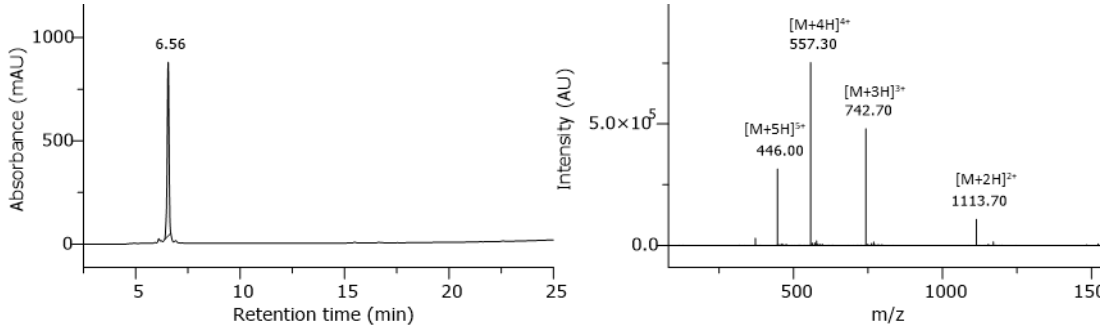

Figure 2.6.5: HPLC chromatogram of purified peptide FOG-1 WT. *Gradient 5–95 % MeCN monitored at 220 nm.*

2.6.6 FOG-1 SCR (peptide competition)

H_2N-RRSIQKMRQPKNSRS-Ahx-Ahx-K-$CONH_2$; peptide was synthesized in 5 µmol scale. After purification (5–50 % MeCN), the 8 x TFA salt product (2.22 mg, 0.71 µmol, 14 % yield) was obtained as a white solid. t_R = 6.68 min. Purity ≥ 99 %. Formula: $C_{93}H_{173}N_{37}O_{24}S$. Molecular weight: 2224.32 Da. HRMS-ESI+ (m/z): $[M+3H]^{3+}$ calcd.: 742.7807; found: 742.7876.

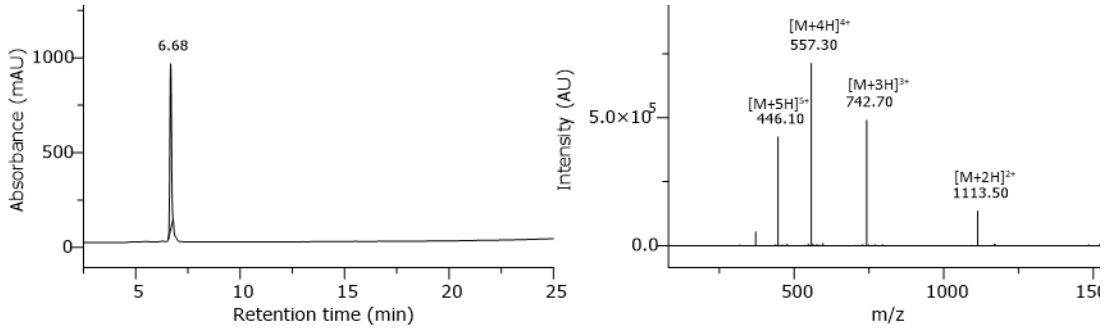

Figure 2.6.6: HPLC chromatogram of purified peptide FOG-1 SCR. *Gradient 5–95 % MeCN monitored at 220 nm.*

2.7 Cell-based methods

2.7.1 Culturing, passaging, freezing and thawing of cells

2.7.1.1 HeLaK, U2OS, HEK293T and HCT116 cells

Adherent Hela Kyoto (HeLaK), U2OS and HEK293T cells were cultured in Dulbecco's Modified Eagle Medium (DMEM, Gibco), HCT116 cells were cultured in McCoy's 5A Modified Medium (Gibco), both supplemented with 10 % heat-inactivated fetal calf serum (FCS, Gibco) and 1 % penicillin/streptomycin (P/S), under humidified conditions at 37 °C with 5 % CO_2 in 10 cm (10 mL medium) or 14.5 cm (20 mL medium) cell culture dishes (Greiner Bio-One). Every two to four days, depending on the confluency of the cells, cell culture medium was exchanged, or cells were subcultured. Therefore, at 80–90 % confluency, used medium was removed, cells were rinsed with an amount of phosphate-buffered saline (PBS) equivalent to 50 % of the original amount of cell culture medium and incubated with an amount of Trypsin/EDTA equivalent to 10 % of the original amount of cell culture medium at 37 °C for 5 minutes. Gentle tapping of the plate ensured complete cell detachment. Trypsin was neutralized with fresh cell culture medium. Appropriate volumes of the resulting suspension according to the desired dilution were transferred to new cell culture dishes containing fresh cell culture medium. Cell viability and cell number were assessed using an automated cell counter (Invitrogen or Shanghai Ruiyu Biotech). To prepare cells for storage, trypsinized cells were pelleted by centrifugation at 1,200 rpm for 5 minutes and washed with PBS. Afterwards, they were resuspended in 1 mL freezing medium (90 % FCS + 10 % DMSO), transferred into cryovials and placed in containers filled with isopropanol for gradual cooling at -80 °C. For extended storage, cryovials were later transferred to liquid nitrogen. For thawing, cryovials were removed from liquid nitrogen and briefly warmed in a 37 °C water bath. To eliminate residual DMSO promptly, the thawed cells were centrifuged at 1,200 rpm for 5 minutes, washed once with PBS, resuspended in fresh cell culture medium and transferred to new cell culture dishes. Cultured cells were regularly replaced, typically every two months. Mycoplasma contamination was routinely checked via polymerase chain reaction (PCR) conducted by a technical assistant.

2.7.1.2 Sf9 cells

Sf9 cells were grown in Sf-900 II SFM medium (Gibco) under conditions of 27 °C with agitation at 90 rpm. Freezing of the cells was performed as described before. The freezing medium was prepared by supplementing the Sf-900 II SFM medium with 30 % FCS and 10 % DMSO.

2.7.2 Transfections

2.7.2.1 Plasmid transfections of HeLaK, U2OS, HEK293T and HCT116 cells

Cells were seeded 24 h prior to transfection according to Table 2.7.2.1.1.

Table 2.7.2.1.1: Cell numbers seeded for transfection in different cell culture dishes

cell culture dish	growth area [cm^2]	cell number
6-well	8.87	1.0×10^5
100/20 mm	58	6.5×10^5
145/20 mm	143	1.6×10^6

Transfections of HeLaK, U2OS and HCT116 cells were performed using FuGENE HD Transfection Reagent (Promega) according to the manufacturer's instructions. Transfection mix was prepared according to Table 2.7.2.1.2.

Table 2.7.2.1.2: Transfection mix for different cell culture dishes

Cell culture dish	Medium [mL]	DNA [µg]	H_2O [µL]	Opti-MEM [µL]	FuGENE HD [µL]
6-well	2	2	to 10	90	8
100/20 mm	10	10	to 50	450	40
145/20 mm	20	20	to 100	900	80

Transfections of HEK293T cells were performed using the calcium phosphate method as previously described (Chen & Okayama, 1987). Unless stated otherwise, cells were harvested for experiments 48 h after transfection.

2.7.2.2 Bacmid transfections of Sf9 cells

Bacmids were generated using the Bac-to-Bac baculovirus expression system (Gibco). The transfection process was carried out using the ExpiFectamine Sf transfection reagent (Gibco) in line with the protocol provided by the manufacturer. To enhance viral

production, the culture medium from the transfected cells was collected one day post-transfection and used to infect a new batch of cells. Following one or two infection cycles, the medium from these infected cultures was harvested and preserved as viral stocks at 4 °C.

2.7.2.3 siRNA transfections of HeLaK cells

To achieve RNAi-mediated knockdown, ON-TARGETplus SMARTpool siRNAs (Horizon Discovery), either targeting ZNF512B mRNA or a non-targeting control, were introduced into cells using the DharmaFECT1 transfection reagent (Horizon Discovery) following the provided protocol. In brief, 1×10^5 HelaK cells were plated in a 6-well plate 24 h prior to transfection. For preparation, 10 µL of 5 µM siRNAs were combined with 190 µL of Opti-MEM reduced serum medium (Gibco). Separately, 4 µL of DharmaFECT1 was mixed with 196 µL of Opti-MEM in another tube. Both mixtures were left to rest for 5 min before being combined and incubated together for 20 min. Meanwhile, cells were rinsed once with PBS and 1.6 mL of DMEM, supplemented with 10 % FCS but without P/S, was added. The final transfection mixture was then added dropwise to the cells, which were incubated for 48 h before further experiments were performed.

2.7.3 Generation of HeLaK cells inducibly expressing GFP or GFP-ZNF512B

Transfections were done as described. 24 h after transfection, selection was started by addition of blasticidin S to the medium at a final concentration of 10 µg/mL. Selection was performed for two weeks. Expression of fusion proteins was induced 48 h before starting experiments by addition of doxycycline to the medium at a final concentration of 1 µg/mL.

2.7.4 Flow cytometry analysis

Flow cytometry analysis was performed using the BD Accuri C6 Plus Flow Cytometer (BD Biosciences). Typically, 200 µL of cell suspensions were used for analysis and 50,000 events were measured. The gate was plotted to forward (FSC) and sideward (SSC)

scatter into the viable cell population of suitable control cells. Data processing was carried out using the included software.

2.7.5 Immunofluorescence (IF) microscopy

IF staining and microscopy were conducted following previously established methods (Herchenrother, Gossen, et al., 2023). In summary, 1×10^5 cells were seeded onto coverslips placed in 24-well plates and grown overnight. The next day, cells were rinsed twice with PBS and fixed for 15 min using 1 % formaldehyde in PBS. Following fixation, cells were treated with a blocking and permeabilization solution consisting of PBS containing 0.1 % Triton X-100 and 1 % BSA (PBS-T + BSA) for 20 min. Cells were then sequentially incubated with primary and secondary antibodies prepared in PBS-T + BSA for 30 minutes each, with three rinses using PBS-T performed between the antibody applications. After a final set of three washes with PBS-T, nuclei were stained with 10 µg/mL Hoechst solution for 3 minutes. After a water rinse, the coverslips were mounted on microscope slides using Fluoromount G mounting medium (SouthernBiotech). Imaging was carried out on a Carl Zeiss Axio Observer.Z1 inverted microscope equipped with an Axiocam 506 mono camera. Images were processed using the Zeiss Zen software (version 3.1, blue edition), and intensity profiles were generated using the ImageJ2 distribution Fiji (Schindelin et al., 2012).

2.7.6 Senescence associated (SA)-β-galactosidase activity staining

To assess SA-β-galactosidase activity *in situ*, 1×10^5 cells were plated onto coverslips within 24-well plates. Control cells were treated with 100 nM doxorubicin (Thermo Fisher Scientific) for two days before staining. The staining procedure followed a previously established protocol (Lee et al., 2006). Briefly, after rinsing the cells in PBS, they were fixed in 3.7 % formaldehyde. Subsequently, cells were incubated overnight at 37 °C in freshly prepared staining solution composed of PBS at pH 6.0, 2 mM $MgCl_2$, 5 mM potassium ferricyanide ($K_3Fe[CN]_6$), 5 mM potassium ferrocyanide ($K_4Fe[CN]_6$) and 1 mg/mL X-gal. After being washed with water, the coverslips were mounted, and cells were visualized using the same procedure as described for IF microscopy.

2.7.7 Terminal deoxynucleotidyl transferase dUTP nick end labeling (TUNEL) assay

TUNEL assays were conducted using the One-Step TUNEL In Situ Apoptosis Kit (Elabscience) according to the kit's instructions. Cells were fixed and permeabilized following the steps outlined for IF microscopy. For generating a positive control, coverslips were treated with DNase I buffer for 5 min at room temperature, followed by incubation with DNase I working solution at 37 °C for 30 min. For the negative control, coverslips were exposed to DNase I buffer under the same conditions without subsequent DNase I treatment. All samples were then incubated with TdT equilibration buffer for 30 min at 37 °C before being treated with the labeling working solution (without enzyme for negative control) for 60 min in a dark, humidified environment at 37 °C. Finally, cells were stained with DAPI working solution for 5 min in the dark at room temperature, and the coverslips were mounted onto slides for imaging, as previously described for IF microscopy.

2.8 DNA-based methods

2.8.1 Generation of eukaryotic expression vectors

Plasmids for protein expression in different cell lines were typically generated via restriction enzyme-based cloning. Therefore, target DNA was amplified via PCR using primers containing specific restriction enzyme recognition sites. DNA fragments and target vectors were then digested using FastDigest restriction enzymes (Thermo Fisher Scientific). Target vectors were additionally dephosphorylated using FastAP thermosensitive alkaline phosphatase (Thermo Fisher Scientific) to avoid backbone relegation. After subsequent agarose gel electrophoresis and gel extraction using the EXTRACTME DNA Clean-Up & Gel-Out kit (Blirt), DNA fragments and target vectors were ligated using T4 DNA Ligase (Thermo Fisher Scientific). *E. coli* cells were transformed with the generated plasmids and incubated on agar plates. Bacterial colonies were tested for the desired plasmids via PCR and used to inoculate suspension cultures. Plasmids were extracted using the EXTRACTME Plasmid Mini kit. DNA concentration was measured using a NanoPhotometer (Implen). DNA sequences of purified plasmids were verified via Sanger sequencing at Microsynth Seqlab using appropriate sequencing primers. Validated plasmids were used for retransformation and purification using the EXTRACTME Plasmid Midi kit. If direct digestion of PCR products turned out

unsuccessful, DNA fragments were subcloned beforehand via TOPO TA cloning. ZNF512B, ZBTB20 and ZNF148 coding sequences were amplified from HeLaK cDNA previously generated in the group. pTetLS was a gift from Prof. Dr. Lienhard Schmitz (Institute of Biochemistry, Medical Faculty, Justus-Liebig University Giessen, Germany). H2B-mRFP (Martin & Cardoso, 2010) was a gift from Prof. Dr. M. Cristina Cardoso (Cell Biology and Epigenetics, Department of Biology, Technical University of Darmstadt, Germany). pFBDM-6xHis-RBBP4 was a gift from Prof. Dr. Joel Mackay (School of Life and Environmental Sciences, University of Sydney, Australia). pFlag-FOXJ1 (Moparthi & Koch, 2020) was a gift from Stefan Koch (Addgene plasmid #153129). pFastBac1 was part of the Bac-to-Bac baculovirus expression system (Gibco). pIRESneo-eGFP (Zink et al., 2017), pEGFP-N2, p3xFLAG-CMV-10, pAB-Gal94 (Baniahmad et al., 1995), p4xUAS-tk-luc, pCMV-lacZ and pBluescript-II-SK(+) were already in stock of the group. Most important plasmid maps (created with SnapGene) can be found in the appendix (Figures 7.1.1–7.1.5).

2.8.2 Polymerase chain reaction (PCR)

PCRs were performed using Q5 High-Fidelity 2X Master Mix (New England Biolabs) following the manufacturer's protocol. Thermocycling conditions for a routine PCR are shown in Table 2.8.2.

Table 2.8.2: Thermocycling protocol for routine PCR with Q5 High-Fidelity DNA Polymerase

Step	Temperature	Time
Initial denaturation	98 °C	30 s
25–35 ×	98 °C	10 s
	*50–72 °C	30 s
	72 °C	30 s/kb
Final extension	72 °C	2 min
Hold	4 °C	∞

**Annealing temperatures were calculated using the NEB T_m Calculator*

2.8.3 Transformation of *E. coli* cells and preparation of bacterial suspension cultures

Chemically competent DH5α *E. coli* strains were used for plasmid amplification. Transformation was carried out via heat shock. Therefore, 50 µL of *E. coli* cells with

added plasmid DNA were incubated on ice for 30 min, followed by incubation at 42 °C for 60 s and another incubation on ice for 5 min. Afterwards, cells were combined with 200 µL SOC medium and incubated for 1 h at 37 °C with gentle shaking at 300 rpm. Subsequently, the mixture was spread directly onto pre-warmed lysogeny broth (LB) agar plates containing suitable antibiotics. Plates were stored overnight at 37 °C. Bacterial suspension cultures were prepared by inoculating 5 mL of LB medium containing appropriate antibiotics and incubation overnight at 37 °C and 150 rpm.

2.8.4 Colony PCR

Bacterial colonies were tested for desired plasmids via PCR with suitable primers using GoTaq DNA Polymerase (Promega). PCR reaction mix was prepared following the manufacturer's instructions but instead of template DNA, a bacterial colony was added using a pipette tip. The same tip was used to inoculate a corresponding suspension culture. Thermocycling was performed under the conditions shown in Table 2.8.4, and generated DNA fragments were analyzed in subsequent agarose gel electrophoresis.

Table 2.8.4: Thermocycling protocol for routine PCR with GoTaq DNA Polymerase

Step	Temperature	Time
Initial denaturation	95 °C	2 min
25–35 ×	95 °C	60 s
	*42–65 °C	60 s
	72 °C	60 s/kb
Final extension	72 °C	5 min
Hold	4 °C	∞

**Annealing temperatures were calculated using the Promega T_m for Oligos Calculator*

2.8.5 TOPO TA cloning

Since 3′ A-overhangs are necessary for TA cloning and PCR products were generated using the Q5 High Fidelity DNA polymerase (New England Biolabs), which is a proofreading polymerase removing these overhangs, DNA fragments were purified using the EXTRACTME DNA Clean-Up & Gel-Out kit (Blirt) and incubated with GoTaq DNA Polymerase (Promega) for 10 min at 72 °C. Subsequently, subcloning was performed using the TOPO TA Cloning kit (Invitrogen) following the manufacturer's instructions. The TOPO cloning reaction was performed with salt for 30 min.

2.8.6 Site-directed mutagenesis (SDM)

Introduction of point mutations into plasmid DNA was done as previously described (Liu & Naismith, 2008). In brief, primers were designed with a primer-primer complementary (PP) part, incorporating the desired mutations, and non-overlapping (NO) parts at the 3′ ends, with annealing temperatures 5–10 °C above the annealing temperature of the primer-primer complementary part. Then, PCR was performed with Q5 High Fidelity DNA polymerase (New England Biolabs) under the thermocycling conditions shown in Table 2.8.6. Afterwards, PCR products were digested with DpnI to remove template DNA.

Table 2.8.6: Thermocycling protocol for SDM with Q5 High-Fidelity DNA Polymerase

Step	Temperature	Time
Initial denaturation	98 °C	30 s
17 ×	98 °C	10 s
	*50–72 °C	30 s
	72 °C	30 s/kb
1 ×	98 °C	10 s
	**50–72 °C	30 s
	72 °C	30 s/kb
Final extension	72 °C	2 min
Hold	4 °C	∞

**Annealing temperature for NO calculated using the NEB T_m Calculator*
***Annealing temperature for PP calculated using the NEB T_m Calculator*

2.9 Protein-based methods

2.9.1 Preparation of nuclear extracts

For nuclear preparation, cells were incubated in 1 mL Hypotonic Lysis buffer (Table 2.9.1) supplemented with 1 µL protease inhibitor mix rotating at 4 °C for 30 min. Afterwards, samples were centrifuged for 10 min at 4 °C and 10,000 rpm. Supernatants were discarded, and nuclei were incubated in SDS sample buffer at 95 °C for 5 min.

Table 2.9.1: Composition of buffer for nuclear extract preparation

Buffer	Concentration	Component
Hypotonic Lysis buffer	10 mM	Tris/Cl pH 8.0
	1 mM	KCl
	1.5 mM	$MgCl_2$

2.9.2 Coomassie Staining

To visualize proteins separated by SDS-PAGE, gels were incubated with Coomassie staining solution overnight at room temperature. The following day, they were incubated with destaining solution multiple times and subsequently immersed in gel saver solution. The documentation of gels was done using an LED light plate (Kaiser) and a digital single-lens reflex (DSLR) camera (Nikon).

2.9.3 Immunoblot

To detect specific proteins separated by SDS-PAGE, gels were equilibrated with transfer buffer for 15 min. Subsequently, proteins were transferred onto a nitrocellulose membrane via semi-dry electroblotting at 200 mA for 1 h. Membranes were then blocked using PBS supplemented with 0.1 % Tween20 (PBS-T) and 5 % milk powder to prevent non-specific antibody binding to the membrane. The primary antibody incubation was carried out in blocking solution overnight at 4 °C with gentle rotation. The following day, membranes were washed three times with PBS-T for 5 min each at room temperature. Next, secondary antibodies conjugated with horseradish peroxidase (HRP) were applied in blocking solution for 1 h at room temperature with gentle shaking. After this, membranes were again washed three times with PBS-T for 5 min each at room temperature. Finally, membranes were incubated with Trident femto Western HRP substrate (GeneTex) and analyzed in a chemiluminescence imager (Intas).

2.9.4 DNase immunoprecipitation (DNase-IP) and peptide competition

Preparation of DNase-digested cell extracts and immunoprecipitation were performed using GFP-Trap Magnetic Particles M-270 (Chromotek) following the manufacturer's protocol. 1×10^6 cells per sample were incubated on ice for 30 min in 200 µL RIPA buffer (Table 2.9.4) supplemented with 25 U DNase I (Thermo Fisher Scientific), 2.5 mM $MgCl_2$ and 0.2 µL protease inhibitor mix. Tubes were inverted several times every 10 min. After centrifugation at 17,000× g for 10 min at 4 °C, supernatants were transferred to fresh tubes and mixed with 300 µL Dilution buffer supplemented with 0.3 µL protease inhibitor mix. Lysates were then incubated rotating for 1 h at 4 °C with 10 µL of GFP-Trap Magnetic Particles M-270, which had been equilibrated with 500 µL Wash buffer beforehand. For peptide competition, lysates were incubated with peptide solution rotating for 1 h at 4 °C prior to incubation with beads. Next, beads were washed three times with 500 µL Wash buffer rotating at 4 °C for 5 min each. Precipitated proteins were eluted by incubation of beads at 95 °C for 5 min in 2×SDS sample buffer.

Table 2.9.4: Composition of buffers for DNase-IP

Buffer	Concentration	Component
RIPA buffer	10 mM	Tris/Cl pH 7.5
	150 mM	NaCl
	0.5 mM	EDTA
	0.1 %	SDS
	1 %	Triton X-100
	1 %	deoxycholate
Dilution buffer	10 mM	Tris/Cl pH 7.5
	150 mM	NaCl
	0.5 mM	EDTA
Wash buffer	10 mM	Tris/Cl pH 7.5
	150 mM	NaCl
	0.05 %	Nonidet P-40 substitute
	0.5 mM	EDTA

2.9.5 MNase immunoprecipitation (MNase-IP), MS sample preparation and native ChIP-qPCR

Preparation of micrococcal nuclease (MNase)-digested nuclear extracts and immunoprecipitation were performed as previously described (Herchenrother, Gossen, et al., 2023; Link et al., 2018; Punzeler et al., 2017; Vardabasso et al., 2015). Nuclei of 4×10^7 cells were isolated by incubation with 5 mL PBS supplemented with 0.3% Triton X-100 and 5 µL protease inhibitor mix for 10 min at 4 °C. Nuclei were then pelleted, washed with PBS and resolved in 500 µL freshly prepared EX100 buffer (Table 2.9.5) supplemented with 2 mM $CaCl_2$ and 0.5 µL protease inhibitor mix. Next, chromatin was digested with 1.5 U MNase (Sigma-Aldrich) for 20 min at 26 °C. Digestion was stopped by adding 10 mM EGTA, and samples were centrifuged for 30 min at 13,000 rpm and 4 °C. Supernatants were transferred to fresh tubes. Samples were subsequently incubated with 25 µL of equilibrated GFP-Trap Magnetic Particles M-270 (Chromotek) overnight rotating at 4 °C. Beads were washed twice with 1 mL Wash buffer I and twice with 1 mL Wash buffer II. For analysis via immunoblot, precipitated proteins were eluted by incubation of beads at 95 °C for 5 min in 2×SDS sample buffer. For analysis via mass spectrometry, precipitated proteins were eluted by incubation of beads with Elution buffer for 30 min at 37 °C and 1,400 rpm in the dark. Supernatants were transferred into fresh tubes, and beads were further incubated in Alkylation buffer for 5 min at 37 °C and 1,400 rpm in the dark. Both eluates were combined and incubated overnight at 25 °C and 800 rpm in the dark. The next day, trypsin digestion was stopped by addition of 1 % trifluoroacetic acid (Thermo Fisher Scientific). For analysis via qPCR, beads were incubated for 30 min at 37 °C in 100 µL TE buffer supplemented with 1 µL RNase A (10 mg/mL, Thermo Fisher Scientific). Afterwards, 5 µL 10 % SDS and 2.5 µL Proteinase K (20 mg/mL, Thermo Fisher Scientific) were added, and beads were incubated at 37 °C for 4 h followed by 65 °C overnight. After centrifugation for 2 min at 5,000 rpm, supernatants were transferred into fresh tubes. Chromatin was purified using the MinElute PCR Purification kit (Qiagen) and analyzed via qPCR.

Table 2.9.5: Composition of buffers for MNase-IP

Buffer	Concentration	Component
EX100	10 mM	HEPES pH 7.6
	100 mM	NaCl
	1.5 mM	$MgCl_2$
	0.5 mM	EGTA
	10 %	Glycerol
	10 mM	β-glycerol phosphate
Wash buffer I	10 mM	Tris/Cl pH 7.5
	150 mM	NaCl
	0.1 %	Nonidet P-40 substitute
Wash buffer II	10 mM	Tris/Cl pH 7.5
	150 mM	NaCl
Elution buffer	2 M	Urea
	50 mM	Tris/Cl pH 7.5
	2 mM	DTT
	20 µg/mL	Trypsin Gold (Promega)
Alkylation buffer	2 M	Urea
	50 mM	Tris/Cl pH 7.5
	10 mM	chloroacetamide
TE buffer	10 mM	Tris/Cl pH 8.1
	1 mM	EDTA

2.9.6 Label-free quantitative mass spectrometry (lfqMS/MS)

2.9.6.1 MS data acquisition

Peptides were desalted on StageTips (Rappsilber et al., 2007) and analyzed by nanoflow liquid chromatography on an EASY-nLC 1000 system (Thermo Fisher Scientific) coupled online to a Q Exactive Plus mass spectrometer (Thermo Fisher Scientific). Peptides were separated on a C18-reversed phase capillary (25 cm long, 75 µm inner diameter) packed with ReproSil-Pur C18-AQ 1.9 µm resin (Dr. Maisch) mounted directly on the electrospray ion source. A gradient from 2 % to 60 % acetonitrile in 0.5 % formic acid at a flow of 225 nL/min was applied for 90 min. The Q Exactive Plus was operated with a Top10 MS/MS spectra acquisition method per MS full scan.

2.9.6.2 MS data analysis

Raw files were processed with MaxQuant (version 1.6.5.0) (Cox & Mann, 2008) against a human uniprot database (81,194 entries). Carbamidomethylation was set as fixed modification while methionine oxidation and protein *N*-acetylation were considered as variable modifications. The search was performed with an initial mass tolerance of 7 ppm mass accuracy for the precursor ion and 20 ppm for the MS/MS spectra in the HCD fragmentation mode. Search results were processed with MaxQuant and filtered with a false discovery rate of 0.01. The 'match-between-runs' option and the label-free quantitation were activated. Protein groups marked as reverse, contaminants, only identified by site and less than 2 peptides (at least 1 unique) were removed. Non-measured values were imputed with a beta distribution at the limit of quantitation. For creating the volcano plots, a p-value of a two-tailed Welch's t-test was calculated. Plots were created using the ggplot2 package (Wickham, 2016).

2.9.7 Expression and purification of recombinant proteins

Expression and purification of recombinant His-ZNF512B (for EMSAs) and His-RBBP4 (for FP) proteins was done as described (Herchenrother, Gossen, et al., 2023). Sf9 cell extracts were prepared three days after infection. Therefore, cells were washed twice with ice-cold PBS and subsequently incubated in Hypotonic buffer (Table 2.9.7) on ice for 10 min, followed by brief vortexing and centrifugation. Nuclei were then incubated in Hypertonic buffer on ice for 20 min. After centrifugation for 10 min at 16,000× g, supernatants were purified via FPLC using the Äkta Start (Cytiva) with a HisTrap HP column (71502768) following the manufacturer's instructions. His-RBBP4 was further purified with a HiTrap Q HP anion exchange column (29051325).

Table 2.9.7: Composition of buffers for protein extraction from Sf9 cells

Buffer	Concentration	Component
Hypotonic buffer	10 mM	HEPES-KOH pH 7.9
	10 mM	KCl
	1.5 mM	$MgCl_2$
Hypertonic buffer	20 mM	HEPES-KOH pH 7.9
	25 %	Glycerol
	420 mM	NaCl
	1.5 mM	$MgCl_2$
	0.2 mM	EDTA

2.9.8 Electrophoretic mobility shift assays (EMSAs)

EMSAs were performed as originally described (van de Nobelen et al., 2010). 300 ng of salmon sperm DNA were used per reaction as unspecific competitor. Cy5-labelled unmethylated or Cy3-labelled methylated (all eight cytosines in a CpG context) double-stranded oligos were used as probes.

2.9.9 Fluorescence polarization (FP)

To determine the dissociation constant (k_D), serial dilutions of RBBP4 protein (10–0 µM) in 50 mM Tris/Cl pH 7.5, 150 mM NaCl and 0.02 % Triton X-100 were combined with 1 nM fluorescently-tagged tracer peptide. Polarization (P) was measured after 60 min using a Spark 20M microplate reader (Tecan). k_D values were then calculated by converting the P values into their corresponding anisotropy (A) values following the equation:

$$A = \frac{2P}{3 - P}$$

These values were plotted versus the respective concentrations of the protein with a non-linear regression according to the following equation:

$$A = A_f + (A_b - A_f)\frac{(L_T + k_D + R_T) - \sqrt{(L_T - k_D - R_T)^2 - 4L_T R_T}}{2L_T}$$

Here, A_f is the anisotropy for the free ligand, A_b is the anisotropy for the fully bound ligand, L_T is the total added concentration of ligand and R_T is the total receptor concentration. For the competitive binding experiments, RBBP4 protein was incubated with tracer peptide in 50 mM Tris/Cl pH 7.5, 150 mM NaCl and 0.02 % Triton X-100 for 60 min to form the protein-tracer complex. Next, serial dilutions (1.0–0.0 mM) of the corresponding peptide were added, with a final concentration of 1 nM tracer and 40 nM protein, and after 60 min, *P* values were measured and plotted against the logarithmic peptide concentration. The inhibitory concentration (IC_{50}) was determined by fitting the dose-response to four parameter logistic (4PL) curves in GraphPad Prism (version 6). Inhibition constant (k_i) values were calculated using the following equation (Nikolovska-Coleska et al., 2004):

$$k_i = \frac{[I]_{50}}{\frac{[L]_{50}}{k_D} + \frac{[P]_0}{k_D} + 1}$$

Here, $[I]_{50}$ is the concentration of free inhibitor at 50 % inhibition, $[L]_{50}$ is the concentration of free labelled ligand at 50 % inhibition and $[P]_0$ is the concentration of free protein at 0 % inhibition.

2.9.10 Luciferase reporter assay

1.5×10^5 HEK293T cells were seeded per well of a 6-well plate and transfected the next day with 1 µg of p4xUAS-tk-luc reporter plasmid, 0.5 µg GAL expression vector and 0.5 µg pCMV-lacZ vector for normalization. After 72 h, cells were directly lysed in well with 200 µL Lysis buffer (Table 2.9.10) for 15 min at room temperature. Supernatants were mixed 1:1 with 100 µL 90 mg/L D-Luciferin/0.8 mM ATP. After 5 sec incubations, luciferase activity was measured by quantifying emitted light with an Orion L plate reader (Titertek-Berthold). Values were normalized to β-galactosidase activity by mixing 5 µL supernatant with 900 µL LacZ buffer and 100 µL 4 g/L OPNG/0.1 M KPO_4 and measuring absorbance at 420 nm when a color change of the mixture occurred.

Table 2.9.10: Composition of buffers for luciferase reporter assay

Buffer	Concentration	Component
Lysis buffer	25 mM	Tris/Cl pH 7.5
	8 mM	$MgCl_2$
	1 mM	EDTA
	1 %	Triton X-100
	15 %	Glycerol
	1 mM	DTT
LacZ buffer	0.1 mM	$MgSO_4$ pH 7.0
	50 mM	Na_2HPO_4
	10 mM	KCl

2.9.11 Structure determination

2.9.11.1 Peptide synthesis

A peptide encompassing residues 419–430 of human ZNF512B was chemically synthesized and purified by ChinaPeptides. The peptide was N-terminally acetylated and C-terminally amidated.

2.9.11.2 Expression and purification of recombinant RBBP4

Expression of recombinant RBBP4 in Sf9 cells was done as previously described (Lejon et al., 2011). Cells were lysed by sonication on ice in Lysis buffer (Table 2.9.11.2) supplemented with a cOmplete EDTA-free protease inhibitor tablet (Roche). Afterwards, 0.1 % NP-40 and 10 µg/mL DNase I were added, and the lysate was clarified by centrifugation. The supernatant was incubated with nickel-nitrilotriacetic acid beads (Qiagen) for 2 h at 4 °C. The beads were then washed with Lysis buffer containing increasing concentrations of imidazole (2, 20 and 40 mM). RBBP4 was eluted with 500 mM imidazole, and the His-tag was cleaved by overnight dialysis at 4 °C in 20 mM Tris/Cl pH 8.0, 150 mM NaCl, 2.5 mM $CaCl_2$ and 500 U thrombin. Next, RBBP4 was purified by size-exclusion chromatography in 20 mM Tris/Cl pH 7.5, 150 mM NaCl and 1 mM DTT using a HiLoad 16/60 Superdex 75 pg column (Cytiva). Fractions containing purified RBBP4 were concentrated to 5 mg/mL and stored at -20 °C.

Table 2.9.11.2: Composition of buffer for extraction of recombinant RBBP4 from Sf9 cells

Buffer	Concentration	Component
Lysis buffer	20 mM	Tris/Cl pH 8.0
	150 mM	NaCl
	10 mM	$MgCl_2$
	1 mM	β-mercaptoethanol

2.9.11.3 Crystallization and structure determination

The ZNF512B peptide was dissolved in demineralized water to a concentration of 10 mM. RBBP4 was mixed with ZNF512B peptide at a molar ratio of 1:2 and incubated on ice for 2 h. Crystallization trials were set up at 4 °C in 96-well plates as sitting drops using 0.2 µL protein solution and 0.1 µL crystallization solution. Single crystals were obtained in 0.1 M MES/imidazole pH 6.5, 40 % ethylene glycol, 20 % PEG 8000 and 0.1 M mixture of carboxylic acids (Morpheus screen, Molecular Dimensions). Crystals were harvested into a cryoprotectant solution containing 25 % glycerol in mother liquor before being transferred to liquid nitrogen. X-ray diffraction data were collected on the MX2 beamline (microfocus) at the Australian Synchrotron at 100 K and a wavelength of 0.9537 Å. The dataset was processed and scaled at 2.2 Å resolution using XDS (Kabsch, 2010) and Scala (Evans, 2006). The RBBP4-ZNF512B structure was solved by molecular replacement using PHENIX phaser-MR (Adams et al., 2002) with RBBP4-FOG-1 (PDB: 2XU7) as a search model without FOG-1 or other ligands. The crystal belonged to space group P 1 21 1, with two molecules in the asymmetric unit. Further model building was performed by iterative rounds of manual model building in real space using COOT (Emsley et al., 2010), followed by refinement using REFMAC5 (Murshudov et al., 2011) and PHENIX (Adams et al., 2002). Validation of the structure was carried out with MolProbity (Davis et al., 2007). Interface analysis was performed using the EBI PISA server (Krissinel & Henrick, 2007) and PDBsum (Laskowski et al., 2018). Figures were generated using PyMOL (DeLano, 2002). Data collection and refinement statistics can be found in Table 2.9.11.3.

Table 2.9.11.3: Data collection and refinement statistics for RBBP4-ZNF512B structure

Data collection	
Space group	P 1 21 1
Cell dimensions a, b, c (Å) α, β, γ (°)	 76.10, 59.58, 101.45 90, 93.77, 90
Resolution (Å)	46.88 - 2.20 (2.32 - 2.20)
R_{merge}	0.156 (1.238)
$CC_{1/2}$	0.991 (0.493)
$I / \sigma I$	6.5 (1.3)
Completeness (%)	100 (100)
Redundancy	3.5 (3.6)
Refinement	
Resolution (Å)	46.88 - 2.20
No. reflections	46302 (4563)
R_{work} / R_{free}	0.21 (0.33) / 0.24 (0.35)
Ramachandran statistics Favoured (%) Allowed (%) Outliers (%)	 97.11 2.63 0.26
Number of non-hydrogen atoms Macromolecules Ligands Solvent	 6185 161 337
Average B-factor	41.40
R.m.s deviations Bond lengths (Å) Bond angles (°)	 0.005 0.80

2.10 RNA-based methods

2.10.1 RNA extraction and RT-qPCR

Total RNA from different human tissues was purchased from Applied Biosystems and BioChain and used as previously described (Wiedemann et al., 2010). RNA extraction was performed as described (Procida et al., 2021). Briefly, total RNA was extracted using the RNeasy Mini kit (Qiagen) with on-column DNase digest using the RNase-Free DNase set (Qiagen) following the manufacturer's protocol. 1 µg total RNA was reverse transcribed using the Transcriptor First Strand cDNA Synthesis kit (Roche) with random hexamer primers according to the manufacturer's instructions. For subsequent qPCR analysis, technical triplicates of 6 µL cDNA (1:20 dilution), 7.5 µL iTaq Universal SYBR Green Supermix (Bio-Rad) and 1.5 µL primer mix (5 µM forward and reverse primer) were prepared. The qPCR thermocycling conditions can be found in Table 2.10.1. Ct values of technical triplicates were averaged, and fold change expression was calculated with the Delta-Delta Ct method, normalizing to HPRT1 expression.

Table 2.10.1: Thermocycling protocol for qPCR with iTaq Universal SYBR Green Supermix

Step	Temperature	Time
Initial denaturation	95 °C	5 min
40 ×	95 °C	3 s
	60 °C	20 s
Melting curve	65–95 °C	12 °C/min

2.10.2 mRNA sequencing and analysis

mRNA sequencing was performed at Biomarker Technologies. Raw sequencing files (FASTQ) were adaptor and quality trimmed using trimGalore (Krueger, 2015). Alignment of the trimmed sequencing reads to the hg19 reference genome (Church et al., 2011) was performed using HISAT2 (version 2.2.1) with '--min-intronlen 30 –max-intronlen 3000' parameters (Kim et al., 2019) and stored as binary alignment maps (BAM). Read count per gene tables based on BAM files were generated within R using the summarizeOverlaps function of the GenomicAlignments package (Lawrence et al., 2013). Normalization of read counts and detection of differentially expressed genes was calculated with DESeq2 (Love et al., 2014) based on the read counts per gene tables. If not indicated differently, significantly differentially expressed genes were selected using a $\log_2$FC threshold of > 1 or < -1 and an adjusted p-value < 0.05. Identification of enriched

biological pathways was performed using clusterProfiler (Wu et al., 2021). Volcano plots were generated with the EnhancedVolcano R package (Blighe et al., 2023).

3 Results

3.1 ZNF512B contains several unidentified but highly conserved domains

Since the number of studies on ZNF512B is rather low (Chapter 1.2.1), I decided to start with a broad analysis of the protein's expression, structure, domains and conservation. Via RT-qPCR, I detected the expression levels of ZNF512B's mRNA in different tissues and cell types (Figure 3.1.1, with help from Lena Paasche, Institute for Genetics, Justus-Liebig University Giessen, Germany). These were relatively low in all tested samples, with the highest levels in brain and tumor tissues.

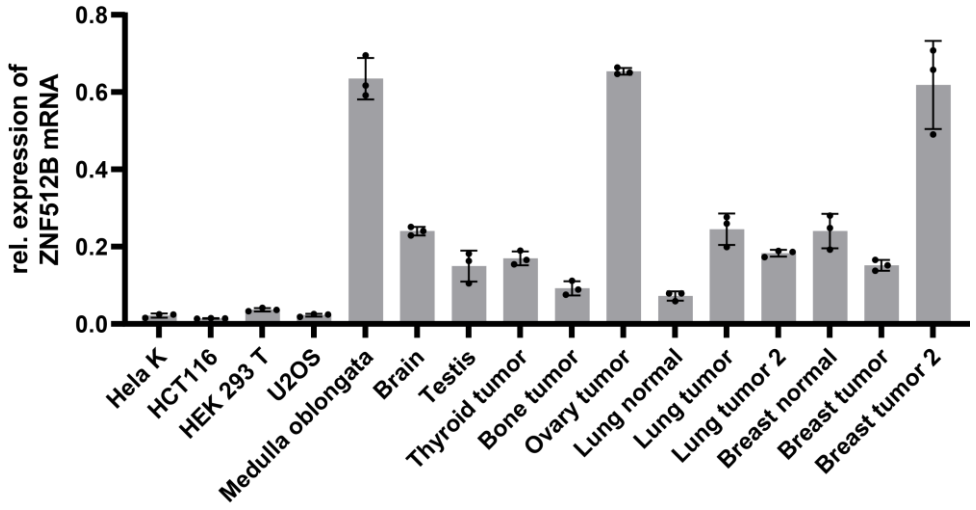

Figure 3.1.1: The levels of ZNF512B mRNA are relatively low in several tissues and cell types. *RT-qPCR to detect relative ZNF512B mRNA expression in different human tissues and cell lines normalized to HPRT1 expression. Depicted is the mean with standard deviation (SD) of three technical replicates.*

As ZNF512B is a nuclear protein (Chapter 1.2.1), I searched its amino acid sequence for a nuclear localization signal (NLS) with cNLS Mapper and could localize a bipartite NLS inside the internal region (Figure 3.1.2A) (Kosugi et al., 2008; Kosugi, Hasebe, Matsumura, et al., 2009; Kosugi, Hasebe, Tomita, et al., 2009). Next, I predicted ordered and disordered protein regions of ZNF512B using PONDR (Figure 3.1.2A) (Li et al., 1999; Oates et al., 2013; Romero et al., 2001). Huge parts of ZNF512B were predicted to be intrinsically disordered, especially its large internal region. The regions predicted as ordered were mainly corresponding to the four ZF pairs. Interestingly, while the known repeat domain and the putative leucine zipper were localized in predicted disordered regions, there were two undefined sections of ZNF512B, in the internal domain and between ZF pairs three and four, that were also predicted as ordered. I decided to have a

closer look at these domains via the AlphaFold protein structure database (Jumper et al., 2021; Varadi et al., 2022). First, I analyzed the complete ZNF512B protein, which was, again, predicted to be largely unstructured (Figure 3.1.2B). Then, I focused on the eight ZF domains (Figure 3.1.2C). While the four typical C_2H_2 ZFs were predicted to form the characteristic ββα fold (Chapter 1.2), intriguingly, all four atypical C_2HC ZFs were predicted to form a αββα structure, with a second α-helix upstream of the two β-sheets. In the region of the putative leucine zipper, two β-sheets are predicted to form (Figure 3.1.2D). Just upstream of that position, one of the additional ordered regions is predicted to form a previously unidentified α-helix (Figure 3.1.2E). Remarkably, the known repeat region is suggested to form a large β-helix (Figure 3.1.2F). Lastly, while analyzing the second additional ordered region inside the internal domain of ZNF512B, I identified an amino acid sequence that, interestingly, resembles the N-terminal NIM, which facilitates direct RBBP4 interaction in several TFs like FOG-1, SALL1/4 and BCL11A (Chapter 1.1.4.1) (Figure 3.1.2G). Therefore, this sequence could potentially also facilitate NuRD interaction.

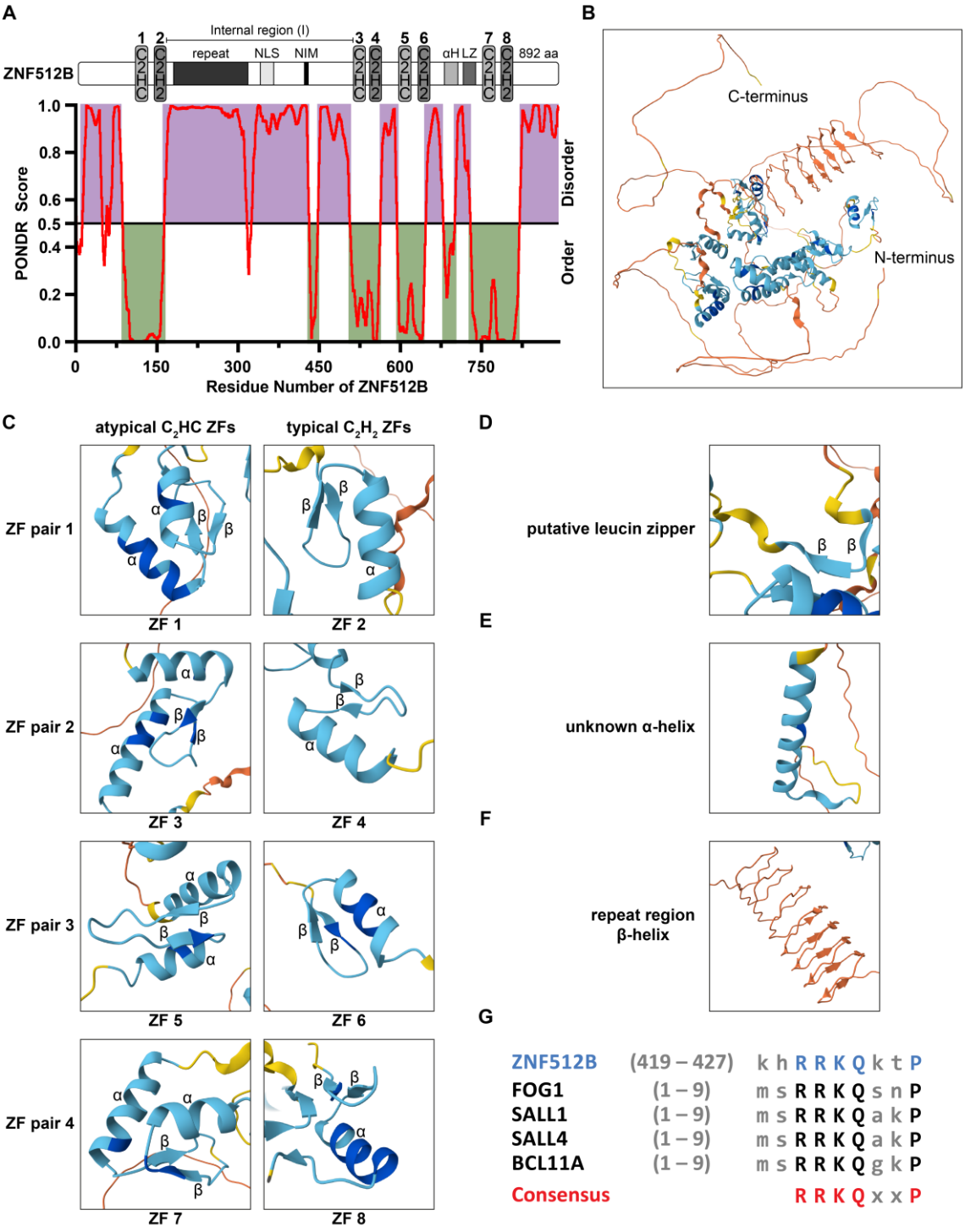

Figure 3.1.2: ZNF512B contains a previously unidentified α-helix and putative NIM. (A) Top: *Schematic depiction of the human ZNF512B protein with four pairs of atypical C_2HC (light grey) and typical C_2H_2 (dark grey) ZFs, a repeat region, an NLS, a putative NIM, an unknown α-helix (αH) and a putative leucine zipper (LZ).* ***Bottom:*** *Ordered and disordered regions of human ZNF512B (NP_065764.1) as predicted by PONDR using the predictor VLXT.* ***(B-F)*** *Snapshots from the AlphaFold protein structure database of* ***(B)*** *the complete ZNF512B structure,* ***(C)*** *the eight ZF domains,* ***(D)*** *the putative leucine zipper,* ***(E)*** *an unknown α-helix and* ***(F)*** *the repeat region folding into a β-helix. α: α-helix, β: β-sheet. Color represents the per-residue model confidence score (pLDDT): Dark blue: Very high (pLDDT > 90), light blue: High (90 > pLDDT > 70), yellow: Low (70 > pLDDT > 50), orange: Very low (pLDDT < 50).* ***(G)*** *Alignment of the internal putative NIM in ZNF512B with the N-terminal NIMs of known NuRD interactors. Capital letters indicate conserved amino acids.*

As a next step, I analyzed the conservation of ZNF512B's domains, since this can already give a hint on their functional relevance. So, I aligned ZNF512B's amino acid sequences from different vertebrate organisms (Figure 3.1.3). As expected, ZNF512B displayed an overall high degree of conservation (Chapter 1.2.1). Especially the ZF domains, the putative leucine zipper, the newly identified α-helix and the putative NIM are very well conserved. The NLS though has two insertions in fish and one in chicken. Interestingly, the repeat region forming the large β-helix is only conserved in mammals.

In summary, I could show that ZNF512B is expressed at low levels in different tissues and cell lines, and identify previously unknown, highly conserved domains, including a putative NIM.

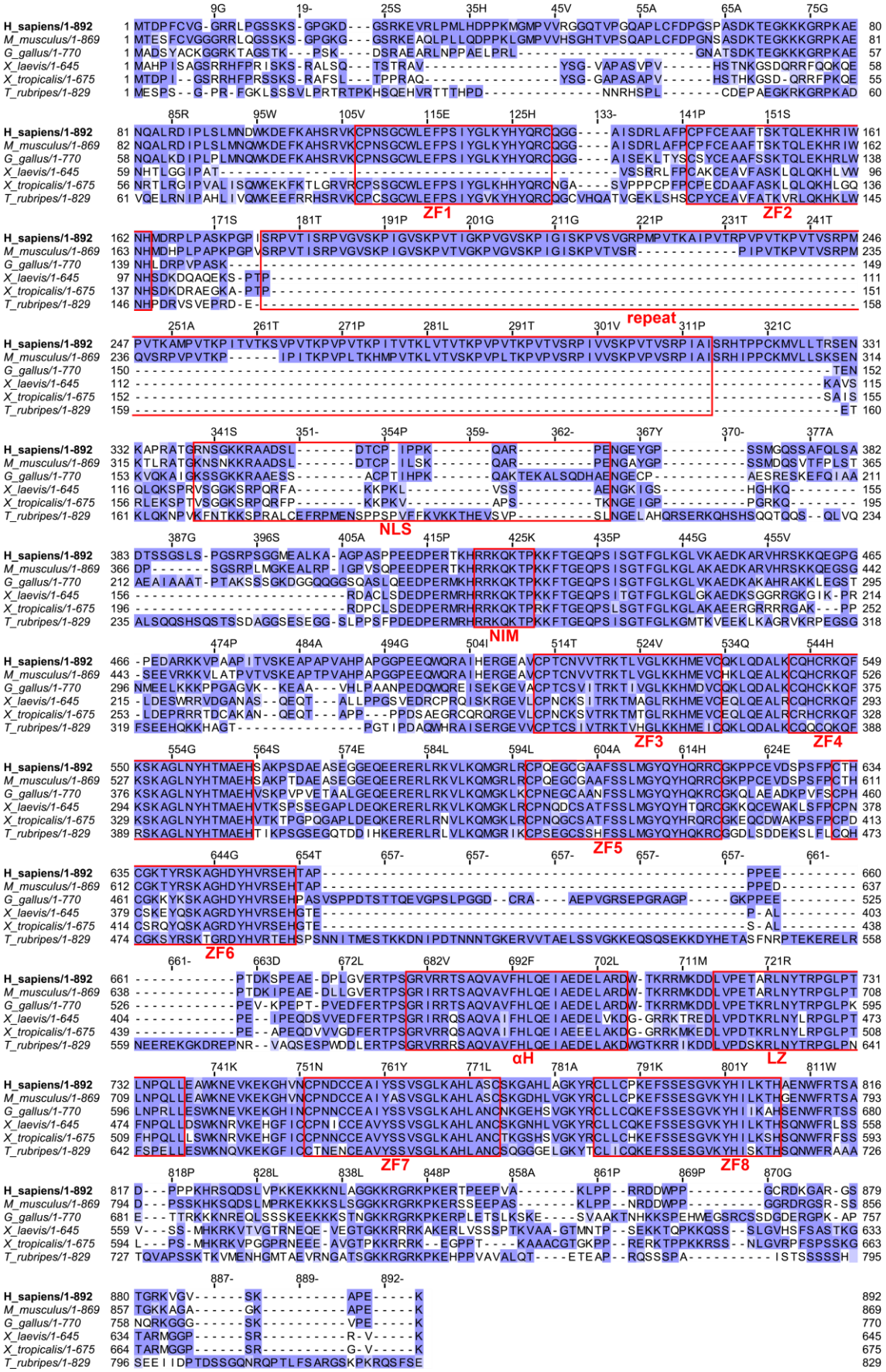

Figure 3.1.3: ZNF512B is highly conserved among vertebrates. *Alignment of ZNF512B protein sequences from H. sapiens (NP_065764.1), M. musculus (NP_001158069.1), G. gallus (NP_001032919.3), X. laevis*

(XP_018093756.1), X. tropicalis (NP_001135637.1) and T. rubripes (XP_029689030.1). Alignment was created in Jalview (version 2.11.3.2) using T-Coffee (version 11.00.8cbe486) with default settings. Color indicates BLOSUM62 score. ZF domains, the repeat region, the NLS, the putative NIM, the unknown α-helix (αH) and the putative leucine zipper (LZ) are indicated by red boxes.

3.2 ZNF512B is an interaction partner of H2A.Z, PWWP2A and HMG20A

ZNF512B is an interactor of H2A.Z-containing nucleosomes as demonstrated in MS experiments (Chapter 1.2.1). So before starting further experiments, I set out to validate this interaction first. I isolated nuclei from several HeLa Kyoto (HeLaK) cell lines previously created in our lab, that were stably expressing either GFP as negative control, GFP-H2A, GFP-macroH2A, GFP-H2A.X, GFP-H2A.Z.1, GFP-H2A.Z.2.1 or GFP-H2A.Z.2.2. I digested their chromatin with MNase to obtain mostly mononucleosomes and performed pull-down experiments using GFP-Trap beads. I analyzed the eluates in immunoblots, applying antibodies against GFP, as control of the immunoprecipitation (IP), against H3, to verify that nucleosomes were still intact, or against ZNF512B (Figure 3.2.1). Surprisingly, ZNF512B was not only pulled down by H2A.Z-containing nucleosomes but also by those containing H2A or any of the other H2A variants without prominent differences. The only exception made nucleosomes containing GFP-H2A.Z.2.2, where only a faint ZNF512B signal was visible. Considering that there were no striking differences in the amount of precipitated ZNF512B for H2A and the different variants, I concluded that the experiment was not suited to detect a preference of ZNF512B for certain nucleosomes.

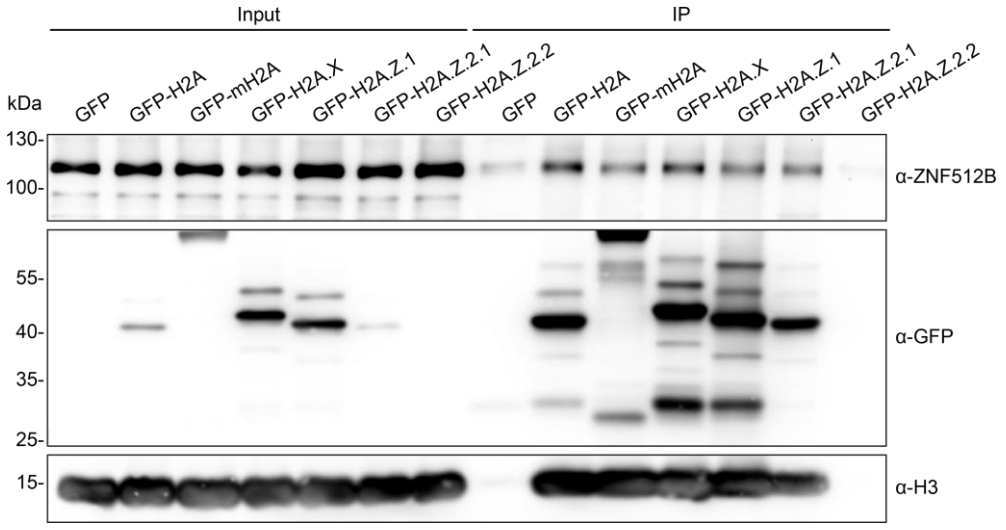

Figure 3.2.1: H2A or H2A variant-containing nucleosomes pull down endogenous ZNF512B. *Immunoblots of MNase-digested nuclear extracts from HeLaK cells stably expressing GFP, GFP-H2A or a GFP-H2A variant after pull-down with GFP-Trap beads detecting ZNF512B, GFP (IP control) or H3 (control of intact nucleosomes).*

I decided to rather pull down ZNF512B and to detect H2A and its variants in the eluates. Therefore, I created HeLaK cell lines inducibly expressing GFP or GFP-ZNF512B under a tetracycline(tet)-dependent promoter through integration into the AAVS1 safe harbor locus via genome editing by CRISPR/Cas9 (Figure 3.2.2A). I selected two clones from each cell line and after induction with doxycycline for 48 h, I analyzed them via flow cytometry (Figure 3.2.2B) and immunofluorescence (IF) microscopy (Figure 3.2.2C). All four clones showed an efficient expression of GFP or GFP-ZNF512B, respectively. However, the GFP-ZNF512B clones had lower expression levels in comparison to the GFP clones. Also, the IF microscopy experiment confirmed the nuclear localization of ZNF512B. Again, I isolated nuclei and digested chromatin with MNase. In a parallel approach, I used DNase I for digestion instead to examine ZNF512B's interaction with free histones. I controlled both digestion methods by analyzing isolated DNA on an agarose gel (Figure 3.2.2D). As expected, with the DNase approach no DNA was left, while with the MNase approach mainly mononucleosomes (~150 bp) and less dinucleosomes (~300 bp) were obtained. I performed IPs with GFP-Trap beads and analyzed the eluates in immunoblots applying antibodies against GFP, as control of the immunoprecipitation, H3, to verify that nucleosomes were still intact, H2A, H2A.X, H2A.Z or macroH2A (Figure 3.2.2E, F). The DNase approach clearly indicated that ZNF512B is not able to pull down any of the free histones (Figure 3.2.2E). The MNase approach on the other hand confirmed an interaction of ZNF512B with nucleosomes containing H2A, H2A.Z or macroH2A with a visible preference for H2A.Z-containing nucleosomes (Figure 3.2.2F).

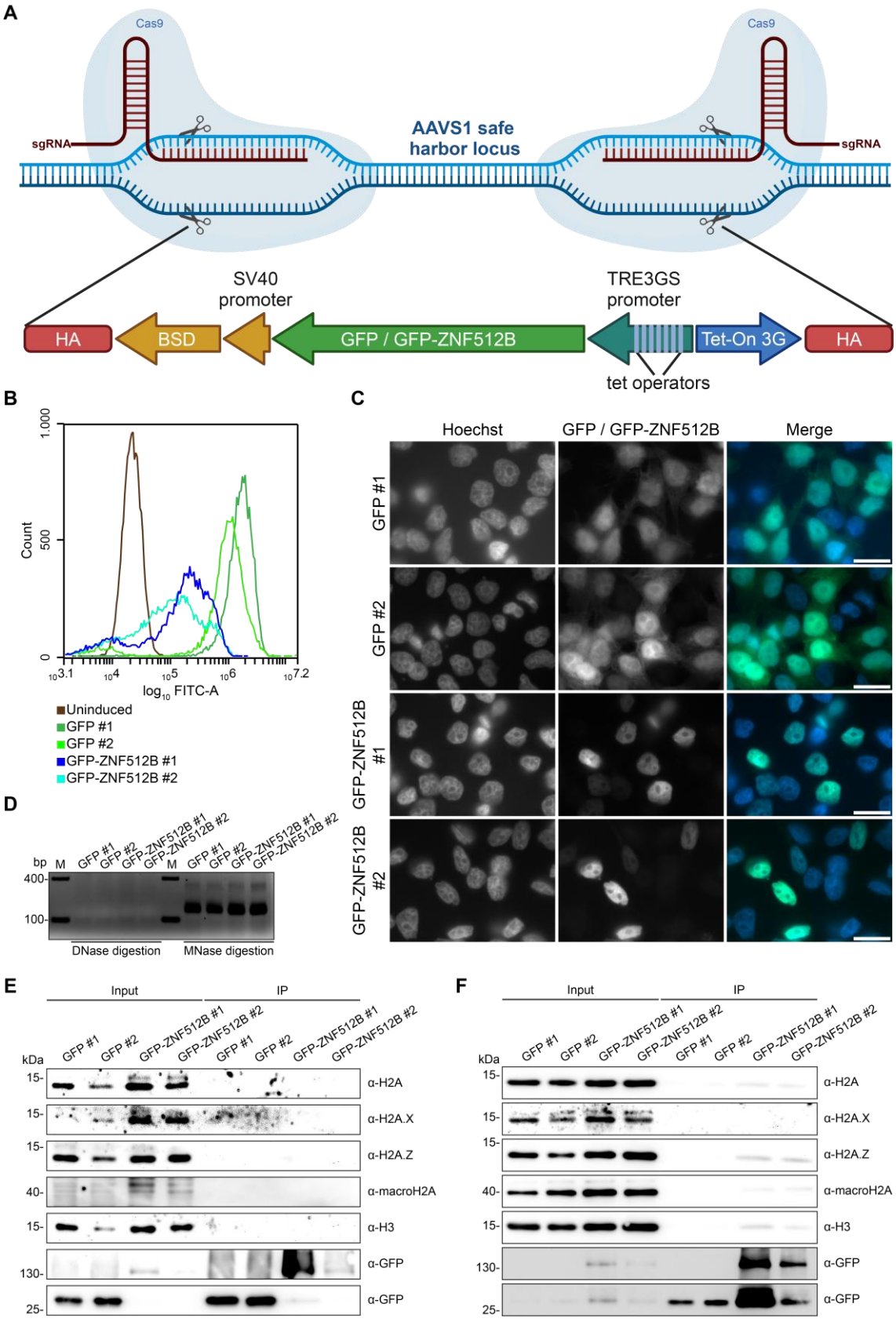

Figure 3.2.2: ZNF512B interacts preferentially with H2A.Z-containing nucleosomes. (A) *Schematic depiction of the creation of HeLaK cell lines inducibly expressing GFP or GFP-ZNF512B under a tetracycline-dependent promoter through integration into the AAVS1 safe harbor locus via genome editing by CRISPR/Cas9. The continuously expressed tet transactivator protein (Tet-On 3G) binds tightly to the*

tet-responsive promoter (TRE3GS, modified to eliminate binding sites for endogenous mammalian TFs) containing tet operators in the presence of doxycycline leading to expression of GFP / GFP-ZNF512B. Continuously expressed blasticidin S deaminase (BSD) confers resistance to blasticidin and was used for selection of two clones per cell line. Homology arms (HA) were used for targeted integration into the AAVS1 safe harbor locus. ***(B)*** *Flow cytometry analysis of uninduced and inducibly expressing GFP or GFP-ZNF512B HeLaK cells. Two clones each.* ***(C)*** *IF microscopy of inducibly expressing GFP or GFP-ZNF512B (green) HeLaK cells co-stained with Hoechst (DNA, blue). Two clones each. Scale bars: 20 µm.* ***(D)*** *Agarose gel of DNase- or MNase-digested chromatin isolated inducibly expressing GFP or GFP-ZNF512B HeLaK cells. Two clones each.* ***(E, F)*** *Immunoblots of* ***(E)*** *DNase-digested cell extracts or* ***(F)*** *MNase-digested nuclear extracts from HeLaK cells inducibly expressing GFP or GFP-ZNF512B after pull-down with GFP-Trap beads detecting H2A or different H2A variants, GFP (IP control) or H3 (control of intact nucleosomes).*

Since ZNF512B is also an interaction partner of the H2A.Z-associated proteins PWWP2A and HMG20A (Chapter 1.2.1), I attempted to verify these interactions next. Given that the expression level of GFP-ZNF512B was strongly varying between the two clones of the inducible cell lines I selected, I chose to use a pool of transiently transfected cells for further experiments to avoid clonal effects and/or off-target effects through genome editing. First, I transfected HeLaK cells with plasmids encoding GFP or GFP-ZNF512B and checked the transfection efficiency by flow cytometry (Figure 3.2.3A) as well as gene expression by RT-qPCR (Figure 3.2.3B, with help from Lena Paasche, Institute for Genetics, Justus-Liebig University Giessen, Germany) and protein level by immunoblot (Figure 3.2.3C). HeLaK cells were efficiently transfected with over 70 % of cells expressing GFP-ZNF512B (Figure 3.2.3A). In addition, the expression level was extremely high in comparison to the endogenous protein (Figure 3.2.3B, C). Then, I prepared MNase-digested nuclear extracts and did immunoblots after pull-down with GFP-Trap beads with antibodies against GFP, H2A.Z, HMG20A or PWWP2A (Figure 3.2.3D). This confirmed once more the interaction between ZNF512B and H2A.Z-containing nucleosomes and moreover the interactions with HMG20A and PWWP2A.

In summary, I showed that ZNF512B is an interactor of H2A-, H2A.Z- and macroH2A-containing nucleosomes with an evident preference for H2A.Z-containing ones as well as an interactor of the H2A.Z-associated proteins PWWP2A and HMG20A.

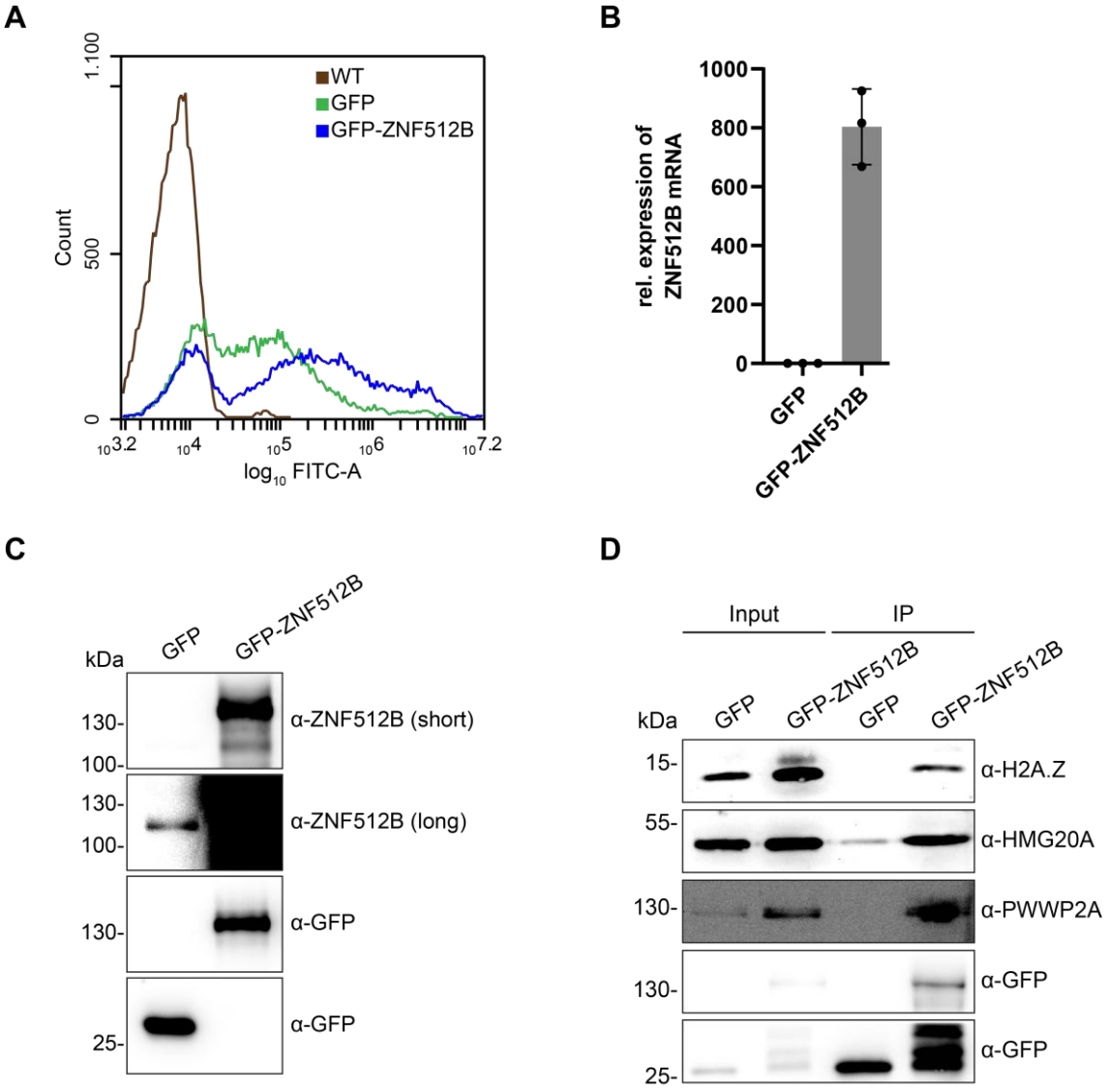

Figure 3.2.3: ZNF512B interacts with H2A.Z-containing nucleosomes and with the H2A.Z-associated proteins PWWP2A and HMG20A. ***(A)*** *Flow cytometry analysis of wild-type (WT) and transiently expressing GFP or GFP-ZNF512B HeLaK cells.* ***(B)*** *RT-qPCR to detect relative ZNF512B mRNA expression upon GFP or GFP-ZNF512B overexpression in HeLaK cells normalized to HPRT1 expression. Depicted is the mean with standard deviation (SD) of three biological replicates.* ***(C)*** *Immunoblots of DNase-digested nuclear extracts from HeLaK cells transiently expressing GFP or GFP-ZNF512B detecting ZNF512B or GFP.* ***(D)*** *Immunoblots of MNase-digested nuclear extracts from HeLaK cells transiently expressing GFP or GFP-ZNF512B after pull-down with GFP-Trap beads detecting H2A.Z, its associated proteins HMG20A or PWWP2A, or GFP (IP control).*

3.3 High levels of ZNF512B lead to the formation of chromatin foci

After I transfected HeLaK cells with GFP or GFP-ZNF512B encoding plasmids for the IP experiments, I also carried out IF microscopy (Figure 3.3.1, with help from Nadine Daus, Institute for Genetics, Justus-Liebig University Giessen, Germany). Unexpectedly, GFP-ZNF512B formed nuclear foci, whose number and sizes directly correlated with the expression level of GFP-ZNF512B. The higher the expression level was, the less, but at the same time larger, foci formed. Astonishingly, staining of DNA revealed that chromatin nearly completely colocalized with GFP-ZNF512B within these foci. This implied that GFP-ZNF512B overexpression induced some sort of chromatin compaction/condensation/aggregation.

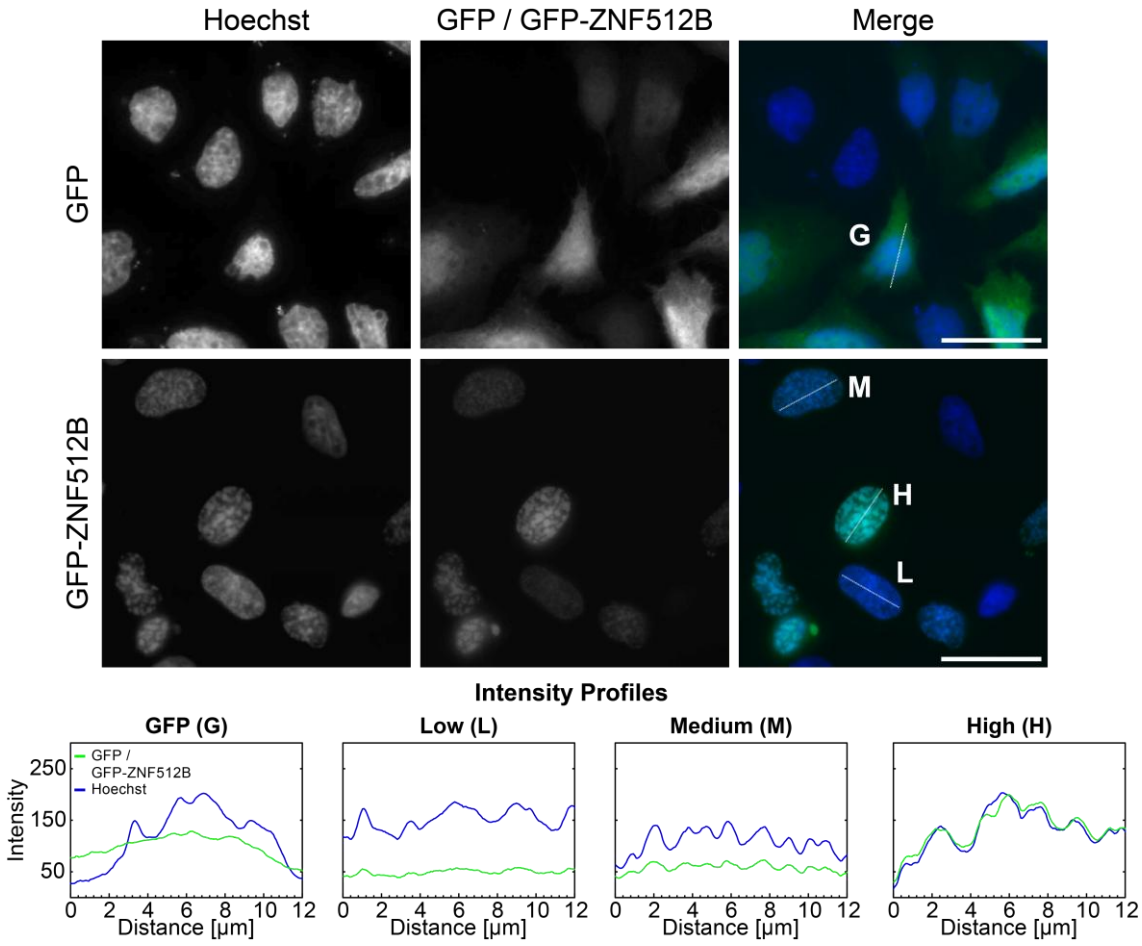

Figure 3.3.1: ZNF512B overexpression leads to formation of nuclear foci colocalizing with chromatin. ***Top:*** *IF microscopy of HeLaK cells expressing GFP or GFP-ZNF512B (green) co-stained with Hoechst (DNA, blue). Scale bars: 20 µm.* ***Bottom:*** *Intensity profiles of nuclear areas from IF pictures (see lines, top) depicting Hoechst and GFP/GFP-ZNF512B fluorescence within cells expressing GFP (G) or low (L), medium (M) or high (H) levels of GFP-ZNF512B.*

To check whether this interesting phenotype was influenced by the position of the GFP-tag, I cloned and transfected a C-terminally tagged ZNF512B-GFP construct and repeated the IF microscopy experiment (Figure 3.3.2A). However, the repositioning of the GFP-tag had no effect on the foci formation or the colocalization with chromatin. To also exclude a cell line-specific phenotype, I further transfected HCT116, HEK293T and U2OS cells with the GFP or GFP-ZNF512B plasmids. In all three alternative cell lines GFP-ZNF512B overexpression led to chromatin condensation as in HeLaK cells (Figure 3.3.2B). Next, I repeated the IF microscopy in addition with an antibody against the mitotic histone PTM H3S10ph (Chapter 1.1.3) to find out whether the observed ZNF512B-forced chromatin compaction foci possibly represented prophase condensation spots (Figure 3.3.2C). This was not the case because these foci were not marked with this mitotic modification.

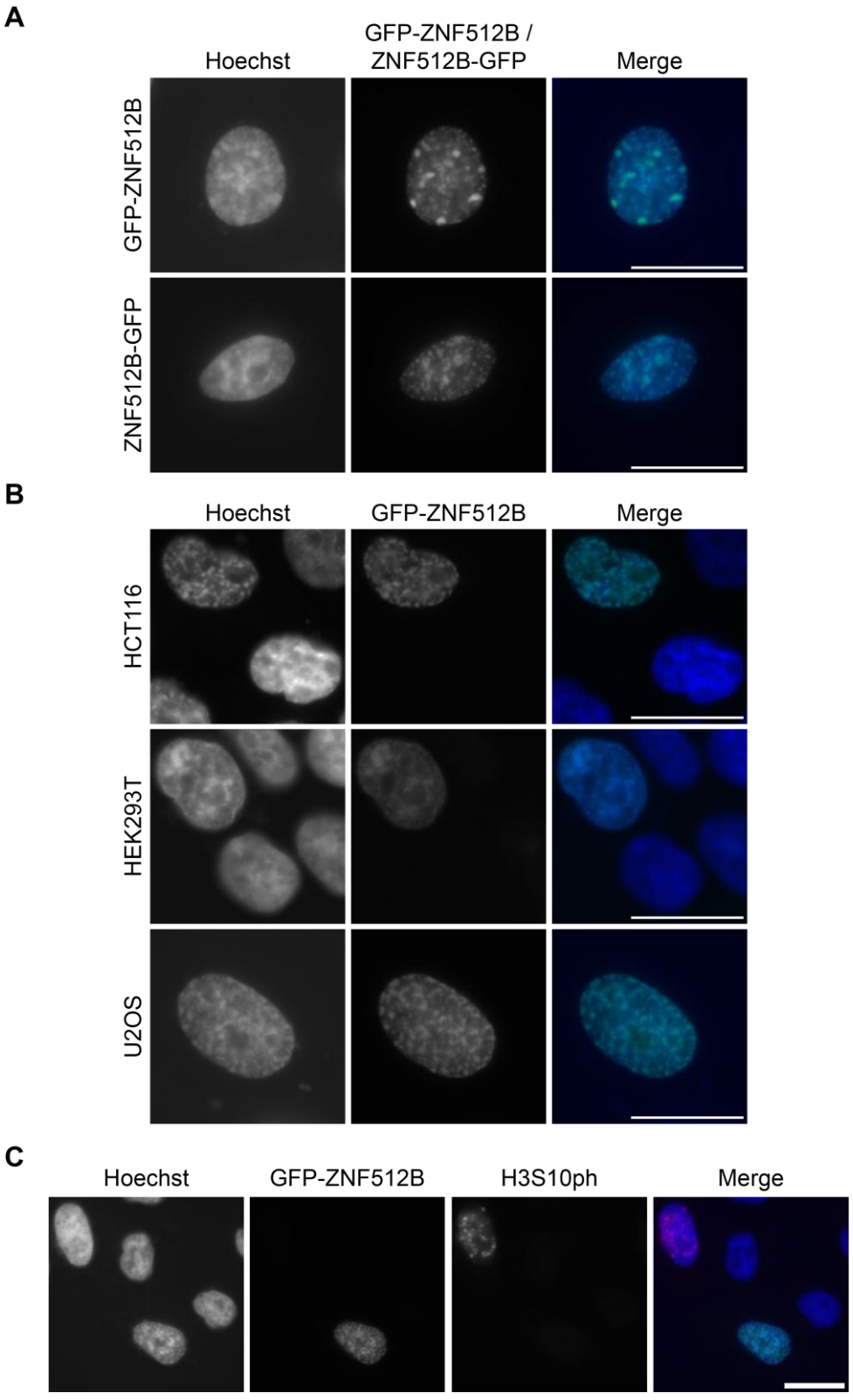

Figure 3.3.2: ZNF512B induced chromatin compaction is not caused by position of the GFP-tag, cell line or mitosis. (A, B) *IF microscopy of Hoechst (DNA, blue) stained* ***(A)*** *HeLaK cells expressing GFP-ZNF512B or ZNF512B-GFP (green) or* ***(B)*** *HCT116, HEK239T or U2OS cells expressing GFP-ZNF512B (green). Scale bars: 20 µm.* ***(C)*** *IF microscopy of Hoechst (DNA, blue) stained HeLaK cells expressing GFP-ZNF512B (green) and co-stained with anti-H3S10ph antibody (red) as mitosis mark. Scale bar: 20 µm.*

The ZNF512B-induced chromatin foci further resembled senescence-associated heterochromatin foci (SAHF), a distinct heterochromatic structure that accumulates in senescent cells (Narita et al., 2003). So, to exclude senescence as the underlying reason for the observed phenotype, I applied a senescence-associated (SA) β-galactosidase staining (Figure 3.3.3A). SA-β-galactosidase is only active in senescent cells at pH 6 and breaks down X-gal in the buffer, marking senescent cells with blue color. This staining in HeLaK cells expressing GFP or GFP-ZNF512B or treated with the senescence-inducing drug doxorubicin as positive control revealed that ZNF512B overexpression did not lead to senescence (Figure 3.3.3B). Since a previous study showed that ZNF512B overexpression led to apoptosis (Chapter 1.2.1), I also employed a terminal deoxynucleotidyl transferase dUTP nick end labeling (TUNEL) assay (Figure 3.3.3C). Here, the 3′-OH ends of DNA fragments, that occur, for instance, through apoptosis-associated digestion by caspases, are labeled with fluorochrome-labeled dUTP by terminal deoxynucleotidyl transferase (TdT) and can subsequently be detected in IF microscopy. This clearly demonstrated that the cells showing the ZNF512B-induced chromatin condensation were not apoptotic (Figure 3.3.3D). Nevertheless, it is noteworthy that I have not been able to create stably transfected cells because the long-term expression of GFP-ZNF512B ultimately led to cell death. These data suggest that apoptosis is not the cause but rather a consequence of the chromatin compaction phenotype.

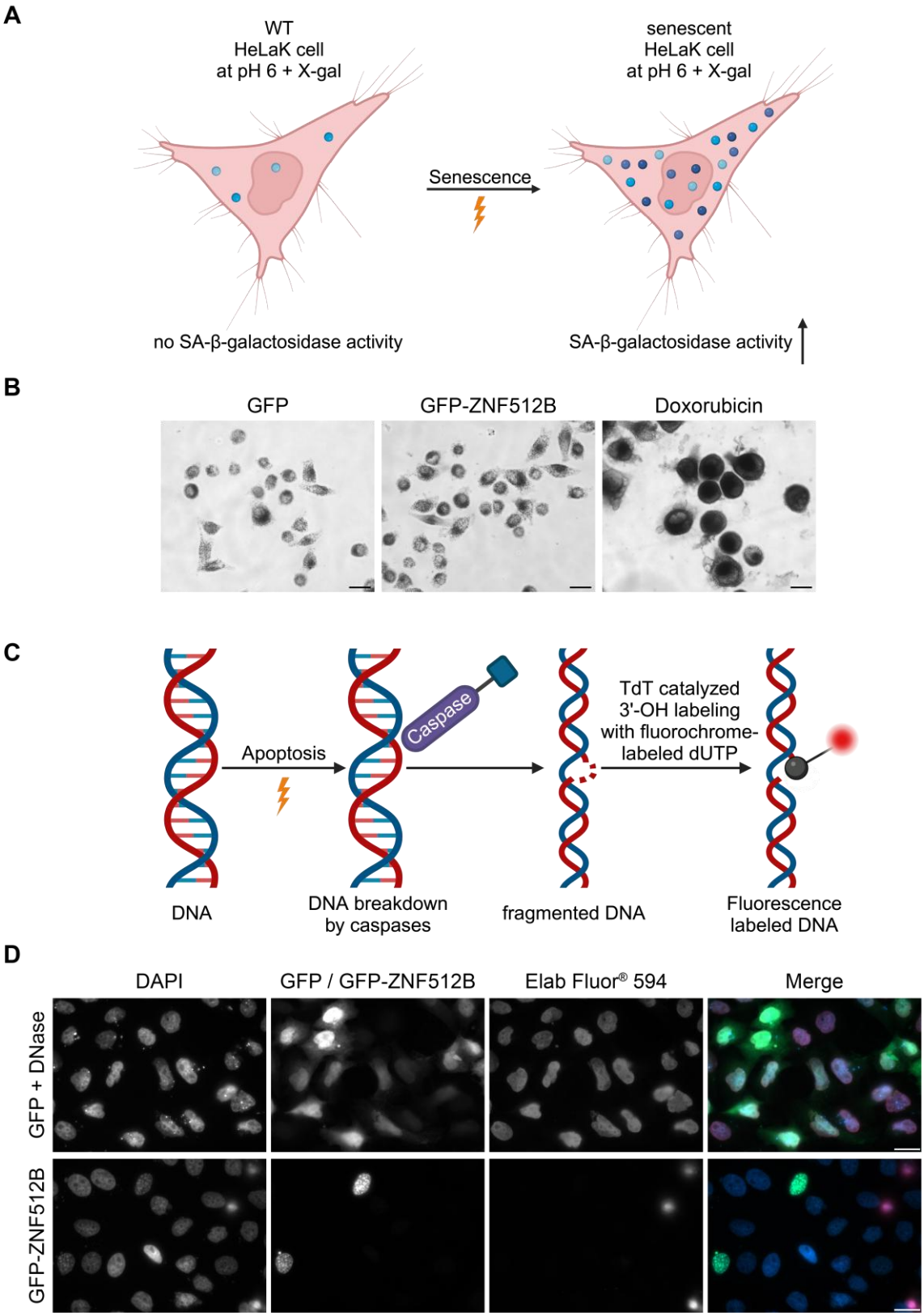

Figure 3.3.3: ZNF512B induced chromatin compaction is not caused by senescence or apoptosis. (A) *Schematic depiction of the SA-β-galactosidase staining. SA-β-galactosidase breaks down X-gal in the buffer only in senescent cells at pH 6, marking them with blue color.* ***(B)*** *Bright-field microscopy of in situ staining for SA-β-galactosidase activity as marker for senescent cells in HeLaK cells expressing GFP or GFP-ZNF512B or treated with doxorubicin as positive control. Scale bars: 20 µm.* ***(C)*** *Schematic depiction of the TUNEL assay. Apoptosis induces DNA breakdown by caspases. Resulting DNA fragments are labeled*

at the 3´-OH ends by TdT with fluorochrome-labeled dUTP. ***(D)*** *IF microscopy of TUNEL assay labeling DNA fragments with Elab Fluor 594 (red) in DAPI (DNA, blue) stained HeLaK cells expressing GFP or GFP-ZNF512B (green). GFP expressing cells were treated with DNase I as positive control. Scale bars: 20 µm.*

As the overexpression of GFP-ZNF512B led to drastic changes in chromatin structure in the form of chromatin compaction foci, I finally decided to analyze histone PTMs in this condition. Histone PTMs play an important role in chromatin organization (Chapter 1.1.3). Due to the high level of chromatin condensation following the ZNF512B overexpression, I suspected to see an increase in repressive histone PTMs, like H3K9me3 and H3K27me3, and a decrease in active histone PTMs, like H3K4me3, H2A.Zac and H3K27ac (Table 1.1.3). I conducted IF microscopy on HeLaK cells transfected with the GFP or GFP-ZNF512B plasmids using antibodies against the aforementioned histone PTMs (Figure 3.3.4). I could not observe greater changes on the general level of the histone PTMs, but, interestingly, the distributions of some of the histone PTMs in the nucleus were different. While histone marks associated with active transcription (H3K4me3, H2A.Zac, H3K27ac) were excluded from the GFP-ZNF512B/chromatin foci, histone marks associated with heterochromatin (H3K27me3, H3K9me3) colocalized with these foci.

To sum up, high expression levels of ZNF512B lead to foci formation and chromatin condensation/aggregation in the nucleus and repressive histone PTMs colocalize with these foci.

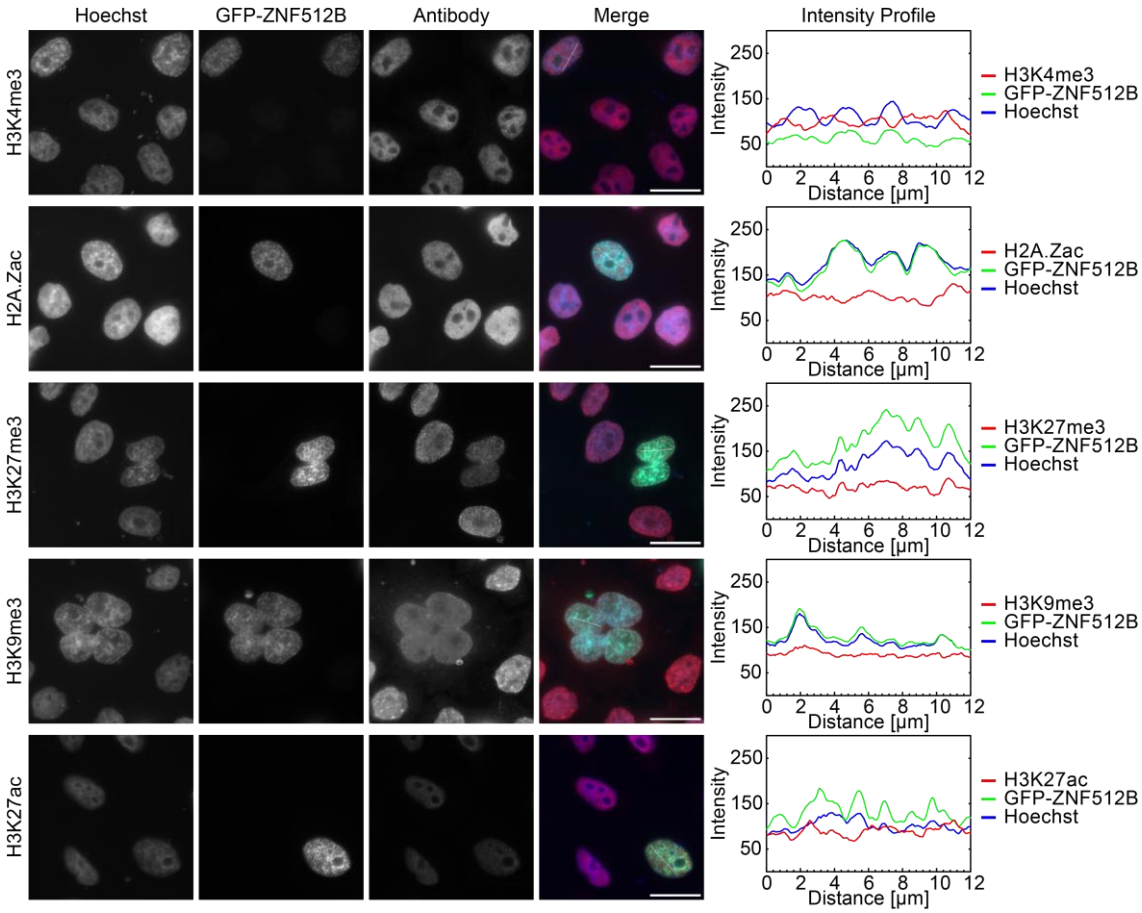

Figure 3.3.4: ZNF512B foci colocalize with repressive and exclude active histone PTMs. Left: *IF microscopy of Hoechst (DNA, blue) stained HeLaK cells expressing GFP-ZNF512B (green) and co-stained with different antibodies against active (H3K4me3, H2A.Zac, H3K27ac) or repressive (H3K27me3, H3K9me3) histone modifications (red). Scale bars: 20 µm.* ***Right:*** *Intensity profiles of nuclear areas from IF pictures (see lines, left) depicting Hoechst, GFP-ZNF512B and respective antibody fluorescence.*

3.4 ZNF512B-induced chromatin compaction is dependent on the zinc finger domains

ZNF512B consists of a large internal region, four pairs of an atypical (C_2HC) ZF followed by a typical (C_2H_2) ZF and several other domains (Chapter 3.1). To better understand the overexpression phenotype, I decided to decipher which domains of ZNF512B are crucial for this condensation/aggregation and focused on the ZF domains first. I started by generating two GFP-ZNF512B constructs in which I either mutated all typical (ΔTypZF) or all atypical (ΔAtypZF) ZF domains by always exchanging the first two cysteines with alanines. I transfected HeLaK cells with these constructs and performed IF microscopy (Figure 3.4.1A). Surprisingly, for both constructs I could mostly observe cells showing the phenotype comparable to wild type GFP-ZNF512B. Some cells looked different, although it is important to note that very strong GFP signals were present in the nucleoli of these cells suggesting improper folding of a substantial percentage of the exogenous

proteins and therefore probably leading to aberrant phenotypes (Alberti & Carra, 2019). I decided to test the individual ZF pairs next and cloned four plasmids, each encoding only a single GFP-tagged ZF pair of ZNF512B, transfected HeLaK cells and performed IF microscopy (Figure 3.4.1B). None of the ZF pairs lead to the overexpression phenotype. All four showed a diffuse GFP signal throughout the nucleus and chromatin was not condensed, but again, very strong GFP signals in the nucleoli hinted at improper folding.

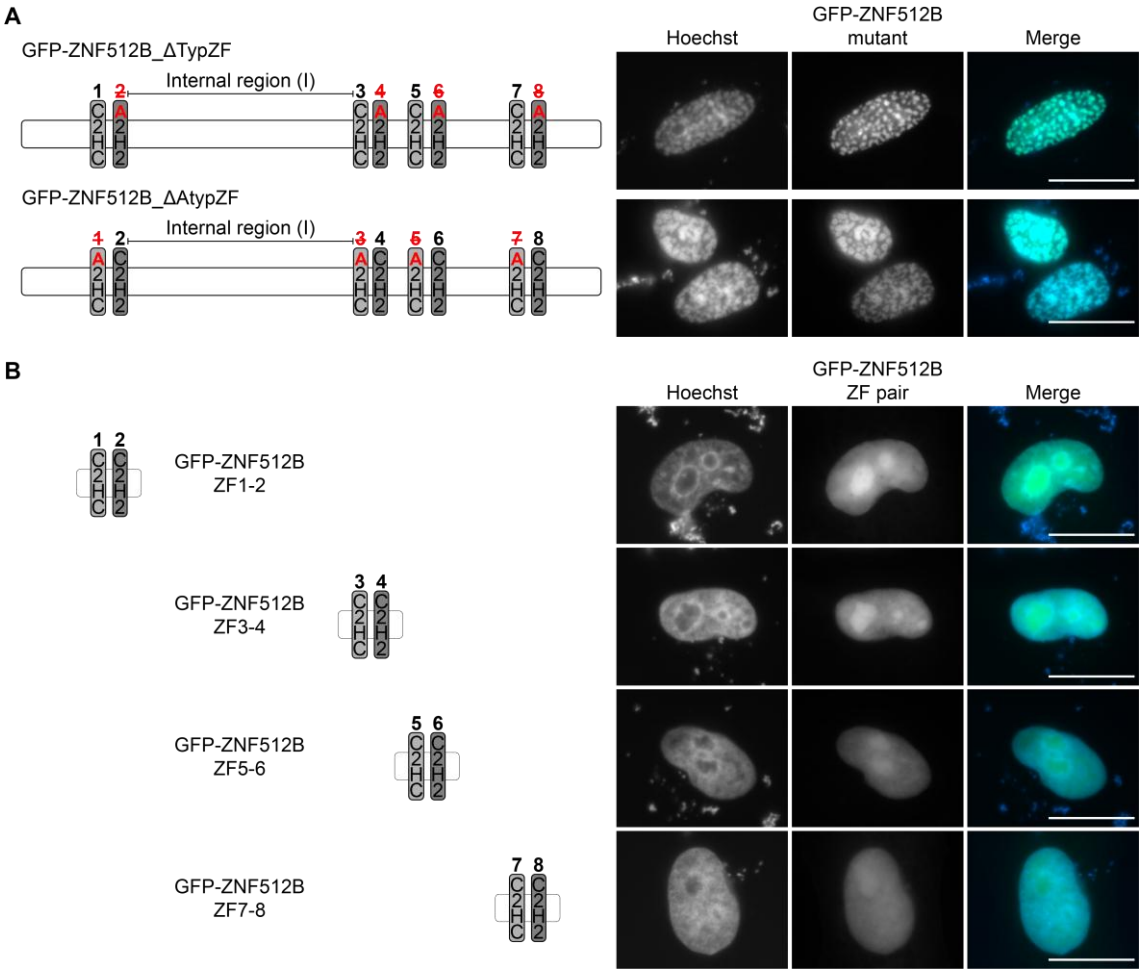

Figure 3.4.1: ZNF512B induced chromatin compaction is not dependent on only typical or atypical ZF domains. (A, B) Left: *Schematic depiction of used constructs.* ***Right:*** *IF microscopy of Hoechst (DNA, blue) stained HeLaK cells expressing* ***(A)*** *GFP-ZNF512B_ΔTypZF (only atypical ZFs) or GFP-ZNF512B_ΔAtypZF (only typical ZFs) (green) or* ***(B)*** *different GFP-tagged ZF pairs of ZNF512B (green). Scale bars: 20 µm.*

Thinking that a possible reason could have been the short length of the single ZF pairs, I finally created several truncation/deletion constructs of GFP-ZNF512B and repeated the IF microscopy experiments (Figure 3.4.2). As before, GFP-ZNF512B showed the overexpression phenotype, forming nuclear protein and chromatin foci. When only the

internal region of ZNF512B without any ZFs was expressed, the phenotype could not be observed anymore. There was a diffuse signal of GFP-ZNF512B_ΔZF throughout the nucleus and foci formation as well as chromatin condensation were absent, implying the ZF domains as necessity for the phenotype. Accordingly, expression of GFP-ZNF512B_ΔI with all ZFs but without the internal region led to the same phenotype as wild type GFP-ZNF512B. Interestingly, stepwise deletion of ZF pairs corresponded with more but smaller protein/DNA foci as they occur at lower expression levels of wild type GFP-ZNF512B, indicating that the extent of the phenotype depends on the number of ZFs. Through the combination of constructs, I could also exclude all the other ZNF512B domains as needed for the overexpression phenotype. Of note, this experiment also verified the location of an NLS inside the internal region, because the GFP-ZNF512B_ΔZF (I_only) construct localized in the nucleus without an additional NLS.

In conclusion, these data show that the ZF domains of ZNF512B are required for the overexpression phenotype.

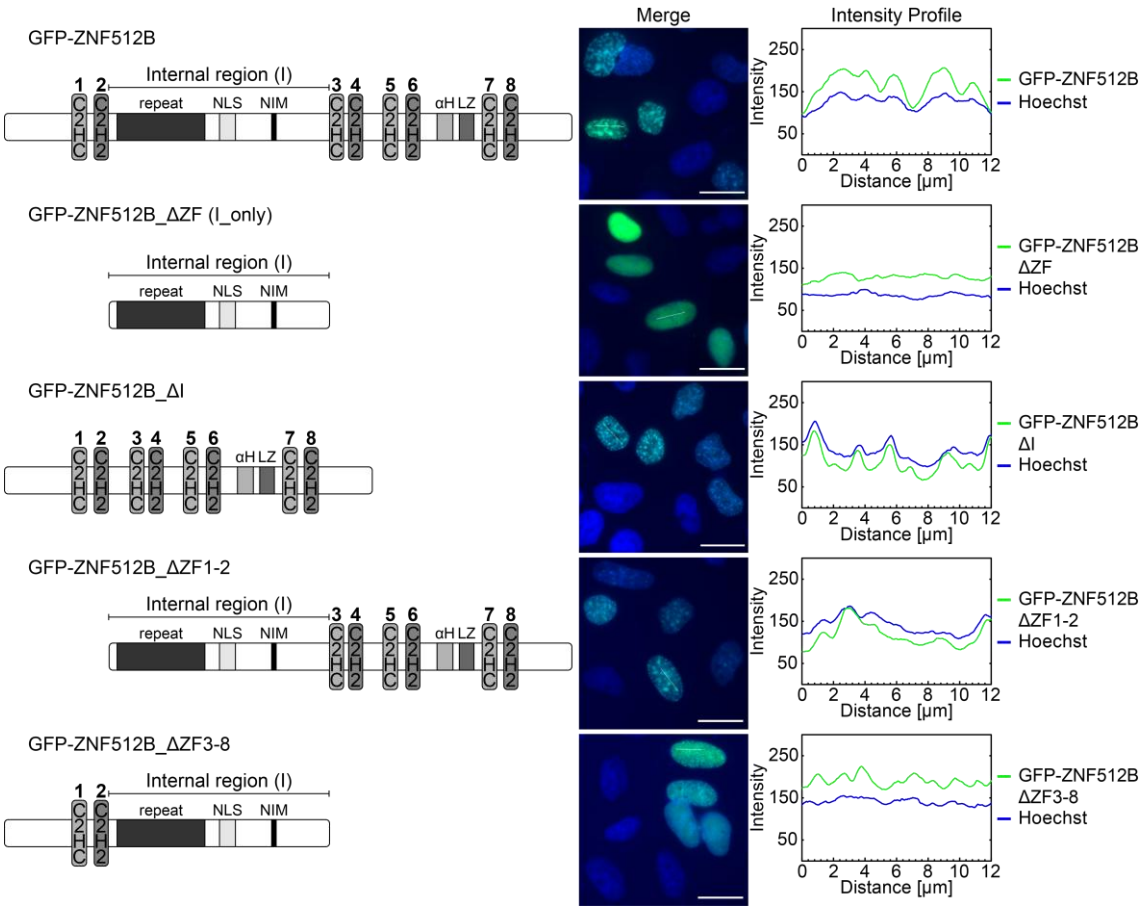

Figure 3.4.2: ZNF512B induced chromatin compaction is dependent on its zinc finger domains. Left: *Schematic depiction of used constructs* ***Middle:*** *IF microscopy of Hoechst (DNA, blue) stained HeLaK cells expressing GFP-ZNF512B, GFP-ZNF512B_ΔZF (internal domain only), GFP-ZNF512B_ΔI (only ZFs*

without internal region), GFP-ZNF512B_ΔZF1-2 or GFP-ZNF512B_ΔZF3-8 (green). Scale bars: 20 µm. ***Right:*** *Intensity profiles of nuclear areas from IF pictures (see lines, middle) depicting Hoechst and GFP constructs fluorescence.*

3.5 ZNF512B is a novel DNA-binding protein

The number of ZF domains in ZNF512B directly influenced the quantity and size of protein and chromatin foci during the overexpression. Therefore, I hypothesized that the ZFs facilitate DNA binding and oligomerization, bringing together ZNF512B proteins and different chromatin domains in the observed foci. To first test ZNF512B's DNA binding ability, Dr. Jörg Leers (Institute for Genetics, Justus-Liebig University Giessen, Germany) expressed and purified recombinant His-tagged ZNF512B (Figure 3.5.1A) and performed electrophoretic mobility shift assays (EMSAs). Since ZNF512B seemingly has an affinity for methylated DNA as shown in affinity purification experiments with semisynthetic dinucleosomes containing different chromatin modifications in the Modification Atlas of Regulation by Chromatin States (MARCS) (Lukauskas et al., 2024), we decided to test unmethylated (Figure 3.5.1B) as well as methylated DNA (Figure 3.5.1C) probes in the EMSAs. The results clearly demonstrated that ZNF512B is capable of binding DNA regardless of its methylation status.

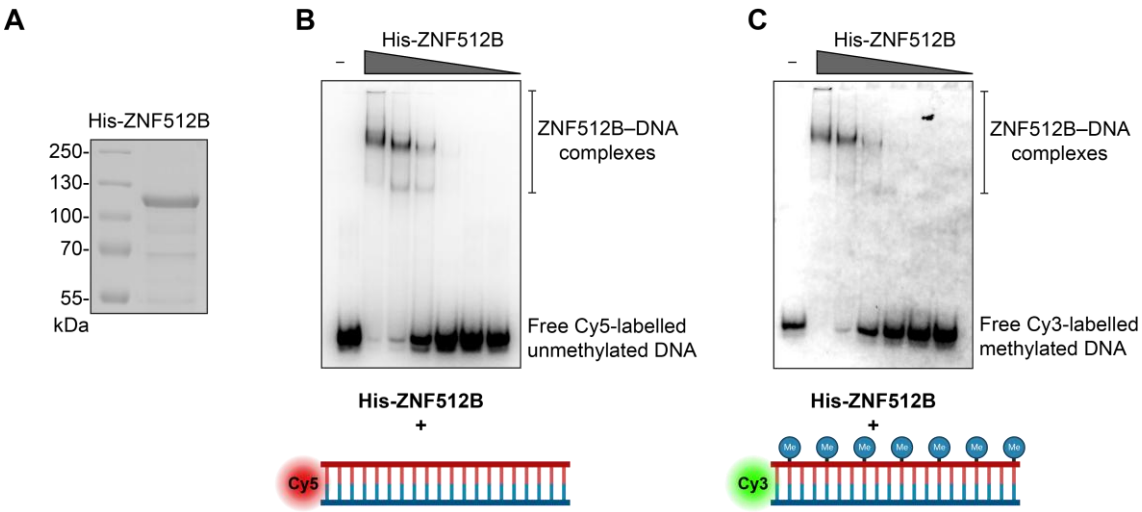

Figure 3.5.1: ZNF512B binds DNA. ***(A)*** *Coomassie brilliant blue-stained SDS-PAGE gel separating purified recombinant His-ZNF512B.* ***(B, C) Top:*** *Electrophoretic Mobility Shift Assays (EMSAs) of* ***(B)*** *Cy5-labelled unmethylated or* ***(C)*** *Cy3-labelled methylated DNA together with increasing amounts of purified recombinant His-ZNF512B protein.* ***Bottom:*** *Schematic depiction of the utilized DNA oligomers.*

Following this detected DNA binding ability, I decided to predict potential DNA binding motifs for ZNF512B's ZFs using a position weight matrix (PWM) predictor for ZF

domains (Persikov et al., 2009; Persikov & Singh, 2014) based on bacterial one-hybrid (B1H) screens (Persikov et al., 2014; Persikov et al., 2015). I predicted the PWM for all ZNF512B ZF domains (Figure 3.5.2). Interestingly, the motifs with the highest confidence were predicted for the atypical ZFs 1 and 5. In general, ZNF512B's ZF domains were predicted to bind AT-rich sequences.

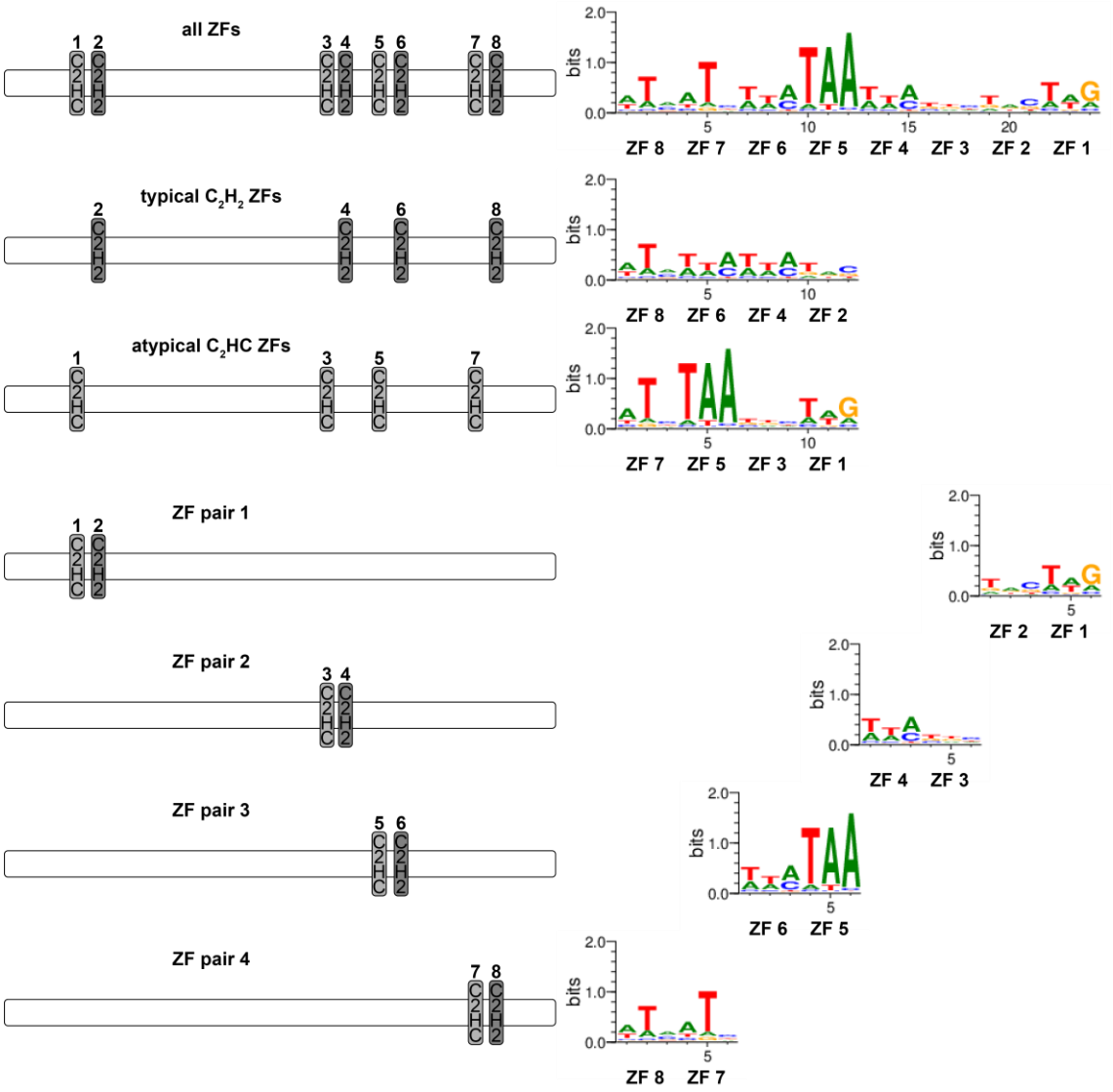

Figure 3.5.2: ZNF512B's ZF domains are predicted to bind AT-rich DNA motifs. Left: *Schematic depiction of the ZF domains used for prediction of the PWMs.* ***Right:*** *Predicted PWMs for the ZF domains of ZNF512B based on B1H datasets.*

To next assess whether ZNF512B can form oligomers, I created FLAG-tagged ZNF512B deletion constructs and used them together with the already existent GFP-tagged ones in co-transfections of HeLaK cells. I analyzed these cells in IF microscopy and could see that the overexpression phenotype was also independent of the used protein-tag

(Figure 3.5.3A). I then proceeded with pull-downs with GFP-Trap beads and immunoblotting (Figure 3.5.3B). I could demonstrate that ZNF512B can indeed oligomerize but only wild type GFP-ZNF512B and GFP-ZNF512B_ΔI could precipitate FLAG-ZNF512B and FLAG-ZNF512B_ΔI respectively. Lastly, I checked whether ZNF512B affects chromatin accessibility. If my hypothesis is correct that overexpressed ZNF512B brings different chromatin domains into closer contact, there should be no direct changes in nucleosome occupancy. I digested nuclear extracts of HeLaK cells transiently transfected with an empty (BlueScript), GFP or GFP-ZNF512B expression vector with MNase and stopped the digestion after several time points. Analysis of the isolated DNA on an agarose gel showed that there were indeed no significant changes in chromatin accessibility between the different samples (Figure 3.5.3C).

In summary, ZNF512B is a novel DNA binding protein that has the ability to oligomerize.

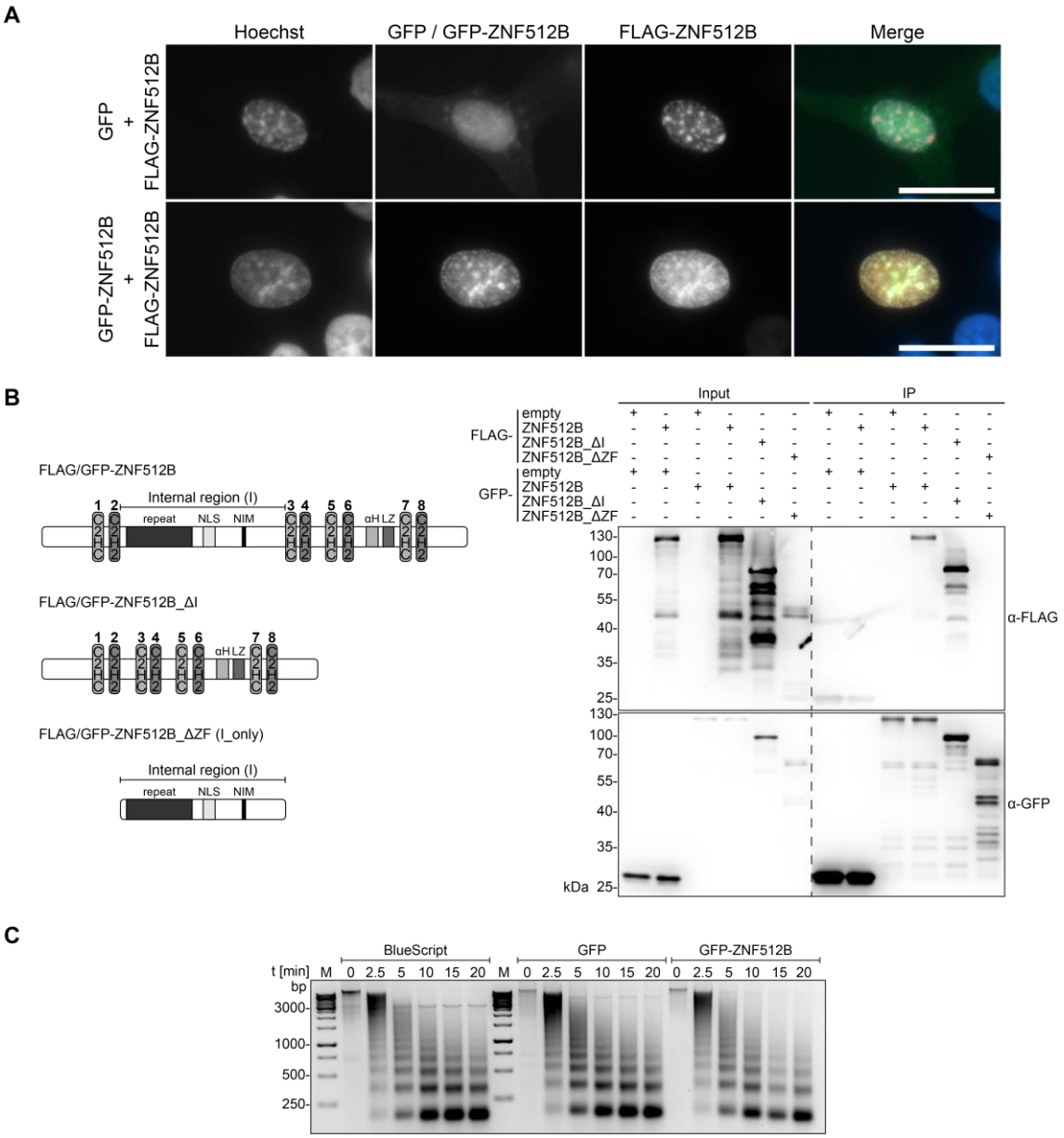

Figure 3.5.3: ZNF512B can form oligomers via its ZF domains. (A) *IF microscopy of Hoechst (DNA, blue) stained HeLaK cells expressing GFP (green) and FLAG-ZNF512B (red) or GFP-ZNF512B (green) and FLAG-ZNF512B (red). Scale bars: 20 µm.* ***(B) Left:*** *Schematic depiction of used constructs.* ***Right:*** *Immunoblots of DNase-digested cell extracts from HeLaK cells expressing GFP, GFP-ZNF512B, GFP-ZNF512B_ΔI or GFP-ZNF512B_ΔZF together with FLAG, FLAG-ZNF512B, FLAG-ZNF512B_ΔI or FLAG-ZNF512B_ΔZF after pull-down with GFP-Trap beads detecting FLAG or GFP (IP control). Dashed line indicates cut membrane.* ***(C)*** *Agarose gel of MNase-digested chromatin isolated from HeLaK cells transfected with an empty vector as control (BlueScript) or expressing GFP or GFP-ZNF512B. MNase digestion was stopped after several time points.*

3.6 ZNF512B is a novel interactor of the NuRD complex

As I identified earlier (Chapter 3.1), the internal region of ZNF512B contains a putative NuRD interaction motif (NIM) (Figure 3.6.1A). To answer the question whether this motif truly facilitates an interaction with the NuRD complex, I first created a GFP-ZNF512B construct bearing the point mutation K423A, as the corresponding lysine in FOG-1 was shown to be essential for NuRD binding (Hong et al., 2005). I then transfected HeLaK cells with the GFP, GFP-ZNF512B or GFP-ZNF512B_K423A plasmids and used their DNase-digested cell extracts for IPs with GFP-Trap beads. Subsequent immunoblots detecting the NuRD components RBBP4, MBD2, HDAC1 or MTA1 clearly confirmed an interaction between ZNF512B and the NuRD complex that is facilitated by the NIM (Figure 3.6.1B).

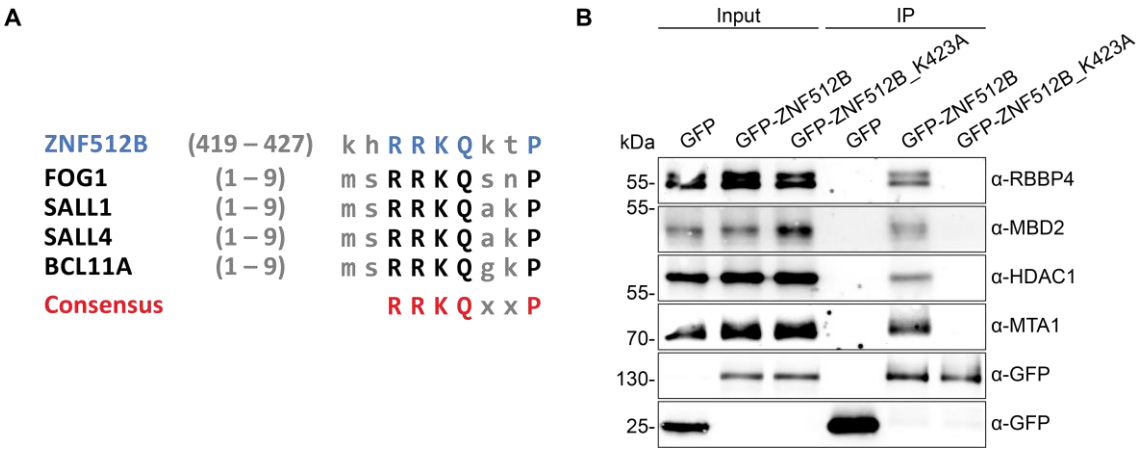

Figure 3.6.1: ZNF512B interacts with the NuRD complex via its NIM. (A) *Alignment of the internal putative NIM in ZNF512B with the N-terminal NIMs of known NuRD interactors. Capital letters indicate conserved amino acids.* ***(B)*** *Immunoblots of DNase-digested cell extracts from HeLaK cells expressing GFP, GFP-ZNF512B or GFP-ZNF512B_K423A after pull-down with GFP-Trap beads detecting NuRD complex members RBBP4, MBD2, HDAC1 or MTA1, or GFP (IP control).*

In addition, I validated this interaction via IF microscopy. The NuRD members RBBP4, MTA1 and CHD4 visibly colocalized with the GFP-ZNF512B foci (Figure 3.6.2A–C). When GFP-ZNF512B_K423A was overexpressed though, they were distributed throughout the nucleus. As expected, the ZNF512B and chromatin condensation foci were still present, since I already established the ZF domains as required for induction of the aggregation phenotype.

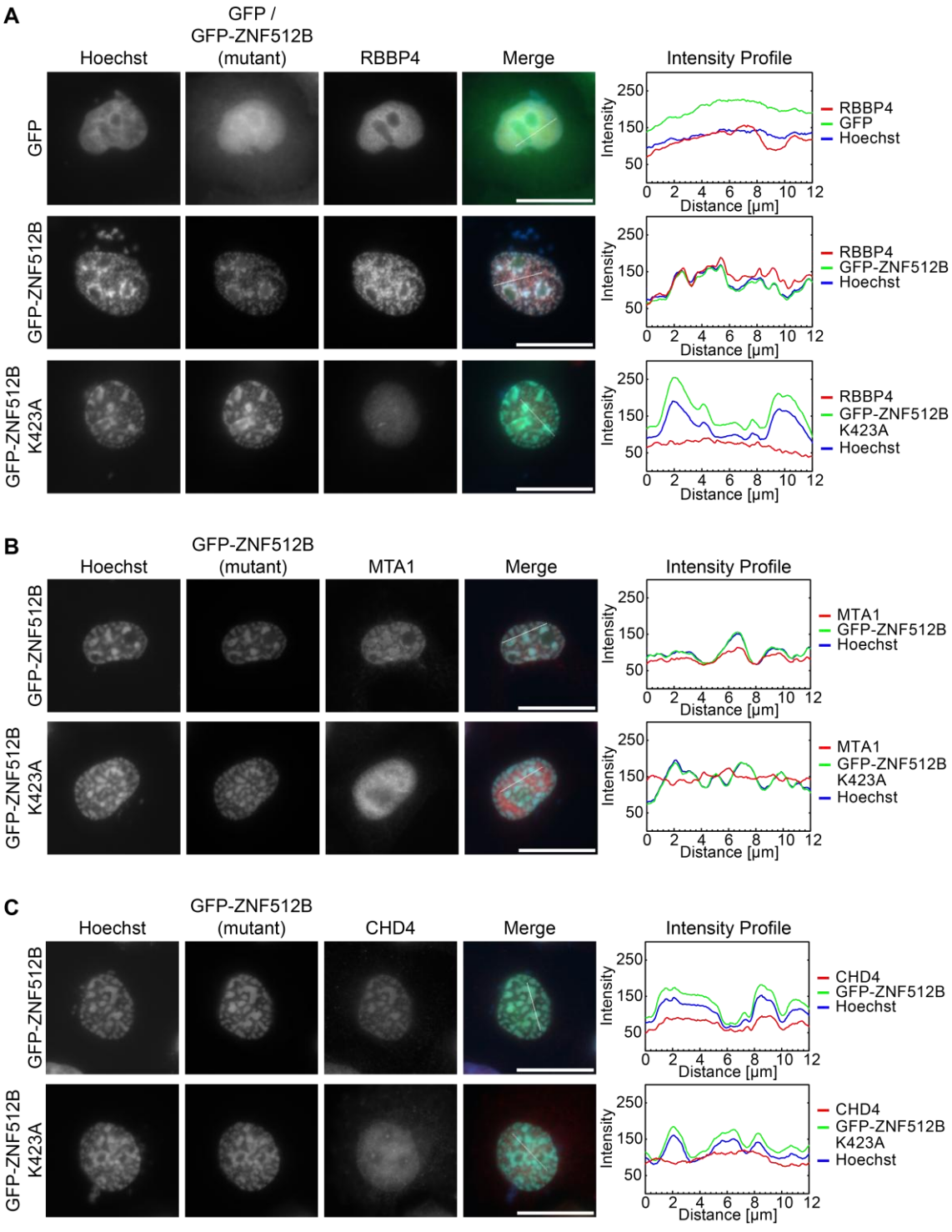

Figure 3.6.2: The NuRD members RBBP4, MTA1 and CHD4 colocalize with ZNF512B-induced chromatin compaction foci. (A–C) Left: *IF microscopy of Hoechst (DNA, blue) stained HeLaK cells expressing GFP, GFP-ZNF512B or GFP-ZNF512B_K423A (green) and co-stained with* ***(A)*** *anti-RBBP4,* ***(B)*** *anti-MTA1 or* ***(C)*** *anti-CHD4 antibody (red). Scale bars: 20 µm.* ***Right:*** *Intensity profiles of nuclear areas from IF pictures (see lines, left) depicting Hoechst, GFP constructs and respective antibody fluorescence.*

I then questioned whether the disruption of the NuRD interaction might affect the histone PTM profiles at the aggregation sites I had observed earlier (Chapter 3.3). To investigate this, I conducted the same IF microscopy experiments as before but used cells expressing GFP-ZNF512B_K423A (Figure 3.6.3A). However, there was no noticeable variation compared to cells expressing GFP-ZNF512B: Active histone PTMs (H3K4me3, H2A.Zac, H3K27ac) were excluded from the GFP-ZNF512B_K423A-induced chromatin foci, while repressive histone PTMs (H3K27me3, H3K9me3) were colocalizing. I further inspected the general level of the different histone PTMs by preparing nuclear extracts from HeLaK cells transfected with the GFP, GFP-ZNF512B or GFP-ZNF512B_K423A plasmids followed by immunoblots detecting H3, as loading control, GFP, as control of the transfection, or the respective histone PTMs (Figure 3.6.3B). The global amount of the examined histone PTMs appeared overall comparable between all three conditions taking slight differences in loading and transfection efficiency into account.

In summary, I showed that ZNF512B interacts with the NuRD complex via an internal NIM and that the histone PTM profiles at ZNF512B-induced chromatin foci are unaffected by this interaction.

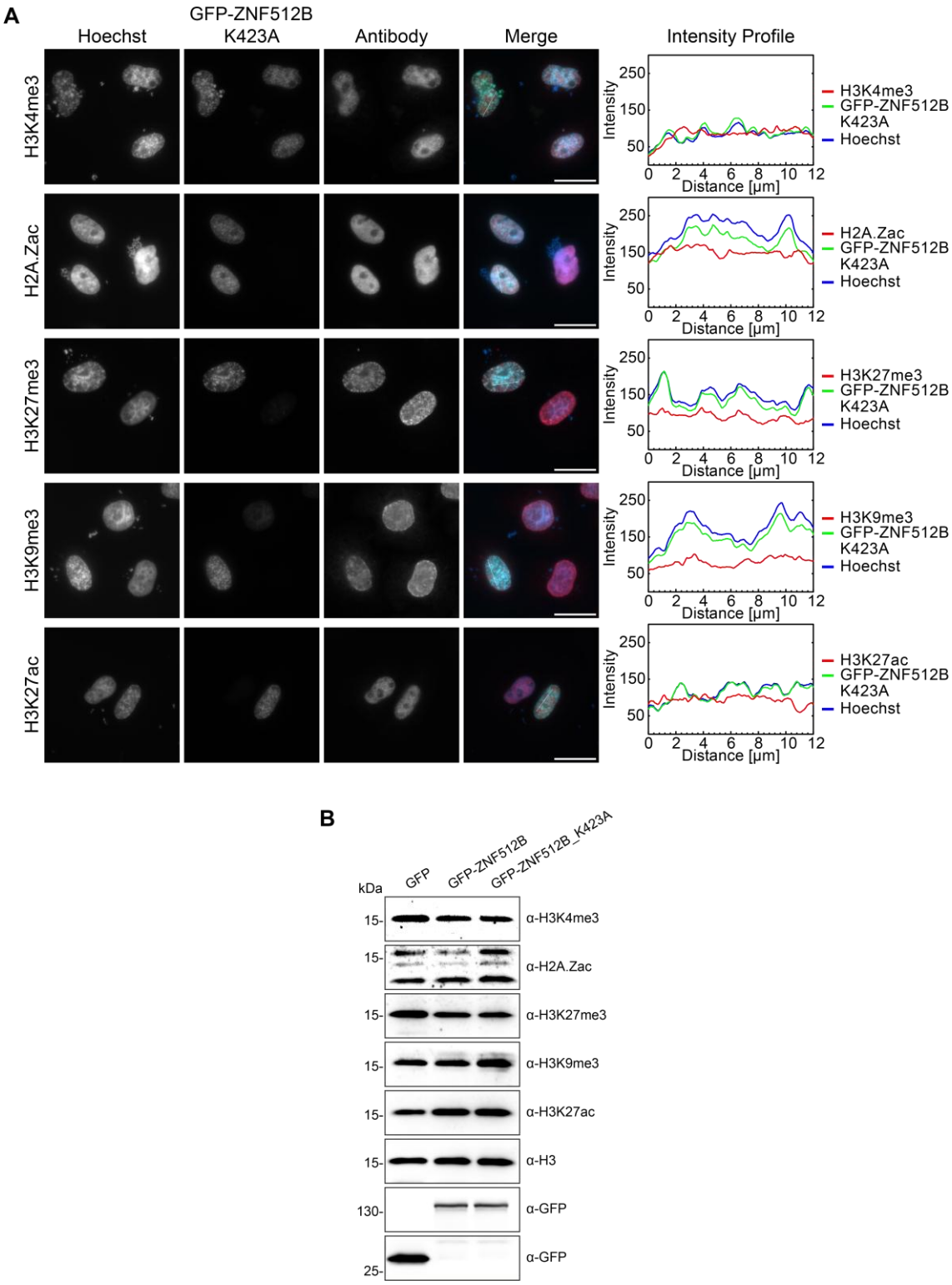

Figure 3.6.3: Loss of NuRD interaction does not influence histone PTM patterns at sites of ZNF512B-induced chromatin aggregation. (A) Left: *IF microscopy of Hoechst (DNA, blue) stained HeLaK cells expressing GFP-ZNF512B_K423A (green) and co-stained with different antibodies against active (H3K4me3, H2A.Zac, H3K27ac) or repressive (H3K27me3, H3K9me3) histone modifications (red). Scale bars: 20 µm.* ***Right:*** *Intensity profiles of nuclear areas from IF pictures (see lines, left) depicting Hoechst, GFP-ZNF512B_K423A and respective antibody fluorescence.* ***(B)*** *Immunoblots of DNase-digested nuclear extracts from HeLaK cells expressing GFP, GFP-ZNF512B or GFP-ZNF512B_K423A detecting active (H3K4me3, H2A.Zac, H3K27ac) or repressive (H3K27me3, H3K9me3) histone modifications, GFP (expression control) or H3 (loading control).*

3.7 ZNF512B interacts with the complete NuRD complex and NIM-independent proteins

To independently verify NuRD binding and to further identify the interactome of ZNF512B, I performed GFP-Trap IPs with MNase-digested nuclear extracts of HeLaK cells transfected with the GFP, GFP-ZNF512B or GFP-ZNF512B_K423A plasmids and used the eluates for label-free quantitative MS (lfqMS/MS) experiments in collaboration with Dr. Falk Butter (Institute of Molecular Virology and Cell Biology, Friedrich-Loeffler-Institute, Federal Research Institute for Animal Health, Greifswald, Germany) (Figure 3.7.1A–D). Remarkably, GFP-ZNF512B pulled down every single member of the NuRD complex, while GFP-ZNF512B_K423A, as anticipated, pulled down none. Once more I could verify the interactions with H2A.Z-containing nucleosomes as well as HMG20A and show that these are NIM-independent. Interestingly, I also discovered some new NIM-independent interactors. To rule out false positives, I applied pull-downs and immunoblots and confirmed the interaction of GFP-ZNF512B and GFP-ZNF512B_K423A with karyopherin subunit alpha 4 (KPNA4), which plays a role in nuclear import (Wing et al., 2022), and URB1 ribosome biogenesis homolog (URB1), a protein that enables RNA binding activity (Shan et al., 2023) (Figure 3.7.1E).

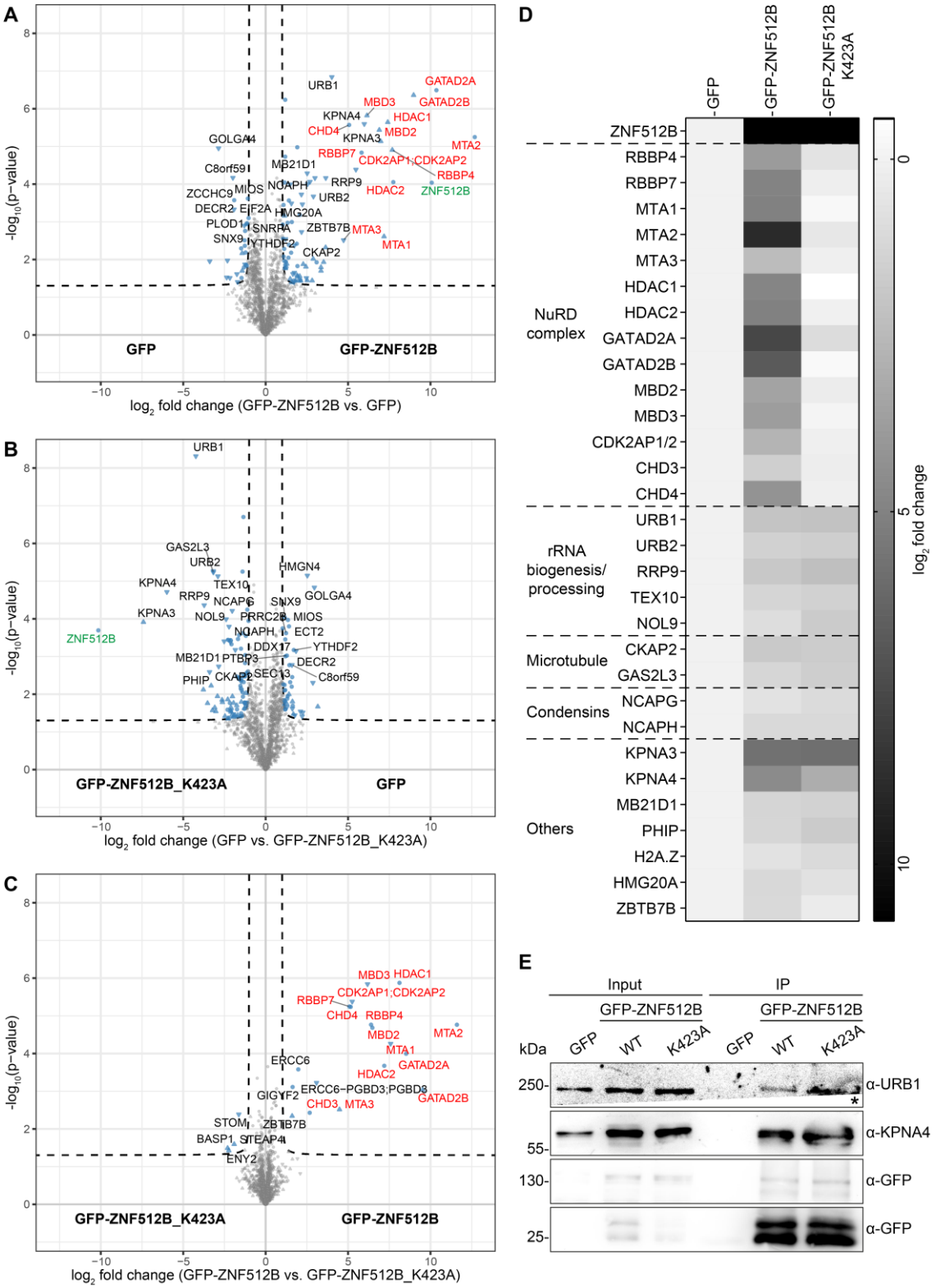

Figure 3.7.1: ZNF512B interacts with the complete NuRD complex and with NIM-independent proteins. ***(A, B, C)*** *Volcano plots of lfqMS/MS data (one representative experiment with four technical replicates per sample) comparing* ***(A)*** *proteins enriched on GFP-ZNF512B with those bound to GFP (control) or* ***(B)*** *proteins enriched on GFP (control) with those bound to GFP-ZNF512B_K423A or* ***(C)*** *proteins enriched on GFP-ZNF512B with those bound to GFP-ZNF512B_K423A. ZNF512B is highlighted in green, NuRD complex members are highlighted in red.* ***(D)*** *Heatmap of significantly enriched interactors of GFP-ZNF512B or GFP-ZNF512B_K423A compared to GFP. Shown is the average log_2 fold change of two independent experiments with four technical replicates per sample each.* ***(E)*** *Immunoblots of MNase-*

digested nuclear extracts from HeLaK cells expressing GFP, GFP-ZNF512B or GFP-ZNF512B_K423A after pull-down with GFP-Trap beads detecting URB1, KPNA4 or GFP (IP control). Asterisk indicates cut membrane.

Subsequently, I created an overview of ZNF512B's interaction network using the STRING database (Figure 3.7.2) (Szklarczyk et al., 2023). In general, ZNF512B's interacting proteins could be sorted into four clusters. The first and largest cluster contains the NuRD complex and its associated proteins, like H2A.Z and HMG20A. The second cluster 'NLS-dependent protein nuclear import complex' contains the two importin subunits KPNA3/4. Then, there is the third cluster 'positive regulation of chromosome condensation' composed of non-SMC condensin I complex subunit G/H (NCAPG/H), cytoskeleton associated protein 2 (CKAP2) and growth arrest specific 2 like 3 (GAS2L3). NCAPG/H are involved in chromosome condensation and stability during meiosis and mitosis (Cai et al., 2022; Liu et al., 2024), CKAP2 is a mitotic spindle protein (McAlear & Bechstedt, 2022) and GAS2L3 is a regulator of cell division binding actin and microtubules (Sharaby et al., 2014). Finally, there is the fourth cluster 'ribosome biogenesis' including URB1/2, testis expressed 10 (TEX10), ribosomal RNA processing 9 (RRP9) and nucleolar protein 9 (NOL9). These proteins all play a role in (pre-)rRNA processing and maturation (Clerget et al., 2020; Finkbeiner et al., 2011; Gordon et al., 2019). Three proteins did not fit any of the clusters: Zinc finger and BTB domain containing 7B (ZBTB7B, also known as ThPOK), pleckstrin homology domain interacting protein (PHIP) and cyclic GMP-AMP synthase (CGAS, also known as MB21D1). ZBTB7B controls $CD4^+$ T cell development by recruitment of the NuRD complex (Gao et al., 2022), PHIP is a H3K4 methylation-binding protein (Morgan et al., 2017) and CGAS functions as a DNA sensor (West et al., 2015).

In summary, the gathered interaction data imply that ZNF512B binds to the complete NuRD complex via its internal NIM. Further, I identified new NIM-independent interactors which are mainly involved in chromosome condensation and ribosome biogenesis.

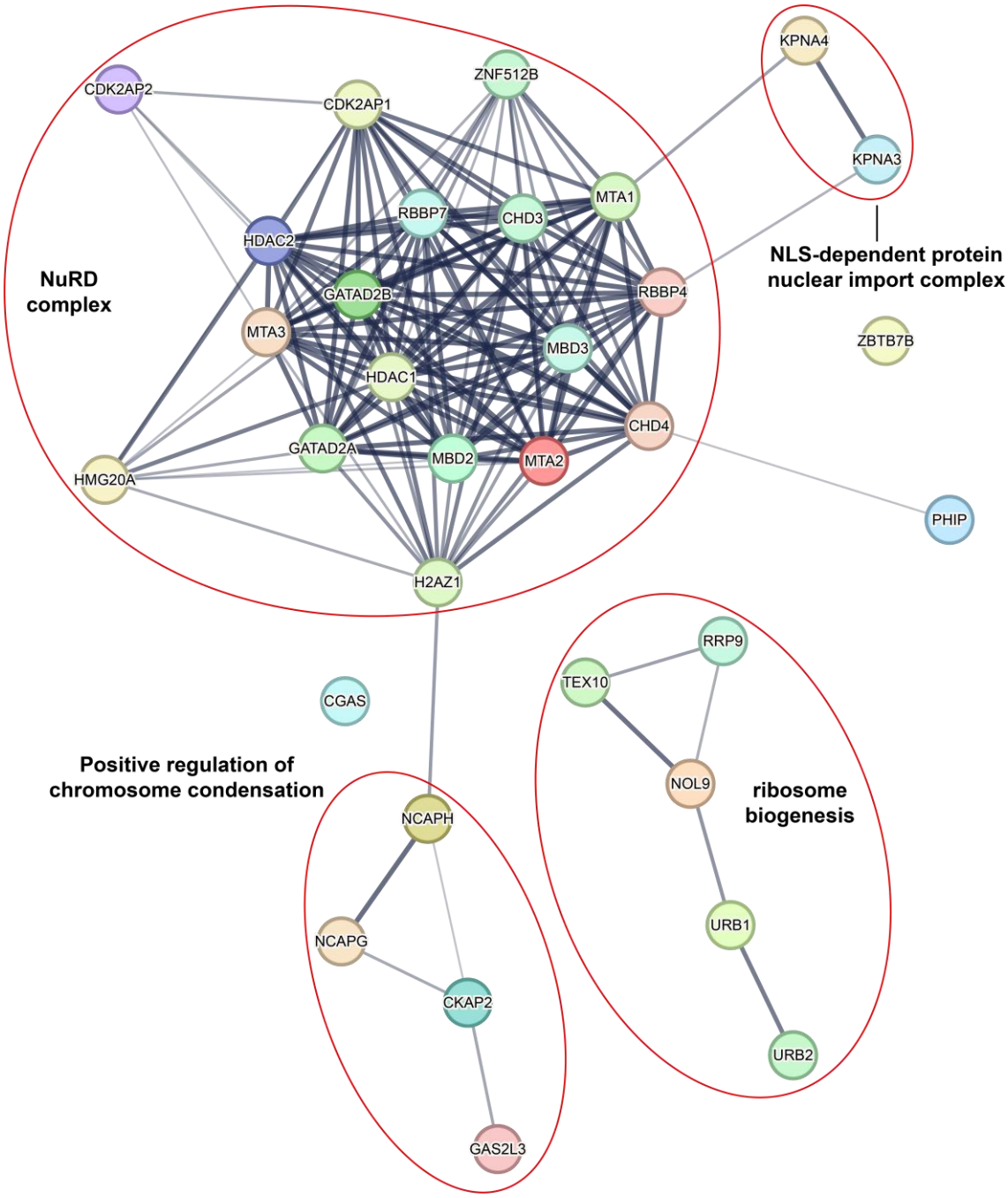

Figure 3.7.2: ZNF512B's interaction network contains four clusters. *Network of ZNF512B interacting proteins based on the lfqMS/MS data created using the STRING database. Red circles indicate clusters. Edges indicate both functional and physical protein associations. Line thickness indicates the strength of data support.*

3.8 ZNF512B affects gene expression in a NuRD-dependent and -independent manner and acts as a transcriptional repressor

After successfully establishing that ZNF512B interacts with the NuRD complex through its NIM, I next proceeded to explore whether it influences gene transcription and if this function is dependent on NuRD binding. To do so, I extracted RNA from HeLaK cells transiently expressing GFP, GFP-ZNF512B (NuRD binding) or GFP-ZNF512B_K423A (loss of NuRD binding) and conducted high-throughput mRNA sequencing (mRNA-seq) in collaboration with Prof. Dr. Marek Bartkuhn and Dr. Tobias Friedrich (Biomedical Informatics and Systems Medicine Science Unit for Basic and Clinical Medicine, Justus-Liebig University Giessen, Germany). The principal component analysis (PCA) revealed that there was high variance between the GFP and the GFP-ZNF512B/GFP-ZNF512B_K423A samples, while the variance between the two ZNF512B constructs was relatively low (Figure 3.8.1A). All three biological replicates per condition produced highly similar results, except for one GFP replicate, which showed some variance to the other two. The sequencing results revealed that, compared to GFP-expressing control cells, approximately 500 or 350 genes were significantly deregulated following GFP-ZNF512B or GFP-ZNF512B_K423A overexpression, respectively (Figure 3.8.1B, C). Among these, 229 genes were uniquely deregulated in cells overexpressing GFP-ZNF512B, while 68 genes were uniquely deregulated in cells overexpressing GFP-ZNF512B_K423A, indicating that ZNF512B influences gene expression in a NuRD-dependent and -independent manner (Figure 3.8.1C). Unexpectedly, the majority of genes that were commonly deregulated or exclusively deregulated by GFP-ZNF512B_K423A were downregulated, whereas most genes exclusively deregulated by GFP-ZNF512B were upregulated (Figure 3.8.1D, E). These upregulated genes were predominantly expressed at very low levels or not at all in GFP control cells (Figure 3.8.1F). Over-representation analysis (ORA) and gene set enrichment analysis (GSEA) for both Gene Ontology (GO) and Kyoto Encyclopedia of Genes and Genomes (KEGG) databases showed that the shared deregulated genes are involved in various biological processes and molecular functions, making it difficult to establish a specific biological connection between ZNF512B and a particular process (Figure 3.8.1G).

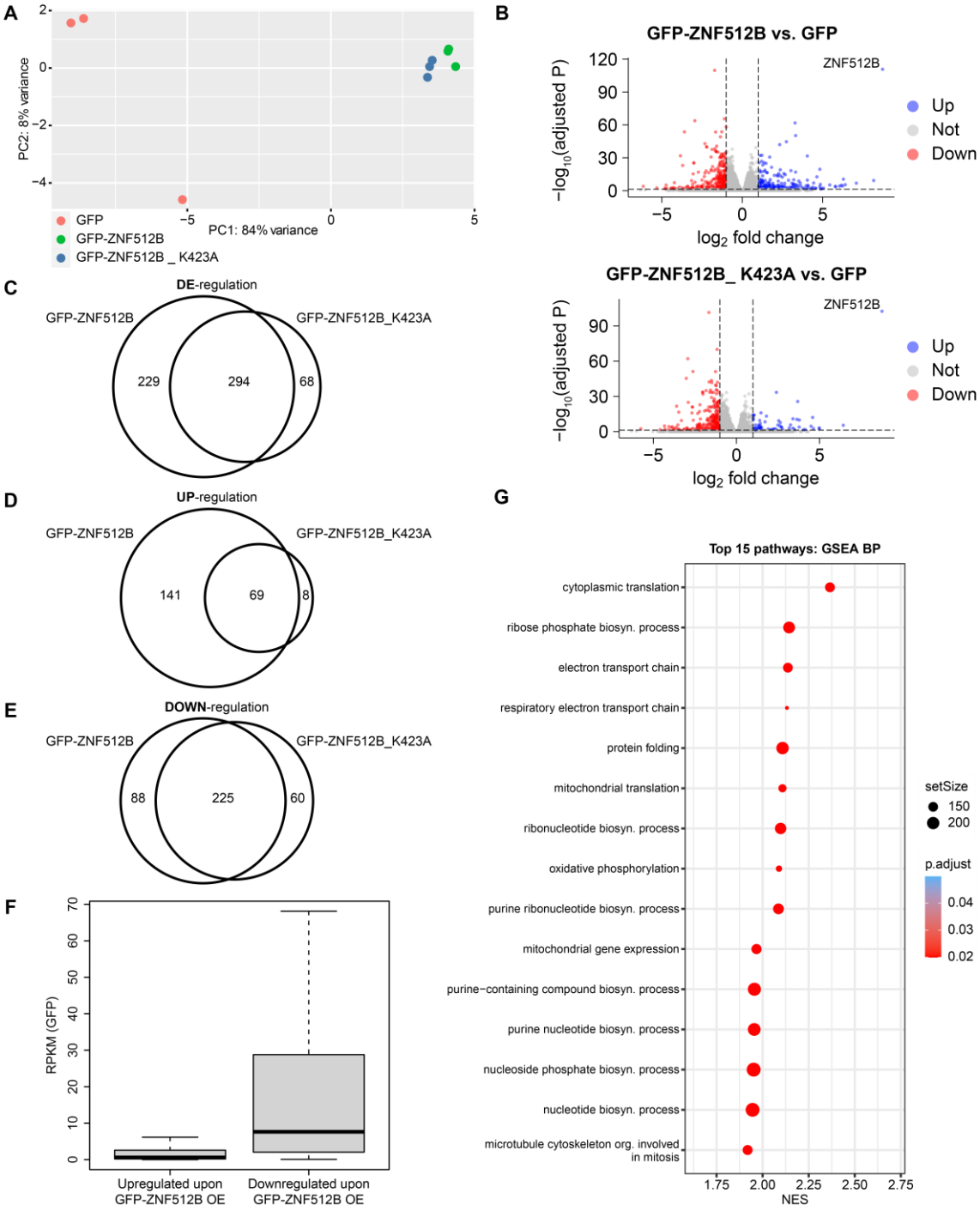

Figure 3.8.1: ZNF512B overexpression affects the transcriptome in a NuRD-dependent and an -independent manner. ***(A)*** *PCA of mRNA-seq data from three replicates each of HeLaK cells expressing GFP, GFP-ZNF512B or GFP-ZNF512B_K423A.* ***(B)*** *Volcano plots showing deregulated genes in GFP-ZNF512B (top) or GFP-ZNF512B_K423A (bottom) expressing HeLaK cells compared to GFP control.* ***(C, D, E)*** *Euler diagrams depicting the overlap of significantly* ***(C)*** *deregulated,* ***(D)*** *upregulated or* ***(E)*** *downregulated genes (log_2 FC > 1 or < -1 and adjusted p-value < 0.05) upon GFP-ZNF512B or GFP-ZNF512B_K523A overexpression compared to GFP control.* ***(F)*** *Box plot depicting gene expression base levels (RPKM) of GFP expressing HeLaK cells. Shown are genes significantly up- or downregulated upon GFP-ZNF512B overexpression (OE).* ***(G)*** *Gene set enrichment analysis (GSEA) for the Gene Ontology (GO) database of deregulated genes upon GFP-ZNF512B and GFP-ZNF512B_K423A overexpression compared to GFP control.*

As I utilized an artificial overexpression system thus far, I next questioned whether the endogenous protein also contributes to the regulation of gene expression. To investigate this, I depleted endogenous ZNF512B in HeLaK cells using siRNA-mediated knock-down (KD). I observed a significant reduction in ZNF512B mRNA and protein levels, confirmed by RT-qPCR, immunoblots and IF microscopy (Figure 3.8.2A–C, with help from Lena Paasche, Institute for Genetics, Justus-Liebig University Giessen, Germany). Subsequently, I performed mRNA-seq on these cells, again in collaboration with Prof. Dr. Marek Bartkuhn and Dr. Tobias Friedrich (Biomedical Informatics and Systems Medicine Science Unit for Basic and Clinical Medicine, Justus-Liebig University Giessen, Germany). The PCA revealed that there was high variance between the control (Ctrl) and the ZNF512B KD, while there was low variance between the two biological replicates of each condition (Figure 3.8.2D). The sequencing results indicated that 18 genes were upregulated and eight were downregulated significantly following ZNF512B depletion, suggesting that it might indeed play a role in transcriptional regulation, however only for a very limited subset of genes (Figure 3.8.2E). ORA and GSEA analyses for GO and KEGG databases showed that the genes deregulated upon ZNF512B depletion are primarily involved in processes related to RNA-processing (Figure 3.8.2F).

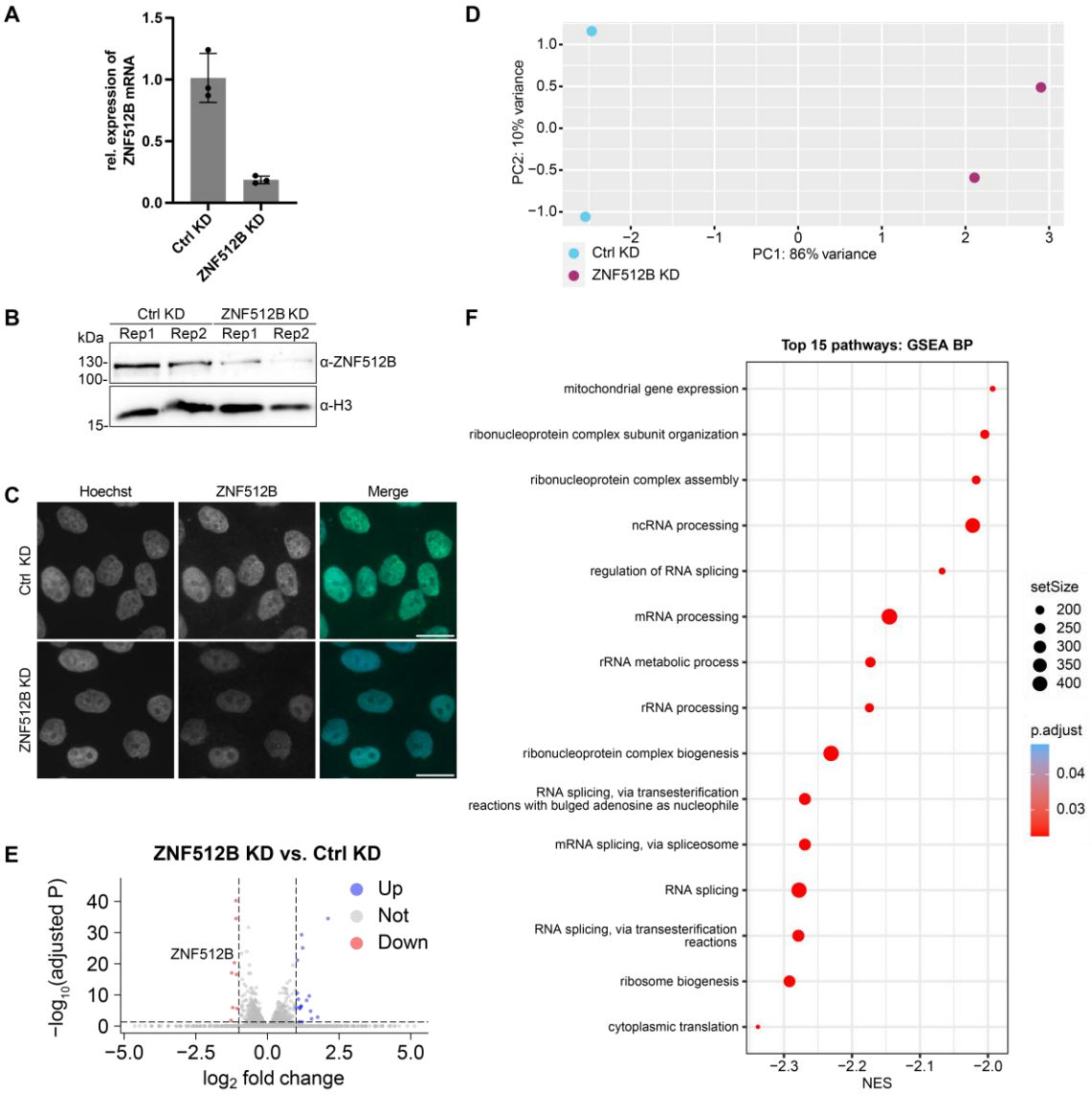

Figure 3.8.2: ZNF512B depletion influences a subset of genes involved in RNA-related processes. (A) *RT-qPCR to detect relative ZNF512B mRNA expression upon siRNA-mediated Ctrl or ZNF512B knock-down (KD) in HeLaK cells normalized to HPRT1 expression. Depicted is the mean with standard deviation (SD) of three biological replicates.* ***(B)*** *Immunoblots of nuclear extracts from two replicates (Rep) each of HeLaK cells upon siRNA-mediated Ctrl or ZNF512B KD detecting ZNF512B or H3 (loading control).* ***(C)*** *IF microscopy of Hoechst (DNA, blue) stained HeLaK cells upon siRNA-mediated Ctrl or ZNF512B KD co-stained with anti-ZNF512B antibody (green). Scale bars: 20 µm.* ***(D)*** *Principal component analysis (PCA) of mRNA-seq data from two replicates each of HeLaK cells upon siRNA-mediated Ctrl or ZNF512B KD.* ***(E)*** *Volcano plot showing deregulated genes in HeLaK cells upon siRNA-mediated ZNF512B KD compared to Ctrl KD.* ***(F)*** *Gene set enrichment analysis (GSEA) for the Gene Ontology (GO) database of deregulated genes upon siRNA-mediated ZNF512B KD compared to Ctrl KD.*

I consequently compared all mRNA-seq data sets from before, showing that there were only some genes upregulated upon overexpression and downregulated upon KD of ZNF512B and vice versa (Figure 3.8.3A). Unfortunately, different strategies to identify direct target genes of ZNF512B that are repressed in a NuRD-dependent manner (comparing downregulated genes upon GFP-ZNF512B overexpression with upregulated

genes upon ZNF512B KD or comparing upregulated genes upon GFP-ZNF512B_K423A overexpression with upregulated genes upon ZNF512B KD) did not return overlapping genes. Nevertheless, to verify the mRNA-seq data, I also validated some genes by RT-qPCR (Figure 3.8.3B, with help from Felix Diegmüller, Institute for Genetics, Justus-Liebig University Giessen, Germany).

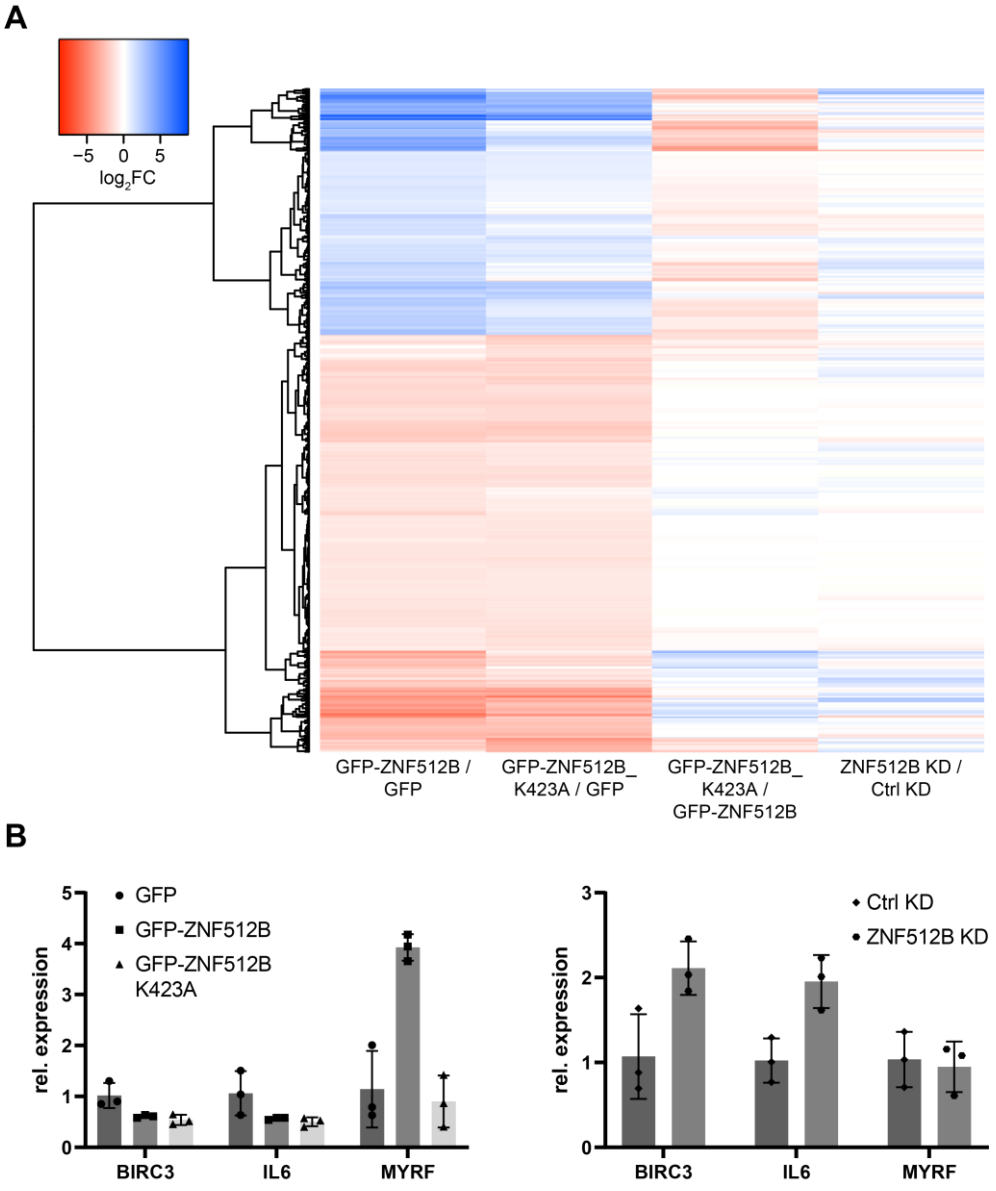

Figure 3.8.3: RT-qPCR verified the ZNF512B mRNA-seq data. (A) *Heatmap of deregulated genes upon GFP-ZNF512B or GFP-ZNF512B_K423A overexpression compared to GFP control, upon GFP-ZNF512B_K423A overexpression compared to GFP-ZNF512B overexpression or upon siRNA-mediated ZNF512B KD compared to Ctrl KD.* ***(B)*** *RT-qPCR to detect relative baculoviral IAP repeat containing 3 (BIRC3), Interleukin 6 (IL6) or myelin regulatory factor (MYRF) mRNA expression upon GFP, GFP-ZNF512B or GFP-ZNF512B_K423A overexpression (top) or upon siRNA-mediated Ctrl or ZNF512B KD (bottom) in HeLaK cells normalized to HPRT1 expression. Depicted is the mean with SD of three biological replicates. mRNA-seq data: BIRC3 and IL6 genes were downregulated upon GFP-ZNF512B and GFP-ZNF512B_K423A overexpression compared to GFP control and upregulated upon ZNF512B KD compared to Ctrl KD; MYRF was upregulated upon GFP-ZNF512B overexpression compared to GFP-ZNF512B_K423A overexpression and GFP control.*

A rational next step was to analyze via chromatin immunoprecipitation (ChIP) on which sites in the genome ZNF512B can be found. Since I already established that ZNF512B can pull down nucleosomes without crosslinking, I decided to conduct native ChIP experiments using MNase for chromatin digestion and GFP-Trap beads for IPs. To first test whether this was a reasonable approach, I prepared nuclear extracts of HeLaK cells transiently expressing GFP, GFP-ZNF512B or GFP-ZNF512B_K423A and performed ChIP-qPCR (Figure 3.8.4). Given that ZNF512B is associated with H2A.Z and HMG20A, I used primers to check two different H2A.Z.1/HMG20A-positive sites (ADAMTS3 gene body and EIF4H promoter) and two different H2A.Z.1/HMG20A-negative sites (GNAI1 gene body and RPL11 gene body) in the genome, which had been characterized before (Herchenrother, Gossen, et al., 2023). Remarkably, for GFP-ZNF512B the H2A.Z.1/HMG20A-positive sites were highly enriched, while unexpectedly, for GFP-ZNF512B_K423A this was not the case. As these results were promising that my approach worked, I decided to continue with high-throughput ChIP sequencing (ChIP-seq). I performed ChIP on nuclear extracts of HeLaK cells transiently expressing GFP, GFP-ZNF512B or GFP-ZNF512B_K423A as before and prepared the sequencing library. Unfortunately, the resulting sequencing data sets have yet to be analyzed.

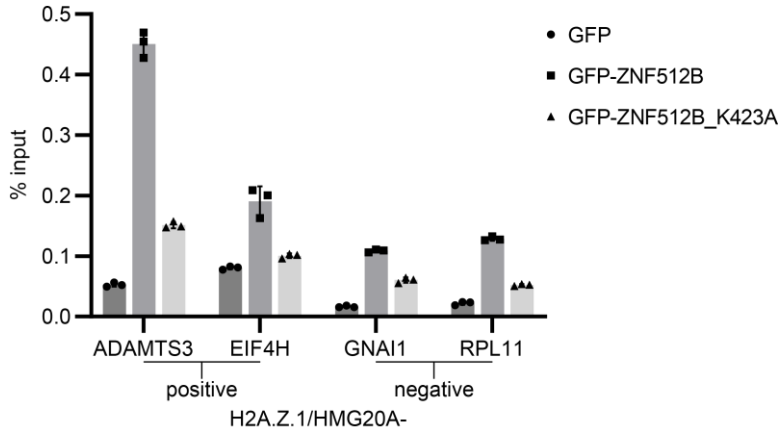

Figure 3.8.4: ZNF512B localizes to H2A.Z.1/HMG20A-positive sites in the genome. *ChIP-qPCR on MNase-digested nuclear extracts from HeLaK cells expressing GFP, GFP-ZNF512B or GFP-ZNF512B_K423A after pull-down with GFP-Trap beads. H2A.Z.1/HMG20A-positive sites: ADAMTS3 gene body and EIF4H promoter. H2A.Z.1/HMG20A-negative sites: GNAI1 gene body and RPL11 gene body. Depicted is the mean with SD of three technical replicates.*

Finally, I employed a luciferase-based reporter assay in HEK293T cells to investigate whether the recruitment of ZNF512B to promoters directly influences transcription

(Figure 3.8.5A, with help from Dr. Jörg Leers and Felix Diegmüller, Institute for Genetics, Justus-Liebig University Giessen, Germany). Therefore, I used various ZNF512B deletion or mutation constructs. These were tagged with a GAL4-tag for recruitment to the promoter of a luciferase reporter gene under the control of an upstream activator sequence (UAS) leading to expression or repression of the luciferase gene depending on the properties of the respective ZNF512B construct. Notably, ZNF512B exhibited a significant repressive effect, indicating a potential role in inhibiting rather than activating transcription (Figure 3.8.5B). The K423A mutation resulted in reduced but still over 50 % repression, suggesting that the interaction with NuRD only partially accounts for the inhibitory effect, as previously suggested by the mRNA-seq analyses. Similarly, the internal region alone without ZFs (ΔZF) led to strong repression comparable to the full-length ZNF512B protein, while the additional K423A mutation (ΔZF_K423A) again reduced but not completely abolished its repressive capability. Interestingly, deleting the entire internal region (ΔI) also diminished but not eliminated the repressive effect, implying the presence of another repressive region within ZNF512B.

Concurrently, these data demonstrate that ZNF512B regulates a subset of genes through both NuRD-dependent and -independent mechanisms, localizes to select H2A.Z.1/HMG20A-positive sites in the genome and functions as a transcriptional repressor.

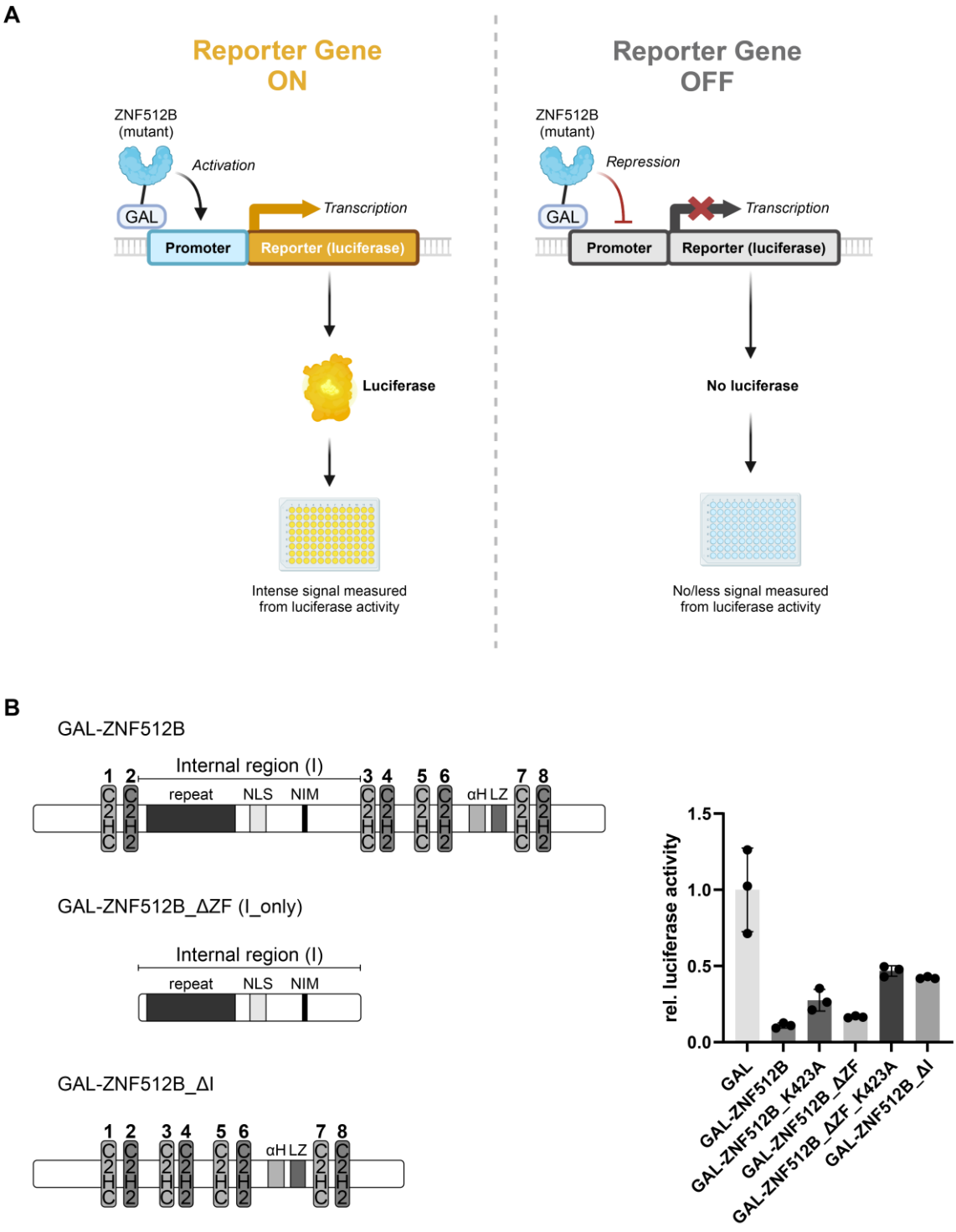

Figure 3.8.5: ZNF512B is a transcriptional repressor. ***(A)*** *Schematic depiction of the luciferase reporter assay. Proteins with GAL4-tag are recruited to the UAS of the luciferase gene promoter leading to expression or repression of the luciferase gene and a measurable difference in the resulting bioluminescence.* ***(B) Left:*** *Schematic depiction of the used constructs.* ***Right:*** *Reporter assay of HEK293T cells expressing luciferase-reporter and GAL control or different GAL-ZNF512B constructs. Depicted is the mean with SD of three biological replicates.*

3.9 ZNF512B directly interacts with RBBP4 of the NuRD complex

Given the significance of the NuRD complex association for ZNF512B's role as a transcriptional repressor, I aimed to examine this interaction in greater detail. All mentioned NIM-containing proteins directly interact with RBBP4 of the NuRD complex (Chapter 1.1.4.1). Therefore, I investigated in collaboration with Prof. Dr. Joel Mackay and Dr. Chandrika Deshpande (School of Life and Environmental Sciences, University of Sydney, Australia) whether ZNF512B also directly interacts with RBBP4. They expressed His-tagged full-length RBBP4 in Sf9 insect cells, purified the protein, reconstituted the RBBP4-ZNF512B complex by combining RBBP4 with a synthetic peptide containing the ZNF512B NIM (residues 419–430) and resolved the X-ray crystal structure of the complex. They identified two copies of the RBBP4-ZNF512B complex in the asymmetric unit with effectively identical conformations. RBBP4 exhibited a barrel-shaped β-propeller fold with a prominent acidic cavity on one of the apical surfaces (Figure 3.9A–C). The electron density map was successfully modeled for residues 10–410, with the exclusion of a likely highly dynamic loop at residues 90–113. The backbone conformation of RBBP4 exhibited a high degree of similarity to that observed in the RBBP4-FOG-1 complex (Protein Data Bank (PDB): 2XU7, (Berman et al., 2000)) (Figure 3.9B). The ZNF512B peptide (419–430) was successfully modeled in the structure with high confidence, revealing that it bound in an extended conformation to the acidic surface of RBBP4 (Figure 3.9C). The complex led to the formation of numerous electrostatic interactions (Figure 3.9D). Generally, the residues in the C-terminal half of the ZNF512B peptide (Q424–F430) exhibited conformations that were highly similar to those of the corresponding residues of FOG-1 in the RBBP4-FOG-1 structure (Figure 3.9E). The side chains of K425, T426 and K428 were observed to project into the solvent, while Q424 and P427 were seen to pack into a broad uncharged groove. K429 was positioned on an acidic surface formed by E41 and D74 in one copy of the complex and E41 and E75 in the other: The RBBP4 backbone underwent a localized reorientation with either D74 or E75 positioned in proximity to the K429 side chain. Similarly, the side-chain positions of ZNF512B residues R422 and K423 occupied the same negatively charged pockets and formed analogous interactions as the corresponding residues in FOG-1 (Figure 3.9C–E). Consequently, R422 formed an ion pair with E231 and the backbone carbonyl of N277, while K423 interacted with the side chains of E126, N128 and E179. It was observed that there were significant differences in the N-terminal segment of the peptide, which was an unexpected finding. In the RBBP4-FOG-1

structure, the side chain of R3 is positioned on an acidic 'shelf', forming electrostatic interactions with the side chains of E231, N277 and E319 (Figure 3.9E). However, in ZNF512B, a rotation of the backbone of R421 reoriented the side chain of this residue, causing it to face away from RBBP4 and towards the solvent. In contrast, the side-chain amino group of K419 occupied the corresponding 'shelf' (Figure 3.9C) and formed interactions with the side chains of E231, N277 and E319 (Figure 3.9D). The side chain of H420 was additionally contributing to this observed reorientation of K419 and R421, through interaction with D318.

In conclusion, ZNF512B directly binds RBBP4 of the NuRD complex via its NIM in a partially distinct way than FOG-1.

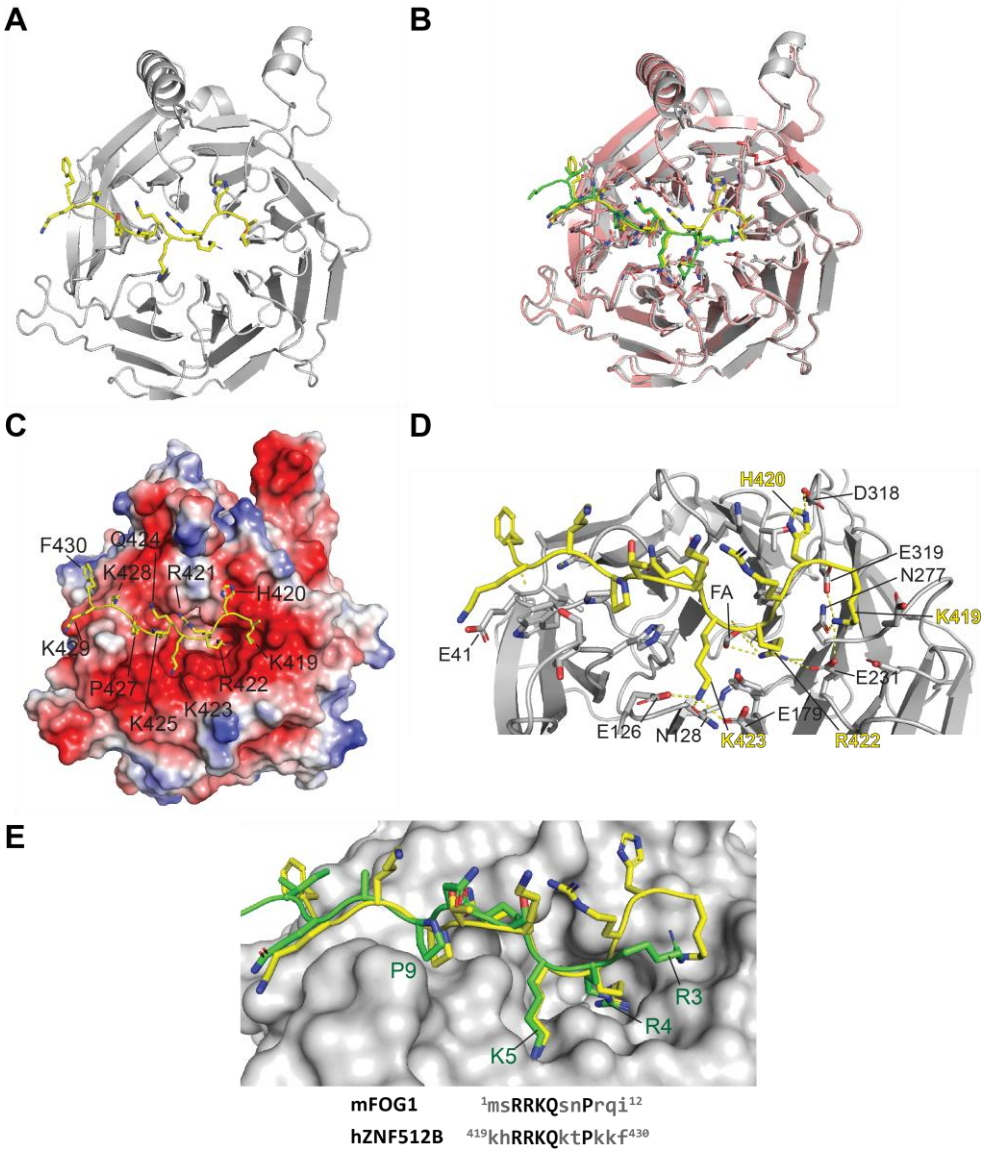

Figure 3.9: ZNF512B directly interacts with RBBP4 of the NuRD complex. ***(A)*** *Ribbon diagram of the RBBP4-ZBF512B complex. RBBP4 is shown in grey and ZNF512B in yellow.* ***(B)*** *Overlay (over backbone*

heavy atoms) of the RBBP4-ZNF512B structure (grey and yellow) with the RBBP4-FOG-1 structure (salmon and green, PDB: 2XU7). ***(C)*** *Same as (A) but with RBBP4 shown as electrostatic potential surface.* ***(D)*** *Close-up of polar interactions (dashed lines) made between RBBP4 and ZNF512B. Residue numbers are indicated in black for RBBP4 and yellow for ZNF512B.* ***(E)*** *Overlay of the structure of FOG-1(1–12) (green, PDB: 2XU7) bound to RBBP4 (grey) with ZNF512B (yellow). Key residues in FOG-1 are labelled. A sequence alignment is shown below, capital letters indicate conserved residues.*

3.10 ZNF512B's interaction with RBBP4 reveals an alternative, internal NuRD-interaction motif

The crystal structure of the RBBP4-ZNF512B complex revealed some unique interactions in comparison to FOG-1 binding to RBBP4. Hence, I wanted to analyze whether the amino acids forming these unique interactions are indeed involved in NuRD binding of ZNF512B in a cellular context. To not exclude other potentially important residues, I decided to test the whole motif. I created a corresponding GFP-ZNF512B alanine point mutant for each residue (K419–F430) and performed IPs followed by immunoblotting (Figure 3.10.1). In accordance with the known NIM and the crystal structure, R422, K423 and P427 were essential for NuRD binding, while K425, T426 and K428 were not. Interestingly, R421 was also not necessary for the interaction as predicted from the crystal structure. Nevertheless, K419, which interacted with RBBP4 in the crystal structure instead of the expected R421, and H420, which formed a new interaction with RBBP4 in comparison to FOG-1, were not essential as well. Q424 was only slightly contributing to NuRD binding, in contrast to the known NIM, and F430 was likewise only partially required. Remarkably, K429, which led to a localized reorientation of the RBBP4 backbone in the crystal structure, was essential for the interaction.

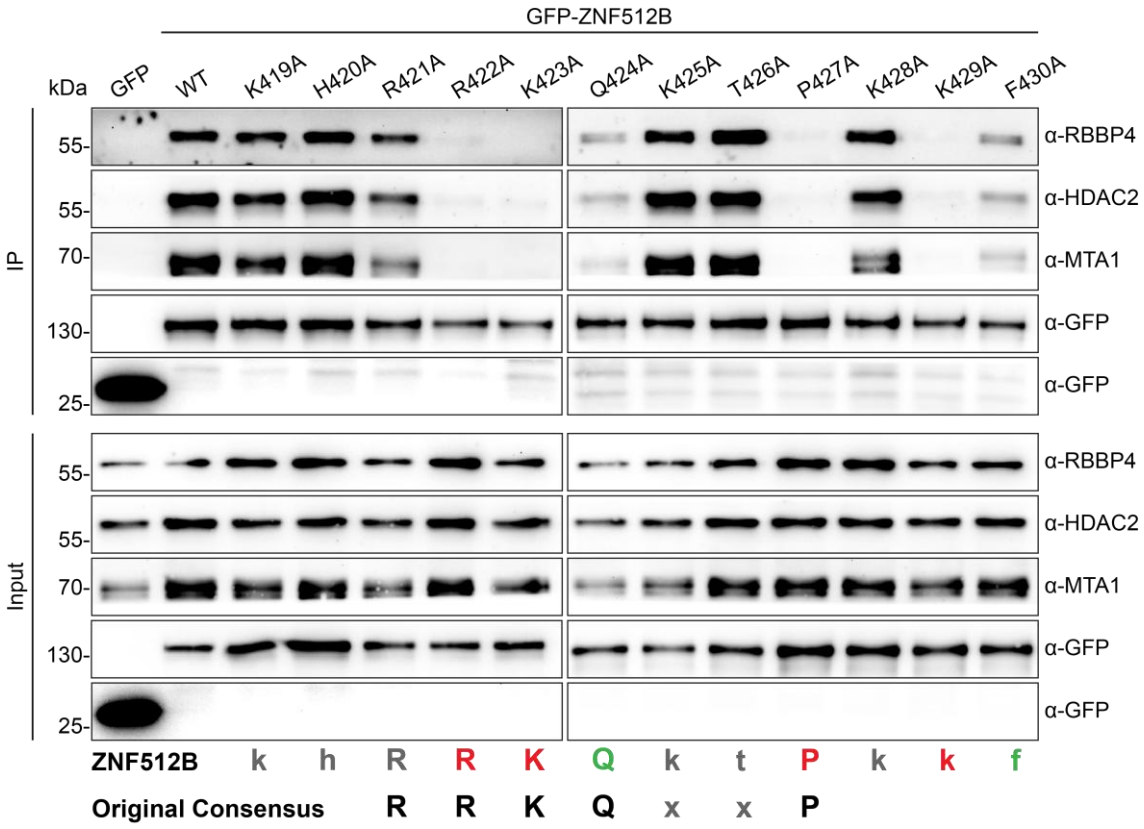

Figure 3.10.1: Distinct amino acids in the ZNF512B NIM are required for NuRD binding. *Immunoblots of DNase-digested cell extracts from HeLaK cells expressing GFP, GFP-ZNF512B or a GFP-ZNF512B point mutant after pull-down with GFP-Trap beads detecting NuRD members RBBP4, HDAC2 or MTA1, or GFP (IP control). ZNF512B residues 419–430 and original NIM consensus sequence are shown below. Capital letters indicate conserved amino acids. Amino acids essential for NuRD binding of ZNF512B are shown in red, amino acids contributing to the interaction are shown in green.*

In addition, I could further confirm my findings in IF microscopy experiments (Figure 3.10.2).

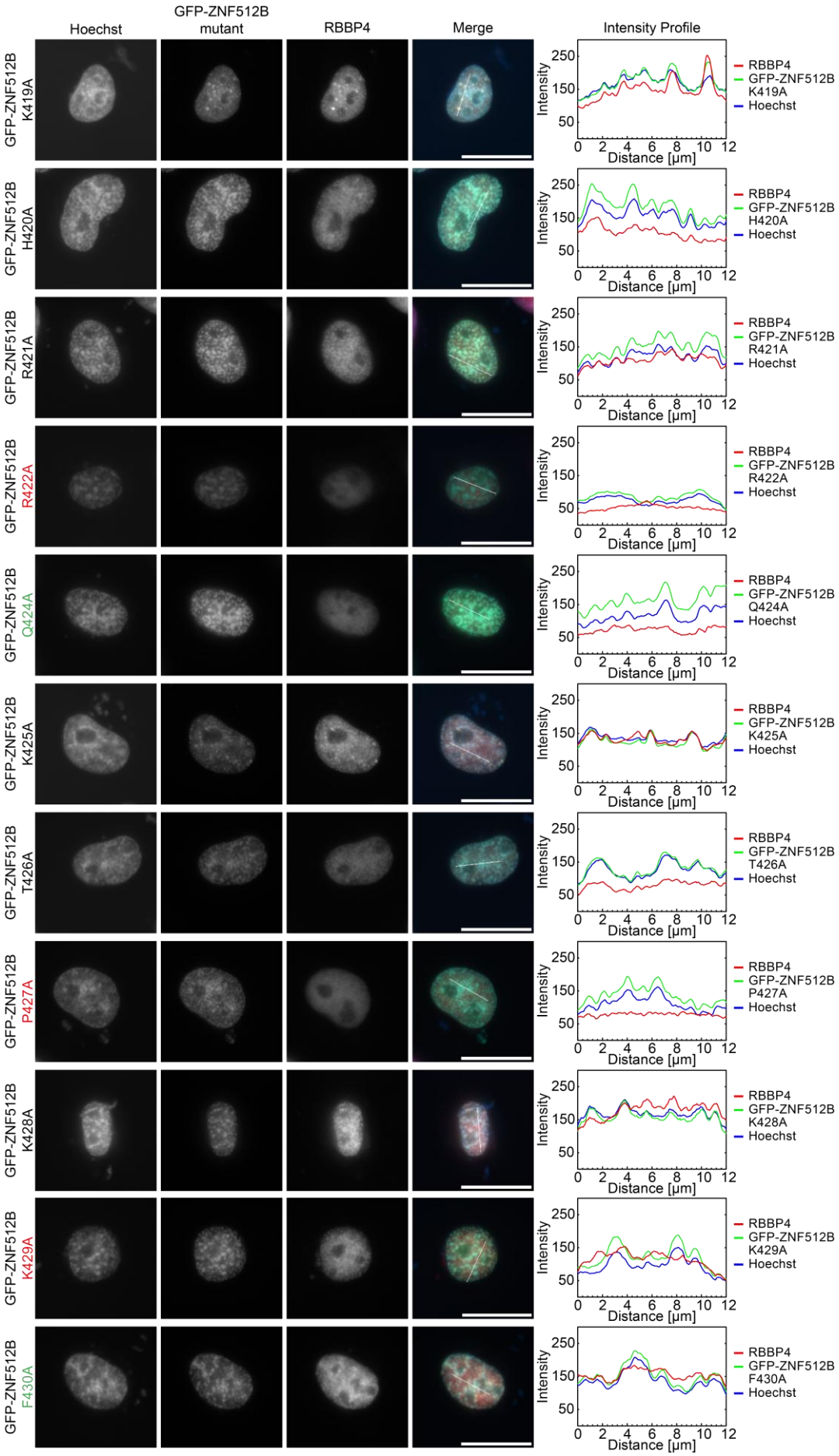
Hoechst
GFP-ZNF512B mutant
RBBP4
Merge
Intensity Profile
GFP-ZNF512B K419A
GFP-ZNF512B H420A
GFP-ZNF512B R421A
GFP-ZNF512B R422A
GFP-ZNF512B Q424A
GFP-ZNF512B K425A
GFP-ZNF512B T426A
GFP-ZNF512B P427A
GFP-ZNF512B K428A
GFP-ZNF512B K429A
GFP-ZNF512B F430A
Intensity
Distance [µm]
RBBP4
GFP-ZNF512B K419A
GFP-ZNF512B H420A
GFP-ZNF512B R421A
GFP-ZNF512B R422A
GFP-ZNF512B Q424A
GFP-ZNF512B K425A
GFP-ZNF512B T426A
GFP-ZNF512B P427A
GFP-ZNF512B K428A
GFP-ZNF512B K429A
GFP-ZNF512B F430A
Hoechst

Figure 3.10.2: RBBP4 does not colocalize with ZNF512B mutations R422A, P427A and K429A. Left: *IF microscopy of Hoechst (DNA, blue) stained HeLaK cells expressing different GFP-ZNF512B point mutants (green) and co-stained with anti-RBBP4 antibody (red). Scale bars: 20 µm. Mutations that impair ZNF512B's NuRD interaction are marked in red, the ones that weaken the interaction are marked in green.* ***Right:*** *Intensity profiles of nuclear areas from IF pictures (see lines, left) depicting Hoechst, GFP-ZNF512B point mutants and anti-RBBP4 antibody fluorescence.*

Following these results, I sought to test two more GFP-ZNF512B mutants in IPs to fully characterize the unusual interaction between ZNF512B and RBBP4. In the crystal structure, K419 of ZNF512B occupied the acidic 'shelf' in RBBP4 which was expected to be occupied by R421 corresponding to R3 in FOG-1. I speculated that if K419 is mutated to an alanine, R421 could take its place on the acidic 'shelf' and vice versa. So, I first created a GFP-ZNF512B_K419A_R421A double mutant. Next, I wondered whether K429, that I had newly identified to be essential for ZNF512B's NuRD interaction, could also be exchanged with a different basic amino acid. Consequently, I created a GFP-ZNF512B_K429R mutant, to check whether an arginine instead of the lysine would be sufficient for NuRD interaction. The GFP-ZNF512B_K419A_R421A double mutant as well as the GFP-ZNF512B_K429R mutant still interacted with the NuRD complex (Figure 3.10.3A), a result I also verified by IF microscopy for the K429R mutant (Figure 3.10.3B). Taking all these data into account, I concluded that the known NIM consensus sequence was unsuitable to properly describe the motif in ZNF512B and questioned whether there were more proteins that might interact with RBBP4 in a comparable way. I used the ScanProsite tool from Expasy (Sigrist et al., 2013) and searched for human proteins containing the adapted NIM sequence 'RKxxxPxK/R'. I found several proteins which had been previously connected to NuRD in direct or rather indirect ways, like zinc-finger E-box binding-homeobox 2 (ZEB2) (Wu et al., 2016). By comparing the NIM sequences within these proteins and ZNF512B with the ones of FOG-1 and others, I finally came up with the hypothesis that two different NIM consensus sequences exist: 1) The known N-terminal NIM 'RRKQxxP' and 2) an internal NIM (iNIM) 'RKxxxPxK' (Figure 3.10.3C).

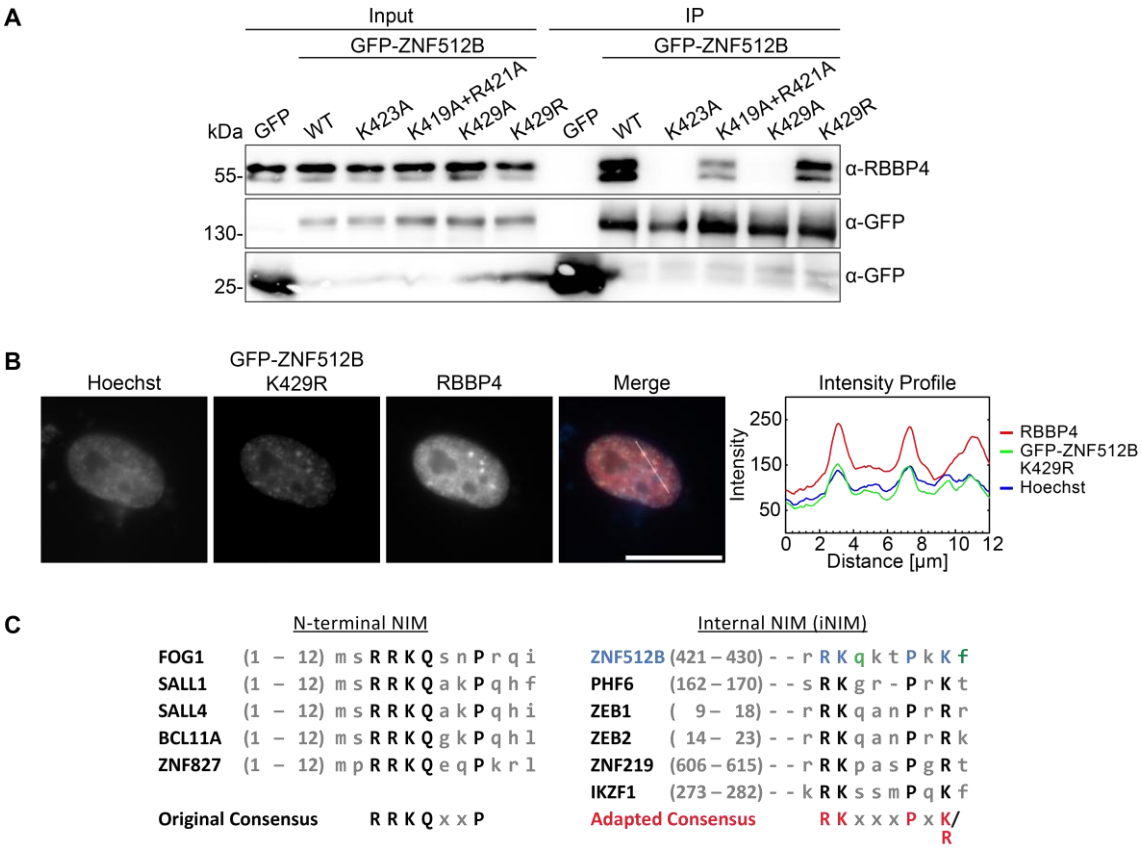

Figure 3.10.3: The ZNF512B-RBBP4 interaction reveals an unusual, additional iNIM consensus sequence. ***(A)*** *Immunoblots of DNase-digested cell extracts from HeLaK cells expressing GFP, GFP-ZNF512B or a GFP-ZNF512B point mutant after pull-down with GFP-Trap beads detecting RBBP4 or GFP (IP control)* ***(B) Left:*** *IF microscopy of a Hoechst (DNA, blue) stained HeLaK cell expressing GFP-ZNF512B_K429R (green) and co-stained with anti-RBBP4 antibody (red). Scale bar: 20 µm.* ***Right:*** *Intensity profile of nuclear area from IF picture (see line, left) depicting Hoechst, GFP-ZNF512B_K429R and anti-RBBP4 antibody fluorescence.* ***(C)*** *Alignments of N-terminal (left) and internal NIM (iNIM, right) sequences. Capital letters indicate conserved amino acids. Green letters indicate amino acids that contribute to but are not essential for ZNF512B's NuRD binding.*

To test my hypothesis and to identify new NuRD interactors, I chose three proteins with an iNIM from my previous search, which had, to my knowledge, not yet been connected to NuRD, namely forkhead box J1 (FOXJ1) (Padua et al., 2023) and zinc finger and BTB domain-containing protein 20 (ZBTB20) (Stoyanov et al., 2023), or which had at least not been connected to direct RBBP4 interaction, namely ZNF148 (also known as ZBP-89) (Woo et al., 2008) (Figure 3.10.4A). I cloned GFP-tagged constructs of these proteins and performed IPs and immunoblots (Figure 3.10.4B, C). None of the three proteins was able to pull down RBBP4. Since the transfection efficiency for GFP-ZNF148 was very low, as visible in the input, I repeated the experiment for this protein, but, again, it did not pull down RBBP4 (Figure 3.10.4D). Finally, to rule out that the GFP-tag interferes with

ZNF148's NuRD interaction, I cloned a FLAG-tagged version of the construct and repeated the experiment (Figure 3.10.4E). Still, it showed no interaction with RBBP4.

In summary, I showed that distinct amino acids in ZNF512B are required for RBBP4 binding and discovered an alternative, internal NuRD-interaction motif (iNIM) that is present in several other proteins.

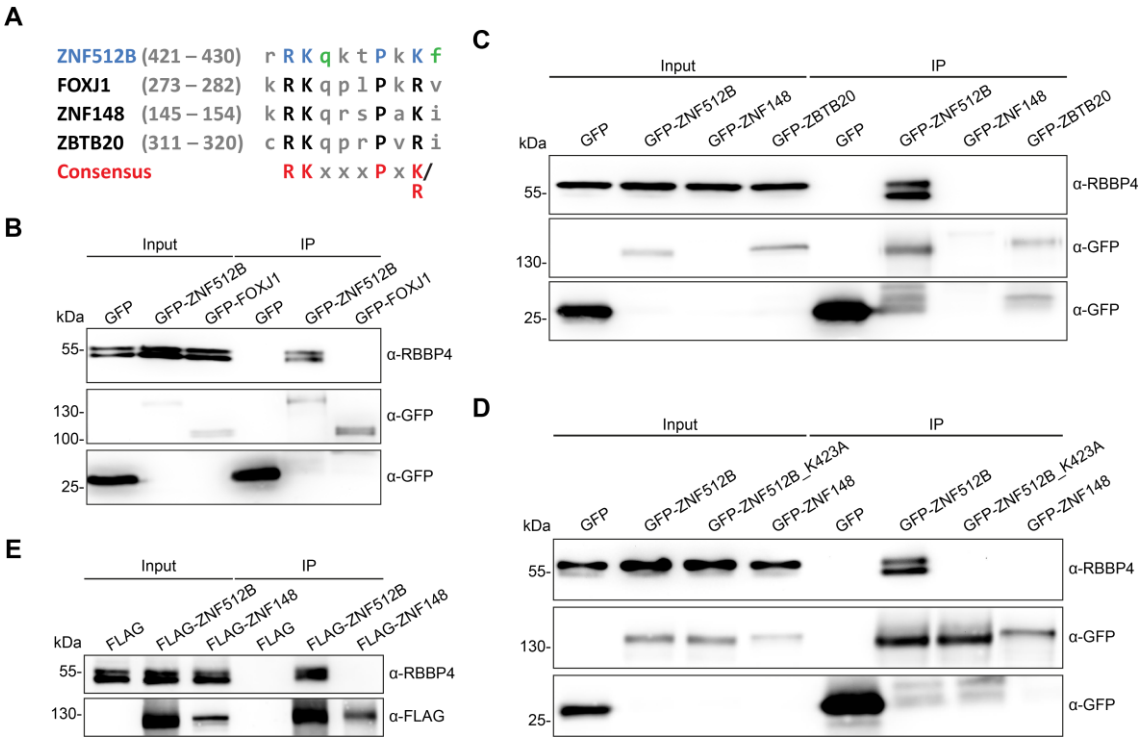

Figure 3.10.4: FOXJ1, ZBTB20 and ZNF148 do not interact with RBBP4. ***(A)*** *Alignment of the iNIM in ZNF512B with the putative iNIMs of FOXJ1, ZNF148 and ZBTB20. Capital letters indicate conserved amino acids. Green letters indicate amino acids that contribute to but are not essential for ZNF512B's NuRD binding.* ***(B–D)*** *Immunoblots of DNase-digested cell extracts from HeLaK cells expressing GFP, GFP-ZNF512B, GFP-ZNF512B_K423A, GFP-FOXJ1, GFP-ZNF148 or GFP-ZBTB20 after pull-down with GFP-Trap beads detecting RBBP4 or GFP (IP control).* ***(E)*** *Immunoblots of DNase-digested cell extracts from HeLaK cells expressing FLAG, FLAG-ZNF512B or FLAG-ZNF148 after pull-down with DYKDDDDK Fab-Trap beads detecting RBBP4 or FLAG (IP control).*

3.11 ZNF512B's iNIM facilitates high affinity binding to RBBP4

Since I hypothesized the existence of two different NIMs, I decided to test whether these confer different binding affinities. I performed a competition experiment by repeating GFP-Trap IPs with cell extracts from HeLaK cells expressing GFP or GFP-ZNF512B but incubated the inputs with different concentrations of FOG-1 NIM, ZNF512B iNIM or scrambled peptides as control. Subsequent immunoblots detecting RBBP4 or MTA1 revealed that > 750 nM FOG-1 NIM peptide were necessary to compete the interaction

between GFP-ZNF512B and NuRD while 250 nM ZNF512B iNIM peptide were already sufficient to do the same (Figure 3.11A, B). To quantify this difference in binding affinities, competitive fluorescence polarization (FP)-based experiments were performed in a collaboration with Prof. Dr. Olalla Vázquez and Dr. Van Tuan Trinh (Chemical Biology, Department of Chemistry, Philipps University Marburg, Germany) using unlabeled ZNF512B iNIM, scrambled ZNF512B iNIM and FOG-1 NIM peptides to displace a ZNF512B tracer from RBBP4 (Figure 3.11C). These experiments demonstrated a strikingly low competitive inhibition constant for the iNIM in ZNF512B (k_i = 19 ± 7 nM) in comparison to the NIM in FOG-1 (k_i = 1200 ± 500 nM), indicating that ZNF512B binds RBBP4 with > 60-fold higher affinity (Figure 3.11D, E).

In summary, the iNIM in ZNF512B facilitates high-affinity binding to RBBP4 of the NuRD complex.

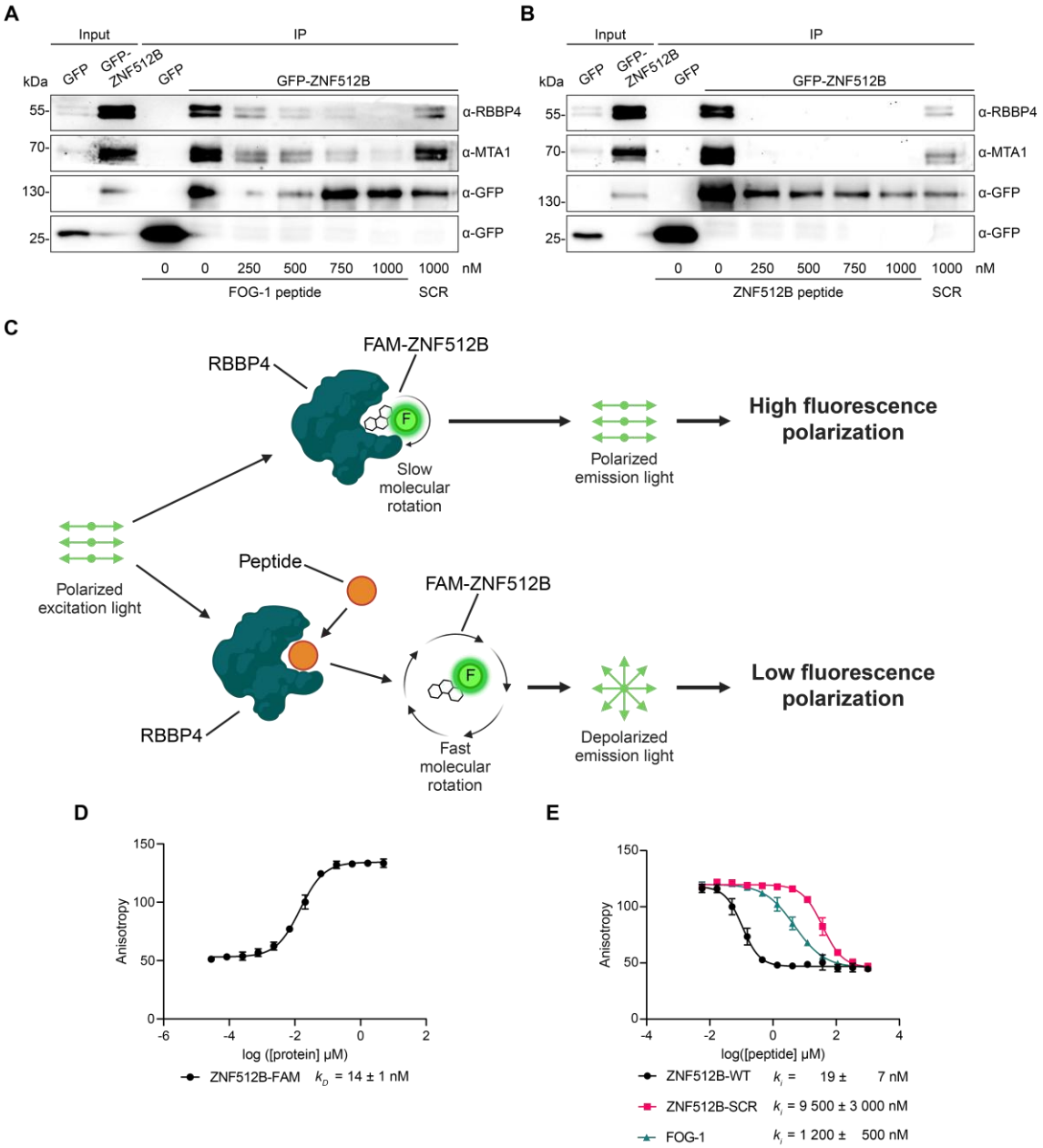

Figure 3.11: ZNF512B binds RBBP4 with high affinity via its iNIM. (A, B) *Immunoblots of DNase-digested cell extracts from HeLaK cells expressing GFP or GFP-ZNF512B incubated with increasing amounts of* ***(A)*** *FOG-1 or* ***(B)*** *ZNF512B NIM peptides or respective scrambled (SCR) control peptides after pull-down with GFP-Trap beads detecting NuRD members RBBP4 or MTA1, or GFP (IP control).* ***(C)*** *Schematic depiction of the FP-based binding experiment. RBBP4 binds the fluorescein (FAM)-labelled ZNF512B tracer leading to high fluorescence polarization. Increasing concentrations of an RBBP4-binding peptide displace the FAM-ZNF512B tracer leading to a measurable difference in fluorescence polarization.* ***(D)*** *FP-based saturation binding experiment of RBBP4 to FAM-labelled ZNF512B.* ***(E)*** *FP-based binding experiment of RBBP4. Competitive experiments of unlabeled FOG-1 NIM (1–12), ZNF512B iNIM and scrambled peptides displacing the FAM-labelled ZNF512B tracer from RBBP4.*

4 Discussion

4.1 ZNF512B contains diverse and highly conserved domains

Through the application of different tools (Figures 3.1.2, 3.1.3), I analyzed the structure and conservation of the known domains of ZNF512B, being the ZFs, the repeat region and the putative leucine zipper, and of previously unidentified domains: an NLS, the here characterized iNIM and an α-helix (Figure 4.1.1). This chapter will mainly focus on the structural aspects of the different domains. Their functional implications will be discussed in the corresponding subsequent chapters.

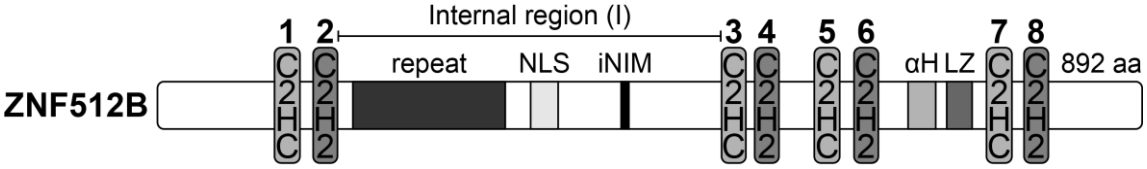

Figure 4.1.1: ZNF512B encompasses diverse domains. *Schematic depiction of the human ZNF512B protein with four pairs of atypical C_2HC (light grey) and typical C_2H_2 (dark grey) ZFs, a repeat region, an NLS, a putative NIM, an unknown α-helix (αH) and a putative leucine zipper (LZ).*

The NLS in the middle of ZNF512B's internal region was predicted by several other tools than just cNLS Mapper, like NLSExplorer (Li et al., 2024) and NLStradamus (Nguyen Ba et al., 2009). However, other NLS's were predicted as well. Through later IF microscopy experiments using a ZNF512B construct including only the internal domain, the position of an NLS inside this region could be verified, since the construct still localized to the nucleus. Nevertheless, ZNF512B could also contain multiple NLS's. Of note, constructs missing the last or the last two ZF pairs, were not localizing to the nucleus anymore without an additional NLS at the C-terminus. Possibly, these constructs were folding in a way that impaired the NLS in the internal region, but it could also hint at an NLS at ZNF512B's C-terminus.

The C_2H_2 ZF domains of ZNF512B are predicted to form a ββα fold with high to very high confidence. This is extremely likely, since it is the typical structure that these ZFs form (Wolfe et al., 2000). The C_2HC ZFs on the other hand are all predicted to have a second α-helix upstream of the ββα fold, again with high to very high confidence. When looking at other C_2HC ZF domains, there are some that form a ββα fold, e.g. in suppression of tumorigenicity 18 (ST18, PDB: 2CS8), and some that also have an additional upstream α-helix, e.g. in ring finger protein 125 (RNF125, PDB: 5DKA). Interestingly, there is also a solution structure of ZFs three and four of ZNF512B

(PDB: 2GQJ) (Figure 4.1.2). In this structure, the atypical C_2HC ZF3 also exhibits an upstream α-helix. So, it seems to be true that ZNF512B's atypical ZFs form in this way. For RNF125, it was shown that a C_2HC ZF domain is essential for binding of the RING domain to ubiquitin conjugating enzyme E2 D1 (UBE2D1) (Bijlmakers et al., 2016). In this particular case, the α-helices of this ZF act as linkers enhancing the ubiquitin ligase activity. The additional α-helices in ZNF512B could possibly function in a similar way and stabilize interactions. It would be interesting to introduce point mutations targeting the α-helices upstream of the atypical ZFs to test if this influences ZNF512B's interaction with the NuRD complex, its DNA binding ability or its oligomerization. The solution structure of ZFs three and four of ZNF512B reveals another interesting aspect, which can also be seen in the predicted structure from the AlphaFold database. While both ZFs in all other pairs in ZNF512B form individual structures that are slightly apart from each other, the downstream α-helix of ZF three is directly connected to ZF four (Figure 4.1.2). It seems as if this ZF pair could be an exception and that both ZFs form one structural domain together. The reason for this could be the shorter distance between ZFs three and four. While the number of amino acids between ZFs one and two, five and six, and seven and eight is twelve, thirteen and eleven respectively, it's just eight amino acids between ZFs three and four. So far, ZF pair two did not show different functionality in comparison to the others, but it could be kept in mind for future studies.

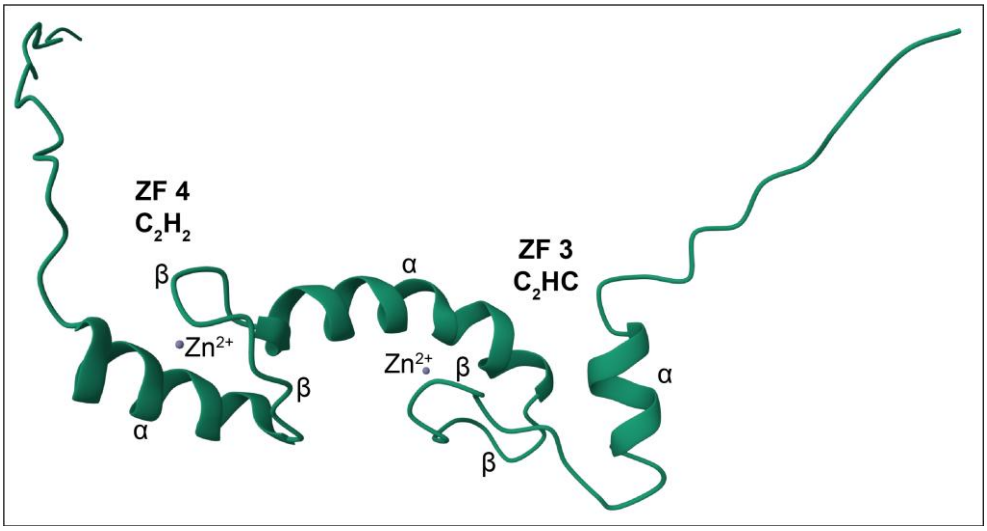

Figure 4.1.2: The atypical C2HC ZF3 of ZNF512B comprises an upstream α-helix. *Solution structure of the ZF domains three and four of human ZNF512B. PDB: 2GQJ. α: α-helix, β: β-sheet.*

The putative leucine zipper in ZNF512B is predicted to form two β-sheets in the structure from the AlphaFold database with high confidence, while the rest of the domain is predicted to be unstructured. Typically, a leucine zipper consists of repeats with a leucine at every seventh position forming an amphipathic α-helix, whose hydrophobic side can dimerize with itself or another α-helix to bind DNA (Krylov & Vinson, 2001). Since leucine zippers can be unstructured in the absence of DNA, it is possible that the prediction in the AlphaFold database is correct but that this domain is a leucine zipper nonetheless (Grigorescu & Rosenberg, 2004). On the other hand, the domain only has three seven amino acid repeats and could be too short to actually dimerize with itself. In addition, I predicted structures of a complex containing two molecules of the putative leucine zipper with and without DNA using AlphaFold 3 (Abramson et al., 2024), but in these it still did not form an α-helix or dimerize. The last few amino acids of the domain also already form the α-helix upstream of the atypical ZF seven. Therefore, it is unlikely that this is indeed a functional leucine zipper. A search with the Basic Local Alignment Search Tool (BLAST) from the National Center for Biotechnology Information did not reveal proteins with a similar domain from which a possible function could be derived (Altschul et al., 1990). Nevertheless, the putative leucine zipper domain of ZNF512B is highly conserved among species and in ZNF512B's paralogue ZNF512. This could hint at relevant functionality, maybe only in a specific isoform of ZNF512B. It could be of interest to test if point mutations targeting the leucines affect ZNF512B's DNA binding, oligomerization or transcriptional repression.

Just upstream of the putative leucine zipper, a previously unknown α-helix in ZNF512B is predicted in the AlphaFold database with high to very high confidence. This domain is also highly conserved across species and in the paralogue ZNF512, again hinting at role in the proteins function. A BLAST search reveals two proteins that have such a domain resembling the one in ZNF512B: General transcription factor IIIC subunit 2 (GTF3C2), which is involved in transcription by RNA polymerase III (Talyzina et al., 2023), and ryanodine receptor 3 (RYR3), which is a calcium channel that may be particularly important in specific brain functions (Murayama & Ogawa, 1996; Zucchi & Ronca-Testoni, 1997). This is interesting, since the MS-based (Figures 3.7.1, 3.7.2) and mRNA-seq (Figure 3.8.2) experiments indicated that ZNF512B could potentially play a role in ribosome biogenesis and is expressed at a higher level in the brain (Figure 3.1.1). Conserved amino acids between the three proteins would be good targets for point

mutations. Further, the α-helix in ZNF512B has one side covered in hydrophobic amino acids. Possibly, the putative leucine zipper dimerizes with the α-helix just upstream, and the two domains form one larger interaction domain. However, different predictions I performed with AlphaFold 3 did not strengthen this hypothesis.

Finally, the repeat region in ZNF512B's internal domain is predicted to form a right-handed, three-faced β-helix with very low confidence in the AlphaFold database. Since the confidence of the prediction is so low, it could very well be that this structure is not real, and that the region is intrinsically disordered. Further, this part of ZNF512B is only conserved in mammals, so either it has a specific function in that class, or it really is not important. However, it was shown that repeats in the protein sequence can form these β-helices, e.g. for pectate lyase and the bacteriophage P22 tailspike (Mitraki et al., 2002). Mutating the repeating amino acids in this region would be a good attempt to see whether it has any influence on ZNF512B's function as transcriptional repressor.

4.2 ZNF512B might play a role in mitosis and RNA processing

LfqMS/MS experiments with cells transiently expressing GFP, GFP-ZNF512B or GFP-ZNF512B_K423A (loss of NuRD interaction) demonstrated that ZNF512B interacts with the complete NuRD complex via its iNIM and further with H2A.Z-containing nucleosomes, HMG20A and newly identified interactors independently from the iNIM (Figure 3.7.1). These proteins could be sorted into clusters via analysis with the STRING database (Figure 3.7.2, Table 4.2).

Table 4.2: Proteins identified in the lfqMS/MS experiments and their cluster from the STRING analysis

Protein	Cluster
RBBP4 RBBP7 MTA1 MTA2 MTA3 HDAC1 HDAC2 GATAD2A GATAD2B MBD2 MBD3 CDK2AP1 CDK2AP2 CHD3 CHD4 H2A.Z HMG20A	**NuRD complex**
KPNA3 KPNA4	**NLS-dependent protein nuclear import complex**
NCAPG NCAPH CKAP2 GAS2L3	**Positive regulation of chromosome condensation**
TEX10 RRP9 NOL9 URB1 URB2	**Ribosome biogenesis**
ZBTB7B PHIP CGAS	**No cluster**

ZBTB7B, PHIP and CGAS (also known as MB21D1) did not fit any cluster. Since ZBTB7B was shown to interact with the NuRD complex (Gao et al., 2022) and its interaction with ZNF512B is also dependent on the iNIM, it is feasible to speculate that it was pulled down via the NuRD complex and may be a member of the corresponding cluster. PHIP was previously shown to bind H3K4 methylation (Morgan et al., 2017). This is surprising since the IF microscopy experiments suggest that H3K4me3 is a histone

PTM excluded from the ZNF512B-induced chromatin foci (Figures 3.3.4, 3.6.3). It could be possible that H3K4me1/me2, which was not tested in this study, colocalizes with these foci and is bound by PHIP, which is subsequently pulled down with ZNF512B. CGAS was shown to act as a DNA sensor (West et al., 2015), so it could also just colocalize with the ZNF512B-induced chromatin foci and be pulled down indirectly. On the other hand, PHIP and CGAS could also just exhibit unspecific binding.

The cluster 'NLS-dependent protein nuclear import complex' includes KPNA3 and KPNA4. Next to their role in nuclear import (Wing et al., 2022), these proteins have been shown to act as chaperones preventing protein aggregation (Doll & Cingolani, 2022). Since ZNF512B overexpression induces protein/chromatin aggregation, it is likely that KPNA3/4 are recruited to ZNF512B/chromatin oligomers 'trying' to prevent their aggregation.

The cluster 'ribosome biogenesis' included several proteins involved in rRNA processing and maturation. This is highly interesting, since the mRNA-seq data showed that KD of ZNF512B influences genes that are likewise mainly associated with RNA-processing (Figure 3.8.2). Since ZF domains can facilitate the binding of RNA (Cassandri et al., 2017), I conducted a preliminary crosslinking immunoprecipitation (CLIP) experiment in collaboration with Dr. Oliver Rossbach (Institute for Biochemistry, Justus-Liebig University Giessen, Germany) to find out whether ZNF512B can directly bind RNA (Figure 4.2.1A). Here, after UV crosslinking and cell lysis, RNA is digested with different concentrations of RNase I, followed by IP of the protein of interest and radioactive labeling of the digested RNA. RNA bound to the protein of interest can then be visualized in autoradiography. CLIP on HeLaK cells transiently expressing GFP or GFP-ZNF512B using GFP-Trap beads or Dynabeads coupled with anti-GFP or anti-FLAG antibody indicated that ZNF512B can indeed bind RNA (Figure 4.2.1B). All these data taken together hint at a role of ZNF512B in RNA processing, which is also often affected in patients with ALS (Alberti et al., 2017; Lehmkuhl & Zarnescu, 2018), the neurodegenerative disorder ZNF512B has been associated with (Jiang et al., 2021). In a different project in our group further experiments are already underway, like CLIP-seq, RNA immunoprecipitation sequencing (RIP-seq) and surveying targets by APOBEC-mediated profiling (STAMP), to analyze which (types of) RNA ZNF512B binds. In addition, the interactions between ZNF512B and the proteins from the 'ribosome biogenesis' cluster should be verified via IPs and immunoblots, and the deregulation of

genes associated with RNA-processing after ZNF512B KD should be validated by RT-qPCR. Further, it will be interesting to find out whether the putative interaction domain in ZNF512B is important for this potential functionality, since GTF3C2, which is involved in transcription by RNA polymerase III (Talyzina et al., 2023), contains a similar domain.

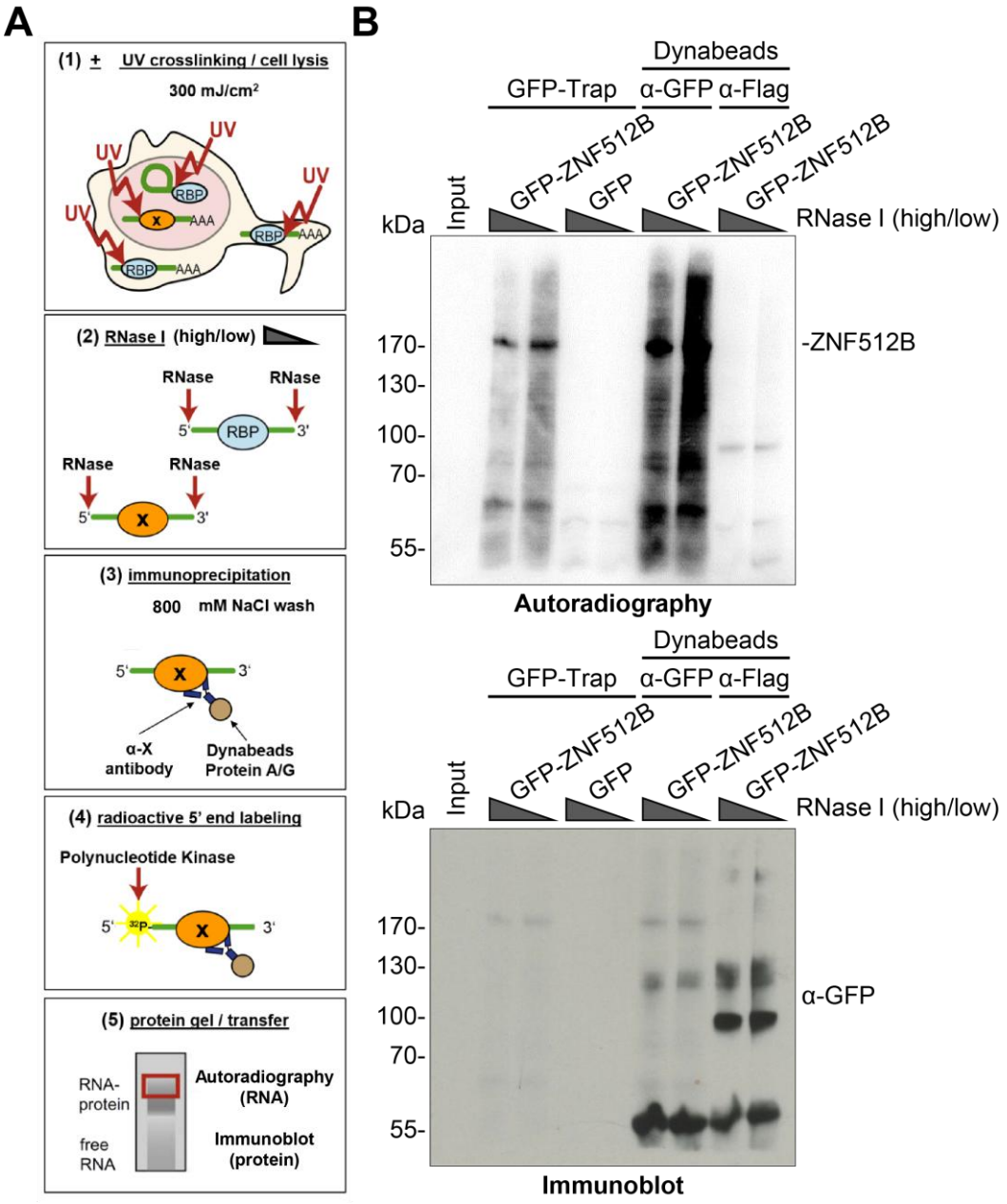

Figure 4.2.1: ZNF512B binds RNA. ***(A)*** *Schematic depiction of a CLIP experiment.* ***(1)*** *Cells are UV crosslinked and lysed.* ***(2)*** *RNA is digested with RNase I in high and low concentrations.* ***(3)*** *IP of the protein of interest using antibody-coupled dynabeads.* ***(4)*** *Polynucleotide kinase is used to label 5′ ends of RNA with radioactive phosphorus-32 (^{32}P).* ***(5)*** *Samples are analyzed in autoradiography visualizing RNA and immunoblot visualizing proteins.* ***(B)*** *Autoradiography* ***(top)*** *and Immunoblot detecting GFP* ***(bottom)*** *of cell extracts from UV crosslinked HeLaK cells expressing GFP or GFP-ZNF512B after digestion with different concentrations of RNase I, pull-down with GFP-Trap beads or Dynabeads coupled with anti-GFP or anti-FLAG antibody and ^{32}P end labeling of RNA.*

Interestingly, the last cluster ‘positive regulation of chromosome condensation’ included multiple proteins involved in mitosis hinting at a possible involvement of ZNF512B in cell division. To further investigate this intriguing idea, live-cell IF microscopy on HeLaK cells transiently expressing H2B-RFP and GFP-ZNF512B was performed together with Dr. Stefanie Wunderlich (Molecular Embryology, Department of Biology, Philipps University Marburg, Germany) using a spinning disk confocal microscope (Figure 4.2.2). This preliminary experiment revealed that ZNF512B is localizing to the mitotic spindle during metaphase. In addition, it appeared as if cells were not able to go through mitosis properly (data not shown). First follow-up IF microscopy experiments in our group verified this localization for endogenous ZNF512B. Notably, it was shown that several members of the NuRD complex like CHD4, MDB3 or HDAC1 also localize to the mitotic spindle (Sakai et al., 2002; Sillibourne et al., 2007; Yokoyama et al., 2013). Since the interaction of ZNF512B with proteins involved in mitosis is iNIM-independent (Figure 3.7.1), it is likely that GFP-ZNF512B_K423A still localizes to the mitotic spindle. Additional IF microscopy experiments should be conducted with GFP-ZNF512B and GFP-ZNF512B_K423A expressing cells and with ZNF512B KD cells to investigate whether the localization of NuRD members to the mitotic spindle is influenced by or even dependent on ZNF512B. For these experiments, cells could also be synchronized, for instance by incubation with a cyclin dependent kinase 1 (CDK1) inhibitor (Vassilev, 2006). Until now, no major mitotic defects for ZNF512B KD cells could be observed, but future, more sensitive and quantitative studies should focus on ZNF512B’s putative role in cell division.

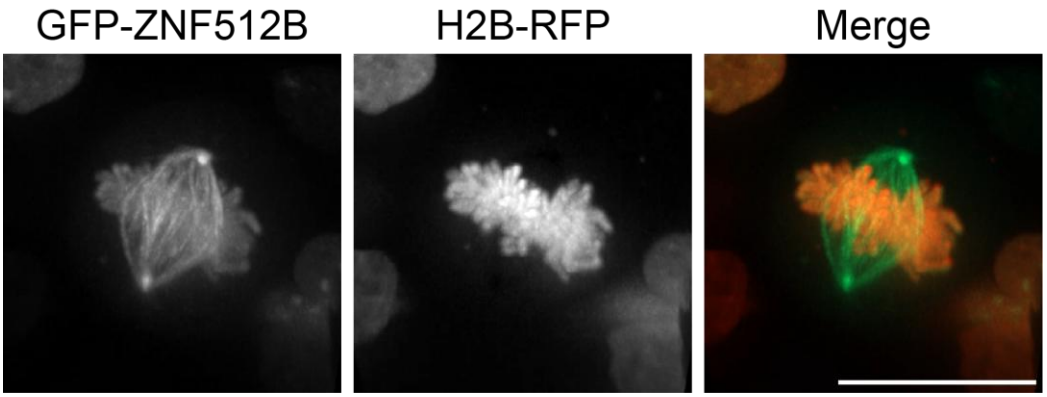

Figure 4.2.2: ZNF512B localizes to the mitotic spindle. *IF microscopy of HeLaK cells expressing GFP-ZNF512B (green) and H2B-RFP (red). Scale bar: 20 µm.*

4.3 ZNF512B binds RBBP4 of the NuRD complex via an iNIM with high affinity

Structural studies (Figure 3.9) and IP (Figure 3.10.1) and IF microscopy (Figure 3.10.2) experiments have shown that ZNF512B directly interacts with RBBP4 of the NuRD complex via an internal domain in a way that is distinct from the interaction via the known N-terminal NIM. Other proteins have been shown to interact with RBBP4 in a similar way (Figure 3.10.3), and I consequently suggested that two different NIM consensus sequences exist, the known N-terminal NIM and an alternative, internal NIM (iNIM). However, NIM consensus sequences appear to be even more diverse and the distinction between NIM and iNIM is not always clear-cut. For instance, adipocyte enhancer-binding protein 2 (AEBP2) (Sun et al., 2018) and the Epstein-Barr virus protein BMRF1 (Salamun et al., 2019) bind RBBP4 via an iNIM but exhibit an amino acid insertion between the first arginine and lysine, and, in addition, AEBP2 is missing the proline (Figure 4.3.1). Several proteins with an N-terminal NIM share this further adapted motif with AEBP2, like PR domain zinc finger proteins 3/16 (PRDM3/16) and, most importantly, histone H3 (Ivanochko et al., 2019; Schmitges et al., 2011). So, the sequence to search for potential new NuRD interacting proteins is not definitive and could be even further adapted to not miss any. On the other hand, the number of false positives will increase if the sequence to search for becomes too generic. It is more promising to limit the number of results with a more specific search sequence to increase the probability of positive hits.

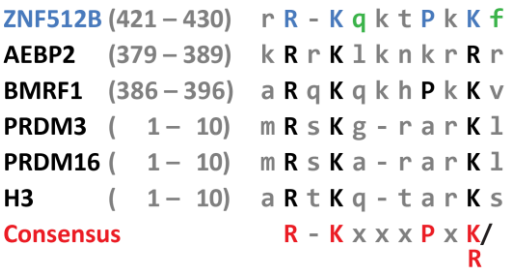

Figure 4.3.1: The (i)NIM sequence can be further adapted. *Alignment of the iNIM in ZNF512B with the (i)NIMs of AEBP2, BMRF1, PRDM3, PRDM16 and H3. Capital letters indicate conserved amino acids. Green letters indicate amino acids that contribute to but are not essential for ZNF512B's NuRD binding.*

Unfortunately, the tested proteins FOXJ1, ZBTB20 and ZNF148 did not show an interaction with RBBP4 in IPs and immunoblots (Figure 3.10.4). There can be several reasons for these results. First, the experimental setup could be unsuited and would need to be optimized for these proteins. For example, the wash buffer during the IP could be too strong or the protein-tag or position of it could inhibit the interaction with RBBP4.

For this reason, the FLAG-tagged construct of ZNF148 was tested, but it also showed no interaction (Figure 3.10.4). Second, the proteins might not interact with the NuRD complex due to adjacent amino acids, other domains, PTMs or the general folding of the protein blocking the iNIM, or due to competition with other interactors, although the last problem should be solved through the overexpression in the presented experiments. Finally, it is possible that these proteins bind the NuRD complex only in specific cell types or stages or under other specific conditions. This could also explain why they have not been identified in previously published MS screens with NuRD members (Kloet et al., 2015; Spruijt et al., 2016). Interestingly, an online-available dissertation (Aghajanirefah, 2012) suggests that ZNF148 binds the NuRD complex only in purely erythroid cells, such as mouse erythroleukemia (MEL) cells, while it interacts with activating complexes, like the p400 complex, in non-erythroid cell lines. This could be the reason why there is no interaction between RBBP4 and ZNF148 in HeLaK cells. I tried to verify the interaction in MEL cells, but, unfortunately, the transfection efficiency of these cells was too low to conduct proper experiments (data not shown). A probable basis for this distinction of ZNF148 between cell lines could be PTMs blocking the iNIM, as mentioned above, since this would be a dynamic mechanism. For H3, there is evidence that trimethylation of K4 inhibits the interaction with RBBP4 in PRC2 (Schmitges et al., 2011). Possibly, the corresponding lysine in ZNF148 is methylated in non-erythroid cells, blocking the NuRD interaction, but unmodified in erythroid cells, leading to the interaction with the complex. It is an intriguing idea that the iNIM could function as a ‘switch’, allowing a protein to change between the recruitment of activating or repressive complexes, as it could be the case for ZNF148. I already exchanged some amino acids in ZNF512B and ZNF148, that could theoretically be modified and are not essential for the NuRD interaction, and started with IPs (data not shown), but further experiments will be needed to test whether this hypothesis is true.

One aspect several NIM- or iNIM-containing proteins have in common is that they can only interact with RBBP4 within the NuRD complex and not in other complexes like PRC2 (Lejon et al., 2011; Salamun et al., 2019). The lfqMS/MS experiments (Figure 3.7.1) demonstrate that this distinction is also true for ZNF512B. A possible reason could be that the (i)NIM-binding pocket in RBBP4 is obstructed when the protein is engaged with PRC2, as structural studies have indicated (Chammas et al., 2020; Nowak et al., 2011). Since H3 and AEBP2 can interact with RBBP4 within PRC2 via their NIM,

this reason is rather unlikely (Kim et al., 2009; Schmitges et al., 2011). It was also suggested that the interaction with a specific complex is facilitated via additional interactions with RBBP4 or subunits that are missing in other complexes (Lejon et al., 2011). This could be another explanation why the here tested iNIM-containing proteins FOXJ1, ZBTB20 and ZNF148 did not show an interaction with RBBP4. For AEBP2, it was shown via isothermal titration calorimetry (ITC) assays with a NIM-binding deficient RBBP4 mutant that its three ZFs bind distinct regions of RBBP4 (Cai et al., 2023). For PRDM3/16, it was similarly suggested that they could have potential secondary interactions with MBD3 of the NuRD complex via their first ZF domain (Ivanochko et al., 2019). Therefore, it is not hard to imagine that one or more domains in ZNF512B could form additional interactions with NuRD. While the IP, IF microscopy and lfqMS/MS experiments (Figures 3.6.1, 3.6.2, 3.7.1) demonstrate that the iNIM in ZNF512B is strictly necessary for the interaction, the question remains whether it is also sufficient for NuRD binding or if other domains of ZNF512B are needed or are at least contributing to the interaction. I conducted a preliminary experiment to examine this question further. I created three GFP-tagged constructs – one construct consisting only of the iNIM sequence of ZNF512B (GFP-ZNF512B_iNIM), one construct containing the N-terminal part of ZNF512B's internal region (GFP-ZNF512B_IN) and one construct containing the C-terminal part of ZNF512B's internal region including the iNIM (GFP-ZNF512B_IC) – and used them for Co-IPs with following immunoblots (Figure 4.3.2). The construct consisting only of the ZNF512B iNIM was not able to pull down RBBP4. However, it is unclear whether the large GFP-tag in comparison to the iNIM interfered with the interaction. The construct containing the N-terminal part of ZNF512B's internal region did not pull down RBBP4, as expected, since it is missing the iNIM. Interestingly, the construct containing the C-terminal part with the iNIM showed a barely visible interaction with RBBP4 compared to full-length ZNF512B. This could hint at additional domains being involved in the interaction between NuRD and ZNF512B. On the other hand, it is possible that this construct was not folded properly, like other constructs before (Figure 3.4.1), and I did not conduct IF microscopy yet to get an insight on this, for example through GFP signals in the nucleoli (Alberti & Carra, 2019). Hence, this data should be taken with caution. Further experiments, like Co-IPs, ITC or FP-based anisotropy assays with truncated ZNF512B constructs or specific point mutations, could shed more light on the question whether multiple ZNF512B domains are involved in the interaction with NuRD. Nevertheless, it is an intriguing idea and could possibly reveal

the function of the upstream α-helices of ZNF512B's atypical ZFs or of the putative interaction domain between ZF pairs three and four. Further, this could explain why PWWP2A is not enriched in the lfqMS/MS data (Figure 3.7.1). PWWP2A only interacts with the M1HR-subunit of the NuRD complex (Link et al., 2018). If ZNF512B relies on additional interactions with members of the remodeler subunit of NuRD, it could preferentially bind to sites where the complete NuRD complex is present.

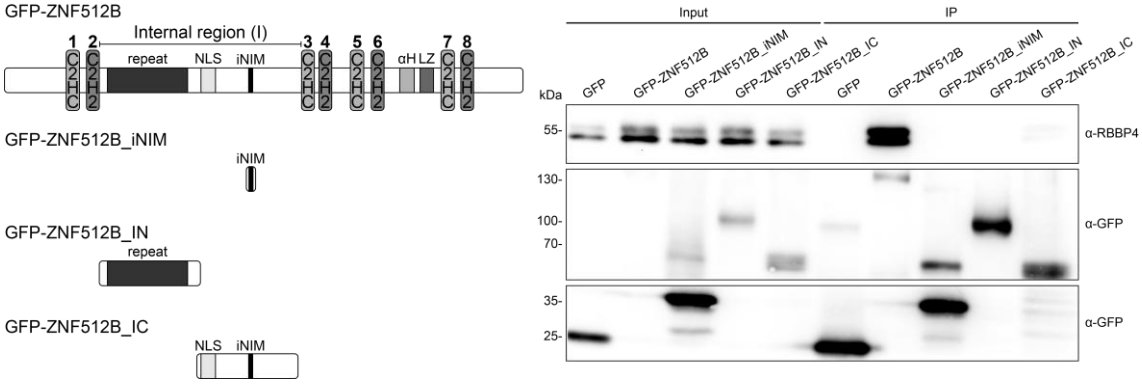

Figure 4.3.2: Additional domains could be involved in ZNF512B's interaction with RBBP4. Left: *Schematic depiction of the used constructs.* ***Right:*** *Immunoblots of DNase-digested cell extracts from HeLaK cells expressing GFP, GFP-ZNF512B, GFP-ZNF512B_iNIM, GFP-ZNF512B_IN or GFP-ZNF512B_IC after pull-down with GFP-Trap beads detecting RBBP4 or GFP (IP control).*

But what about the iNIM itself? It was shown that the NIM in FOG-1 not only binds to RBBP4 but also to MTA1 (Hong et al., 2005). Further, it was demonstrated by performing pull-down experiments with immobilized FOG-1 that a NIM-binding deficient RBBP4 mutant could still be pulled down in the presence of MTA1 (Lejon et al., 2011). Since the residues in RBBP4, that interact with the NIM in FOG-1, are buried within the complex, it was suggested that RBBP4 and MTA1 binding the same molecule of FOG-1 is unlikely and that they rather bind the NIM in different molecules of FOG-1. This was further proposed as the reason for FOG-1 being able to bind to the NuRD complex but not to PRC2. So, can MTA1 also bind the iNIM in ZNF512B? The IP competition experiments with FOG-1 and ZNF512B peptides clearly showed that ZNF512B cannot pull down MTA1 when also no RBBP4 is pulled down (Figure 3.11). Of course, the peptides could just bind to MTA1 as well in this case. More insight can be gained from another competition experiment I performed as part of a collaboration with Prof. Dr. Olalla Vázquez and Dr. Van Tuan Trinh (Chemical Biology, Department of Chemistry, Philipps University Marburg, Germany). In this case, an RBBP4 dual inhibitor peptide, that binds the (i)NIM-binding pocket as well as the MTA1-binding pocket in RBBP4, was used for

competition (Figure 4.3.3A). In this experiment, ZNF512B could clearly pull down MTA1, while it was unable to pull down RBBP4, indicating that MTA1 can indeed bind ZNF512B (Figure 4.3.3B, unpublished data).

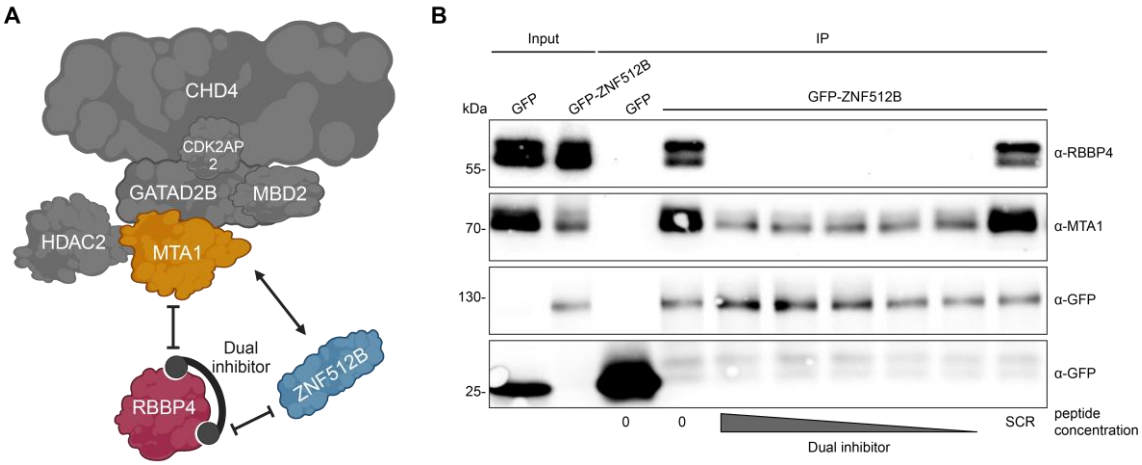

Figure 4.3.3: ZNF512B pulls down MTA1 when RBBP4 is bound by a dual inhibitor. (A) *Schematic depiction of the dual inhibitor's binding mode.* ***(B)*** *Immunoblots of DNase-digested cell extracts from HeLaK cells expressing GFP or GFP-ZNF512B incubated with increasing amounts of an RBBP4 dual inhibitor or a respective scrambled control peptide (SCR) after pull-down with GFP-Trap beads detecting NuRD members RBBP4 or MTA1, or GFP (IP control). Dual inhibitor peptide composition and concentrations are not indicated due to confidentiality of unpublished data.*

This result could further mean two things: 1) While the previously used peptides could also bind MTA1, preventing it from binding to ZNF512B, the dual inhibitor peptide could not, or 2) MTA1 can only bind to ZNF512B when it is not engaged with RBBP4. This could be clarified with IP experiments using an immobilized ZNF512B together with a (i)NIM-binding deficient RBBP4 mutant and MTA1, as done for FOG-1 (Lejon et al., 2011). If the first case is true, ZNF512B should be able to pull down MTA1 and RBBP4 in this experiment, and if the second case is true, it should not be able to pull down either of them. The second case is particularly intriguing, since this could be the main difference between the NIM and the iNIM. When MTA1 is engaged with RBBP4, the (i)NIM-binding pocket of MTA1 could be positioned in a way that it can be accessed by proteins, which have the NIM at a flexible N-terminus, while it is inaccessible by proteins, which have an iNIM (Figure 4.3.4). This could also explain the much higher affinity of ZNF512B's iNIM for RBBP4 in comparison to FOG-1's NIM (Figure 3.11). While only one ZNF512B protein could be able to bind to RBBP4 via its iNIM, two FOG-1 proteins could bind to RBBP4 and MTA1 in parallel, so that they can both exhibit a lower binding

affinity. This strong binding affinity of ZNF512B for RBBP4 might be used to optimize NuRD inhibitors that are already in development (Zhang et al., 2024).

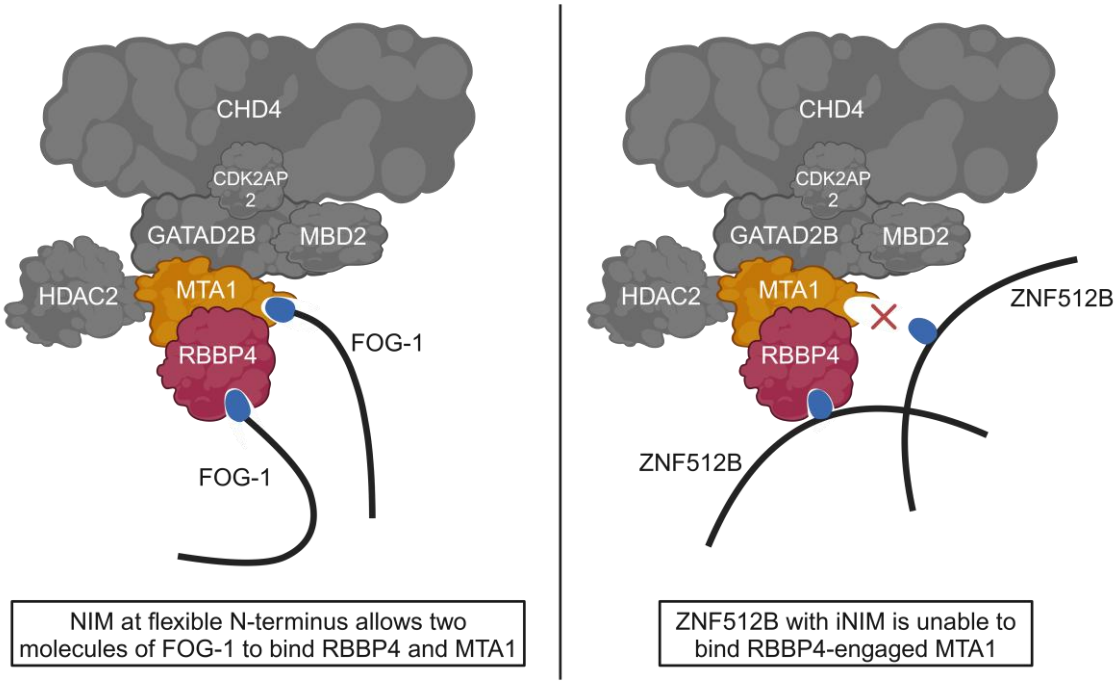

Figure 4.3.4: The ability of different proteins to bind MTA1, when engaged with RBBP4, may depend on the type of NIM. *Schematic depiction of the proposed binding difference between NIM and iNIM. Proteins with a NIM at a flexible N-terminus could bind MTA1, when engaged with RBBP4, while proteins with an iNIM could be unable to do so. (i)NIMs are indicated in blue. Adapted from (Lejon et al., 2011).*

4.4 ZNF512B is a transcriptional repressor

mRNA-seq experiments after overexpression of GFP, GFP-ZNF512B or GFP-ZNF512B_K423A (loss of NuRD binding) and after ZNF512B KD (Figures 3.8.1–3.8.3), and a luciferase reporter assay with different ZNF512B constructs (Figure 3.8.5) established ZNF512B as a strong repressor of gene transcription. Interestingly, ZNF512B can also facilitate gene repression independently of its interaction with the NuRD complex. Here, it would be of interest to repeat the reporter assays with additional constructs to find out which domains are responsible for this NuRD independent function. It is possible that the repeat region, the ZF domains and the putative interaction domain between ZF pairs three and four play a role in gene repression, potentially through the recruitment of some of the iNIM-independent interactors, such as the condensin complex subunits NCAPG/H.

One unexpected finding was that, in contrast, most genes exclusively deregulated upon overexpression of GFP-ZNF512B were upregulated. These genes were primarily

expressed at very low levels or not at all in the GFP expressing control cells (Figure 3.8.1). Therefore, due to ZNF512B's high expression level and strong binding affinity for NuRD, the complex may be recruited 'away' from genes that are repressed by it in the control cells, leading to the upregulation of those genes.

The small number of deregulated genes after ZNF512B KD (Figure 3.8.2) could be a consequence of its low expression level in HeLaK cells (Figure 3.1.1). One possible explanation for this is that ZNF512B just regulates a very small number of genes, as it was shown for other ZFPs, like ZFP568 (Yang, Wang, Hoang, et al., 2017), ZFP64 (Lu et al., 2018), ZNF558 (Johansson et al., 2022) or ZNF410 (Lan et al., 2021). Analysis of the existing ChIP-seq data and future ChIP-seq and cleavage under targets and release using nuclease (CUT&RUN) experiments with endogenous ZNF512B could explore this possibility further. Nevertheless, together with the lfqMS/MS data, the deregulated genes still hint at a possible involvement of ZNF512B in RNA-processing (Chapter 4.2). As mentioned, these genes should additionally be verified in RT-qPCR experiments. Further, it would be interesting to perform RNAseq-based alternative splicing analysis after ZNF512B KD.

4.5 ZNF512B is a DNA-binding protein

In this study, EMSAs were applied to demonstrate that ZNF512B is capable of binding DNA (Figure 3.5.1). Of note, the sequence for the utilized DNA oligomers was derived from the H19 promoter, because in a previous mRNA-seq experiment, ZNF512B seemed to strongly deregulate that gene (data not shown). If the hypothesis regarding the overexpression phenotype is true, it should be the ZF domains facilitating the DNA binding ability. Although this is in general very likely, the experiments in this study do not clearly show it. Therefore, it would be advisable to repeat the EMSAs with the different ZNF512B truncation/deletion constructs including mutations of the repeat region and the putative interaction domain between ZF pairs three and four. It will be particularly interesting to test the typical/atypical ZF mutants and separate ZF pairs, since they were able to induce the overexpression phenotype individually and should therefore exhibit the same DNA binding ability.

Unmethylated as well as methylated DNA probes were tested in the EMSAs (Figure 3.5.1), because in affinity purification experiments with semisynthetic

dinucleosomes containing different chromatin modifications shown in MARCS, ZNF512B demonstrates a preference for DNA methylation (Lukauskas et al., 2024) (Figure 4.5.1). However, the EMSAs did not experimentally determine a higher affinity of ZNF512B for methylated DNA. Analysis of the NuRD complex members in MARCS gives a possible explanation for ZNF512B's affinity for methylated DNA in these experiments (Figure 4.5.1). It seems as if ZNF512B is just pulled down together with the NuRD complex, which has an affinity for methylated DNA due to its MBD2 subunit (Schmolka et al., 2023). Notably, the data from MARCS also demonstrates ZNF512B's affinity for H2A.Z-containing nucleosomes.

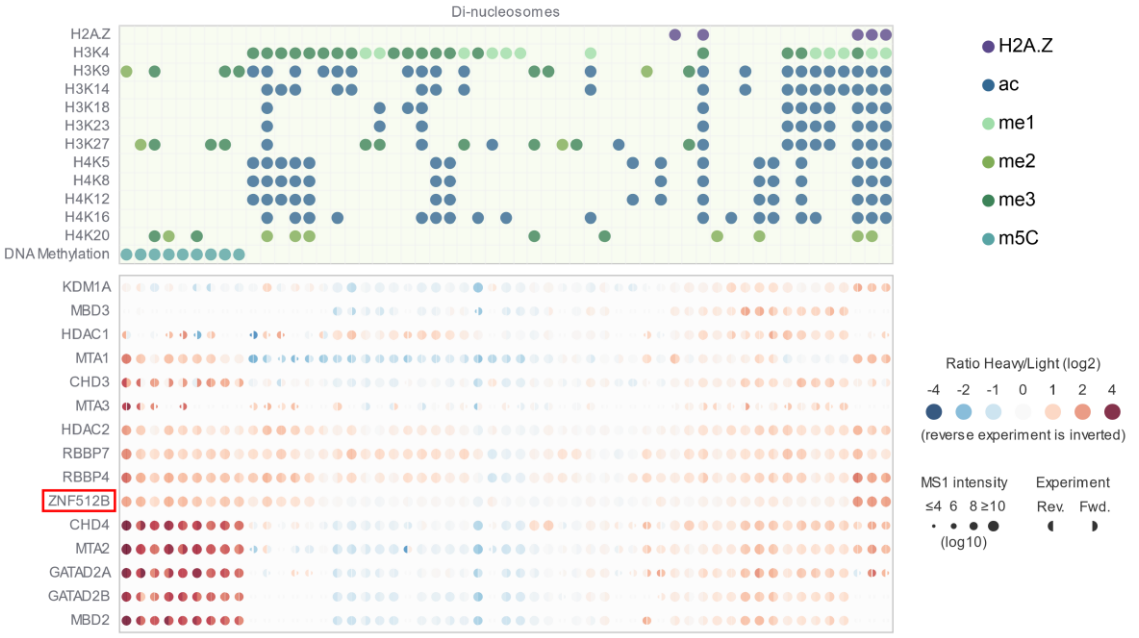

Figure 4.5.1: ZNF512B and the NuRD complex members show an affinity for DNA methylation. *Heatmap visualization of the enrichment of ZNF512B and different members of the NuRD complex after affinity purification experiments with semisynthetic dinucleosomes containing different chromatin modifications. The results shown here are in whole based upon data generated in MARCS (Lukauskas et al., 2024).*

Further, the predicted potential DNA binding motifs for ZNF512B's ZF domains were, in general, AT-rich sequences (Figure 3.5.2). Interestingly, the NIM-containing NuRD interactor SALL4 was demonstrated to exhibit a distinctive affinity for AT-rich sequences, which are recognized by a pair of ZFs located at its C-terminus (Watson et al., 2023). Possibly, ZNF512B could act in a similar manner. On the other hand, repetitive and non-consecutive TTC sequences were recently suggested as ZNF512B's DNA binding motif (Ma et al., 2024). Together with Dr. Jörg Leers (Institute for Genetics, Justus-Liebig

University Giessen, Germany), these different sequences were tested in a preliminary experiment, performing an EMSA with 1) the suggested sequence from Ma & Zhang et al., 2) the sequence predicted for all ZF domains of ZNF512B and 3) the sequence from the H19 promoter, that was utilized earlier (Figure 4.5.2). This experiment showed no specificity of ZNF512B for any of the three sequences. Therefore, further experiments are needed to determine ZNF512B's DNA binding motif, such as ChIP-seq with endogenous ZNF512B, DNA immunoprecipitation sequencing (DIP-seq) or systematic evolution of ligands by exponential enrichment (SELEX). We have already started with SELEX experiments but have unfortunately encountered problems with the solubility of the ZNF512B protein.

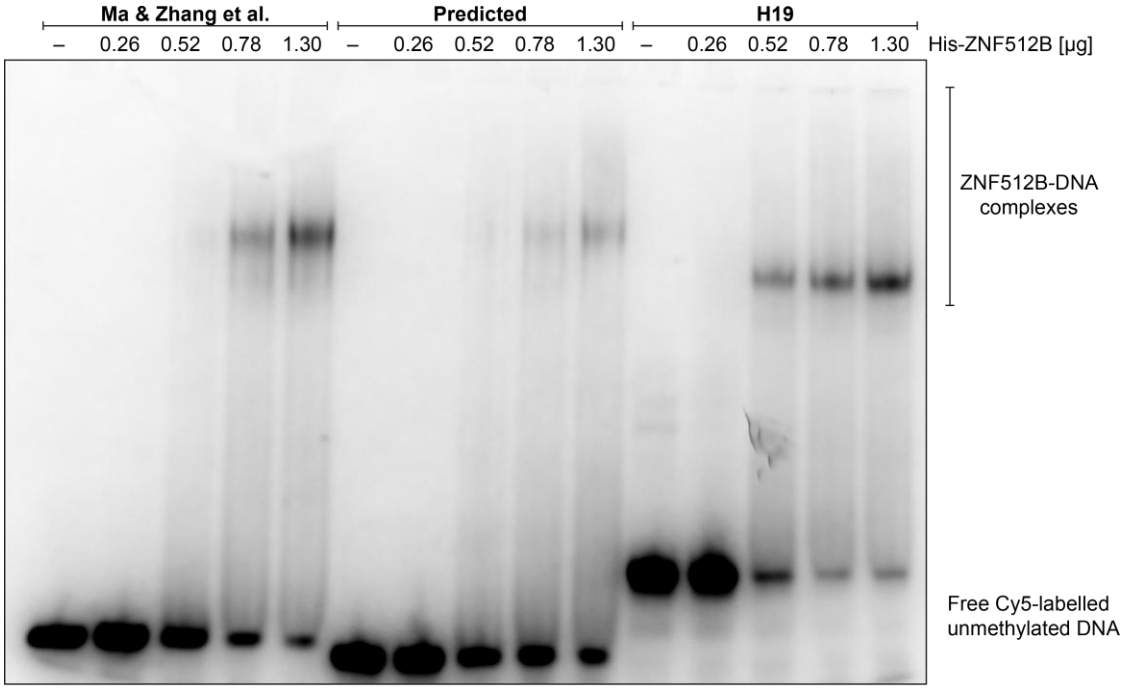

Figure 4.5.2: ZNF512B binds different DNA oligos without specificity. Top: *EMSA of different Cy5-labelled unmethylated DNA together with increasing amounts of purified recombinant His-ZNF512B protein.* ***Bottom:*** *Sequences of the utilized DNA oligomers.* ***Ma & Zhang et al.:*** *Binding sequence of ZNF512B as suggested by (Ma et al., 2024).* ***Predicted:*** *Binding sequence of ZNF512B as predicted by me using a PWM predictor for ZF domains (Persikov et al., 2009; Persikov & Singh, 2014).* ***H19:*** *Part of the mouse H19 promoter as used before.*

4.6 ZNF512B has the ability to oligomerize

IPs followed by immunoblots demonstrated that GFP-tagged ZNF512B can pull down FLAG-tagged ZNF512B (Figure 3.5.3). The constructs with only the ZF domains were

also able to pull down each other, while the constructs containing only the internal region were not. If the hypothesis regarding the overexpression phenotype is correct, the ZF domains should facilitate oligomerization. Nevertheless, in these experiments the putative interaction domain between ZF pairs three and four could also be responsible. Therefore, further experiments with constructs containing point mutations targeting the putative interaction domain should be performed. Further, these experiments do not clearly show that ZNF512B does truly oligomerize. It is also possible that some of the NIM-independent interactors are bound by FLAG-tagged and GFP-tagged ZNF512B leading to the collective precipitation. To conclusively assess whether ZNF512B oligomerizes, size-exclusion chromatography with multi-angle light scattering (SEC-MALS), analytical ultracentrifugation or mass photometry experiments should be performed. Another possible indication that ZNF512B does in fact oligomerize, is its putative inclusion of several NLS's (Chapter 4.1). These can be bound by proteins involved in nuclear import, like KPNA3/4, to chaperone aggregation-prone proteins (Bourgeois et al., 2020). To test if the ZF pairs of ZNF512B could in theory be responsible for the oligomerization, I predicted the structure of a complex containing two molecules of the first ZF pair using AlphaFold 3 (Figure 4.6). Remarkably, the ZF pairs were predicted to be intertwined with each other, strengthening the idea that ZNF512B can indeed oligomerize via these domains.

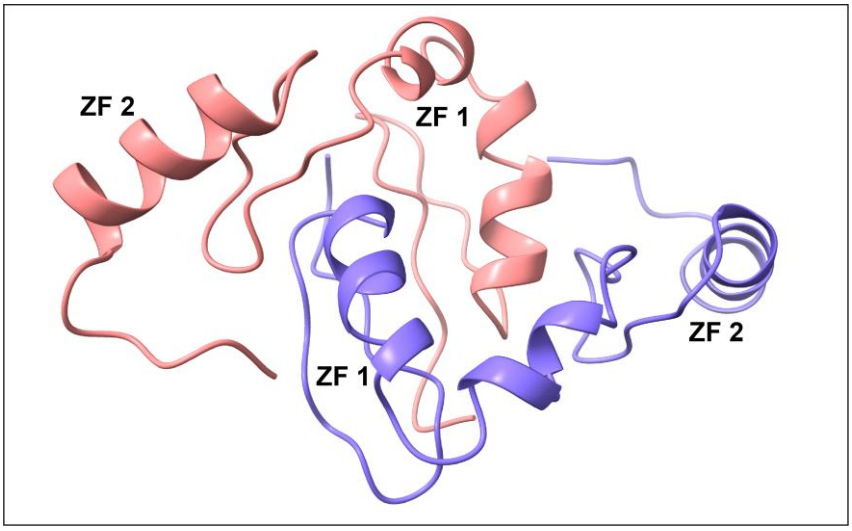

Figure 4.6: Two molecules of the first ZF pair of ZNF512B are predicted to form a complex. *Structure of a complex of two molecules of the first ZF pair of ZNF512B predicted using AlphaFold 3. Molecular graphics done with UCSF ChimeraX, developed by the Resource for Biocomputing, Visualization, and Informatics at the University of California, San Francisco, with support from National Institutes of Health R01-GM129325 and the Office of Cyber Infrastructure and Computational Biology, National Institute of Allergy and Infectious Diseases (Goddard et al., 2018; Meng et al., 2023; Pettersen et al., 2021).*

4.7 Overexpression of ZNF512B leads to chromatin and protein foci formation dependent on its zinc finger domains

In this study, IF microscopy experiments demonstrated that overexpression of ZNF512B induces the formation of chromatin compaction/condensation/aggregation foci in the nucleus (Figure 3.3.1). Further IF microscopy experiments and different assays could exclude the type and position of the protein-tag, the cell line, mitotic arrest, senescence and apoptosis as underlying reasons for this phenotype (Figures 3.3.2, 3.3.3). Especially apoptosis was an important point to analyze since one publication stated that overexpression of ZNF512B leads to apoptosis (Tili et al., 2010). A TUNEL assay confirmed that the cells overexpressing ZNF512B and showing the chromatin condensation phenotype were not apoptotic (Figure 3.3.3). For the positive control, cells were treated with DNase I, as recommended in the manufacturer's instructions of the TUNEL assay kit, to demonstrate that the labeling of DNA fragments, as they occur during apoptosis, worked as intended. To make the experiment even more convincing, it would be of advantage to include an apoptosis control in the future, e.g. by treating the cells with camptothecin (Liskova et al., 2022) or etoposide (Bailly, 2023), to establish that the labeling works in actually apoptotic cells. Nevertheless, the manufacturer of the TUNEL assay kit tested the successful detection of camptothecin-induced apoptosis in HeLa cells (Elabscience, 2024). Furthermore, the number of apoptotic cells for the ZNF512B overexpression was on the same level as for the control GFP overexpression in flow cytometry experiments with propidium iodide (PI) (data not shown), and apoptosis marker genes were not upregulated in the mRNA-seq experiments (Figure 3.8.1). Therefore, it is likely that the observed phenotype is indeed not a consequence of apoptosis. Nonetheless, the consistent chromatin condensation seems to be detrimental to the cells in the long term and to ultimately cause apoptosis, because it was not possible to create stably transfected cell lines expressing ZNF512B. Still, the mentioned publication states that ZNF512B overexpression leads to apoptosis already after 24 h and that the KD of the protein leads to a decrease in apoptotic cells, which would hint at a direct effect of ZNF512B (Tili et al., 2010). However, in that study the ZNF512B overexpression and KD were compared to the same WT apoptosis control, so it is unclear whether the observed effects are just a consequence of the transfections or of ZNF512B. Future live-cell IF microscopy experiments would be suited to analyze the development and time course of the overexpression phenotype in detail and could also reveal possible problems with mitosis in the cells (Chapter 4.2).

Notably, the chromatin compaction/condensation/aggregation phenotype could not be observed in cells inducibly expressing ZNF512B (Figure 3.2.2). IF microscopy experiments demonstrated that the extent of the phenotype correlates with the expression level of ZNF512B (Figure 3.3.1). This was generally lower in the inducible cell lines and possibly too low to lead to the observed phenotype.

I have hypothesized that the overexpression phenotype is induced through DNA binding and oligomerization of ZNF512B facilitated by its ZF domains (Chapters 3.5, 4.5, 4.6). A surprising discovery was that just the atypical and just the typical ZF domains could induce the phenotype (Figure 3.4.1). This would mean that both ZF types in ZNF512B facilitate DNA binding as well as oligomerization on their own, which would be a rather unique capability. For the corresponding experiments, mutants of ZNF512B were used, in which always the first two cysteines of the typical or atypical ZF domains were exchanged for alanines (Figure 3.4.1). To validate that the ZF domains are impaired, future experiments should be repeated with mutants, in which all cysteines/histidines of the ZF domains are exchanged.

Still, there are other possible explanations for the overexpression phenotype. Recently, it was proposed that ZNF512 and ZNF512B initiate the formation of pericentric heterochromatin through binding TTC sequences and recruitment of SUV39H1/2 (Ma et al., 2024). However, this hypothesis has to be treated with caution. First, the recruitment of SUV39H1/2 through ZNF512B could not be identified in the lfqMS/MS experiments (Figure 3.7.1) nor in any other published MS study. Second, the EMSA could not show an increased affinity of ZNF512B for the suggested DNA sequence (Figure 4.5.2). Third, the mentioned publication focuses mainly on ZNF512 and not on ZNF512B and thus does not show the results of some experiments for the latter. Finally, if the foci in the overexpression phenotype were induced heterochromatin foci, a generally higher level of heterochromatic histone PTMs and changes in nucleosome occupancy would be expectable; both were not observed in my experiments (Figures 3.5.3, 3.6.3). Assay for transposase-accessible chromatin using sequencing (ATAC-seq) and chromosome conformation capture (3C)-based methods would be beneficial to further analyze the spatial organization of chromatin when ZNF512B is overexpressed.

One possible alternative explanation for the overexpression phenotype could be that ZNF512B forms condensates via liquid-liquid phase separation (LLPS), as it was also

shown for other ZFPs, like GATA-binding factor 3 (GATA3) (Chen et al., 2023). This could be tested by the addition of 1,6-hexanediol to the cell medium. This alcohol should dissolve the observed foci if they are indeed LLPS condensates (Duster et al., 2021; Ulianov et al., 2021). Further, it was reported that the zinc concentration is highly important for the phase separation behavior of ZF domains (Shih et al., 2022), and zinc homeostasis and LLPS aggregates have been linked to ALS (Y. Chen et al., 2024). ZNF512B contains eight ZF domains and is expressed at an extremely high level during its overexpression (Figure 3.2.3). It is possible that the zinc concentration in the cells is insufficient to properly stabilize all ZF domains, which leads to impacted phase separation and the formation of the observed foci. Zinc supplementation experiments could shed light on this possibility.

I am aware of the non-physiological challenges of such a rather artificial overexpression system. Still, I am convinced that it can offer new insights into ZNF512B biology, since it demonstrates how higher levels of ZNF512B can negatively influence the cells, as I will discuss in more detail in the next chapter.

4.8 High levels of ZNF512B could be connected to neurodegenerative diseases and cancer

RT-qPCR experiments demonstrated that ZNF512B's mRNA is expressed across different tissues and cell types at low levels with the highest amounts in brain and tumor tissues (Figure 3.1.1). Yet, it needs to be mentioned that for this experiment only one biological replicate with three technical replicates was tested per tissue and cell line. Therefore, the data should be taken with caution and the experiment needs to be repeated with more biological replicates for higher reliability. Further, even though HPRT1 is one of the most stable reference genes for normalization (S. Y. Lee et al., 2022), including a second reference gene, like HMBS (Ahn et al., 2021), could make the results more convincing especially when comparing different tissues and cell lines. Nevertheless, the results are comparable to what has been published about ZNF512B's expression levels so far – it was shown that it is broadly expressed across tissues and cell types (Tili et al., 2010) and that it is enriched in brain and neuronal cells (Nagase et al., 1999) – and what can be derived from available databases, like The Human Protein Atlas (Karlsson et al., 2021). Since it has been associated with ALS (Jiang et al., 2021), a neurodegenerative disorder that affects motor neurons, it is intriguing to analyze ZNF512B's function in these cell

types. In a different project in our group, ZNF512B knock-out mouse embryonic stem cells (mESCs) were already created that are to be differentiated into neural progenitor cells (NPCs) and motor neurons, if possible. These experiments will explore ZNF512B's role in these cell types. Further, ZNF512B is generally expressed at relatively low levels (Figure 3.1.1). This could have different reasons. Possibly, ZNF512B fulfills its function during development and differentiation and is no longer necessary in a higher amount in fully differentiated cells. Our mentioned work on ZNF512B in mESCs could also answer this question. Next, ZNF512B may in general only be needed in a small amount. It could just regulate a small number of genes (Chapter 4.4), so that no high amount of protein is required. Another possible explanation is that higher levels of ZNF512B are detrimental to cells. In this study, overexpression of ZNF512B induced a severe aggregation phenotype, which is dependent on the expression level, and long-term expression on a high level eventually lead to cell death. Protein aggregation has also been connected to several neurodegenerative diseases, like ALS (Y. Chen et al., 2024; Pasha et al., 2021). In this context, it is also interesting to see that ZNF512B levels are elevated in tumor tissues, as detected by the RT-qPCR experiment (Figure 3.1.1). Analysis of different cancer tissues using The Cancer Genome Atlas (TCGA) from the Center for Cancer Genomics of the National Cancer Institute showed that in most cases, in which ZNF512B is affected, its levels are elevated instead of reduced (Figure 4.8). As ZNF512B is a strong transcriptional repressor (Figures 3.8.1, 3.8.5), it is possible that higher levels unspecifically repress tumor suppressor genes, in turn promoting carcinogenesis. On the other hand, overexpression of ZNF512B leads to the increased expression of genes that are usually not expressed or only on low level (Figure 3.8.1). If this includes oncogenes in specific tissues or cell types, it could likewise induce tumor development. If high levels of ZNF512B are a cause or a consequence of cancer will be an intriguing aspect to find out.

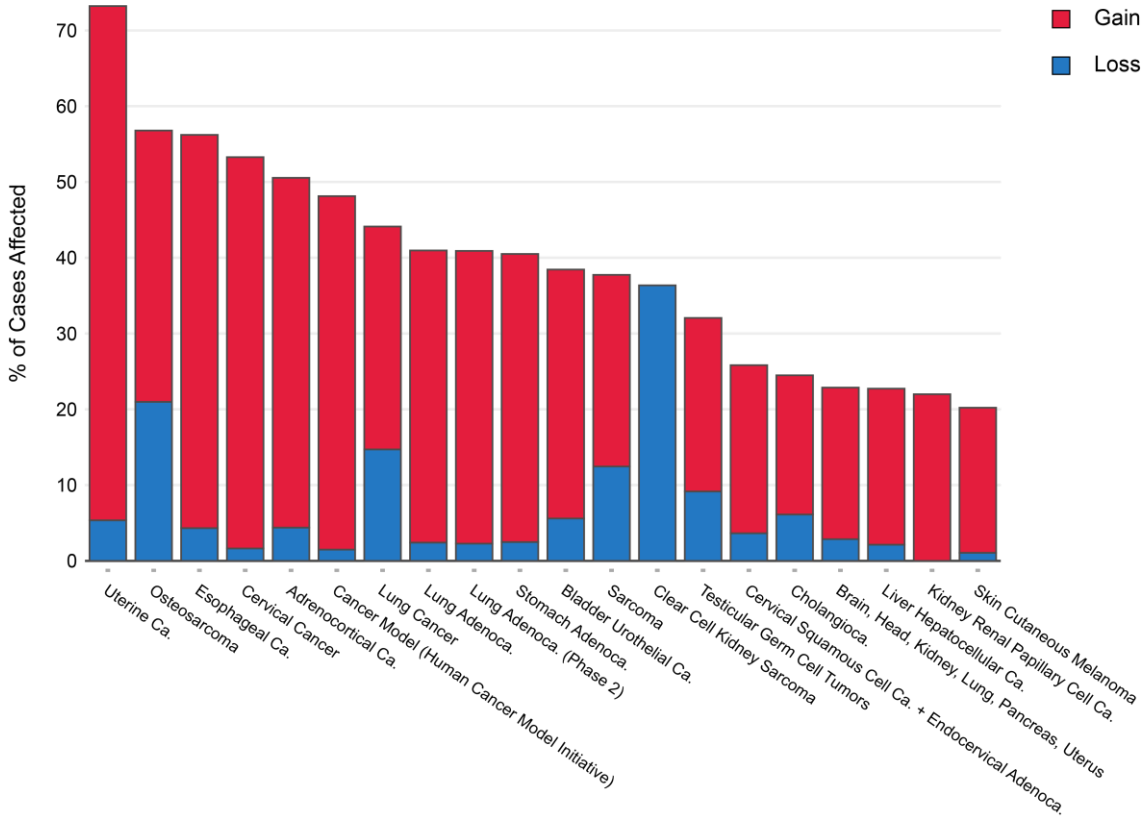

Figure 4.8: ZNF512B levels are mostly elevated in cancer tissues if affected. *Shown is the percentage of cases in which the ZNF512B gene is affected in different cancer tissues. Cases in which ZNF512B levels are elevated are indicated in red, cases in which ZNF512B levels are reduced are indicated in blue. To increase accessibility of the data, project names were reduced to names of the analyzed tissues. Ca.: carcinoma. The results shown here are in whole based upon data generated by the TCGA Research Network: https://www.cancer.gov/tcga.*

4.9 ZNF512B is an interactor of H2A.Z-containing nucleosomes

ZNF512B was shown to act as an interactor of the histone variant H2A.Z and its associated proteins PWWP2A and HMG20A (Herchenrother, Gossen, et al., 2023; Link et al., 2018; Punzeler et al., 2017; Vardabasso et al., 2015). In this study, pull-down experiments with cell lines stably expressing GFP, GFP-H2A or different GFP-H2A variants showed a signal of ZNF512B for every cell line (Figure 3.2.1). A possible explanation for this could be ZNF512B's low expression level in HeLaK cells (Figure 3.1.1). IPs with cell lines inducibly expressing ZNF512B demonstrated that it preferentially pulls down H2A.Z-containing nucleosomes (Figure 3.2.2). ZNF512B's interaction with H2A.Z was further verified in IPs and lfqMS/MS experiments with cells transiently expressing ZNF512B (Figure 3.2.3, 3.7.1). The affinity of ZNF512B for H2A.Z-containing nucleosomes can also be seen in MARCS (Figure 4.5.1). Therefore, all published and here presented data clearly demonstrate that ZNF512B acts as a specific

interactor of H2A.Z-containing nucleosomes. But does ZNF512B preferentially interact with a specific isoform of H2A.Z? Based on this study, that question cannot be answered. In previous lfqMS/MS experiments, ZNF512B did not show a preference for H2A.Z.1 or H2A.Z.2.1 (Punzeler et al., 2017; Vardabasso et al., 2015). However, cell lines stably expressing H2A.Z.1- or H2A.Z.2.1-containing nucleosomes were used, as in this study (Figure 3.2.1), possibly leading to the same problems due to ZNF512B's low expression level. A possible solution would be to endogenously tag the different H2A.Z isoforms and repeat the pull-down experiments with ZNF512B. In this way, antibodies against the different tags could be used to detect whether there is a difference in the amounts of precipitated H2A.Z isoforms.

So, how does ZNF512B interact with H2A.Z? Pull-down experiments with DNase- and MNase-digested extracts showed that ZNF512B can bind H2A.Z-containing nucleosomes but not free histones. Hence, it is likely that ZNF512B does not directly bind H2A.Z but rather needs the chromatin context to interact with this histone variant. Other interactors, like HMG20A or the NuRD complex, and/or specific DNA motifs could be needed to recruit ZNF512B to H2A.Z-containing nucleosomes. The lfqMS/MS experiments demonstrated that NuRD binding is not needed for the interaction between ZNF512B and H2A.Z/HMG20A (Figure 3.7.1). However, the ChIP-qPCR experiment showed that ZNF512B is less enriched at specific H2A.Z-positive sites without the NuRD interaction (Figure 3.8.4). This experiment must be taken with caution, since it was performed with a single biological replicate per condition and should be repeated. It could mean though, that ZNF512B preferentially localizes to H2A.Z-containing nucleosomes at specific sites, where HMG20A and the complete NuRD complex are also localized. If NuRD interaction is lost, ZNF512B could also localize to other H2A.Z/HMG20A sites. Because of a preference for sites with the complete NuRD complex, ZNF512B and PWWP2A could only colocalize at few sites in the genome, due to PWWP2A's specificity for the M1HR-subunit of NuRD (Chapter 4.3). HMG20A could be the 'bridge' between ZNF512B and H2A.Z. Future pull-down and ChIP-seq/CUT&RUN experiments should also be performed in HMG20A KD cells, to see whether the interaction between ZNF512B and H2A.Z is affected.

4.10 Summary & Outlook

This study verifies ZNF512B as an interactor of H2A.Z-containing nucleosomes and its associated protein HMG20A (Figure 4.10). It demonstrates that ZNF512B interacts with the NuRD complex through direct binding of RBBP4 via an alternative, internal NIM present in several other proteins. Further, it shows that ZNF512B acts as a transcriptional repressor dependent and independent of the NuRD interaction, and that elevated levels of ZNF512B induce protein and chromatin aggregation in the nucleus, presumably facilitated by DNA binding and oligomerization of the ZF domains. Finally, it identifies NIM-independent interactors of ZNF512B and suggests a role for the protein in mitosis and RNA-processing. Still, there are major open questions regarding ZNF512B's functionality. How is it recruited to H2A.Z-containing nucleosomes and specific sites in the genome? What is the DNA-binding motif? Which genes are directly regulated by ZNF512B? How exactly does the overexpression phenotype develop and what implications does it have for the endogenous protein? Future research, especially in additional cell types and with focus on the endogenous protein, will shed light on these intriguing questions. Altogether, this study contributes to a better understanding of ZNF512B's functionality and consequently also of the mechanisms underlying H2A.Z's activity. It may have implications for diseases in which ZNF512B expression is deregulated, such as neurodegenerative diseases and cancer, and suggests the existence of additional proteins as potential NuRD interactors.

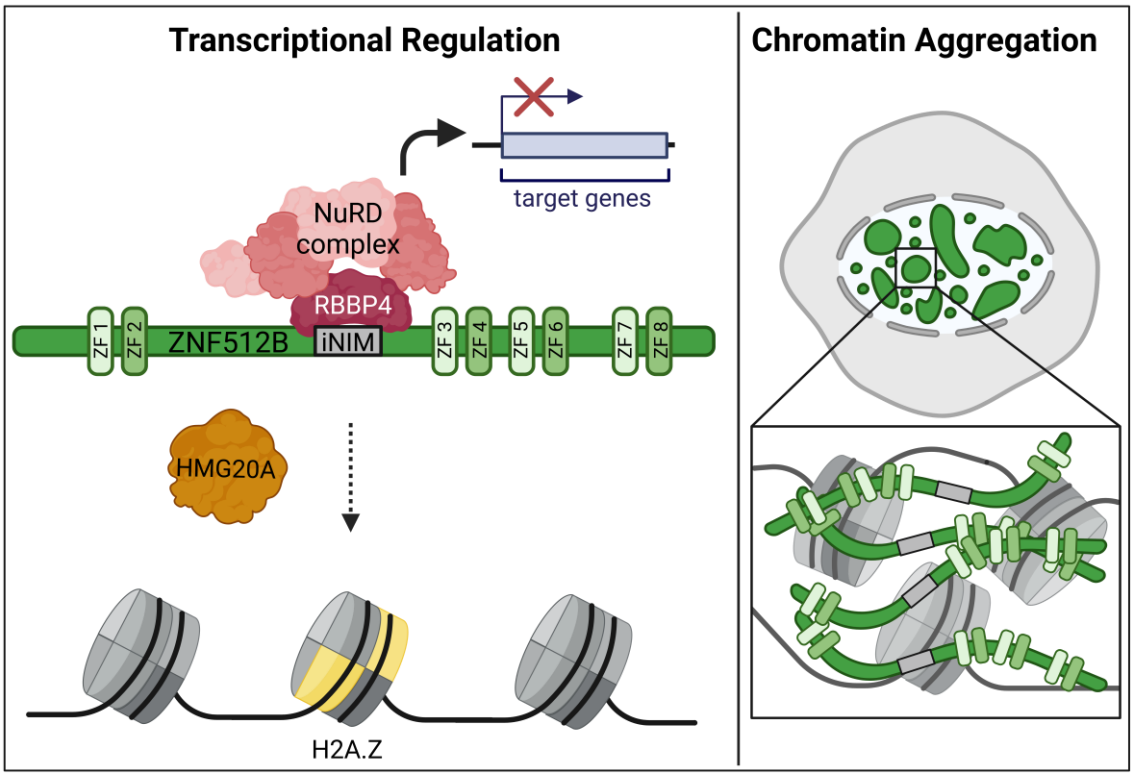

Figure 4.10: ZNF512B's functions in transcriptional regulation and chromatin aggregation. *The H2A.Z- and HMG20A-associated protein ZNF512B interacts with RBBP4 of the NuRD complex via an iNIM and acts as transcriptional repressor in NuRD-dependent and -independent ways. Elevated levels of ZNF512B induce protein and chromatin aggregation in the nucleus. Created in BioRender.com.*

5 References

Abramson, J., Adler, J., Dunger, J., Evans, R., Green, T., Pritzel, A., Ronneberger, O., Willmore, L., Ballard, A. J., Bambrick, J., Bodenstein, S. W., Evans, D. A., Hung, C. C., O'Neill, M., Reiman, D., Tunyasuvunakool, K., Wu, Z., Zemgulyte, A., Arvaniti, E., . . . Jumper, J. M. (2024). Accurate structure prediction of biomolecular interactions with AlphaFold 3. *Nature*, *630*(8016), 493-500. https://doi.org/10.1038/s41586-024-07487-w

Adams, P. D., Grosse-Kunstleve, R. W., Hung, L. W., Ioerger, T. R., McCoy, A. J., Moriarty, N. W., Read, R. J., Sacchettini, J. C., Sauter, N. K., & Terwilliger, T. C. (2002). PHENIX: building new software for automated crystallographic structure determination. *Acta Crystallogr D Biol Crystallogr*, *58*(Pt 11), 1948-1954. https://doi.org/10.1107/s0907444902016657

Aghajanirefah, A. (2012). *The Role of ZBP-89 in Globin Regulation*

Ahn, H. R., Baek, G. O., Yoon, M. G., Son, J. A., You, D., Yoon, J. H., Cho, H. J., Kim, S. S., Cheong, J. Y., & Eun, J. W. (2021). HMBS is the most suitable reference gene for RT-qPCR in human HCC tissues and blood samples. *Oncol Lett*, *22*(5), 791. https://doi.org/10.3892/ol.2021.13052

Al-Naama, N., Mackeh, R., & Kino, T. (2020). C(2)H(2)-Type Zinc Finger Proteins in Brain Development, Neurodevelopmental, and Other Neuropsychiatric Disorders: Systematic Literature-Based Analysis. *Front Neurol*, *11*, 32. https://doi.org/10.3389/fneur.2020.00032

Alatwi, H. E., & Downs, J. A. (2015). Removal of H2A.Z by INO80 promotes homologous recombination. *EMBO Rep*, *16*(8), 986-994. https://doi.org/10.15252/embr.201540330

Alberti, S., & Carra, S. (2019). Nucleolus: A Liquid Droplet Compartment for Misbehaving Proteins. *Curr Biol*, *29*(19), R930-R932. https://doi.org/10.1016/j.cub.2019.08.013

Alberti, S., Mateju, D., Mediani, L., & Carra, S. (2017). Granulostasis: Protein Quality Control of RNP Granules. *Front Mol Neurosci*, *10*, 84. https://doi.org/10.3389/fnmol.2017.00084

Albig, W., & Doenecke, D. (1997). The human histone gene cluster at the D6S105 locus. *Hum Genet*, *101*(3), 284-294. https://doi.org/10.1007/s004390050630

Albig, W., Kioschis, P., Poustka, A., Meergans, K., & Doenecke, D. (1997). Human histone gene organization: nonregular arrangement within a large cluster. *Genomics*, *40*(2), 314-322. https://doi.org/10.1006/geno.1996.4592

Altaf, M., Auger, A., Monnet-Saksouk, J., Brodeur, J., Piquet, S., Cramet, M., Bouchard, N., Lacoste, N., Utley, R. T., Gaudreau, L., & Cote, J. (2010). NuA4-dependent acetylation of nucleosomal histones H4 and H2A directly stimulates incorporation of H2A.Z by the SWR1 complex. *J Biol Chem*, *285*(21), 15966-15977. https://doi.org/10.1074/jbc.M110.117069

Altschul, S. F., Gish, W., Miller, W., Myers, E. W., & Lipman, D. J. (1990). Basic local alignment search tool. *J Mol Biol*, *215*(3), 403-410. https://doi.org/10.1016/S0022-2836(05)80360-2

Andrade de Oliveira, K., Sengupta, S., Yadav, A. K., & Clarke, R. (2023). The complex nature of heterogeneity and its roles in breast cancer biology and therapeutic responsiveness. *Front Endocrinol (Lausanne)*, *14*, 1083048. https://doi.org/10.3389/fendo.2023.1083048

Auger, A., Galarneau, L., Altaf, M., Nourani, A., Doyon, Y., Utley, R. T., Cronier, D., Allard, S., & Cote, J. (2008). Eaf1 is the platform for NuA4 molecular assembly that evolutionarily links chromatin acetylation to ATP-dependent exchange of

histone H2A variants. *Mol Cell Biol*, *28*(7), 2257-2270. https://doi.org/10.1128/MCB.01755-07

Avila-Lopez, P. A., Guerrero, G., Nunez-Martinez, H. N., Peralta-Alvarez, C. A., Hernandez-Montes, G., Alvarez-Hilario, L. G., Herrera-Goepfert, R., Albores-Saavedra, J., Villegas-Sepulveda, N., Cedillo-Barron, L., Montes-Gomez, A. E., Vargas, M., Schnoor, M., Recillas-Targa, F., & Hernandez-Rivas, R. (2021). H2A.Z overexpression suppresses senescence and chemosensitivity in pancreatic ductal adenocarcinoma. *Oncogene*, *40*(11), 2065-2080. https://doi.org/10.1038/s41388-021-01664-1

Bailly, C. (2023). Etoposide: A rider on the cytokine storm. *Cytokine*, *168*, 156234. https://doi.org/10.1016/j.cyto.2023.156234

Ballestar, E., & Wolffe, A. P. (2001). Methyl-CpG-binding proteins. Targeting specific gene repression. *Eur J Biochem*, *268*(1), 1-6. https://doi.org/10.1046/j.1432-1327.2001.01869.x

Baniahmad, A., Leng, X., Burris, T. P., Tsai, S. Y., Tsai, M. J., & O'Malley, B. W. (1995). The tau 4 activation domain of the thyroid hormone receptor is required for release of a putative corepressor(s) necessary for transcriptional silencing. *Mol Cell Biol*, *15*(1), 76-86. https://doi.org/10.1128/MCB.15.1.76

Banks, C. A. S., Miah, S., Adams, M. K., Eubanks, C. G., Thornton, J. L., Florens, L., & Washburn, M. P. (2018). Differential HDAC1/2 network analysis reveals a role for prefoldin/CCT in HDAC1/2 complex assembly. *Sci Rep*, *8*(1), 13712. https://doi.org/10.1038/s41598-018-32009-w

Bannister, A. J., & Kouzarides, T. (2011). Regulation of chromatin by histone modifications. *Cell Res*, *21*(3), 381-395. https://doi.org/10.1038/cr.2011.22

Bao, Y., & Shen, X. (2011). SnapShot: Chromatin remodeling: INO80 and SWR1. *Cell*, *144*(1), 158-158 e152. https://doi.org/10.1016/j.cell.2010.12.024

Basta, J., & Rauchman, M. (2015). The nucleosome remodeling and deacetylase complex in development and disease. *Transl Res*, *165*(1), 36-47. https://doi.org/10.1016/j.trsl.2014.05.003

Becker, P. B., Ruppert, S., & Schutz, G. (1987). Genomic footprinting reveals cell type-specific DNA binding of ubiquitous factors. *Cell*, *51*(3), 435-443. https://doi.org/10.1016/0092-8674(87)90639-8

Bednar, J., & Dimitrov, S. (2011). Chromatin under mechanical stress: from single 30 nm fibers to single nucleosomes. *FEBS J*, *278*(13), 2231-2243. https://doi.org/10.1111/j.1742-4658.2011.08153.x

Beisel, C., Imhof, A., Greene, J., Kremmer, E., & Sauer, F. (2002). Histone methylation by the Drosophila epigenetic transcriptional regulator Ash1. *Nature*, *419*(6909), 857-862. https://doi.org/10.1038/nature01126

Bellucci, L., Dalvai, M., Kocanova, S., Moutahir, F., & Bystricky, K. (2013). Activation of p21 by HDAC inhibitors requires acetylation of H2A.Z. *PLOS ONE*, *8*(1), e54102. https://doi.org/10.1371/journal.pone.0054102

Berman, H. M., Westbrook, J., Feng, Z., Gilliland, G., Bhat, T. N., Weissig, H., Shindyalov, I. N., & Bourne, P. E. (2000). The Protein Data Bank. *Nucleic acids research*, *28*(1), 235-242. https://doi.org/10.1093/nar/28.1.235

Berta, D. G., Kuisma, H., Valimaki, N., Raisanen, M., Jantti, M., Pasanen, A., Karhu, A., Kaukomaa, J., Taira, A., Cajuso, T., Nieminen, S., Penttinen, R. M., Ahonen, S., Lehtonen, R., Mehine, M., Vahteristo, P., Jalkanen, J., Sahu, B., Ravantti, J., . . . Aaltonen, L. A. (2021). Deficient H2A.Z deposition is associated with genesis of uterine leiomyoma. *Nature*, *596*(7872), 398-403. https://doi.org/10.1038/s41586-021-03747-1

Bharath, M. M., Chandra, N. R., & Rao, M. R. (2003). Molecular modeling of the chromatosome particle. *Nucleic acids research*, *31*(14), 4264-4274. https://doi.org/10.1093/nar/gkg481

Bijlmakers, M. J., Teixeira, J. M., Boer, R., Mayzel, M., Puig-Sarries, P., Karlsson, G., Coll, M., Pons, M., & Crosas, B. (2016). A C2HC zinc finger is essential for the RING-E2 interaction of the ubiquitin ligase RNF125. *Sci Rep*, *6*, 29232. https://doi.org/10.1038/srep29232

Billon, P., & Cote, J. (2013). Precise deposition of histone H2A.Z in chromatin for genome expression and maintenance. *Biochim Biophys Acta*, *1819*(3-4), 290-302. https://doi.org/10.1016/j.bbagrm.2011.10.004

Binda, O., Sevilla, A., LeRoy, G., Lemischka, I. R., Garcia, B. A., & Richard, S. (2013). SETD6 monomethylates H2AZ on lysine 7 and is required for the maintenance of embryonic stem cell self-renewal. *Epigenetics*, *8*(2), 177-183. https://doi.org/10.4161/epi.23416

Bird, A. P. (1986). CpG-rich islands and the function of DNA methylation. *Nature*, *321*(6067), 209-213. https://doi.org/10.1038/321209a0

Blighe, K., Rana, S., & Lewis, M. (2023). EnhancedVolcalo: Publication-ready volcano plots with enhanced colouring and labelling. *R package version 1.18.0*. https://doi.org/10.18129/B9.bioc.EnhancedVolcano

Bonisch, C., Schneider, K., Punzeler, S., Wiedemann, S. M., Bielmeier, C., Bocola, M., Eberl, H. C., Kuegel, W., Neumann, J., Kremmer, E., Leonhardt, H., Mann, M., Michaelis, J., Schermelleh, L., & Hake, S. B. (2012). H2A.Z.2.2 is an alternatively spliced histone H2A.Z variant that causes severe nucleosome destabilization. *Nucleic acids research*, *40*(13), 5951-5964. https://doi.org/10.1093/nar/gks267

Boulasiki, P., Tan, X. W., Spinelli, M., & Riccio, A. (2023). The NuRD Complex in Neurodevelopment and Disease: A Case of Sliding Doors. *Cells*, *12*(8). https://doi.org/10.3390/cells12081179

Bourgeois, B., Hutten, S., Gottschalk, B., Hofweber, M., Richter, G., Sternat, J., Abou-Ajram, C., Gobl, C., Leitinger, G., Graier, W. F., Dormann, D., & Madl, T. (2020). Nonclassical nuclear localization signals mediate nuclear import of CIRBP. *Proc Natl Acad Sci U S A*, *117*(15), 8503-8514. https://doi.org/10.1073/pnas.1918944117

Bowerman, S., & Wereszczynski, J. (2016). Effects of MacroH2A and H2A.Z on Nucleosome Dynamics as Elucidated by Molecular Dynamics Simulations. *Biophys J*, *110*(2), 327-337. https://doi.org/10.1016/j.bpj.2015.12.015

Brahma, S., Udugama, M. I., Kim, J., Hada, A., Bhardwaj, S. K., Hailu, S. G., Lee, T. H., & Bartholomew, B. (2017). INO80 exchanges H2A.Z for H2A by translocating on DNA proximal to histone dimers. *Nat Commun*, *8*(1), 15616. https://doi.org/10.1038/ncomms15616

Bruce, K., Myers, F. A., Mantouvalou, E., Lefevre, P., Greaves, I., Bonifer, C., Tremethick, D. J., Thorne, A. W., & Crane-Robinson, C. (2005). The replacement histone H2A.Z in a hyperacetylated form is a feature of active genes in the chicken. *Nucleic acids research*, *33*(17), 5633-5639. https://doi.org/10.1093/nar/gki874

Buschbeck, M., & Hake, S. B. (2017). Variants of core histones and their roles in cell fate decisions, development and cancer. *Nat Rev Mol Cell Biol*, *18*(5), 299-314. https://doi.org/10.1038/nrm.2016.166

Cai, L., Liu, B., Cao, Y., Sun, T., & Li, Y. (2023). Unveiling the molecular structure and role of RBBP4/7: implications for epigenetic regulation and cancer research. *Front Mol Biosci*, *10*, 1276612. https://doi.org/10.3389/fmolb.2023.1276612

Cai, X., Gao, J., Shi, C., Guo, W. Z., Guo, D., & Zhang, S. (2022). The role of NCAPG in various of tumors. *Biomed Pharmacother*, *155*, 113635. https://doi.org/10.1016/j.biopha.2022.113635

Cai, Y., Jin, J., Florens, L., Swanson, S. K., Kusch, T., Li, B., Workman, J. L., Washburn, M. P., Conaway, R. C., & Conaway, J. W. (2005). The mammalian YL1 protein is a shared subunit of the TRRAP/TIP60 histone acetyltransferase and SRCAP complexes. *J Biol Chem*, *280*(14), 13665-13670. https://doi.org/10.1074/jbc.M500001200

Cai, Y., Jin, J., Tomomori-Sato, C., Sato, S., Sorokina, I., Parmely, T. J., Conaway, R. C., & Conaway, J. W. (2003). Identification of new subunits of the multiprotein mammalian TRRAP/TIP60-containing histone acetyltransferase complex. *J Biol Chem*, *278*(44), 42733-42736. https://doi.org/10.1074/jbc.C300389200

Cakmakci, N. G., Lerner, R. S., Wagner, E. J., Zheng, L., & Marzluff, W. F. (2008). SLIP1, a factor required for activation of histone mRNA translation by the stem-loop binding protein. *Mol Cell Biol*, *28*(3), 1182-1194. https://doi.org/10.1128/MCB.01500-07

Cao, R., Wang, L., Wang, H., Xia, L., Erdjument-Bromage, H., Tempst, P., Jones, R. S., & Zhang, Y. (2002). Role of histone H3 lysine 27 methylation in Polycomb-group silencing. *Science*, *298*(5595), 1039-1043. https://doi.org/10.1126/science.1076997

Cassandri, M., Smirnov, A., Novelli, F., Pitolli, C., Agostini, M., Malewicz, M., Melino, G., & Raschella, G. (2017). Zinc-finger proteins in health and disease. *Cell Death Discov*, *3*, 17071. https://doi.org/10.1038/cddiscovery.2017.71

Chammas, P., Mocavini, I., & Di Croce, L. (2020). Engaging chromatin: PRC2 structure meets function. *Br J Cancer*, *122*(3), 315-328. https://doi.org/10.1038/s41416-019-0615-2

Chen, C., & Okayama, H. (1987). High-efficiency transformation of mammalian cells by plasmid DNA. *Mol Cell Biol*, *7*(8), 2745-2752. https://doi.org/10.1128/mcb.7.8.2745-2752.1987

Chen, L., Conaway, R. C., & Conaway, J. W. (2013). Multiple modes of regulation of the human Ino80 SNF2 ATPase by subunits of the INO80 chromatin-remodeling complex. *Proc Natl Acad Sci U S A*, *110*(51), 20497-20502. https://doi.org/10.1073/pnas.1317092110

Chen, X., Huang, M. F., Fan, D. M., He, Y. H., Zhang, W. J., Ding, J. C., Peng, B. L., Pan, X., Liu, Y., Du, J., Li, Y., Liu, Z. Y., Xie, B. L., Kuang, Z. J., Yi, J., & Liu, W. (2024). CARM1 hypermethylates the NuRD chromatin remodeling complex to promote cell cycle gene expression and breast cancer development. *Nucleic acids research*, *52*(12), 6811-6829. https://doi.org/10.1093/nar/gkae329

Chen, Y., Pei, X., Chen, L., & Chen, L. (2024). A dynamic regulatory switch for phase separation of FUS protein: Zinc ions and zinc finger domain. *Biochem Biophys Res Commun*, *710*, 149862. https://doi.org/10.1016/j.bbrc.2024.149862

Chen, Y., Wan, Y., Pei, X., Wang, T., Ma, Z., & Chen, L. (2023). GATA3 ZnF2-defective mutant condensation underlies type I IFN-activating in breast cancer. *bioRxiv*, 2023.2005.2002.538687. https://doi.org/10.1101/2023.05.02.538687

Choi, J., Heo, K., & An, W. (2009). Cooperative action of TIP48 and TIP49 in H2A.Z exchange catalyzed by acetylation of nucleosomal H2A. *Nucleic acids research*, *37*(18), 5993-6007. https://doi.org/10.1093/nar/gkp660

Church, D. M., Schneider, V. A., Graves, T., Auger, K., Cunningham, F., Bouk, N., Chen, H. C., Agarwala, R., McLaren, W. M., Ritchie, G. R., Albracht, D., Kremitzki, M., Rock, S., Kotkiewicz, H., Kremitzki, C., Wollam, A., Trani, L., Fulton, L., Fulton,

R., . . . Hubbard, T. (2011). Modernizing reference genome assemblies. *PLoS Biol*, *9*(7), e1001091. https://doi.org/10.1371/journal.pbio.1001091

Clapier, C. R., Iwasa, J., Cairns, B. R., & Peterson, C. L. (2017). Mechanisms of action and regulation of ATP-dependent chromatin-remodelling complexes. *Nat Rev Mol Cell Biol*, *18*(7), 407-422. https://doi.org/10.1038/nrm.2017.26

Clerget, G., Bourguignon-Igel, V., Marmier-Gourrier, N., Rolland, N., Wacheul, L., Manival, X., Charron, C., Kufel, J., Mereau, A., Senty-Segault, V., Tollervey, D., Lafontaine, D. L. J., Branlant, C., & Rederstorff, M. (2020). Synergistic defects in pre-rRNA processing from mutations in the U3-specific protein Rrp9 and U3 snoRNA. *Nucleic acids research*, *48*(7), 3848-3868. https://doi.org/10.1093/nar/gkaa066

Cole, L., Kurscheid, S., Nekrasov, M., Domaschenz, R., Vera, D. L., Dennis, J. H., & Tremethick, D. J. (2021). Multiple roles of H2A.Z in regulating promoter chromatin architecture in human cells. *Nat Commun*, *12*(1), 2524. https://doi.org/10.1038/s41467-021-22688-x

Colino-Sanguino, Y., Clark, S. J., & Valdes-Mora, F. (2022). The H2A.Z-nuclesome code in mammals: emerging functions. *Trends Genet*, *38*(3), 273-289. https://doi.org/10.1016/j.tig.2021.10.003

Colino-Sanguino, Y., Cornett, E. M., Moulder, D., Smith, G. C., Hrit, J., Cordeiro-Spinetti, E., Vaughan, R. M., Krajewski, K., Rothbart, S. B., Clark, S. J., & Valdes-Mora, F. (2019). A Read/Write Mechanism Connects p300 Bromodomain Function to H2A.Z Acetylation. *iScience*, *21*, 773-788. https://doi.org/10.1016/j.isci.2019.10.053

Connacher, J., von Gruning, H., & Birkholtz, L. (2022). Histone Modification Landscapes as a Roadmap for Malaria Parasite Development. *Front Cell Dev Biol*, *10*, 848797. https://doi.org/10.3389/fcell.2022.848797

Coon, J. J., Ueberheide, B., Syka, J. E., Dryhurst, D. D., Ausio, J., Shabanowitz, J., & Hunt, D. F. (2005). Protein identification using sequential ion/ion reactions and tandem mass spectrometry. *Proc Natl Acad Sci U S A*, *102*(27), 9463-9468. https://doi.org/10.1073/pnas.0503189102

Corona, D. F., & Tamkun, J. W. (2004). Multiple roles for ISWI in transcription, chromosome organization and DNA replication. *Biochim Biophys Acta*, *1677*(1-3), 113-119. https://doi.org/10.1016/j.bbaexp.2003.09.018

Cox, J., & Mann, M. (2008). MaxQuant enables high peptide identification rates, individualized p.p.b.-range mass accuracies and proteome-wide protein quantification. *Nat Biotechnol*, *26*(12), 1367-1372. https://doi.org/10.1038/nbt.1511

Dang, W., & Bartholomew, B. (2007). Domain architecture of the catalytic subunit in the ISW2-nucleosome complex. *Mol Cell Biol*, *27*(23), 8306-8317. https://doi.org/10.1128/MCB.01351-07

Davis, I. W., Leaver-Fay, A., Chen, V. B., Block, J. N., Kapral, G. J., Wang, X., Murray, L. W., Arendall, W. B., 3rd, Snoeyink, J., Richardson, J. S., & Richardson, D. C. (2007). MolProbity: all-atom contacts and structure validation for proteins and nucleic acids. *Nucleic Acids Res*, *35*(Web Server issue), W375-383. https://doi.org/10.1093/nar/gkm216

de Castro, R. O., Carbajal, A., Previato de Almeida, L., Goitea, V., Griffin, C. T., & Pezza, R. J. (2022). Mouse Chd4-NURD is required for neonatal spermatogonia survival and normal gonad development. *Epigenetics Chromatin*, *15*(1), 16. https://doi.org/10.1186/s13072-022-00448-5

DeLano, W. L. (2002). The PyMOL Molecular Graphics System. *Delano Scientific, San Carlos*.

Demetriadou, C., Koufaris, C., & Kirmizis, A. (2020). Histone N-alpha terminal modifications: genome regulation at the tip of the tail. *Epigenetics Chromatin*, *13*(1), 29. https://doi.org/10.1186/s13072-020-00352-w

Doll, S. G., & Cingolani, G. (2022). Importin alpha/beta and the tug of war to keep TDP-43 in solution: quo vadis? *Bioessays*, *44*(12), e2200181. https://doi.org/10.1002/bies.202200181

Dong, M., Chen, J., Deng, Y., Zhang, D., Dong, L., & Sun, D. (2021). H2AFZ Is a Prognostic Biomarker Correlated to TP53 Mutation and Immune Infiltration in Hepatocellular Carcinoma. *Front Oncol*, *11*, 701736. https://doi.org/10.3389/fonc.2021.701736

Doyon, Y., Selleck, W., Lane, W. S., Tan, S., & Cote, J. (2004). Structural and functional conservation of the NuA4 histone acetyltransferase complex from yeast to humans. *Mol Cell Biol*, *24*(5), 1884-1896. https://doi.org/10.1128/MCB.24.5.1884-1896.2004

Draker, R., Ng, M. K., Sarcinella, E., Ignatchenko, V., Kislinger, T., & Cheung, P. (2012). A combination of H2A.Z and H4 acetylation recruits Brd2 to chromatin during transcriptional activation. *PLoS Genet*, *8*(11), e1003047. https://doi.org/10.1371/journal.pgen.1003047

Dunn, C. J., Sarkar, P., Bailey, E. R., Farris, S., Zhao, M., Ward, J. M., Dudek, S. M., & Saha, R. N. (2017). Histone Hypervariants H2A.Z.1 and H2A.Z.2 Play Independent and Context-Specific Roles in Neuronal Activity-Induced Transcription of Arc/Arg3.1 and Other Immediate Early Genes. *eNeuro*, *4*(4). https://doi.org/10.1523/ENEURO.0040-17.2017

Duster, R., Kaltheuner, I. H., Schmitz, M., & Geyer, M. (2021). 1,6-Hexanediol, commonly used to dissolve liquid-liquid phase separated condensates, directly impairs kinase and phosphatase activities. *J Biol Chem*, *296*, 100260. https://doi.org/10.1016/j.jbc.2021.100260

Eirin-Lopez, J. M., Gonzalez-Romero, R., Dryhurst, D., Ishibashi, T., & Ausio, J. (2009). The evolutionary differentiation of two histone H2A.Z variants in chordates (H2A.Z-1 and H2A.Z-2) is mediated by a stepwise mutation process that affects three amino acid residues. *BMC Evol Biol*, *9*(1), 31. https://doi.org/10.1186/1471-2148-9-31

Eirin-Lopez, J. M., Ishibashi, T., & Ausio, J. (2008). H2A.Bbd: a quickly evolving hypervariable mammalian histone that destabilizes nucleosomes in an acetylation-independent way. *FASEB J*, *22*(1), 316-326. https://doi.org/10.1096/fj.07-9255com

El Abdellaoui-Soussi, F., Yunes-Leites, P. S., Lopez-Maderuelo, D., Garcia-Marques, F., Vazquez, J., Redondo, J. M., & Gomez-Del Arco, P. (2022). Interplay between the Chd4/NuRD Complex and the Transcription Factor Znf219 Controls Cardiac Cell Identity. *International journal of molecular sciences*, *23*(17). https://doi.org/10.3390/ijms23179565

Elabscience. (2024). *One-step TUNEL In Situ Apoptosis Kit (Red, Elab Fluor® 594) (E-CK-A322)*. Retrieved 04.12.2024 from https://www.elabscience.com/p/one-step-tunel-in-situ-apoptosis-kit-red-elab-fluor-594--e-ck-a322

Emsley, P., Lohkamp, B., Scott, W. G., & Cowtan, K. (2010). Features and development of Coot. *Acta Crystallogr D Biol Crystallogr*, *66*(Pt 4), 486-501. https://doi.org/10.1107/S0907444910007493

Eom, K. S., Cheong, J. S., & Lee, S. J. (2016). Structural Analyses of Zinc Finger Domains for Specific Interactions with DNA. *J Microbiol Biotechnol*, *26*(12), 2019-2029. https://doi.org/10.4014/jmb.1609.09021

Etier, A., Dumetz, F., Chereau, S., & Ponts, N. (2022). Post-Translational Modifications of Histones Are Versatile Regulators of Fungal Development and Secondary Metabolism. *Toxins (Basel)*, *14*(5). https://doi.org/10.3390/toxins14050317

Evans, P. (2006). Scaling and assessment of data quality. *Acta Crystallogr D Biol Crystallogr*, *62*(Pt 1), 72-82. https://doi.org/10.1107/S0907444905036693

Faast, R., Thonglairoam, V., Schulz, T. C., Beall, J., Wells, J. R., Taylor, H., Matthaei, K., Rathjen, P. D., Tremethick, D. J., & Lyons, I. (2001). Histone variant H2A.Z is required for early mammalian development. *Curr Biol*, *11*(15), 1183-1187. https://doi.org/10.1016/s0960-9822(01)00329-3

Fardi, M., Solali, S., & Farshdousti Hagh, M. (2018). Epigenetic mechanisms as a new approach in cancer treatment: An updated review. *Genes Dis*, *5*(4), 304-311. https://doi.org/10.1016/j.gendis.2018.06.003

Finkbeiner, E., Haindl, M., & Muller, S. (2011). The SUMO system controls nucleolar partitioning of a novel mammalian ribosome biogenesis complex. *EMBO J*, *30*(6), 1067-1078. https://doi.org/10.1038/emboj.2011.33

Flemming, W. (1882). *Zellsubstanz, Kern und Zelltheilung*. Vogel. https://books.google.de/books?id=iTsAAAAAQAAJ

Fritz, A. J., Sehgal, N., Pliss, A., Xu, J., & Berezney, R. (2019). Chromosome territories and the global regulation of the genome. *Genes Chromosomes Cancer*, *58*(7), 407-426. https://doi.org/10.1002/gcc.22732

Fujimoto, S., Seebart, C., Guastafierro, T., Prenni, J., Caiafa, P., & Zlatanova, J. (2012). Proteome analysis of protein partners to nucleosomes containing canonical H2A or the variant histones H2A.Z or H2A.X. *Biol Chem*, *393*(1-2), 47-61. https://doi.org/10.1515/BC-2011-216

Gao, N., Li, Y., Li, J., Gao, Z., Yang, Z., Li, Y., Liu, H., & Fan, T. (2020). Long Non-Coding RNAs: The Regulatory Mechanisms, Research Strategies, and Future Directions in Cancers. *Front Oncol*, *10*, 598817. https://doi.org/10.3389/fonc.2020.598817

Gao, Y., Zamisch, M., Vacchio, M., Chopp, L., Ciucci, T., Paine, E. L., Lyons, G. C., Nie, J., Xiao, Q., Zvezdova, E., Love, P. E., Vinson, C. R., Jenkins, L. M., & Bosselut, R. (2022). NuRD complex recruitment to Thpok mediates CD4(+) T cell lineage differentiation. *Sci Immunol*, *7*(72), eabn5917. https://doi.org/10.1126/sciimmunol.abn5917

Gevry, N., Chan, H. M., Laflamme, L., Livingston, D. M., & Gaudreau, L. (2007). p21 transcription is regulated by differential localization of histone H2A.Z. *Genes Dev*, *21*(15), 1869-1881. https://doi.org/10.1101/gad.1545707

Giaimo, B. D., Ferrante, F., Herchenrother, A., Hake, S. B., & Borggrefe, T. (2019). The histone variant H2A.Z in gene regulation. *Epigenetics Chromatin*, *12*(1), 37. https://doi.org/10.1186/s13072-019-0274-9

Giaimo, B. D., Ferrante, F., Vallejo, D. M., Hein, K., Gutierrez-Perez, I., Nist, A., Stiewe, T., Mittler, G., Herold, S., Zimmermann, T., Bartkuhn, M., Schwarz, P., Oswald, F., Dominguez, M., & Borggrefe, T. (2018). Histone variant H2A.Z deposition and acetylation directs the canonical Notch signaling response. *Nucleic acids research*, *46*(16), 8197-8215. https://doi.org/10.1093/nar/gky551

Gibson, T. J., Postma, J. P., Brown, R. S., & Argos, P. (1988). A model for the tertiary structure of the 28 residue DNA-binding motif ('zinc finger') common to many

eukaryotic transcriptional regulatory proteins. *Protein Eng*, *2*(3), 209-218. https://doi.org/10.1093/protein/2.3.209

Goddard, T. D., Huang, C. C., Meng, E. C., Pettersen, E. F., Couch, G. S., Morris, J. H., & Ferrin, T. E. (2018). UCSF ChimeraX: Meeting modern challenges in visualization and analysis. *Protein Sci*, *27*(1), 14-25. https://doi.org/10.1002/pro.3235

Gordon, J., Pillon, M. C., & Stanley, R. E. (2019). Nol9 Is a Spatial Regulator for the Human ITS2 Pre-rRNA Endonuclease-Kinase Complex. *J Mol Biol*, *431*(19), 3771-3786. https://doi.org/10.1016/j.jmb.2019.07.007

Greenberg, R. S., Long, H. K., Swigut, T., & Wysocka, J. (2019). Single Amino Acid Change Underlies Distinct Roles of H2A.Z Subtypes in Human Syndrome. *Cell*, *178*(6), 1421-1436 e1424. https://doi.org/10.1016/j.cell.2019.08.002

Grigorescu, A. A., & Rosenberg, J. M. (2004). DNA Sequence Recognition by Proteins. In W. J. Lennarz & M. D. Lane (Eds.), *Encyclopedia of Biological Chemistry* (pp. 788-793). Elsevier. https://doi.org/https://doi.org/10.1016/B0-12-443710-9/00682-7

Grune, T., Brzeski, J., Eberharter, A., Clapier, C. R., Corona, D. F., Becker, P. B., & Muller, C. W. (2003). Crystal structure and functional analysis of a nucleosome recognition module of the remodeling factor ISWI. *Mol Cell*, *12*(2), 449-460. https://doi.org/10.1016/s1097-2765(03)00273-9

Hardy, S., Jacques, P. E., Gevry, N., Forest, A., Fortin, M. E., Laflamme, L., Gaudreau, L., & Robert, F. (2009). The euchromatic and heterochromatic landscapes are shaped by antagonizing effects of transcription on H2A.Z deposition. *PLoS Genet*, *5*(10), e1000687. https://doi.org/10.1371/journal.pgen.1000687

Hashimoto, H., Liu, Y., Upadhyay, A. K., Chang, Y., Howerton, S. B., Vertino, P. M., Zhang, X., & Cheng, X. (2012). Recognition and potential mechanisms for replication and erasure of cytosine hydroxymethylation. *Nucleic acids research*, *40*(11), 4841-4849. https://doi.org/10.1093/nar/gks155

Heitz, E. (1928). *"Das" Heterochromatin der Moose*. Bornträger. https://books.google.de/books?id=3JwgSQAACAAJ

Hendzel, M. J., Wei, Y., Mancini, M. A., Van Hooser, A., Ranalli, T., Brinkley, B. R., Bazett-Jones, D. P., & Allis, C. D. (1997). Mitosis-specific phosphorylation of histone H3 initiates primarily within pericentromeric heterochromatin during G2 and spreads in an ordered fashion coincident with mitotic chromosome condensation. *Chromosoma*, *106*(6), 348-360. https://doi.org/10.1007/s004120050256

Herchenrother, A., Gossen, S., Friedrich, T., Reim, A., Daus, N., Diegmuller, F., Leers, J., Sani, H. M., Gerstner, S., Schwarz, L., Stellmacher, I., Szymkowiak, L. V., Nist, A., Stiewe, T., Borggrefe, T., Mann, M., Mackay, J. P., Bartkuhn, M., Borchers, A., . . . Hake, S. B. (2023). The H2A.Z and NuRD associated protein HMG20A controls early head and heart developmental transcription programs. *Nat Commun*, *14*(1), 472. https://doi.org/10.1038/s41467-023-36114-x

Herchenrother, A., Wunderlich, T. M., Lan, J., & Hake, S. B. (2023). Spotlight on histone H2A variants: From B to X to Z. *Semin Cell Dev Biol*, *135*, 3-12. https://doi.org/10.1016/j.semcdb.2022.03.025

Hochheimer, A., Zhou, S., Zheng, S., Holmes, M. C., & Tjian, R. (2002). TRF2 associates with DREF and directs promoter-selective gene expression in Drosophila. *Nature*, *420*(6914), 439-445. https://doi.org/10.1038/nature01167

Hoffmann, A., & Spengler, D. (2019). Chromatin Remodeling Complex NuRD in Neurodevelopment and Neurodevelopmental Disorders. *Front Genet*, *10*, 682. https://doi.org/10.3389/fgene.2019.00682

Hong, J., Feng, H., Wang, F., Ranjan, A., Chen, J., Jiang, J., Ghirlando, R., Xiao, T. S., Wu, C., & Bai, Y. (2014). The catalytic subunit of the SWR1 remodeler is a histone chaperone for the H2A.Z-H2B dimer. *Mol Cell*, *53*(3), 498-505. https://doi.org/10.1016/j.molcel.2014.01.010

Hong, W., Nakazawa, M., Chen, Y. Y., Kori, R., Vakoc, C. R., Rakowski, C., & Blobel, G. A. (2005). FOG-1 recruits the NuRD repressor complex to mediate transcriptional repression by GATA-1. *EMBO J*, *24*(13), 2367-2378. https://doi.org/10.1038/sj.emboj.7600703

Horikoshi, N., Sato, K., Shimada, K., Arimura, Y., Osakabe, A., Tachiwana, H., Hayashi-Takanaka, Y., Iwasaki, W., Kagawa, W., Harata, M., Kimura, H., & Kurumizaka, H. (2013). Structural polymorphism in the L1 loop regions of human H2A.Z.1 and H2A.Z.2. *Acta Crystallogr D Biol Crystallogr*, *69*(Pt 12), 2431-2439. https://doi.org/10.1107/S090744491302252X

Hornbeck, P. V., Zhang, B., Murray, B., Kornhauser, J. M., Latham, V., & Skrzypek, E. (2015). PhosphoSitePlus, 2014: mutations, PTMs and recalibrations. *Nucleic acids research*, *43*(Database issue), D512-520. https://doi.org/10.1093/nar/gku1267

Hossain, M. A., Barrow, J. J., Shen, Y., Haq, M. I., & Bungert, J. (2015). Artificial zinc finger DNA binding domains: versatile tools for genome engineering and modulation of gene expression. *J Cell Biochem*, *116*(11), 2435-2444. https://doi.org/10.1002/jcb.25226

Hotchkiss, R. D. (1948). The quantitative separation of purines, pyrimidines, and nucleosides by paper chromatography. *J Biol Chem*, *175*(1), 315-332. https://www.ncbi.nlm.nih.gov/pubmed/18873306

Hsu, J. Y., Sun, Z. W., Li, X., Reuben, M., Tatchell, K., Bishop, D. K., Grushcow, J. M., Brame, C. J., Caldwell, J. A., Hunt, D. F., Lin, R., Smith, M. M., & Allis, C. D. (2000). Mitotic phosphorylation of histone H3 is governed by Ipl1/aurora kinase and Glc7/PP1 phosphatase in budding yeast and nematodes. *Cell*, *102*(3), 279-291. https://doi.org/10.1016/s0092-8674(00)00034-9

Hussen, B. M., Shoorei, H., Mohaqiq, M., Dinger, M. E., Hidayat, H. J., Taheri, M., & Ghafouri-Fard, S. (2021). The Impact of Non-coding RNAs in the Epithelial to Mesenchymal Transition. *Front Mol Biosci*, *8*, 665199. https://doi.org/10.3389/fmolb.2021.665199

Ignarski, M., Islam, R., & Muller, R. U. (2019). Long Non-Coding RNAs in Kidney Disease. *International journal of molecular sciences*, *20*(13). https://doi.org/10.3390/ijms20133276

Iouzalen, N., Moreau, J., & Mechali, M. (1996). H2A.ZI, a new variant histone expressed during Xenopus early development exhibits several distinct features from the core histone H2A. *Nucleic acids research*, *24*(20), 3947-3952. https://doi.org/10.1093/nar/24.20.3947

Ivanochko, D., Halabelian, L., Henderson, E., Savitsky, P., Jain, H., Marcon, E., Duan, S., Hutchinson, A., Seitova, A., Barsyte-Lovejoy, D., Filippakopoulos, P., Greenblatt, J., Lima-Fernandes, E., & Arrowsmith, C. H. (2019). Direct interaction between the PRDM3 and PRDM16 tumor suppressors and the NuRD chromatin remodeling complex. *Nucleic acids research*, *47*(3), 1225-1238. https://doi.org/10.1093/nar/gky1192

Jansen, A., & Verstrepen, K. J. (2011). Nucleosome positioning in Saccharomyces cerevisiae. *Microbiol Mol Biol Rev*, *75*(2), 301-320. https://doi.org/10.1128/MMBR.00046-10

Jenuwein, T., & Allis, C. D. (2001). Translating the histone code. *Science*, *293*(5532), 1074-1080. https://doi.org/10.1126/science.1063127

Jiang, H., Yang, B., Wang, F., Li, K., Zhu, Y., Liu, B., Ren, H., Tian, S., Xu, Y., Pang, A., & Yang, X. (2021). Association of Single Nucleotide Polymorphism at rs2275294 in the ZNF512B Gene with Prognosis in Amyotrophic Lateral Sclerosis. *Neuromolecular Med*, *23*(2), 242-246. https://doi.org/10.1007/s12017-020-08634-y

Jing, Y., Li, X., Liu, Z., & Li, X. D. (2022). Roles of Negatively Charged Histone Lysine Acylations in Regulating Nucleosome Structure and Dynamics. *Front Mol Biosci*, *9*, 899013. https://doi.org/10.3389/fmolb.2022.899013

Johansson, P. A., Brattas, P. L., Douse, C. H., Hsieh, P., Adami, A., Pontis, J., Grassi, D., Garza, R., Sozzi, E., Cataldo, R., Jonsson, M. E., Atacho, D. A. M., Pircs, K., Eren, F., Sharma, Y., Johansson, J., Fiorenzano, A., Parmar, M., Fex, M., . . . Jakobsson, J. (2022). A cis-acting structural variation at the ZNF558 locus controls a gene regulatory network in human brain development. *Cell Stem Cell*, *29*(1), 52-69 e58. https://doi.org/10.1016/j.stem.2021.09.008

Johnson, L., Cao, X., & Jacobsen, S. (2002). Interplay between two epigenetic marks. DNA methylation and histone H3 lysine 9 methylation. *Curr Biol*, *12*(16), 1360-1367. https://doi.org/10.1016/s0960-9822(02)00976-4

Jumper, J., Evans, R., Pritzel, A., Green, T., Figurnov, M., Ronneberger, O., Tunyasuvunakool, K., Bates, R., Zidek, A., Potapenko, A., Bridgland, A., Meyer, C., Kohl, S. A. A., Ballard, A. J., Cowie, A., Romera-Paredes, B., Nikolov, S., Jain, R., Adler, J., . . . Hassabis, D. (2021). Highly accurate protein structure prediction with AlphaFold. *Nature*, *596*(7873), 583-589. https://doi.org/10.1038/s41586-021-03819-2

Kabsch, W. (2010). Xds. *Acta Crystallogr D Biol Crystallogr*, *66*(Pt 2), 125-132. https://doi.org/10.1107/S0907444909047337

Karlsson, M., Zhang, C., Mear, L., Zhong, W., Digre, A., Katona, B., Sjostedt, E., Butler, L., Odeberg, J., Dusart, P., Edfors, F., Oksvold, P., von Feilitzen, K., Zwahlen, M., Arif, M., Altay, O., Li, X., Ozcan, M., Mardinoglu, A., . . . Lindskog, C. (2021). A single-cell type transcriptomics map of human tissues. *Sci Adv*, *7*(31). https://doi.org/10.1126/sciadv.abh2169

Keogh, M. C., Mennella, T. A., Sawa, C., Berthelet, S., Krogan, N. J., Wolek, A., Podolny, V., Carpenter, L. R., Greenblatt, J. F., Baetz, K., & Buratowski, S. (2006). The Saccharomyces cerevisiae histone H2A variant Htz1 is acetylated by NuA4. *Genes Dev*, *20*(6), 660-665. https://doi.org/10.1101/gad.1388106

Kim, D., Paggi, J. M., Park, C., Bennett, C., & Salzberg, S. L. (2019). Graph-based genome alignment and genotyping with HISAT2 and HISAT-genotype. *Nat Biotechnol*, *37*(8), 907-915. https://doi.org/10.1038/s41587-019-0201-4

Kim, H., Kang, K., & Kim, J. (2009). AEBP2 as a potential targeting protein for Polycomb Repression Complex PRC2. *Nucleic acids research*, *37*(9), 2940-2950. https://doi.org/10.1093/nar/gkp149

Kim, K., Punj, V., Choi, J., Heo, K., Kim, J. M., Laird, P. W., & An, W. (2013). Gene dysregulation by histone variant H2A.Z in bladder cancer. *Epigenetics Chromatin*, *6*(1), 34. https://doi.org/10.1186/1756-8935-6-34

Kimura, A., & Horikoshi, M. (1998). Tip60 acetylates six lysines of a specific class in core histones in vitro. *Genes Cells*, *3*(12), 789-800. https://doi.org/10.1046/j.1365-2443.1998.00229.x

Kloet, S. L., Baymaz, H. I., Makowski, M., Groenewold, V., Jansen, P. W., Berendsen, M., Niazi, H., Kops, G. J., & Vermeulen, M. (2015). Towards elucidating the stability, dynamics and architecture of the nucleosome remodeling and deacetylase complex by using quantitative interaction proteomics. *FEBS J*, *282*(9), 1774-1785. https://doi.org/10.1111/febs.12972

Klug, A. (2010). The discovery of zinc fingers and their development for practical applications in gene regulation and genome manipulation. *Q Rev Biophys*, *43*(1), 1-21. https://doi.org/10.1017/S0033583510000089

Kobor, M. S., Venkatasubrahmanyam, S., Meneghini, M. D., Gin, J. W., Jennings, J. L., Link, A. J., Madhani, H. D., & Rine, J. (2004). A protein complex containing the conserved Swi2/Snf2-related ATPase Swr1p deposits histone variant H2A.Z into euchromatin. *PLoS Biol*, *2*(5), E131. https://doi.org/10.1371/journal.pbio.0020131

Komar, D., & Juszczynski, P. (2020). Rebelled epigenome: histone H3S10 phosphorylation and H3S10 kinases in cancer biology and therapy. *Clin Epigenetics*, *12*(1), 147. https://doi.org/10.1186/s13148-020-00941-2

Kornberg, R. D. (1977). Structure of chromatin. *Annu Rev Biochem*, *46*, 931-954. https://doi.org/10.1146/annurev.bi.46.070177.004435

Koschmann, C., Nunez, F. J., Mendez, F., Brosnan-Cashman, J. A., Meeker, A. K., Lowenstein, P. R., & Castro, M. G. (2017). Mutated Chromatin Regulatory Factors as Tumor Drivers in Cancer. *Cancer Res*, *77*(2), 227-233. https://doi.org/10.1158/0008-5472.CAN-16-2301

Kosugi, S., Hasebe, M., Entani, T., Takayama, S., Tomita, M., & Yanagawa, H. (2008). Design of peptide inhibitors for the importin alpha/beta nuclear import pathway by activity-based profiling. *Chem Biol*, *15*(9), 940-949. https://doi.org/10.1016/j.chembiol.2008.07.019

Kosugi, S., Hasebe, M., Matsumura, N., Takashima, H., Miyamoto-Sato, E., Tomita, M., & Yanagawa, H. (2009). Six classes of nuclear localization signals specific to different binding grooves of importin alpha. *J Biol Chem*, *284*(1), 478-485. https://doi.org/10.1074/jbc.M807017200

Kosugi, S., Hasebe, M., Tomita, M., & Yanagawa, H. (2009). Systematic identification of cell cycle-dependent yeast nucleocytoplasmic shuttling proteins by prediction of composite motifs. *Proc Natl Acad Sci U S A*, *106*(25), 10171-10176. https://doi.org/10.1073/pnas.0900604106

Kouzarides, T. (2007). Chromatin modifications and their function. *Cell*, *128*(4), 693-705. https://doi.org/10.1016/j.cell.2007.02.005

Kreienbaum, C., Paasche, L. W., & Hake, S. B. (2022). H2A.Z's 'social' network: functional partners of an enigmatic histone variant. *Trends Biochem Sci*, *47*(11), 909-920. https://doi.org/10.1016/j.tibs.2022.04.014

Krissinel, E., & Henrick, K. (2007). Inference of macromolecular assemblies from crystalline state. *J Mol Biol*, *372*(3), 774-797. https://doi.org/10.1016/j.jmb.2007.05.022

Krogan, N. J., Kim, M., Tong, A., Golshani, A., Cagney, G., Canadien, V., Richards, D. P., Beattie, B. K., Emili, A., Boone, C., Shilatifard, A., Buratowski, S., & Greenblatt, J. (2003). Methylation of histone H3 by Set2 in Saccharomyces cerevisiae is linked to transcriptional elongation by RNA polymerase II. *Mol Cell Biol*, *23*(12), 4207-4218. https://doi.org/10.1128/MCB.23.12.4207-4218.2003

Krueger, F. (2015). Trim Galore: A Wrapper Tool around Cutadapt and FASTQC to Consistently Apply Quality and Adapter Trimming to FASTQ Files. *Babraham Institute: Cambridge, UK*, *516*, 517.

Krylov, D., & Vinson, C. R. (2001). Leucine Zipper. In *eLS*. https://doi.org/https://doi.org/10.1038/npg.els.0003001

Kunert, N., & Brehm, A. (2009). Novel Mi-2 related ATP-dependent chromatin remodelers. *Epigenetics*, *4*(4), 209-211. https://doi.org/10.4161/epi.8933

Kuo, M. H., Brownell, J. E., Sobel, R. E., Ranalli, T. A., Cook, R. G., Edmondson, D. G., Roth, S. Y., & Allis, C. D. (1996). Transcription-linked acetylation by Gcn5p of histones H3 and H4 at specific lysines. *Nature*, *383*(6597), 269-272. https://doi.org/10.1038/383269a0

Kusch, T., Florens, L., Macdonald, W. H., Swanson, S. K., Glaser, R. L., Yates, J. R., 3rd, Abmayr, S. M., Washburn, M. P., & Workman, J. L. (2004). Acetylation by Tip60 is required for selective histone variant exchange at DNA lesions. *Science*, *306*(5704), 2084-2087. https://doi.org/10.1126/science.1103455

Lai, A. Y., & Wade, P. A. (2011). Cancer biology and NuRD: a multifaceted chromatin remodelling complex. *Nat Rev Cancer*, *11*(8), 588-596. https://doi.org/10.1038/nrc3091

Laity, J. H., Lee, B. M., & Wright, P. E. (2001). Zinc finger proteins: new insights into structural and functional diversity. *Curr Opin Struct Biol*, *11*(1), 39-46. https://doi.org/10.1016/s0959-440x(00)00167-6

Lamaa, A., Humbert, J., Aguirrebengoa, M., Cheng, X., Nicolas, E., Cote, J., & Trouche, D. (2020). Integrated analysis of H2A.Z isoforms function reveals a complex interplay in gene regulation. *eLife*, *9*, e53375. https://doi.org/10.7554/eLife.53375

Lan, X., Ren, R., Feng, R., Ly, L. C., Lan, Y., Zhang, Z., Aboreden, N., Qin, K., Horton, J. R., Grevet, J. D., Mayuranathan, T., Abdulmalik, O., Keller, C. A., Giardine, B., Hardison, R. C., Crossley, M., Weiss, M. J., Cheng, X., Shi, J., & Blobel, G. A. (2021). ZNF410 Uniquely Activates the NuRD Component CHD4 to Silence Fetal Hemoglobin Expression. *Mol Cell*, *81*(2), 239-254 e238. https://doi.org/10.1016/j.molcel.2020.11.006

Larriba, E., & del Mazo, J. (2016). Role of Non-Coding RNAs in the Transgenerational Epigenetic Transmission of the Effects of Reprotoxicants. *International journal of molecular sciences*, *17*(4), 452. https://doi.org/10.3390/ijms17040452

Lashgari, A., Millau, J. F., Jacques, P. E., & Gaudreau, L. (2017). Global inhibition of transcription causes an increase in histone H2A.Z incorporation within gene bodies. *Nucleic acids research*, *45*(22), 12715-12722. https://doi.org/10.1093/nar/gkx879

Laskowski, R. A., Jablonska, J., Pravda, L., Varekova, R. S., & Thornton, J. M. (2018). PDBsum: Structural summaries of PDB entries. *Protein Sci*, *27*(1), 129-134. https://doi.org/10.1002/pro.3289

Lauberth, S. M., & Rauchman, M. (2006). A conserved 12-amino acid motif in Sall1 recruits the nucleosome remodeling and deacetylase corepressor complex. *J Biol Chem*, *281*(33), 23922-23931. https://doi.org/10.1074/jbc.M513461200

Lawrence, M., Huber, W., Pages, H., Aboyoun, P., Carlson, M., Gentleman, R., Morgan, M. T., & Carey, V. J. (2013). Software for computing and annotating genomic ranges. *PLoS Comput Biol*, *9*(8), e1003118. https://doi.org/10.1371/journal.pcbi.1003118

Lee, B. Y., Han, J. A., Im, J. S., Morrone, A., Johung, K., Goodwin, E. C., Kleijer, W. J., DiMaio, D., & Hwang, E. S. (2006). Senescence-associated beta-galactosidase is

lysosomal beta-galactosidase. *Aging Cell*, *5*(2), 187-195. https://doi.org/10.1111/j.1474-9726.2006.00199.x

Lee, K. H., Bosco, A., O'Sullivan, M., Song, Y., Metcalfe, J., Yu, K., Mullins, B. J., Loh, R., & Zhang, G. (2022). Identifying gene network patterns and associated cellular immune responses in children with or without nut allergy. *World Allergy Organ J*, *15*(2), 100631. https://doi.org/10.1016/j.waojou.2022.100631

Lee, S. Y., Choe, Y. H., Han, J. H., Hwang, G., Choi, M. Y., Thakur, G., Jo, C. H., Oh, S. J., Lee, W. J., Rho, G. J., Lee, S. L., & Hwang, T. S. (2022). HPRT1 Most Suitable Reference Gene for Accurate Normalization of mRNA Expression in Canine Dermal Tissues with Radiation Therapy. *Genes (Basel)*, *13*(11). https://doi.org/10.3390/genes13111928

Lehmkuhl, E. M., & Zarnescu, D. C. (2018). Lost in Translation: Evidence for Protein Synthesis Deficits in ALS/FTD and Related Neurodegenerative Diseases. *Adv Neurobiol*, *20*, 283-301. https://doi.org/10.1007/978-3-319-89689-2_11

Lejon, S., Thong, S. Y., Murthy, A., AlQarni, S., Murzina, N. V., Blobel, G. A., Laue, E. D., & Mackay, J. P. (2011). Insights into association of the NuRD complex with FOG-1 from the crystal structure of an RbAp48.FOG-1 complex. *J Biol Chem*, *286*(2), 1196-1203. https://doi.org/10.1074/jbc.M110.195842

Lewis, T. S., Sokolova, V., Jung, H., Ng, H., & Tan, D. (2021). Structural basis of chromatin regulation by histone variant H2A.Z. *Nucleic acids research*, *49*(19), 11379-11391. https://doi.org/10.1093/nar/gkab907

Li, D. Q., & Kumar, R. (2010). Mi-2/NuRD complex making inroads into DNA-damage response pathway. *Cell Cycle*, *9*(11), 2071-2079. https://doi.org/10.4161/cc.9.11.11735

Li, X., Han, M., Zhang, H., Liu, F., Pan, Y., Zhu, J., Liao, Z., Chen, X., & Zhang, B. (2022). Structures and biological functions of zinc finger proteins and their roles in hepatocellular carcinoma. *Biomark Res*, *10*(1), 2. https://doi.org/10.1186/s40364-021-00345-1

Li, X., & Li, X. D. (2021). Integrative Chemical Biology Approaches to Deciphering the Histone Code: A Problem-Driven Journey. *Acc Chem Res*, *54*(19), 3734-3747. https://doi.org/10.1021/acs.accounts.1c00463

Li, X., Romero, P., Rani, M., Dunker, A. K., & Obradovic, Z. (1999). Predicting Protein Disorder for N-, C-, and Internal Regions. *Genome Inform Ser Workshop Genome Inform*, *10*, 30-40. https://www.ncbi.nlm.nih.gov/pubmed/11072340

Li, Y.-F., Pan, X., & Shen, H.-B. (2024). Discovering nuclear localization signal universe through a novel deep learning model with interpretable attention units. *bioRxiv*, 2024.2008.2010.606103. https://doi.org/10.1101/2024.08.10.606103

Link, S., Spitzer, R. M. M., Sana, M., Torrado, M., Volker-Albert, M. C., Keilhauer, E. C., Burgold, T., Punzeler, S., Low, J. K. K., Lindstrom, I., Nist, A., Regnard, C., Stiewe, T., Hendrich, B., Imhof, A., Mann, M., Mackay, J. P., Bartkuhn, M., & Hake, S. B. (2018). PWWP2A binds distinct chromatin moieties and interacts with an MTA1-specific core NuRD complex. *Nat Commun*, *9*(1), 4300. https://doi.org/10.1038/s41467-018-06665-5

Liskova, V., Kajsik, M., Chovancova, B., Roller, L., & Krizanova, O. (2022). Camptothecin, triptolide, and apoptosis inducer kit have differential effects on mitochondria in colorectal carcinoma cells. *FEBS Open Bio*, *12*(5), 913-924. https://doi.org/10.1002/2211-5463.13401

Lister, R., Pelizzola, M., Dowen, R. H., Hawkins, R. D., Hon, G., Tonti-Filippini, J., Nery, J. R., Lee, L., Ye, Z., Ngo, Q. M., Edsall, L., Antosiewicz-Bourget, J., Stewart, R., Ruotti, V., Millar, A. H., Thomson, J. A., Ren, B., & Ecker, J. R. (2009). Human

DNA methylomes at base resolution show widespread epigenomic differences. *Nature*, *462*(7271), 315-322. https://doi.org/10.1038/nature08514

Liu, C., Han, X., Zhang, S., Huang, M., Guo, B., Zhao, Z., Yang, S., Jin, J., Pu, W., & Yu, H. (2024). The role of NCAPH in cancer treatment. *Cell Signal*, *121*, 111262. https://doi.org/10.1016/j.cellsig.2024.111262

Liu, H., & Naismith, J. H. (2008). An efficient one-step site-directed deletion, insertion, single and multiple-site plasmid mutagenesis protocol. *BMC Biotechnol*, *8*, 91. https://doi.org/10.1186/1472-6750-8-91

Liu, X., Li, B., & GorovskyMa. (1996). Essential and nonessential histone H2A variants in Tetrahymena thermophila. *Mol Cell Biol*, *16*(8), 4305-4311. https://doi.org/10.1128/MCB.16.8.4305

Liu, Y., Khan, A. R., & Gan, Y. (2022). C2H2 Zinc Finger Proteins Response to Abiotic Stress in Plants. *International journal of molecular sciences*, *23*(5). https://doi.org/10.3390/ijms23052730

Long, M., Sun, X., Shi, W., Yanru, A., Leung, S. T. C., Ding, D., Cheema, M. S., MacPherson, N., Nelson, C. J., Ausio, J., Yan, Y., & Ishibashi, T. (2019). A novel histone H4 variant H4G regulates rDNA transcription in breast cancer. *Nucleic acids research*, *47*(16), 8399-8409. https://doi.org/10.1093/nar/gkz547

Love, M. I., Huber, W., & Anders, S. (2014). Moderated estimation of fold change and dispersion for RNA-seq data with DESeq2. *Genome Biol*, *15*(12), 550. https://doi.org/10.1186/s13059-014-0550-8

Lu, B., Klingbeil, O., Tarumoto, Y., Somerville, T. D. D., Huang, Y. H., Wei, Y., Wai, D. C., Low, J. K. K., Milazzo, J. P., Wu, X. S., Cao, Z., Yan, X., Demerdash, O. E., Huang, G., Mackay, J. P., Kinney, J. B., Shi, J., & Vakoc, C. R. (2018). A Transcription Factor Addiction in Leukemia Imposed by the MLL Promoter Sequence. *Cancer Cell*, *34*(6), 970-981 e978. https://doi.org/10.1016/j.ccell.2018.10.015

Luger, K., Mader, A. W., Richmond, R. K., Sargent, D. F., & Richmond, T. J. (1997). Crystal structure of the nucleosome core particle at 2.8 A resolution. *Nature*, *389*(6648), 251-260. https://doi.org/10.1038/38444

Luk, E., Ranjan, A., Fitzgerald, P. C., Mizuguchi, G., Huang, Y., Wei, D., & Wu, C. (2010). Stepwise histone replacement by SWR1 requires dual activation with histone H2A.Z and canonical nucleosome. *Cell*, *143*(5), 725-736. https://doi.org/10.1016/j.cell.2010.10.019

Lukauskas, S., Tvardovskiy, A., Nguyen, N. V., Stadler, M., Faull, P., Ravnsborg, T., Ozdemir Aygenli, B., Dornauer, S., Flynn, H., Lindeboom, R. G. H., Barth, T. K., Brockers, K., Hauck, S. M., Vermeulen, M., Snijders, A. P., Muller, C. L., DiMaggio, P. A., Jensen, O. N., Schneider, R., & Bartke, T. (2024). Decoding chromatin states by proteomic profiling of nucleosome readers. *Nature*, *627*(8004), 671-679. https://doi.org/10.1038/s41586-024-07141-5

Lumpkin, R. J., Gu, H., Zhu, Y., Leonard, M., Ahmad, A. S., Clauser, K. R., Meyer, J. G., Bennett, E. J., & Komives, E. A. (2017). Site-specific identification and quantitation of endogenous SUMO modifications under native conditions. *Nat Commun*, *8*(1), 1171. https://doi.org/10.1038/s41467-017-01271-3

Ma, R., Zhang, Y., Zhang, J., Zhang, P., Liu, Z., Fan, Y., Wang, H. T., Zhang, Z., & Zhu, B. (2024). Targeting pericentric non-consecutive motifs for heterochromatin initiation. *Nature*, *631*(8021), 678-685. https://doi.org/10.1038/s41586-024-07640-5

Magana-Acosta, M., & Valadez-Graham, V. (2020). Chromatin Remodelers in the 3D Nuclear Compartment. *Front Genet*, *11*, 600615. https://doi.org/10.3389/fgene.2020.600615

Malgieri, G., Palmieri, M., Russo, L., Fattorusso, R., Pedone, P. V., & Isernia, C. (2015). The prokaryotic zinc-finger: structure, function and comparison with the eukaryotic counterpart. *FEBS J*, *282*(23), 4480-4496. https://doi.org/10.1111/febs.13503

Mao, Z., Pan, L., Wang, W., Sun, J., Shan, S., Dong, Q., Liang, X., Dai, L., Ding, X., Chen, S., Zhang, Z., Zhu, B., & Zhou, Z. (2014). Anp32e, a higher eukaryotic histone chaperone directs preferential recognition for H2A.Z. *Cell Res*, *24*(4), 389-399. https://doi.org/10.1038/cr.2014.30

Martin, R. M., & Cardoso, M. C. (2010). Chromatin condensation modulates access and binding of nuclear proteins. *FASEB J*, *24*(4), 1066-1072. https://doi.org/10.1096/fj.08-128959

Marzluff, W. F., Wagner, E. J., & Duronio, R. J. (2008). Metabolism and regulation of canonical histone mRNAs: life without a poly(A) tail. *Nat Rev Genet*, *9*(11), 843-854. https://doi.org/10.1038/nrg2438

Matthews, J. M., Bhati, M., Lehtomaki, E., Mansfield, R. E., Cubeddu, L., & Mackay, J. P. (2009). It takes two to tango: the structure and function of LIM, RING, PHD and MYND domains. *Curr Pharm Des*, *15*(31), 3681-3696. https://doi.org/10.2174/138161209789271861

McAlear, T. S., & Bechstedt, S. (2022). The mitotic spindle protein CKAP2 potently increases formation and stability of microtubules. *eLife*, *11*. https://doi.org/10.7554/eLife.72202

McGhee, J. D., & Felsenfeld, G. (1980). Nucleosome structure. *Annu Rev Biochem*, *49*, 1115-1156. https://doi.org/10.1146/annurev.bi.49.070180.005343

Meng, E. C., Goddard, T. D., Pettersen, E. F., Couch, G. S., Pearson, Z. J., Morris, J. H., & Ferrin, T. E. (2023). UCSF ChimeraX: Tools for structure building and analysis. *Protein Sci*, *32*(11), e4792. https://doi.org/10.1002/pro.4792

Merry, C. R., Forrest, M. E., Sabers, J. N., Beard, L., Gao, X. H., Hatzoglou, M., Jackson, M. W., Wang, Z., Markowitz, S. D., & Khalil, A. M. (2015). DNMT1-associated long non-coding RNAs regulate global gene expression and DNA methylation in colon cancer. *Hum Mol Genet*, *24*(21), 6240-6253. https://doi.org/10.1093/hmg/ddv343

Mertins, P., Qiao, J. W., Patel, J., Udeshi, N. D., Clauser, K. R., Mani, D. R., Burgess, M. W., Gillette, M. A., Jaffe, J. D., & Carr, S. A. (2013). Integrated proteomic analysis of post-translational modifications by serial enrichment. *Nat Methods*, *10*(7), 634-637. https://doi.org/10.1038/nmeth.2518

Michaille, J. J., Tili, E., Calin, G. A., Garin, J., Louwagie, M., & Croce, C. M. (2005). Cloning and characterization of cDNAs expressed during chick development and encoding different isoforms of a putative zinc finger transcriptional regulator. *Biochimie*, *87*(11), 939-949. https://doi.org/10.1016/j.biochi.2005.06.008

Miller, A., Ralser, M., Kloet, S. L., Loos, R., Nishinakamura, R., Bertone, P., Vermeulen, M., & Hendrich, B. (2016). Sall4 controls differentiation of pluripotent cells independently of the Nucleosome Remodelling and Deacetylation (NuRD) complex. *Development*, *143*(17), 3074-3084. https://doi.org/10.1242/dev.139113

Mitraki, A., Miller, S., & van Raaij, M. J. (2002). Review: conformation and folding of novel beta-structural elements in viral fiber proteins: the triple beta-spiral and triple beta-helix. *J Struct Biol*, *137*(1-2), 236-247. https://doi.org/10.1006/jsbi.2002.4447

Mizuguchi, G., Shen, X., Landry, J., Wu, W. H., Sen, S., & Wu, C. (2004). ATP-driven exchange of histone H2AZ variant catalyzed by SWR1 chromatin remodeling complex. *Science*, *303*(5656), 343-348. https://doi.org/10.1126/science.1090701

Mohrmann, L., & Verrijzer, C. P. (2005). Composition and functional specificity of SWI2/SNF2 class chromatin remodeling complexes. *Biochim Biophys Acta*, *1681*(2-3), 59-73. https://doi.org/10.1016/j.bbaexp.2004.10.005

Moore, L. D., Le, T., & Fan, G. (2013). DNA methylation and its basic function. *Neuropsychopharmacology*, *38*(1), 23-38. https://doi.org/10.1038/npp.2012.112

Moparthi, L., & Koch, S. (2020). A uniform expression library for the exploration of FOX transcription factor biology. *Differentiation*, *115*, 30-36. https://doi.org/10.1016/j.diff.2020.08.002

Morgan, M. A. J., Rickels, R. A., Collings, C. K., He, X., Cao, K., Herz, H. M., Cozzolino, K. A., Abshiru, N. A., Marshall, S. A., Rendleman, E. J., Sze, C. C., Piunti, A., Kelleher, N. L., Savas, J. N., & Shilatifard, A. (2017). A cryptic Tudor domain links BRWD2/PHIP to COMPASS-mediated histone H3K4 methylation. *Genes Dev*, *31*(19), 2003-2014. https://doi.org/10.1101/gad.305201.117

Morrison, A. J., & Shen, X. (2009). Chromatin remodelling beyond transcription: the INO80 and SWR1 complexes. *Nat Rev Mol Cell Biol*, *10*(6), 373-384. https://doi.org/10.1038/nrm2693

Murayama, T., & Ogawa, Y. (1996). Properties of Ryr3 ryanodine receptor isoform in mammalian brain. *J Biol Chem*, *271*(9), 5079-5084. https://doi.org/10.1074/jbc.271.9.5079

Murshudov, G. N., Skubak, P., Lebedev, A. A., Pannu, N. S., Steiner, R. A., Nicholls, R. A., Winn, M. D., Long, F., & Vagin, A. A. (2011). REFMAC5 for the refinement of macromolecular crystal structures. *Acta Crystallogr D Biol Crystallogr*, *67*(Pt 4), 355-367. https://doi.org/10.1107/S0907444911001314

Mylonas, C., Lee, C., Auld, A. L., Cisse, II, & Boyer, L. A. (2021). A dual role for H2A.Z.1 in modulating the dynamics of RNA polymerase II initiation and elongation. *Nat Struct Mol Biol*, *28*(5), 435-442. https://doi.org/10.1038/s41594-021-00589-3

Nagase, T., Ishikawa, K., Kikuno, R., Hirosawa, M., Nomura, N., & Ohara, O. (1999). Prediction of the coding sequences of unidentified human genes. XV. The complete sequences of 100 new cDNA clones from brain which code for large proteins in vitro. *DNA Res*, *6*(5), 337-345. https://doi.org/10.1093/dnares/6.5.337

Nakamura, T., Mori, T., Tada, S., Krajewski, W., Rozovskaia, T., Wassell, R., Dubois, G., Mazo, A., Croce, C. M., & Canaani, E. (2002). ALL-1 is a histone methyltransferase that assembles a supercomplex of proteins involved in transcriptional regulation. *Mol Cell*, *10*(5), 1119-1128. https://doi.org/10.1016/s1097-2765(02)00740-2

Narita, M., Nunez, S., Heard, E., Narita, M., Lin, A. W., Hearn, S. A., Spector, D. L., Hannon, G. J., & Lowe, S. W. (2003). Rb-mediated heterochromatin formation and silencing of E2F target genes during cellular senescence. *Cell*, *113*(6), 703-716. https://doi.org/10.1016/s0092-8674(03)00401-x

Narkaj, K., Stefanelli, G., Wahdan, M., Azam, A. B., Ramzan, F., Steininger, C. F. D., Jr., Walters, B. J., & Zovkic, I. B. (2018). Blocking H2A.Z Incorporation via Tip60 Inhibition Promotes Systems Consolidation of Fear Memory in Mice. *eneuro*, *5*(5), ENEURO.0378-0318.2018. https://doi.org/10.1523/ENEURO.0378-18.2018

Nguyen Ba, A. N., Pogoutse, A., Provart, N., & Moses, A. M. (2009). NLStradamus: a simple Hidden Markov Model for nuclear localization signal prediction. *BMC Bioinformatics*, *10*, 202. https://doi.org/10.1186/1471-2105-10-202

Nikolovska-Coleska, Z., Wang, R., Fang, X., Pan, H., Tomita, Y., Li, P., Roller, P. P., Krajewski, K., Saito, N. G., Stuckey, J. A., & Wang, S. (2004). Development and optimization of a binding assay for the XIAP BIR3 domain using fluorescence polarization. *Anal Biochem*, *332*(2), 261-273. https://doi.org/10.1016/j.ab.2004.05.055

Ning, P., Yang, X., Yang, B., Zhao, Q., Huang, H., An, R., Chen, Y., Hu, F., Xu, Z., & Xu, Y. (2018). Meta-analysis of the association between ZNF512B polymorphism rs2275294 and risk of amyotrophic lateral sclerosis. *Neurol Sci*, *39*(7), 1261-1266. https://doi.org/10.1007/s10072-018-3411-5

Nowak, A. J., Alfieri, C., Stirnimann, C. U., Rybin, V., Baudin, F., Ly-Hartig, N., Lindner, D., & Muller, C. W. (2011). Chromatin-modifying complex component Nurf55/p55 associates with histones H3 and H4 and polycomb repressive complex 2 subunit Su(z)12 through partially overlapping binding sites. *J Biol Chem*, *286*(26), 23388-23396. https://doi.org/10.1074/jbc.M110.207407

Oates, M. E., Romero, P., Ishida, T., Ghalwash, M., Mizianty, M. J., Xue, B., Dosztanyi, Z., Uversky, V. N., Obradovic, Z., Kurgan, L., Dunker, A. K., & Gough, J. (2013). D(2)P(2): database of disordered protein predictions. *Nucleic acids research*, *41*(Database issue), D508-516. https://doi.org/10.1093/nar/gks1226

Oberdoerffer, P., & Sinclair, D. A. (2007). The role of nuclear architecture in genomic instability and ageing. *Nat Rev Mol Cell Biol*, *8*(9), 692-702. https://doi.org/10.1038/nrm2238

Obri, A., Ouararhni, K., Papin, C., Diebold, M. L., Padmanabhan, K., Marek, M., Stoll, I., Roy, L., Reilly, P. T., Mak, T. W., Dimitrov, S., Romier, C., & Hamiche, A. (2014). ANP32E is a histone chaperone that removes H2A.Z from chromatin. *Nature*, *505*(7485), 648-653. https://doi.org/10.1038/nature12922

Olins, D. E., & Olins, A. L. (2003). Chromatin history: our view from the bridge. *Nat Rev Mol Cell Biol*, *4*(10), 809-814. https://doi.org/10.1038/nrm1225

Olson, N. M., Kroc, S., Johnson, J. A., Zahid, H., Ycas, P. D., Chan, A., Kimbrough, J. R., Kalra, P., Schonbrunn, E., & Pomerantz, W. C. K. (2020). NMR Analyses of Acetylated H2A.Z Isoforms Identify Differential Binding Interactions with the Bromodomain of the NURF Nucleosome Remodeling Complex. *Biochemistry*, *59*(20), 1871-1880. https://doi.org/10.1021/acs.biochem.0c00159

Osakabe, A., Lorkovic, Z. J., Kobayashi, W., Tachiwana, H., Yelagandula, R., Kurumizaka, H., & Berger, F. (2018). Histone H2A variants confer specific properties to nucleosomes and impact on chromatin accessibility. *Nucleic acids research*, *46*(15), 7675-7685. https://doi.org/10.1093/nar/gky540

Padua, M. B., Helm, B. M., Wells, J. R., Smith, A. M., Bellchambers, H. M., Sridhar, A., & Ware, S. M. (2023). Congenital heart defects caused by FOXJ1. *Hum Mol Genet*, *32*(14), 2335-2346. https://doi.org/10.1093/hmg/ddad065

Papamichos-Chronakis, M., Watanabe, S., Rando, O. J., & Peterson, C. L. (2011). Global regulation of H2A.Z localization by the INO80 chromatin-remodeling enzyme is essential for genome integrity. *Cell*, *144*(2), 200-213. https://doi.org/10.1016/j.cell.2010.12.021

Papin, C., Le Gras, S., Ibrahim, A., Salem, H., Karimi, M. M., Stoll, I., Ugrinova, I., Schroder, M., Fontaine-Pelletier, E., Omran, Z., Bronner, C., Dimitrov, S., & Hamiche, A. (2021). CpG Islands Shape the Epigenome Landscape. *J Mol Biol*, *433*(6), 166659. https://doi.org/10.1016/j.jmb.2020.09.018

Pasha, T., Zatorska, A., Sharipov, D., Rogelj, B., Hortobagyi, T., & Hirth, F. (2021). Karyopherin abnormalities in neurodegenerative proteinopathies. *Brain*, *144*(10), 2915-2932. https://doi.org/10.1093/brain/awab201

Patel, K., Solomon, P. D., Walshe, J. L., Low, J. K. K., & Mackay, J. P. (2021). The bromodomains of BET family proteins can recognize diacetylated histone H2A.Z. *Protein Sci*, *30*(2), 464-476. https://doi.org/10.1002/pro.4006

Peng, Y., Clark, K. J., Campbell, J. M., Panetta, M. R., Guo, Y., & Ekker, S. C. (2014). Making designer mutants in model organisms. *Development*, *141*(21), 4042-4054. https://doi.org/10.1242/dev.102186

Perell, G. T., Mishra, N. K., Sudhamalla, B., Ycas, P. D., Islam, K., & Pomerantz, W. C. K. (2017). Specific Acetylation Patterns of H2A.Z Form Transient Interactions with the BPTF Bromodomain. *Biochemistry*, *56*(35), 4607-4615. https://doi.org/10.1021/acs.biochem.7b00648

Persikov, A. V., Osada, R., & Singh, M. (2009). Predicting DNA recognition by Cys2His2 zinc finger proteins. *Bioinformatics*, *25*(1), 22-29. https://doi.org/10.1093/bioinformatics/btn580

Persikov, A. V., Rowland, E. F., Oakes, B. L., Singh, M., & Noyes, M. B. (2014). Deep sequencing of large library selections allows computational discovery of diverse sets of zinc fingers that bind common targets. *Nucleic acids research*, *42*(3), 1497-1508. https://doi.org/10.1093/nar/gkt1034

Persikov, A. V., & Singh, M. (2014). De novo prediction of DNA-binding specificities for Cys2His2 zinc finger proteins. *Nucleic acids research*, *42*(1), 97-108. https://doi.org/10.1093/nar/gkt890

Persikov, A. V., Wetzel, J. L., Rowland, E. F., Oakes, B. L., Xu, D. J., Singh, M., & Noyes, M. B. (2015). A systematic survey of the Cys2His2 zinc finger DNA-binding landscape. *Nucleic acids research*, *43*(3), 1965-1984. https://doi.org/10.1093/nar/gku1395

Pettersen, E. F., Goddard, T. D., Huang, C. C., Meng, E. C., Couch, G. S., Croll, T. I., Morris, J. H., & Ferrin, T. E. (2021). UCSF ChimeraX: Structure visualization for researchers, educators, and developers. *Protein Sci*, *30*(1), 70-82. https://doi.org/10.1002/pro.3943

Phillips, J. E., & Corces, V. G. (2009). CTCF: master weaver of the genome. *Cell*, *137*(7), 1194-1211. https://doi.org/10.1016/j.cell.2009.06.001

Procida, T., Friedrich, T., Jack, A. P. M., Peritore, M., Bonisch, C., Eberl, H. C., Daus, N., Kletenkov, K., Nist, A., Stiewe, T., Borggrefe, T., Mann, M., Bartkuhn, M., & Hake, S. B. (2021). JAZF1, A Novel p400/TIP60/NuA4 Complex Member, Regulates H2A.Z Acetylation at Regulatory Regions. *International journal of molecular sciences*, *22*(2), 678. https://doi.org/10.3390/ijms22020678

Punzeler, S., Link, S., Wagner, G., Keilhauer, E. C., Kronbeck, N., Spitzer, R. M., Leidescher, S., Markaki, Y., Mentele, E., Regnard, C., Schneider, K., Takahashi, D., Kusakabe, M., Vardabasso, C., Zink, L. M., Straub, T., Bernstein, E., Harata, M., Leonhardt, H., . . . Hake, S. B. (2017). Multivalent binding of PWWP2A to H2A.Z regulates mitosis and neural crest differentiation. *EMBO J*, *36*(15), 2263-2279. https://doi.org/10.15252/embj.201695757

Ramzan, F., Baumbach, J., Monks, A. D., & Zovkic, I. B. (2020). Histone H2A.Z is required for androgen receptor-mediated effects on fear memory. *Neurobiol Learn Mem*, *175*, 107311. https://doi.org/10.1016/j.nlm.2020.107311

Ramzan, F., Creighton, S. D., Hall, M., Baumbach, J., Wahdan, M., Poulson, S. J., Michailidis, V., Stefanelli, G., Narkaj, K., Tao, C. S., Khan, D., Steininger, C. F. D., Jr., Walters, B. J., Monks, D. A., Martin, L. J., & Zovkic, I. B. (2020). Sex-

specific effects of the histone variant H2A.Z on fear memory, stress-enhanced fear learning and hypersensitivity to pain. *Sci Rep*, *10*(1), 14331. https://doi.org/10.1038/s41598-020-71229-x

Rappsilber, J., Mann, M., & Ishihama, Y. (2007). Protocol for micro-purification, enrichment, pre-fractionation and storage of peptides for proteomics using StageTips. *Nat Protoc*, *2*(8), 1896-1906. https://doi.org/10.1038/nprot.2007.261

Reddy, S. D., Pakala, S. B., Molli, P. R., Sahni, N., Karanam, N. K., Mudvari, P., & Kumar, R. (2012). Metastasis-associated protein 1/histone deacetylase 4-nucleosome remodeling and deacetylase complex regulates phosphatase and tensin homolog gene expression and function. *J Biol Chem*, *287*(33), 27843-27850. https://doi.org/10.1074/jbc.M112.348474

Reid, X. J., Low, J. K. K., & Mackay, J. P. (2023). A NuRD for all seasons. *Trends Biochem Sci*, *48*(1), 11-25. https://doi.org/10.1016/j.tibs.2022.06.002

Richmond, T. J., & Davey, C. A. (2003). The structure of DNA in the nucleosome core. *Nature*, *423*(6936), 145-150. https://doi.org/10.1038/nature01595

Rinn, J. L., Kertesz, M., Wang, J. K., Squazzo, S. L., Xu, X., Brugmann, S. A., Goodnough, L. H., Helms, J. A., Farnham, P. J., Segal, E., & Chang, H. Y. (2007). Functional demarcation of active and silent chromatin domains in human HOX loci by noncoding RNAs. *Cell*, *129*(7), 1311-1323. https://doi.org/10.1016/j.cell.2007.05.022

Robert, F., Hardy, S., Nagy, Z., Baldeyron, C., Murr, R., Dery, U., Masson, J. Y., Papadopoulo, D., Herceg, Z., & Tora, L. (2006). The transcriptional histone acetyltransferase cofactor TRRAP associates with the MRN repair complex and plays a role in DNA double-strand break repair. *Mol Cell Biol*, *26*(2), 402-412. https://doi.org/10.1128/MCB.26.2.402-412.2006

Robertson, K. D. (2005). DNA methylation and human disease. *Nat Rev Genet*, *6*(8), 597-610. https://doi.org/10.1038/nrg1655

Romero, P., Obradovic, Z., Li, X., Garner, E. C., Brown, C. J., & Dunker, A. K. (2001). Sequence complexity of disordered protein. *Proteins*, *42*(1), 38-48. https://doi.org/10.1002/1097-0134(20010101)42:1<38::aid-prot50>3.0.co;2-3

Romhanyi, D., Szabo, K., Kemeny, L., & Groma, G. (2023). Histone and Histone Acetylation-Related Alterations of Gene Expression in Uninvolved Psoriatic Skin and Their Effects on Cell Proliferation, Differentiation, and Immune Responses. *International journal of molecular sciences*, *24*(19). https://doi.org/10.3390/ijms241914551

Ruhl, D. D., Jin, J., Cai, Y., Swanson, S., Florens, L., Washburn, M. P., Conaway, R. C., Conaway, J. W., & Chrivia, J. C. (2006). Purification of a human SRCAP complex that remodels chromatin by incorporating the histone variant H2A.Z into nucleosomes. *Biochemistry*, *45*(17), 5671-5677. https://doi.org/10.1021/bi060043d

Ryan, D. P., Sundaramoorthy, R., Martin, D., Singh, V., & Owen-Hughes, T. (2011). The DNA-binding domain of the Chd1 chromatin-remodelling enzyme contains SANT and SLIDE domains. *EMBO J*, *30*(13), 2596-2609. https://doi.org/10.1038/emboj.2011.166

Sakai, H., Urano, T., Ookata, K., Kim, M. H., Hirai, Y., Saito, M., Nojima, Y., & Ishikawa, F. (2002). MBD3 and HDAC1, two components of the NuRD complex, are localized at Aurora-A-positive centrosomes in M phase. *J Biol Chem*, *277*(50), 48714-48723. https://doi.org/10.1074/jbc.M208461200

Salamun, S. G., Sitz, J., De La Cruz-Herrera, C. F., Yockteng-Melgar, J., Marcon, E., Greenblatt, J., Fradet-Turcotte, A., & Frappier, L. (2019). The Epstein-Barr Virus

BMRF1 Protein Activates Transcription and Inhibits the DNA Damage Response by Binding NuRD. *J Virol*, *93*(22). https://doi.org/10.1128/JVI.01070-19

Sales-Gil, R., Kommer, D. C., de Castro, I. J., Amin, H. A., Vinciotti, V., Sisu, C., & Vagnarelli, P. (2021). Non-redundant functions of H2A.Z.1 and H2A.Z.2 in chromosome segregation and cell cycle progression. *EMBO Rep*, *22*(11), e52061. https://doi.org/10.15252/embr.202052061

Sankaran, V. G., Menne, T. F., Xu, J., Akie, T. E., Lettre, G., Van Handel, B., Mikkola, H. K., Hirschhorn, J. N., Cantor, A. B., & Orkin, S. H. (2008). Human fetal hemoglobin expression is regulated by the developmental stage-specific repressor BCL11A. *Science*, *322*(5909), 1839-1842. https://doi.org/10.1126/science.1165409

Sawicka, A., & Seiser, C. (2012). Histone H3 phosphorylation - a versatile chromatin modification for different occasions. *Biochimie*, *94*(11), 2193-2201. https://doi.org/10.1016/j.biochi.2012.04.018

Scacchetti, A., Schauer, T., Reim, A., Apostolou, Z., Campos Sparr, A., Krause, S., Heun, P., Wierer, M., & Becker, P. B. (2020). Drosophila SWR1 and NuA4 complexes are defined by DOMINO isoforms. *eLife*, *9*, e56325. https://doi.org/10.7554/eLife.56325

Schindelin, J., Arganda-Carreras, I., Frise, E., Kaynig, V., Longair, M., Pietzsch, T., Preibisch, S., Rueden, C., Saalfeld, S., Schmid, B., Tinevez, J. Y., White, D. J., Hartenstein, V., Eliceiri, K., Tomancak, P., & Cardona, A. (2012). Fiji: an open-source platform for biological-image analysis. *Nat Methods*, *9*(7), 676-682. https://doi.org/10.1038/nmeth.2019

Schmitges, F. W., Prusty, A. B., Faty, M., Stutzer, A., Lingaraju, G. M., Aiwazian, J., Sack, R., Hess, D., Li, L., Zhou, S., Bunker, R. D., Wirth, U., Bouwmeester, T., Bauer, A., Ly-Hartig, N., Zhao, K., Chan, H., Gu, J., Gut, H., . . . Thoma, N. H. (2011). Histone methylation by PRC2 is inhibited by active chromatin marks. *Mol Cell*, *42*(3), 330-341. https://doi.org/10.1016/j.molcel.2011.03.025

Schmolka, N., Karemaker, I. D., Cardoso da Silva, R., Recchia, D. C., Spegg, V., Bhaskaran, J., Teske, M., de Wagenaar, N. P., Altmeyer, M., & Baubec, T. (2023). Dissecting the roles of MBD2 isoforms and domains in regulating NuRD complex function during cellular differentiation. *Nat Commun*, *14*(1), 3848. https://doi.org/10.1038/s41467-023-39551-w

Schneider, J., Sundaravinayagam, D., Blume, A., Marg, A., Grunwald, S., Metzler, E., Escobar, H., Muthel, S., Wang, H., Wollersheim, T., Weber-Carstens, S., Akalin, A., Di Virgilio, M., Tursun, B., & Spuler, S. (2023). Disintegration of the NuRD Complex in Primary Human Muscle Stem Cells in Critical Illness Myopathy. *International journal of molecular sciences*, *24*(3). https://doi.org/10.3390/ijms24032772

Schubert, H. L., Wittmeyer, J., Kasten, M. M., Hinata, K., Rawling, D. C., Heroux, A., Cairns, B. R., & Hill, C. P. (2013). Structure of an actin-related subcomplex of the SWI/SNF chromatin remodeler. *Proc Natl Acad Sci U S A*, *110*(9), 3345-3350. https://doi.org/10.1073/pnas.1215379110

Schultz, D. C., Ayyanathan, K., Negorev, D., Maul, G. G., & Rauscher, F. J., 3rd. (2002). SETDB1: a novel KAP-1-associated histone H3, lysine 9-specific methyltransferase that contributes to HP1-mediated silencing of euchromatic genes by KRAB zinc-finger proteins. *Genes Dev*, *16*(8), 919-932. https://doi.org/10.1101/gad.973302

Sedkov, Y., Cho, E., Petruk, S., Cherbas, L., Smith, S. T., Jones, R. S., Cherbas, P., Canaani, E., Jaynes, J. B., & Mazo, A. (2003). Methylation at lysine 4 of histone

H3 in ecdysone-dependent development of Drosophila. *Nature*, *426*(6962), 78-83. https://doi.org/10.1038/nature02080

Shan, L., Xu, G., Yao, R. W., Luan, P. F., Huang, Y., Zhang, P. H., Pan, Y. H., Zhang, L., Gao, X., Li, Y., Cao, S. M., Gao, S. X., Yang, Z. H., Li, S., Yang, L. Z., Wang, Y., Wong, C. C. L., Yu, L., Li, J., . . . Chen, L. L. (2023). Nucleolar URB1 ensures 3' ETS rRNA removal to prevent exosome surveillance. *Nature*, *615*(7952), 526-534. https://doi.org/10.1038/s41586-023-05767-5

Sharaby, Y., Lahmi, R., Amar, O., Elbaz, I., Lerer-Goldshtein, T., Weiss, A. M., Appelbaum, L., & Tzur, A. (2014). Gas2l3 is essential for brain morphogenesis and development. *Dev Biol*, *394*(2), 305-313. https://doi.org/10.1016/j.ydbio.2014.08.006

Shi, D., Huang, Y., & Bai, C. (2023). Studies of the Mechanism of Nucleosome Dynamics: A Review on Multifactorial Regulation from Computational and Experimental Cases. *Polymers (Basel)*, *15*(7). https://doi.org/10.3390/polym15071763

Shih, P. Y., Fang, Y. L., Shankar, S., Lee, S. P., Hu, H. T., Chen, H., Wang, T. F., Hsia, K. C., & Hsueh, Y. P. (2022). Phase separation and zinc-induced transition modulate synaptic distribution and association of autism-linked CTTNBP2 and SHANK3. *Nat Commun*, *13*(1), 2664. https://doi.org/10.1038/s41467-022-30353-0

Sigrist, C. J., de Castro, E., Cerutti, L., Cuche, B. A., Hulo, N., Bridge, A., Bougueleret, L., & Xenarios, I. (2013). New and continuing developments at PROSITE. *Nucleic acids research*, *41*(Database issue), D344-347. https://doi.org/10.1093/nar/gks1067

Sillibourne, J. E., Delaval, B., Redick, S., Sinha, M., & Doxsey, S. J. (2007). Chromatin remodeling proteins interact with pericentrin to regulate centrosome integrity. *Mol Biol Cell*, *18*(9), 3667-3680. https://doi.org/10.1091/mbc.e06-07-0604

Spruijt, C. G., Luijsterburg, M. S., Menafra, R., Lindeboom, R. G., Jansen, P. W., Edupuganti, R. R., Baltissen, M. P., Wiegant, W. W., Voelker-Albert, M. C., Matarese, F., Mensinga, A., Poser, I., Vos, H. R., Stunnenberg, H. G., van Attikum, H., & Vermeulen, M. (2016). ZMYND8 Co-localizes with NuRD on Target Genes and Regulates Poly(ADP-Ribose)-Dependent Recruitment of GATAD2A/NuRD to Sites of DNA Damage. *Cell Rep*, *17*(3), 783-798. https://doi.org/10.1016/j.celrep.2016.09.037

Statello, L., Guo, C. J., Chen, L. L., & Huarte, M. (2021). Gene regulation by long non-coding RNAs and its biological functions. *Nat Rev Mol Cell Biol*, *22*(2), 96-118. https://doi.org/10.1038/s41580-020-00315-9

Stefanelli, G., Makowski, C. E., Brimble, M. A., Hall, M., Reda, A., Creighton, S. D., Leonetti, A. M., McLean, T. A. B., Zakaria, J. M., Baumbach, J., Greer, C. B., Davidoff, A. M., Walters, B. J., Murphy, P. J., & Zovkic, I. B. (2021). The histone chaperone Anp32e regulates memory formation, transcription, and dendritic morphology by regulating steady-state H2A.Z binding in neurons. *Cell Rep*, *36*(7), 109551. https://doi.org/10.1016/j.celrep.2021.109551

Stoyanov, D., Stoyanov, G. S., Ivanov, M. N., Spasov, R. H., & Tonchev, A. B. (2023). Transcription Factor Zbtb20 as a Regulator of Malignancy and Its Practical Applications. *International journal of molecular sciences*, *24*(18). https://doi.org/10.3390/ijms241813763

Strahl, B. D., & Allis, C. D. (2000). The language of covalent histone modifications. *Nature*, *403*(6765), 41-45. https://doi.org/10.1038/47412

Subramanian, V., Fields, P. A., & Boyer, L. A. (2015). H2A.Z: a molecular rheostat for transcriptional control. *F1000Prime Rep*, *7*, 01. https://doi.org/10.12703/P7-01

Suka, N., Suka, Y., Carmen, A. A., Wu, J., & Grunstein, M. (2001). Highly specific antibodies determine histone acetylation site usage in yeast heterochromatin and euchromatin. *Mol Cell*, *8*(2), 473-479. https://doi.org/10.1016/s1097-2765(01)00301-x

Sun, A., Li, F., Liu, Z., Jiang, Y., Zhang, J., Wu, J., & Shi, Y. (2018). Structural and biochemical insights into human zinc finger protein AEBP2 reveals interactions with RBBP4. *Protein Cell*, *9*(8), 738-742. https://doi.org/10.1007/s13238-017-0483-6

Suto, R. K., Clarkson, M. J., Tremethick, D. J., & Luger, K. (2000). Crystal structure of a nucleosome core particle containing the variant histone H2A.Z. *Nat Struct Biol*, *7*(12), 1121-1124. https://doi.org/10.1038/81971

Szklarczyk, D., Kirsch, R., Koutrouli, M., Nastou, K., Mehryary, F., Hachilif, R., Gable, A. L., Fang, T., Doncheva, N. T., Pyysalo, S., Bork, P., Jensen, L. J., & von Mering, C. (2023). The STRING database in 2023: protein-protein association networks and functional enrichment analyses for any sequenced genome of interest. *Nucleic acids research*, *51*(D1), D638-D646. https://doi.org/10.1093/nar/gkac1000

Tachibana, M., Sugimoto, K., Fukushima, T., & Shinkai, Y. (2001). Set domain-containing protein, G9a, is a novel lysine-preferring mammalian histone methyltransferase with hyperactivity and specific selectivity to lysines 9 and 27 of histone H3. *J Biol Chem*, *276*(27), 25309-25317. https://doi.org/10.1074/jbc.M101914200

Talbert, P. B., Ahmad, K., Almouzni, G., Ausio, J., Berger, F., Bhalla, P. L., Bonner, W. M., Cande, W. Z., Chadwick, B. P., Chan, S. W., Cross, G. A., Cui, L., Dimitrov, S. I., Doenecke, D., Eirin-Lopez, J. M., Gorovsky, M. A., Hake, S. B., Hamkalo, B. A., Holec, S., . . . Henikoff, S. (2012). A unified phylogeny-based nomenclature for histone variants. *Epigenetics Chromatin*, *5*(1), 7. https://doi.org/10.1186/1756-8935-5-7

Talyzina, A., Han, Y., Banerjee, C., Fishbain, S., Reyes, A., Vafabakhsh, R., & He, Y. (2023). Structural basis of TFIIIC-dependent RNA polymerase III transcription initiation. *Mol Cell*, *83*(15), 2641-2652 e2647. https://doi.org/10.1016/j.molcel.2023.06.015

Tamaru, H., & Selker, E. U. (2001). A histone H3 methyltransferase controls DNA methylation in Neurospora crassa. *Nature*, *414*(6861), 277-283. https://doi.org/10.1038/35104508

Tang, S., Huang, X., Wang, X., Zhou, X., Huang, H., Qin, L., Tao, H., Wang, Q., & Tao, Y. (2020). Vital and Distinct Roles of H2A.Z Isoforms in Hepatocellular Carcinoma. *Onco Targets Ther*, *13*, 4319-4337. https://doi.org/10.2147/OTT.S243823

Thatcher, T. H., & Gorovsky, M. A. (1994). Phylogenetic analysis of the core histones H2A, H2B, H3, and H4. *Nucleic acids research*, *22*(2), 174-179. https://doi.org/10.1093/nar/22.2.174

Tie, F., Banerjee, R., Stratton, C. A., Prasad-Sinha, J., Stepanik, V., Zlobin, A., Diaz, M. O., Scacheri, P. C., & Harte, P. J. (2009). CBP-mediated acetylation of histone H3 lysine 27 antagonizes Drosophila Polycomb silencing. *Development*, *136*(18), 3131-3141. https://doi.org/10.1242/dev.037127

Tili, E., Michaille, J. J., Liu, C. G., Alder, H., Taccioli, C., Volinia, S., Calin, G. A., & Croce, C. M. (2010). GAM/ZFp/ZNF512B is central to a gene sensor circuitry involving cell-cycle regulators, TGFbeta effectors, Drosha and microRNAs with

opposite oncogenic potentials. *Nucleic acids research*, *38*(21), 7673-7688. https://doi.org/10.1093/nar/gkq637

Torchy, M. P., Hamiche, A., & Klaholz, B. P. (2015). Structure and function insights into the NuRD chromatin remodeling complex. *Cell Mol Life Sci*, *72*(13), 2491-2507. https://doi.org/10.1007/s00018-015-1880-8

Tran, H. G., Steger, D. J., Iyer, V. R., & Johnson, A. D. (2000). The chromo domain protein chd1p from budding yeast is an ATP-dependent chromatin-modifying factor. *EMBO J*, *19*(10), 2323-2331. https://doi.org/10.1093/emboj/19.10.2323

Ulianov, S. V., Velichko, A. K., Magnitov, M. D., Luzhin, A. V., Golov, A. K., Ovsyannikova, N., Kireev, II, Gavrikov, A. S., Mishin, A. S., Garaev, A. K., Tyakht, A. V., Gavrilov, A. A., Kantidze, O. L., & Razin, S. V. (2021). Suppression of liquid-liquid phase separation by 1,6-hexanediol partially compromises the 3D genome organization in living cells. *Nucleic acids research*, *49*(18), 10524-10541. https://doi.org/10.1093/nar/gkab249

Urrutia, R. (2003). KRAB-containing zinc-finger repressor proteins. *Genome Biol*, *4*(10), 231. https://doi.org/10.1186/gb-2003-4-10-231

Valdes-Mora, F., Song, J. Z., Statham, A. L., Strbenac, D., Robinson, M. D., Nair, S. S., Patterson, K. I., Tremethick, D. J., Stirzaker, C., & Clark, S. J. (2012). Acetylation of H2A.Z is a key epigenetic modification associated with gene deregulation and epigenetic remodeling in cancer. *Genome Res*, *22*(2), 307-321. https://doi.org/10.1101/gr.118919.110

van Daal, A., & Elgin, S. C. (1992). A histone variant, H2AvD, is essential in Drosophila melanogaster. *Mol Biol Cell*, *3*(6), 593-602. https://doi.org/10.1091/mbc.3.6.593

van de Nobelen, S., Rosa-Garrido, M., Leers, J., Heath, H., Soochit, W., Joosen, L., Jonkers, I., Demmers, J., van der Reijden, M., Torrano, V., Grosveld, F., Delgado, M. D., Renkawitz, R., Galjart, N., & Sleutels, F. (2010). CTCF regulates the local epigenetic state of ribosomal DNA repeats. *Epigenetics Chromatin*, *3*(1), 19. https://doi.org/10.1186/1756-8935-3-19

Varadi, M., Anyango, S., Deshpande, M., Nair, S., Natassia, C., Yordanova, G., Yuan, D., Stroe, O., Wood, G., Laydon, A., Zidek, A., Green, T., Tunyasuvunakool, K., Petersen, S., Jumper, J., Clancy, E., Green, R., Vora, A., Lutfi, M., . . . Velankar, S. (2022). AlphaFold Protein Structure Database: massively expanding the structural coverage of protein-sequence space with high-accuracy models. *Nucleic acids research*, *50*(D1), D439-D444. https://doi.org/10.1093/nar/gkab1061

Vardabasso, C., Gaspar-Maia, A., Hasson, D., Punzeler, S., Valle-Garcia, D., Straub, T., Keilhauer, E. C., Strub, T., Dong, J., Panda, T., Chung, C. Y., Yao, J. L., Singh, R., Segura, M. F., Fontanals-Cirera, B., Verma, A., Mann, M., Hernando, E., Hake, S. B., & Bernstein, E. (2015). Histone Variant H2A.Z.2 Mediates Proliferation and Drug Sensitivity of Malignant Melanoma. *Mol Cell*, *59*(1), 75-88. https://doi.org/10.1016/j.molcel.2015.05.009

Vassilev, L. T. (2006). Cell cycle synchronization at the G2/M phase border by reversible inhibition of CDK1. *Cell Cycle*, *5*(22), 2555-2556. https://doi.org/10.4161/cc.5.22.3463

Vavra, K. J., Allis, C. D., & Gorovsky, M. A. (1982). Regulation of histone acetylation in Tetrahymena macro- and micronuclei. *J Biol Chem*, *257*(5), 2591-2598. https://www.ncbi.nlm.nih.gov/pubmed/7061439

Vrana, K. E., Churchill, M. E., Tullius, T. D., & Brown, D. D. (1988). Mapping functional regions of transcription factor TFIIIA. *Mol Cell Biol*, *8*(4), 1684-1696. https://doi.org/10.1128/mcb.8.4.1684-1696.1988

Wang, H., Cao, R., Xia, L., Erdjument-Bromage, H., Borchers, C., Tempst, P., & Zhang, Y. (2001). Purification and functional characterization of a histone H3-lysine 4-specific methyltransferase. *Mol Cell*, *8*(6), 1207-1217. https://doi.org/10.1016/s1097-2765(01)00405-1

Wang, L., Xiao, J., Chi, H., & Liu, J. (2024). The elevated expression of ZNF512B indicates favorable prognosis in Colon Adenocarcinoma. *Asian J Surg*. https://doi.org/10.1016/j.asjsur.2024.08.238

Wang, Y., Shankar, S. R., Kher, D., Ling, B. M., & Taneja, R. (2013). Sumoylation of the basic helix-loop-helix transcription factor sharp-1 regulates recruitment of the histone methyltransferase G9a and function in myogenesis. *J Biol Chem*, *288*(24), 17654-17662. https://doi.org/10.1074/jbc.M113.463257

Watson, J. A., Pantier, R., Jayachandran, U., Chhatbar, K., Alexander-Howden, B., Kruusvee, V., Prendecki, M., Bird, A., & Cook, A. G. (2023). Structure of SALL4 zinc finger domain reveals link between AT-rich DNA binding and Okihiro syndrome. *Life Sci Alliance*, *6*(3). https://doi.org/10.26508/lsa.202201588

West, A. P., Khoury-Hanold, W., Staron, M., Tal, M. C., Pineda, C. M., Lang, S. M., Bestwick, M., Duguay, B. A., Raimundo, N., MacDuff, D. A., Kaech, S. M., Smiley, J. R., Means, R. E., Iwasaki, A., & Shadel, G. S. (2015). Mitochondrial DNA stress primes the antiviral innate immune response. *Nature*, *520*(7548), 553-557. https://doi.org/10.1038/nature14156

West, M. H., & Bonner, W. M. (1980). Histone 2A, a heteromorphous family of eight protein species. *Biochemistry*, *19*(14), 3238-3245. https://doi.org/10.1021/bi00555a022

Wickham, H. (2016). *ggplot2: Elegant Graphics for Data Analysis*. Springer. https://doi.org/10.1007/978-3-319-24277-4

Widom, J. (1989). Toward a unified model of chromatin folding. *Annu Rev Biophys Biophys Chem*, *18*, 365-395. https://doi.org/10.1146/annurev.bb.18.060189.002053

Wiedemann, S. M., Mildner, S. N., Bonisch, C., Israel, L., Maiser, A., Matheisl, S., Straub, T., Merkl, R., Leonhardt, H., Kremmer, E., Schermelleh, L., & Hake, S. B. (2010). Identification and characterization of two novel primate-specific histone H3 variants, H3.X and H3.Y. *J Cell Biol*, *190*(5), 777-791. https://doi.org/10.1083/jcb.201002043

Willhoft, O., Ghoneim, M., Lin, C. L., Chua, E. Y. D., Wilkinson, M., Chaban, Y., Ayala, R., McCormack, E. A., Ocloo, L., Rueda, D. S., & Wigley, D. B. (2018). Structure and dynamics of the yeast SWR1-nucleosome complex. *Science*, *362*(6411), eaat7716. https://doi.org/10.1126/science.aat7716

Wing, C. E., Fung, H. Y. J., & Chook, Y. M. (2022). Karyopherin-mediated nucleocytoplasmic transport. *Nat Rev Mol Cell Biol*, *23*(5), 307-328. https://doi.org/10.1038/s41580-021-00446-7

Wolfe, S. A., Nekludova, L., & Pabo, C. O. (2000). DNA recognition by Cys2His2 zinc finger proteins. *Annu Rev Biophys Biomol Struct*, *29*, 183-212. https://doi.org/10.1146/annurev.biophys.29.1.183

Woo, A. J., Moran, T. B., Schindler, Y. L., Choe, S. K., Langer, N. B., Sullivan, M. R., Fujiwara, Y., Paw, B. H., & Cantor, A. B. (2008). Identification of ZBP-89 as a novel GATA-1-associated transcription factor involved in megakaryocytic and erythroid development. *Mol Cell Biol*, *28*(8), 2675-2689. https://doi.org/10.1128/MCB.01945-07

Wratting, D., Thistlethwaite, A., Harris, M., Zeef, L. A., & Millar, C. B. (2012). A conserved function for the H2A.Z C terminus. *J Biol Chem*, *287*(23), 19148-19157. https://doi.org/10.1074/jbc.M111.317990

Wu, L. M., Wang, J., Conidi, A., Zhao, C., Wang, H., Ford, Z., Zhang, L., Zweier, C., Ayee, B. G., Maurel, P., Zwijsen, A., Chan, J. R., Jankowski, M. P., Huylebroeck, D., & Lu, Q. R. (2016). Zeb2 recruits HDAC-NuRD to inhibit Notch and controls Schwann cell differentiation and remyelination. *Nat Neurosci*, *19*(8), 1060-1072. https://doi.org/10.1038/nn.4322

Wu, T., Hu, E., Xu, S., Chen, M., Guo, P., Dai, Z., Feng, T., Zhou, L., Tang, W., Zhan, L., Fu, X., Liu, S., Bo, X., & Yu, G. (2021). clusterProfiler 4.0: A universal enrichment tool for interpreting omics data. *Innovation (Camb)*, *2*(3), 100141. https://doi.org/10.1016/j.xinn.2021.100141

Xiao, F. H., Wang, H. T., & Kong, Q. P. (2019). Dynamic DNA Methylation During Aging: A "Prophet" of Age-Related Outcomes. *Front Genet*, *10*, 107. https://doi.org/10.3389/fgene.2019.00107

Xiao, H., Sandaltzopoulos, R., Wang, H. M., Hamiche, A., Ranallo, R., Lee, K. M., Fu, D., & Wu, C. (2001). Dual functions of largest NURF subunit NURF301 in nucleosome sliding and transcription factor interactions. *Mol Cell*, *8*(3), 531-543. https://doi.org/10.1016/s1097-2765(01)00345-8

Xie, X., Wu, Q., Zhang, K., Liu, Y., Zhang, N., Chen, Q., Wang, L., Li, W., Zhang, J., & Liu, Y. (2021). O-GlcNAc modification regulates MTA1 transcriptional activity during breast cancer cell genotoxic adaptation. *Biochim Biophys Acta Gen Subj*, *1865*(8), 129930. https://doi.org/10.1016/j.bbagen.2021.129930

Xu, Q., Xi, Y., Ma, S., Wang, J., Li, J., Han, C., Li, L., Wang, J., & Liu, H. (2022). Transcriptome profiling of morphogenetic differences between contour and flight feathers in duck. *Br Poult Sci*, *63*(5), 597-604. https://doi.org/10.1080/00071668.2022.2026292

Xue, Y., Wong, J., Moreno, G. T., Young, M. K., Cote, J., & Wang, W. (1998). NURD, a novel complex with both ATP-dependent chromatin-remodeling and histone deacetylase activities. *Mol Cell*, *2*(6), 851-861. https://doi.org/10.1016/s1097-2765(00)80299-3

Yadav, P., Subbarayalu, P., Medina, D., Nirzhor, S., Timilsina, S., Rajamanickam, S., Eedunuri, V. K., Gupta, Y., Zheng, S., Abdelfattah, N., Huang, Y., Vadlamudi, R., Hromas, R., Meltzer, P., Houghton, P., Chen, Y., & Rao, M. K. (2022). M6A RNA Methylation Regulates Histone Ubiquitination to Support Cancer Growth and Progression. *Cancer Res*, *82*(10), 1872-1889. https://doi.org/10.1158/0008-5472.CAN-21-2106

Yanagisawa, Y., Ito, E., Yuasa, Y., & Maruyama, K. (2002). The human DNA methyltransferases DNMT3A and DNMT3B have two types of promoters with different CpG contents. *Biochim Biophys Acta*, *1577*(3), 457-465. https://doi.org/10.1016/s0167-4781(02)00482-7

Yang, P., Wang, Y., Hoang, D., Tinkham, M., Patel, A., Sun, M. A., Wolf, G., Baker, M., Chien, H. C., Lai, K. N., Cheng, X., Shen, C. J., & Macfarlan, T. S. (2017). A placental growth factor is silenced in mouse embryos by the zinc finger protein ZFP568. *Science*, *356*(6339), 757-759. https://doi.org/10.1126/science.aah6895

Yang, P., Wang, Y., & Macfarlan, T. S. (2017). The Role of KRAB-ZFPs in Transposable Element Repression and Mammalian Evolution. *Trends Genet*, *33*(11), 871-881. https://doi.org/10.1016/j.tig.2017.08.006

Yang, Y., Luan, Y., Feng, Q., Chen, X., Qin, B., Ren, K. D., & Luan, Y. (2021). Epigenetics and Beyond: Targeting Histone Methylation to Treat Type 2 Diabetes

Mellitus. *Front Pharmacol*, *12*, 807413. https://doi.org/10.3389/fphar.2021.807413

Yokoyama, H., Nakos, K., Santarella-Mellwig, R., Rybina, S., Krijgsveld, J., Koffa, M. D., & Mattaj, I. W. (2013). CHD4 is a RanGTP-dependent MAP that stabilizes microtubules and regulates bipolar spindle formation. *Curr Biol*, *23*(24), 2443-2451. https://doi.org/10.1016/j.cub.2013.09.062

Yu, H., Wang, J., Lackford, B., Bennett, B., Li, J. L., & Hu, G. (2021). INO80 promotes H2A.Z occupancy to regulate cell fate transition in pluripotent stem cells. *Nucleic acids research*, *49*(12), 6739-6755. https://doi.org/10.1093/nar/gkab476

Zhang, B., Day, D. S., Ho, J. W., Song, L., Cao, J., Christodoulou, D., Seidman, J. G., Crawford, G. E., Park, P. J., & Pu, W. T. (2013). A dynamic H3K27ac signature identifies VEGFA-stimulated endothelial enhancers and requires EP300 activity. *Genome Res*, *23*(6), 917-927. https://doi.org/10.1101/gr.149674.112

Zhang, J., Gao, X., & Yu, L. (2021). Roles of Histone Deacetylases in Acute Myeloid Leukemia With Fusion Proteins. *Front Oncol*, *11*, 741746. https://doi.org/10.3389/fonc.2021.741746

Zhang, K., Jacob, S., Dozmorov, M., Babic, I., Nurmemmedov, E., & Faber, A. C. (2024). R9: A novel NuRD complex inhibitor for targeted therapy in triple negative breast cancer (TNBC). *Cancer Res*, *84*(6). https://doi.org/10.1158/1538-7445.AM2024-5976

Zhang, Y., Ku, W. L., Liu, S., Cui, K., Jin, W., Tang, Q., Lu, W., Ni, B., & Zhao, K. (2017). Genome-wide identification of histone H2A and histone variant H2A.Z-interacting proteins by bPPI-seq. *Cell Res*, *27*(10), 1258-1274. https://doi.org/10.1038/cr.2017.112

Zink, L. M., Delbarre, E., Eberl, H. C., Keilhauer, E. C., Bonisch, C., Punzeler, S., Bartkuhn, M., Collas, P., Mann, M., & Hake, S. B. (2017). H3.Y discriminates between HIRA and DAXX chaperone complexes and reveals unexpected insights into human DAXX-H3.3-H4 binding and deposition requirements. *Nucleic acids research*, *45*(10), 5691-5706. https://doi.org/10.1093/nar/gkx131

Zlatanova, J., & Thakar, A. (2008). H2A.Z: view from the top. *Structure*, *16*(2), 166-179. https://doi.org/10.1016/j.str.2007.12.008

Zucchi, R., & Ronca-Testoni, S. (1997). The sarcoplasmic reticulum Ca2+ channel/ryanodine receptor: modulation by endogenous effectors, drugs and disease states. *Pharmacol Rev*, *49*(1), 1-51. https://www.ncbi.nlm.nih.gov/pubmed/9085308

6 Acknowledgements / Danksagung

„[…] Danke sagen ist schwer
Manche haben‘s im Blut und manche haben‘s verlernt
Dank dem Busfahrer, es fühlt sich gut an, wenn du‘s von Herzen machst
Du denkst ‚warum?‘, doch der Busfahrer merkt sich das
Und auf einmal lächelt er und sagt ‚gern geschehen‘
Und du kannst in seinem Blick ein wenig Wärme sehen
Also schmeiß deine Bedenken über Bord
Es ist ein kleines grenzenloses Wort […]“

aus „Danke“ von Teesy

Danke, Sandra, dass du mir die Möglichkeit gegeben hast in deiner Arbeitsgruppe meine Doktorarbeit anzufertigen. Schon damals im Vorstellungsgespräch habe ich schnell gemerkt, dass wir beide auf einer Wellenlänge sind und ich eine einzigartige Professorin vor mir sitzen habe. Deine ansteckende Begeisterung und Leidenschaft für die Forschung haben mir einen ganz neuen Blick auf die Wissenschaft gegeben. Danke für deine Unterstützung in allen Lebenslagen und dafür, dass du das Potential in mir siehst, wenn ich es nicht tue. Du hast maßgeblich dazu beigetragen, dass meine Entscheidung nach Gießen zu kommen eine der besten meines Lebens geworden ist.

Danke, Alexander, für die Übernahme des Zweitgutachtens und den stets klugen und hilfreichen Input im TAC, im „NuRD-Meeting“ und in den vielen, tollen Jahren im TRR81.

Danke, Marek, dass du als dritter Prüfer dabei bist, für die Kollaboration und für die viele, bioinformatische Hilfe in den letzten Jahren. Es macht immer Spaß sich mit dir auszutauschen, ob während oder außerhalb der Arbeitszeit, und ich bin sehr froh, dass du uns nach deinem Wechsel trotzdem erhalten geblieben bist.

Danke, Oli, dass du als vierter Prüfer zur Verfügung stehst, für die Kollaboration und dass uns durch dich Sophie erhalten geblieben ist. Ich freue mich schon, bald endlich mal Zeit zu haben, gemeinsam ein Spiel zu schauen.

Thanks to all our wonderful collaboration partners. Falk, Joel and Chandrika, Olalla and Marco, thanks to you and your amazing work, this project lead to a great publication.

Danke, Sonja, hier schon einmal für die zukünftigen Erziehungstipps. Wir beide sind wirklich das absolute „Dream Team“. Ich bin froh, dich in meinem Leben zu haben, und freue mich auch schon auf die Cocktails im nächsten… ;)

Danke, Nadine, für deine ganze Unterstützung im Labor und die Therapie-Sitzungen, wenn es mal nicht so läuft wie geplant oder der Laborsegen schief hängt. Ich vermisse wirklich das Sofa in deinem Büro und bin froh, wenn wir uns in Zukunft endlich wieder häufiger sehen.

Danke, Felix, für deinen Musikgeschmack. Nach meinem Vorstellungsgespräch habe ich Steffi auf die Frage, wie die Leute so waren, geantwortet, dass zumindest schonmal jemand ein Bandshirt anhatte. Wer hätte gedacht, was für eine tolle Freundschaft daraus

einmal entstehen würde. Danke, dass ich mich immer auf dich verlassen kann, ob im Labor oder außerhalb. Ich freue mich schon auf viele, weitere Konzerte mit dir.

Danke, Carlotta, dass du versprochen hast, niemals aus Gießen wegzuziehen, weil du weißt, dass es mir das Herz brechen würde. Danke für die gemeinsamen Musicalperformances, die Gespräche, die unvergleichliche Gastfreundschaft und deine (fast immer) ungeschlagen gute Laune.

Danke, Lena, meine „Partnerin in ZNF crime“. Danke, dass ich im Labor immer auf dich zählen kann, deine Unterstützung in den letzten Monaten hat mir wirklich extrem geholfen. Ich freu mich schon, dass ich dir das wohl alles bald heimzahlen darf… Und danke, dass DU wenigstens für immer in der Gegend bleibst ;)

Thank you, Jie, for all your input and all the great and hilarious pranks you are playing all the time in the lab. It is always nice to laugh together with you.

Danke, Jörg, für deine wissenschaftliche Unterstützung, aber auch für deine unbeschwerte Art die Dinge anzugehen und für die oft sehr unterhaltsamen Anekdoten aus dem Institut.

Danke, Joline, für deine Unterstützung und dass man bei dir immer auf ein offenes Ohr trifft, egal wie die Stimmung gerade ist.

Danke, Dennis, für deine unglaublich freundliche Art, die ihresgleichen sucht, und dass mein bei dir immer einen Snack für jede Ernährungspräferenz bekommt.

Danke an alle Bachelor- und Masterstudentinnen, die ich über die Jahre betreuen durfte. Ich konnte immer etwas lernen und jede Arbeit hat irgendwie zum Projekt beigetragen.

Danke an alle unsere Hiwis, ihr haltet den Laden am Laufen und ich bin dankbar, dass wir euch als Unterstützung haben.

Danke, Tara, Andreas, Sandy, Konstantin, Tobi und David, dass ihr mich damals so herzlich bei euch aufgenommen habt und mir den Start deutlich einfacher gemacht habt.

Danke, Sophie, dass du die beste erste Masterstudentin warst, die ich mir hätte wünschen können. Deine Arbeit hat das ganze Projekt so richtig ins Rollen gebracht und ich bin sehr dankbar dafür.

Danke an die anderen Snitches, dass ihr einfach eine wunderbare Gruppe von Menschen seid, die mir einen Grund gegeben hat, auch am Wochenende in Gießen zu sein ;)

Danke an Verena und Fabian, alle meine Freunde und alle dazwischen und außerhalb, für die Unterstützung über all die Jahre und das Verständnis, vor allem in den letzten Monaten.

Danke von tiefstem Herzen an meine gesamte Familie. Ohne eure immer schon bedingungslose Unterstützung wäre das alles hier nicht möglich gewesen.

Und zu guter Letzt: Danke, Steffi, für einfach alles! Ohne dich wäre ich nicht da, wo ich heute bin. Mein größter und wichtigster Erfolg während meiner PhD-Zeit wird immer sein, dass ich dich zu meiner Frau gemacht habe.

7 Appendix

7.1 Plasmid maps

7.1.1 pIRESneo-eGFP-ZNF512B

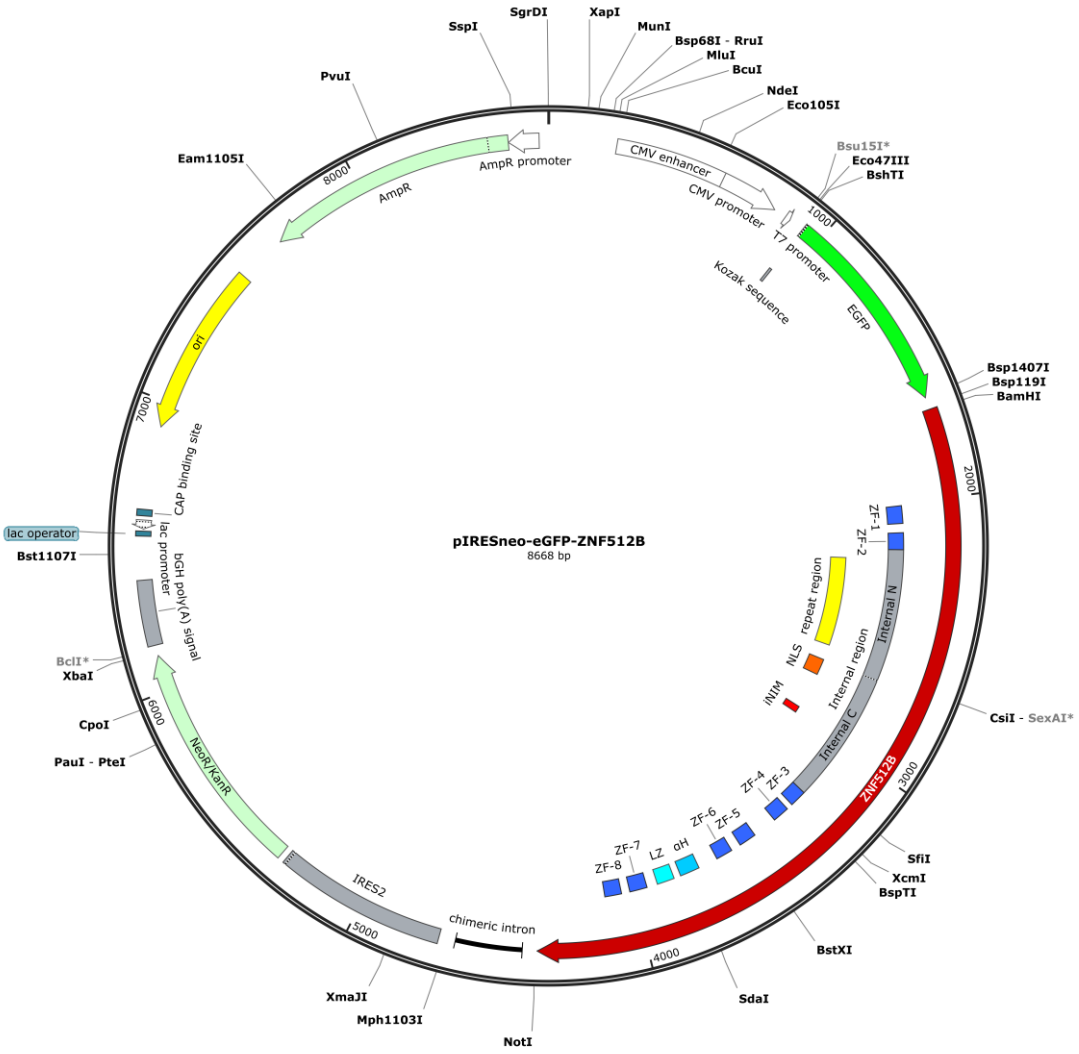

Figure 7.1.1: Plasmid map for pIRESneo-eGFP-ZNF512B. *Vector for eukaryotic expression of N-terminally GFP-tagged human ZNF512B.*

7.1.2 pEGFP-N2-ZNF512B

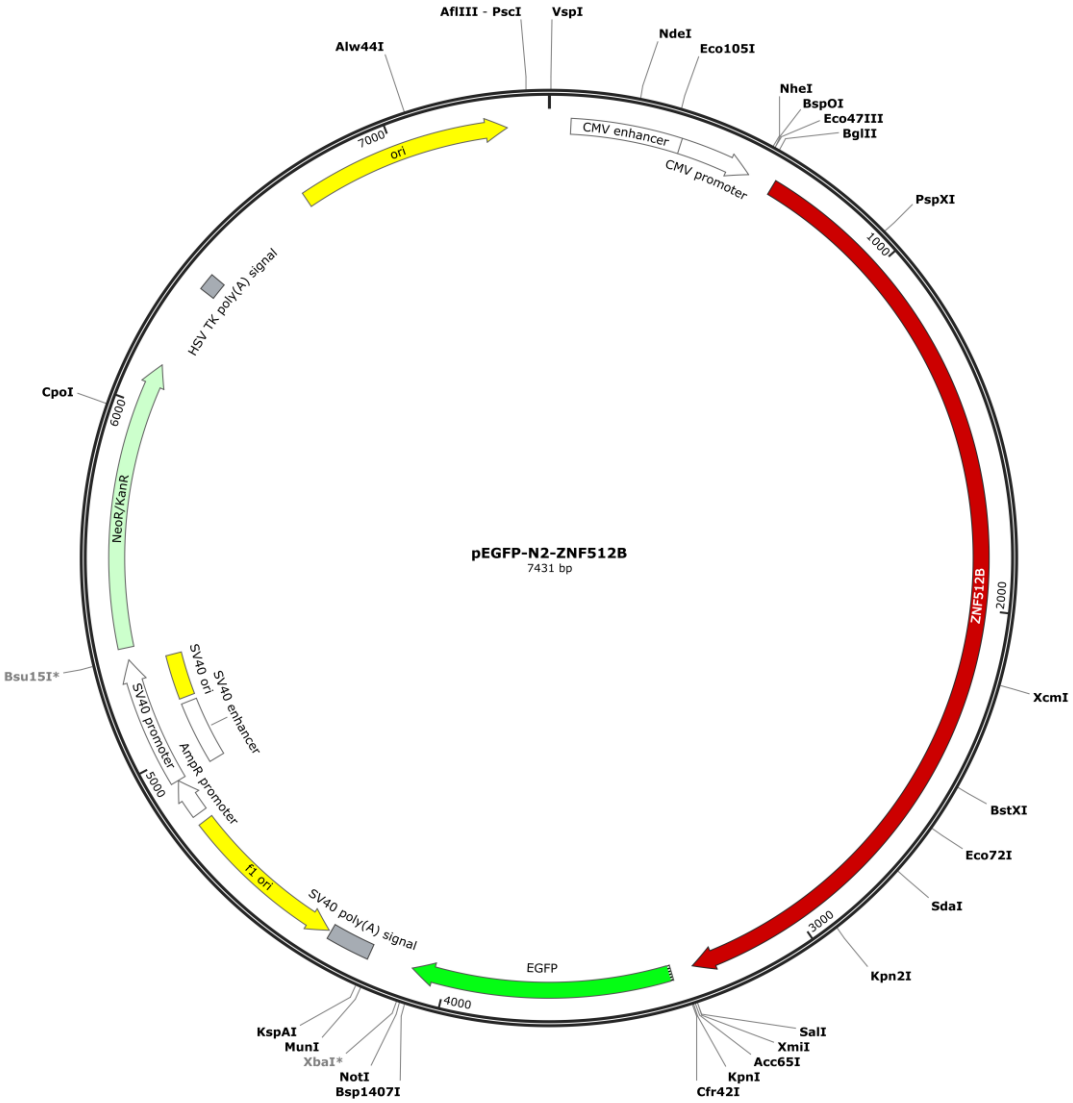

Figure 7.1.2: Plasmid map for pEGFP-N2-ZNF512B. *Vector for eukaryotic expression of C-terminally GFP-tagged human ZNF512B.*

7.1.3 p3xFLAG-ZNF512B

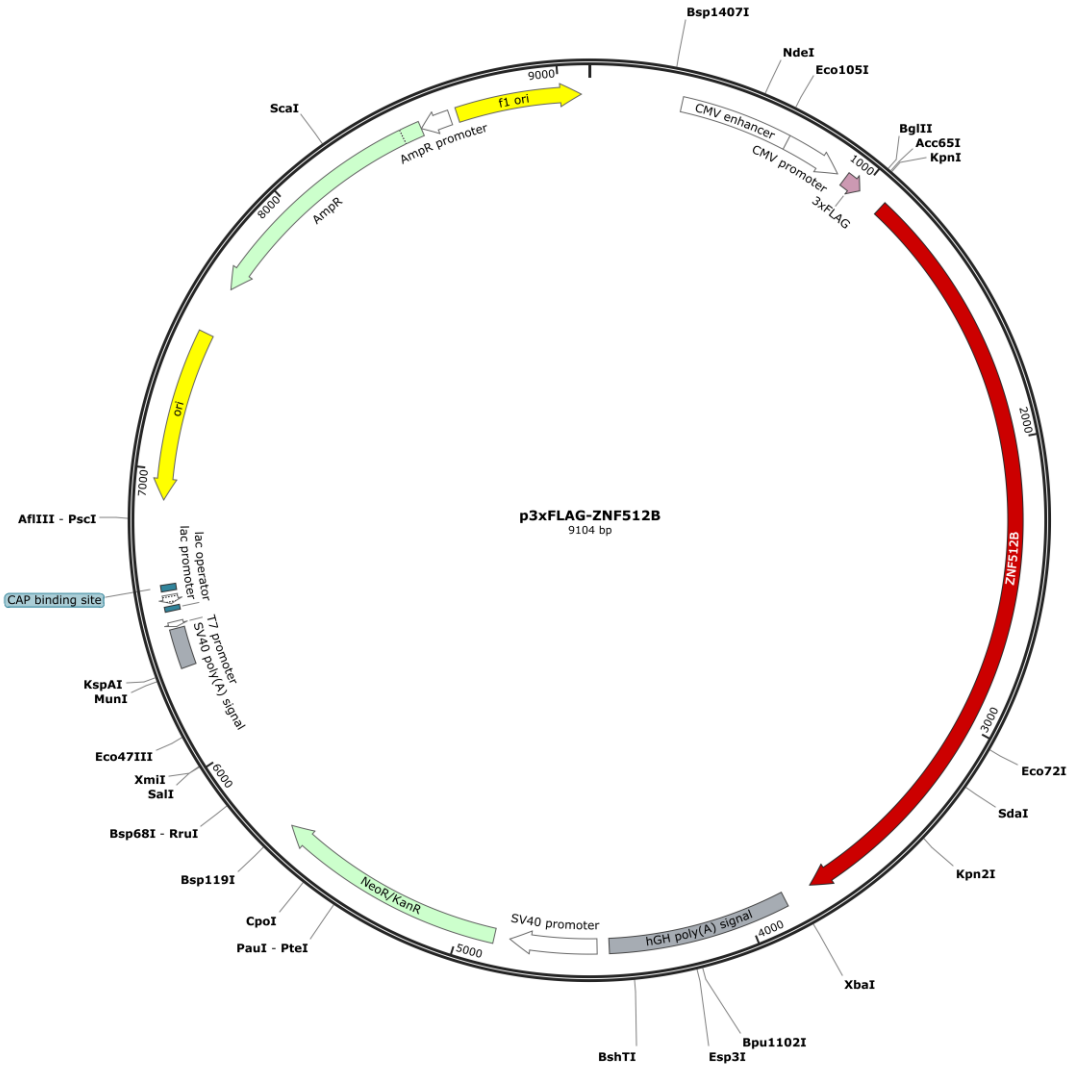

Figure 7.1.3: Plasmid map for p3xFLAG-ZNF512B. *Vector for eukaryotic expression of N-terminally FLAG-tagged human ZNF512B.*

7.1.4 pTetLS-eGFP-ZNF512B

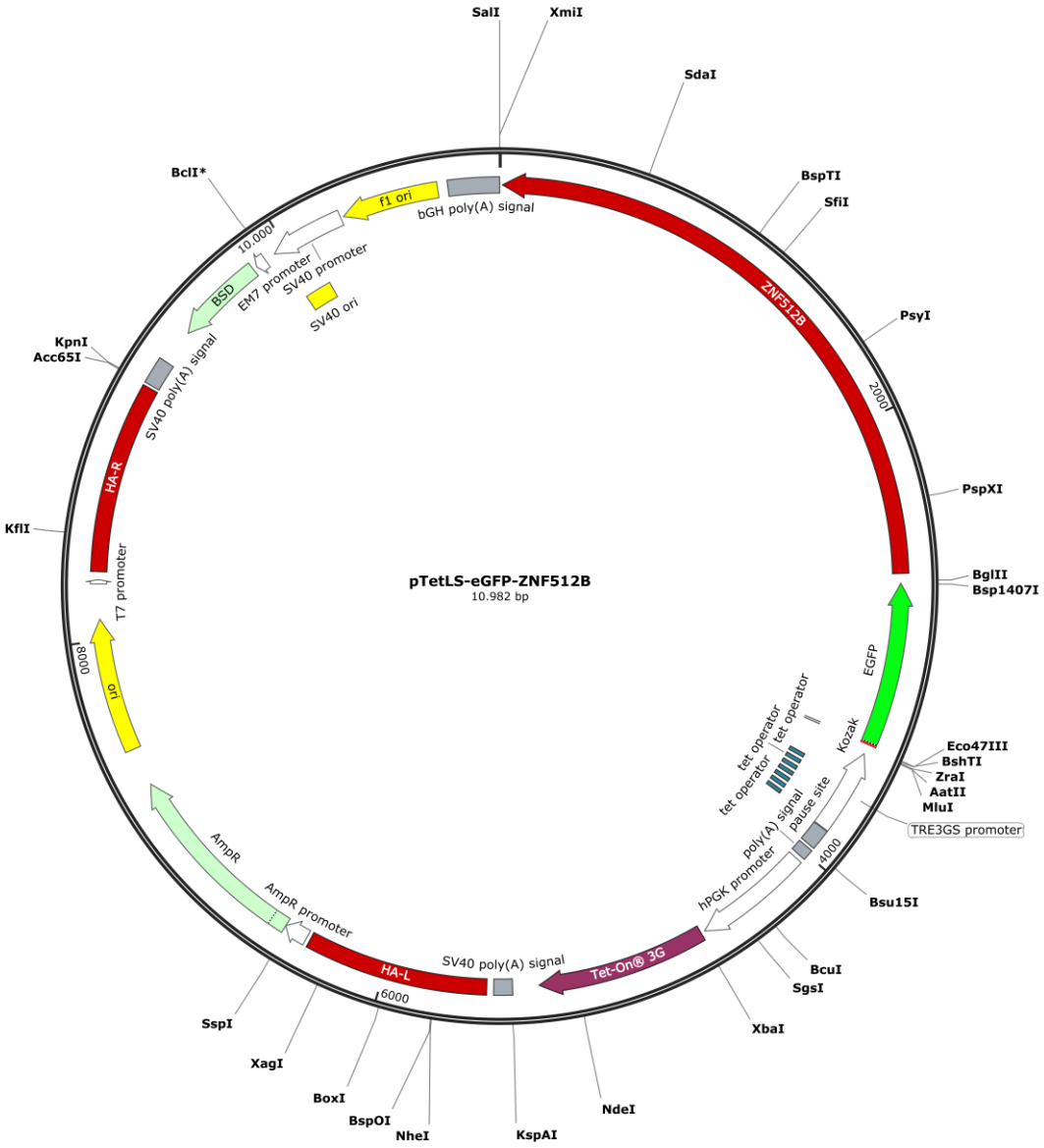

Figure 7.1.4: Plasmid map for pTetLS-eGFP-ZNF512B. *Vector for the generation of cell lines inducibly expressing N-terminally GFP-tagged human ZNF512B under a tet-dependent promoter through integration into the AAVS1 safe harbor locus.*

7.1.5 pAB-Gal94

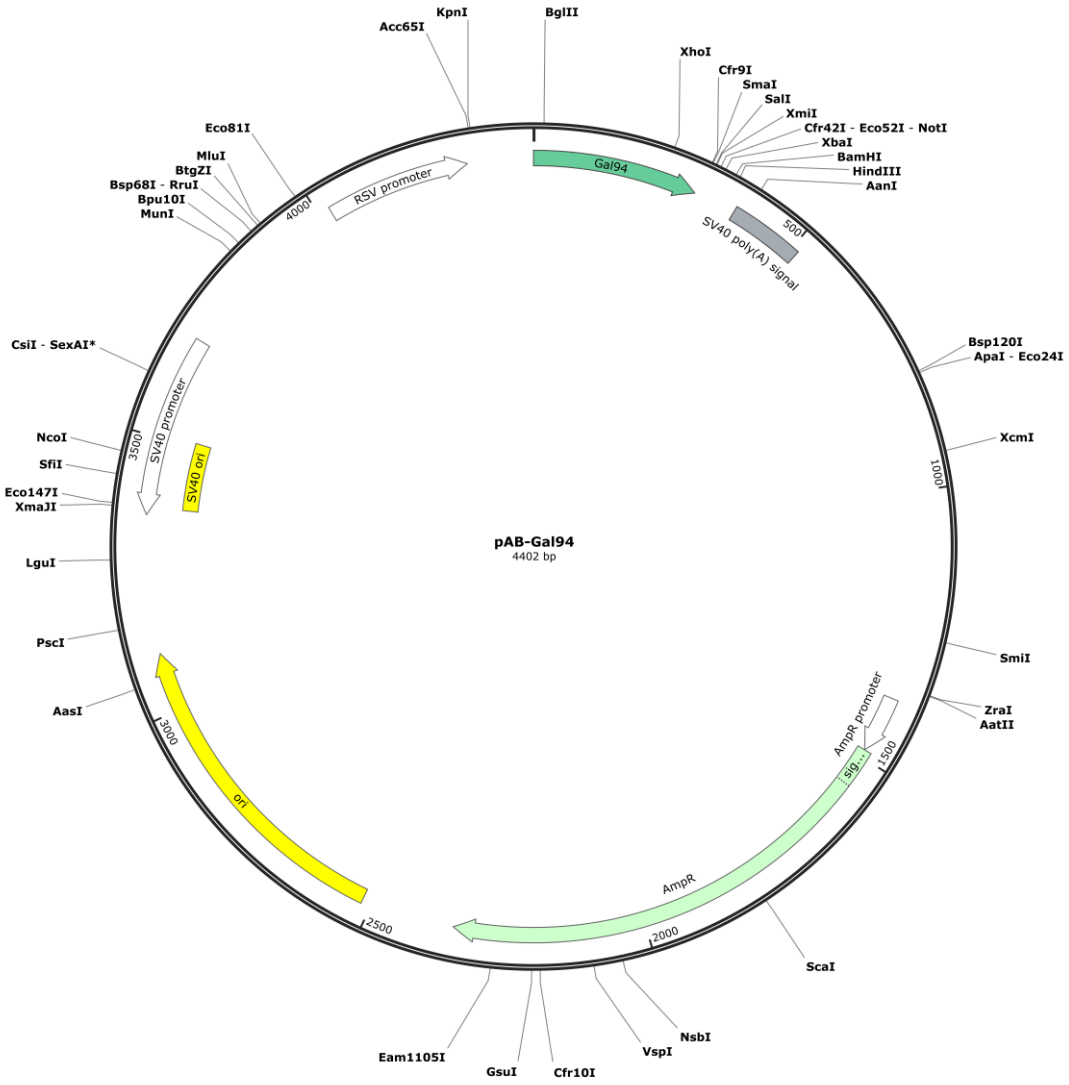

Figure 7.1.5: Plasmid map for pAB-Gal94. *Vector for eukaryotic expression of N-terminally GAL-tagged proteins used in the luciferase reporter assay.*